The Role of the Fiber/Matrix Interphase

in the Static and Fatigue Behavior

of Polymeric Matrix Composite Laminates

by

Robert Edward Swain III

Dissertation submitted to the Faculty of the

Virginia Polytechnic Institute and State University

in partial fulfillment of the requirements for the degree of

Doctor of Philosophy

in

Engineering Mechanics

APPROVED:

Kenneth L. Reifsnider, Chairman

Mark S. Cramer

Scott L. Hendricks

Jack L. Lytton

Wayne W. Stinchcomb

February, 1992

Blacksburg, Virginia

The Role of the Fiber/Matrix Interphase

in the Static and Fatigue Behavior

of Polymeric Matrix Composite Laminates

by

Robert Edward Swain III

Kenneth L. Reifsnider, Chairman

Engineering Mechanics

(ABSTRACT)

Within the past several years, researchers have detected the presence of a third "phase" between the bulk fiber phase and bulk matrix phase in a polymeric matrix composite. This finite-thickness region — termed the *interphase* — possesses mechanical, physical, and chemical properties that are distinct from the fiber and matrix constituents. Thus, the interphase embodies the characteristics of the fiber/matrix bond, including the strength and stiffness of the bond. In essence, the interphase represents the composite *system*, since it defines the level of synergistic interaction that occurs between the load-carrying fibers and the binding matrix material.

Recent interest in the interphase has spawned international conferences and a technical journal devoted to its study. Despite this spate of research, some very fundamental questions about the interphase have remained unanswered. One such question is: "What is best for the _____ performance of a composite, a strong or weak or intermediate-strength interphase?" It is surprising that this question is even asked, since, until recently, it had been assumed that the stronger the fiber/matrix bond, the better the composite behavior. It is now known that this adage is far from true.

Two formidable challenges await those who wish to correlate the strength of the interphase to the mechanical performance of polymeric matrix composite materials. First, one seeks to systematically alter the interphase in order to exploit this variable. In this study, fourteen material systems representing permutations of four carbon fibers, three matrix systems, percentages of fiber surface treatment, and three sizing conditions have been examined. Secondly, one needs to quantitatively characterize the properties of the resultant interphase in order to correlate the bond condition to the

composite's mechanical behavior. This investigation utilizes two techniques, the Continuous Ball Indentation Test and transverse flexure testing, as a means of interrogating the strength of the interphase.

The influence of the interphase on the tensile and compressive strength and modulus of cross-plied laminates possessing a center hole is investigated. Unnotched angle-ply ($[\pm 45]_{ns}$) laminates are also tested in order to assess the role of the interphase in the strength of a "matrix-dominated" laminate.

Fully-reversed ($R = -1$), axial fatigue of notched cross-plied laminates from each of the fourteen material systems is performed. During fatigue testing several data are monitored, including cycles to failure, dynamic modulus, and notch temperature. The tension-tension ($R = 0.1$) fatigue response of the unnotched angle-ply laminates is also studied. Results from X-ray radiography of fatigue-damaged specimens help to explain the relationship between the interphase and the initiation and propagation of life-critical damage mechanisms.

Having observed the formative role played by the interphase in the performance of these laminates, an attempt is made to introduce variables representing the interphase into micromechanical models of composite behavior.

Dedication

This work is dedicated to the hope and joy that accompanies the anticipation of my and Susan's first child, due in ten weeks.

Acknowledgements

The author would like to thank the following people for their contribution to this work:

- Dr. K. L. Reifsnider, for serving as the author's advisor and mentor throughout his graduate study. Though his technical skill is without parallel, it pales in comparison to his sense of humanity.
- Dr. W. W. Stinchcomb, for serving on the author's graduate committee and for the careful insight that helped shape many of the investigative directions detailed herein. His door is *always* open.
- Drs. M. S. Cramer, S. L. Hendricks, and J. L. Lytton for serving on the author's graduate committee. Their questions during the author's oral preliminary exam were tough and fair and largely unanswered.
- The United States Air Force, especially Lt. Suzanne Guihard, for allowing access into the collective expertise of two ongoing research projects. This work would not exist were it not for that opportunity.
- The McDonnell Aircraft Company, in particular, Gail Hahn and Mindy Schowengerdt, for providing assistance in obtaining materials and for answering numerous technical questions.

- The Northrop Corporation, in particular, Dr. Anna Yen, for supplying the author with material systems and for taking the time to answer any and all questions.
- Dexter Hysol, in particular, Raymond Wong, for supplying numerous material systems and for his patience in addressing countless technical questions. His assistance was invaluable.
- Gregg Owens of Amoco Performance Products, for taking the time to respond to the author's many questions about their material systems.
- Jennifer Elmore, for her immeasurable assistance with this investigation. Without her help, the author would have spent *years* performing the countless tasks that are essential in executing a thorough experimental study.
- Robert Brightup, for his many hours spent in laminate fabrication, specimen creation, X-ray radiography, etc., etc., etc.
- Jack Lesko, for introducing the author to the indentation test performed in this investigation. Jack took it upon himself to run *all* of the McAir compression tests. Surely, this is one of the most talented men the author will ever meet.
- Kami Razvan, for introducing the author to the Dynamic Signal Analysis technique and for providing the data acquisition software used throughout this investigation. His expert supervision of the laboratories allowed for the unfettered execution of the experimental work.
- Mehran Elahi, for assisting the author in the interpretation of the Dynamic Signal Analysis data.
- Scott Case, for running *all* of the indentation tests in this study. Multiply fourteen specimens by twenty data points and twenty minutes per point. The author is grateful that Scott does not charge interest on the time that he is owed.
- Shin Steven Lee, for performing the SEM work in this investigation.
- Chuck Chandler, for his expertise and assistance in the fabrication of many of the laminates used in this study.

- Susan Devereaux and Matt Stinchcomb, for creating laminates, running C-scans, and taking X-ray radiographs.
- To the fellow students of the Materials Response Group, for their friendship and camaraderie.
- Barbara Wengert, Sheila Collins, and the ESM clerical staff, especially Cindy Hopkins, for all of their help.
- Bob Davis, Archie Montgomery, Bill Shaver, and Danny Reed for cutting all of panels into precise specimens.
- Mr. and Mrs. Robert Swain Jr., the author's parents, for their constant love and support which has guided and sustained the author to this point in time.
- Mr. and Mrs. Vincent Kordack, the author's in-laws, for their overt love and support in all of the author's endeavors.
- Susan Kordack Swain, for allowing the author to pursue his dreams. Now the author and his wife can dream together.

Table of Contents

List of Illustrations

List of Tables

Introduction and Literature Review

The Interphase

Since the advent of polymeric matrix composite materials as viable structural materials, scientists and engineers have ardently pursued the creation of the "perfect" composite material. This "perfect" material would satisfy all of their demanding structural requirements; i.e., it would possess high specific tensile and compressive longitudinal strength and stiffness, high specific shear strength and stiffness, excellent fatigue and impact behavior, exhibit the ability to retain these properties at high temperature, and be low cost, just to name a few typical traits. In the pursuit of this ideal material over the past thirty years (or more), material engineers have focused primarily on improving the composite's two "main" constituents: the fiber and the matrix. An extreme amount of effort has been expended in the creation of stronger, stiffer, and lighter fibers. This effort has been equally matched in the pursuit of tougher, damage resistant, damage tolerant, temperature resistant, and processable matrix systems. Throughout this venture, one very important aspect has been virtually ignored; namely, the nature of the adhesion between the "main" constituents and its effect on the resultant composite performance.

In June of 1968, ASTM Committee D-30 on High Modulus Fibers and Their Composites sponsored the symposium "Interfaces in Composites." Nearly *eighteen years later* the First Inter-

national Conference on Composite Interfaces convened, the first major, international conference devoted to the fiber/matrix interface in this two-decade time period. Yet, it seems that the emergence of this conference series has issued in a renaissance in the study of the composite interface. As of this writing, the International Conference on Composite Interfaces has met for a second and third time with the fourth meeting set for May of 1992. In addition, a new peer-reviewed journal entitled, *Composite Interfaces*, has appeared, and several books and numerous journal articles have been written, all towards the understanding of the composite interface. The scientific and engineering community has re-awakened to the importance of how the fiber and matrix interact, and how this interaction influences the behavior of the final composite product.

The renewed interest in the fiber/matrix bond has forced the technical community to discard outdated prejudices and formulate new, realistic concepts to better frame the problem at hand. One extremely useful concept is embodied in the term "interphase" — a term found in the work of Sharpe in the early 1970's [1,2]. Several researchers have published data purporting the existence of a region that lies between the bulk fiber material and the bulk matrix material [3]. This "interphase" region is a zone in which the fiber and matrix phases are chemically and/or mechanically combined, or, otherwise, indistinct. The interphase may be a diffusion zone, a nucleation zone, a chemical reaction zone, etc., or any combination of the above. The word "interface" now properly refers to a two-dimensional border separating distinct phases, e.g., fiber, matrix, and interphase phases [4]; unfortunately, the words "interface" and "interphase" are sometimes interchanged carelessly. Jayaraman, *et al.* [3], conclude that the interphase may possess such features as:

- a finite dimension or thickness,
- elastic or inelastic response,
- a degree of anisotropy,
- tensorial bond strength measuring adhesion to the fibers,
- tensorial bond strength measuring adhesion to the matrix, and,
- tensorial values of modulus, coefficient of thermal expansion, Poisson's ratio and strength (possibly functions of position in the radial and azimuthal directions).

It is necessary to devote several paragraphs to describe how an "interphase" arises in a conventional carbon fiber/polymeric matrix composite. This discussion will detail the role of the fiber surface treatment and fiber sizing in the formation of the interphase region at least as it applies to the material systems under consideration in this study.

In the creation of a carbon fiber, a polymeric precursor made of polyacrylonitrile (PAN) is exposed to extremely high temperatures in an attempt to graphitize the precursor. The graphitized fiber leaves the furnace and soon encounters an electrolytic bath which serves as a "surface treatment". The purpose of this treatment is two-fold [5]: first, the liquid attacks the very weak and disoriented outer graphite layers on the fiber surface. It effectively removes these weak layers, and, in doing so, creates microscopic pits and crevices that change the total surface area of the fiber. If one subscribes to the mechanical interlocking theory of adhesion, the creation of such potential "interlocking" sites is thought to promote stronger bonding. The second purpose of the treatment is to deposit chemical groups onto the fiber surface. Surface chemical analysis frequently reveals the presence of oxygen and nitrogen on the surface of carbon fibers that have been surface treated. It is thought that the introduction of these chemical groups serves to encourage polar-polar bonding with epoxy matrices and alter the surface energy of the fiber which may, in turn, promote fiber wetting [5].

A considerable amount of work has been published by Drzal, and Madhukar and Drzal [5-10], examining the differences in the mechanical behavior of epoxy matrix composites possessing surface treated and non-surface treated fibers. Drzal contends that the bond strength of non-surface treated fibers is limited by the presence of the weak graphitic layers. Published failure analyses [5] indicate traces of fiber on both sides of a fractured non-surface treated fiber/matrix bond. The removal of these weak layers during surface treatment is largely responsible for the subsequent increase in surface treated fiber/matrix bond strength, in Drzal's opinion [5]. Other researchers have begun investigating the effect of "levels" of fiber surface treatment on the performance of polymeric matrix composites. At least three variables may be altered in an attempt to change the level of surface treatment (when treated via an electrolytic bath as described above): time of treatment, concentration of the electrolytic solution, and the charge in the solution. Which, and to what extent, each

of these three variables is altered in developing different surface treatment levels is proprietary information of the fiber supplier. Levels representing 10%, 20%, 50%, 100%, 200%, etc., of the standard surface treatment have been studied in an attempt to determine the "optimum" level for the particular composite and loading mode under investigation [11-19]. Due to the rather arbitrary manner in which the 100% surface treatment is defined, and because of the inaccurate procedure responsible for altering surface treatments, criticisms have been voiced concerning one's ability to attribute differences in bond strengths to fibers receiving, say, 10%, 20%, and 50% of standard surface treatment levels; such precise designations do not necessarily reflect corresponding physical (or chemical) changes in the fiber surface. Such criticisms are not applicable to comparisons made between surface treated and non-surface treated fibers, however [20].

After the fiber has received its surface treatment, it typically enters another bath, this time to obtain a "sizing". This sizing (also called a "finish" [21]) is often simply an uncured epoxy occurring in solution. Upon drying, a region of uncured or partially cross-linked epoxy, estimated to be between 100-200 nm in thickness [21] surrounds each fiber (others estimate the thickness to be nearly 500 nm [22]). This "coating" serves at least two purposes. First, the sizing noticeably improves the handleability of the fibers, resulting in less "fuzzing". Secondly, if the fibers are ultimately to be impregnated with an epoxy matrix system, the epoxy sizing acts as a "primer", i.e., it provides an attractive and compatible surface for the matrix to bond to. Drzal [21] has studied the effect of fiber sizing on the fiber/epoxy bond strength and has concluded that the sizing creates a layer that possesses unique mechanical properties. Because the curing agent is forced to migrate from the bulk matrix into the sizing, a gradation of properties exists, transitioning from the bulk matrix properties to a material with higher strength, higher modulus, and lower fracture toughness. Experiments with single fibers embedded in an epoxy coupons [21] has revealed that when the fiber broke, if a sizing had been applied, the failure grew perpendicularly into the matrix region. If no sizing had been applied, the fracture would run along the fiber/matrix interface.

It is clear from the above discussion that both fiber surface treatment and fiber sizing play a significant role in the formation and quality of the fiber/matrix bond. By treating these two procedures as variables, one can create dramatically different interphase regions: surface treated fibers

with no sizing, non-surface treated fibers with sizings, fibers treated to X% of the industry standard that are sized with different epoxy formulations, and all the other permutations inherent within this set. It is important to emphasize that several other factors may influence the formation of an interphase. From this point forth, the *interphase* region will refer to the idealized phase within a composite existing between the bulk fiber and the bulk matrix that has resulted from bringing the fiber — with the presence or absence of surface treatment and sizing — into intimate contact with the matrix system.

Prior to leaving the discussion about the interphase, a brief note about *spelling* will be somewhat illuminating. There is a strong desire to form an adjective out of the word "interphase". The author, in the past, has used the word "interphasial" for this purpose [4]. Upon reflection, this seems to be misspelled. The ending "-ial" simply comes from the tendency to make the word sound like "interfacial". It is likely that the true ending for this adjective is, instead, "-al", just as the adjective for "base" is "basal". Until the author definitively finds the correct spelling for this adjective, the word "interfacial" will be used in its place. The reader is asked not to confuse the adjective "interfacial" with a term describing a two-dimensional boundary. Whenever "interfacial" is used, it will describe a three-dimensional region.

The Interphase and its Influence on Composite Performance

Given that a unique interphase exists in an as-processed composite, several questions surround the role of this interphase and its relationship to the resultant composite. One extremely fundamental question is: "What is best for the _____ performance of the composite, a strong or weak or intermediate-strength interphase?" It is surprising that this question is even asked, since, only recently has experimental evidence convinced the populace that stronger interphases are not always better interphases. Indeed, the ceramic composite community has known for years that weak fiber/matrix bonds allow threatening cracks to diffuse through the material and not lead to instan-

taneous failure. Such a critical eye has been cast on the role of fiber/matrix bonding in the performance of polymeric matrix composites only within the past several years.

Recent work on the role of the interphase in the static performance of carbon fiber/epoxy composites has been performed by Madhukar and Drzal [8-10]. In these works, the longitudinal tensile and compressive strength, as well as the shear strength of unidirectional laminates have been correlated to a measure of the fiber/matrix bond strength. It is clear from these studies and studies of similar focus [11-19] that the quality of the bond between the fiber and the matrix is an essential factor in the determination of the static performance of the material. One common aspect that exists among all the investigations discussed thus far, has been the simplicity of the laminate configurations and loading modes chosen to study the interphase. The motivation behind this is clear: in order to relate composite performance directly to the interphase, one wishes to keep the failure modes as simple as possible. While such work has considerable merit, the composite community awaits studies relating the interphase to the performance of engineering laminates under realistic static and fatigue loading conditions.

Noticeably absent from the literature, however, is a study concentrating on the role of the fiber/matrix interphase in the long-term performance of polymeric matrix composite materials. In 1988, Verpoest, *et al.* [18], observed, "it is surprising to find out that, to the best of our knowledge, no literature data are available on the influence of interface strength on the damage development during fatigue loading." While several researchers have hypothesized on the importance of the interphase to fatigue performance [23-26], to the present author's knowledge, only two such experimental studies exist, as detailed below.

Shih and Ebert [27] examined the ability of silane coupling treatments to alter the bond strength of glass fiber to epoxy, and the effect that this bond strength had on the performance of these composites under four-point flexural fatigue. They concluded, "using interlaminar shear strength as an indication of the interface strength, it was found that composites having a higher interface strength would possess a greater fatigue performance" [27]. Yet, they also found that the fatigue failure sequence was independent of the bond strength provided that the final failure was in flexural tension. This finding is indicative of the constraint placed upon the specimen in the flexural fatigue

loading mode. In other words, the failure modes available to a composite loaded in flexural fatigue are very limited. Hence, the performance of the different bond strength materials to flexural fatigue was only moderately illustrative of the role of the fiber/matrix bond in the fatigue process.

Vincent, *et al.* [28], also studied the role of interphases on the flexural fatigue behavior of unidirectional glass/epoxy composites. They indicated that the fatigue failure process is highly dependent on the materials' resistance to the nucleation of cracking. Thus, just as in Shih and Ebert's work, stronger bonding — resulting in a delay in the onset of cracking — resulted in longer fatigue lives. Again, the criticisms leveled against flexural fatigue remain relevant.

It is important to highlight a common thread that has run through every study that attempts to correlate interphase strength with the performance of the resultant composite: the correlations made in all such studies are *highly* dependent on the method in which interphase strength is measured. Due to the minute size of the interphase region (perhaps on the order of a tenth of a fiber diameter [3]), no technique has been developed that allows for the *direct* measurement of the shear strength and tensile strength of the interphase. The technical community has been forced to develop methods that necessitate a level of "inference" in order to quantify such bond strengths. Popular "interphase strength" measurement techniques may be divided into two general types: single fiber tests (fiber pull-out, critical fiber length, microindentation, and microdebonding) and laminate tests (short beam shear, transverse tension, transverse flexure, and Dynamic Mechanical Analysis) [3]. When one attempts to infer interphase strength from the results of single fiber tests, one is ignoring the complex stress state that arises in a "real" composite. In a "real" composite, the interphase is influenced by the surrounding fibers, irregular fiber spacing, and variations in matrix morphology [3]. When one attempts to infer interphase strength from the results of laminate tests, one is claiming that a global, macroscopic measure is directly attributable to a highly local failure phenomena. Such inferences are likely to introduce considerable error when estimating the true "average" interphase strength. The lack of a universally accepted method to measure interphase strength has clouded previous attempts to correlate bonding condition to macroscopic composite properties.

Opportunities

Two recent Air Force research programs have recognized the need to understand the role of the interphase in the behavior of high-performance, aircraft-structure composite materials [29,30]. Each program examines at least twenty different carbon fiber/polymeric composite material systems towards the goal of determining which system best satisfies the demanding design requirements for both fighter and commercial aircraft. One variable exploited in these twenty-plus material systems is the nature of the fiber/matrix interphase. The McDonnell Aircraft Company (abbreviated throughout this work as "McAir"), recipient of one of the two Air Force research programs (contract number F33615-88-C-5452), has sought to alter the interphase by varying the level of the industry-standard surface treatment (a "state-of-the-art electrolytic oxidative surface treatment" [29]); levels of 20%, 50%, 100%, and 200% of the standard treatment were employed. Material systems were also created using different fiber sizing formulations.

The Northrop Corporation, recipient of the other Air Force research program (contract number F33615-88-C-5447), chose to alter the resultant fiber/matrix bond through a slightly different route. Instead of experimenting with gradations of surface treatment, they chose to examine only two levels: 0% and 100%. They, too, experimented with different fiber sizings, and allowed the presence of the sizing to add to their combination of material systems. In other words, for a given fiber and matrix, the following four combinations existed: no surface treatment, no sizing; no surface treatment, sizing; surface treatment, no sizing; surface treatment, sizing.

Both companies have devoted nearly three years to the characterization of their particular material systems. Included in their investigations is an encompassing examination of the materials' static mechanical properties. Of all the materials tested, the materials that exhibited superior performance in certain, critical mechanical tests (e.g., longitudinal, unidirectional compressive strength and modulus, and longitudinal and transverse unidirectional tensile strength [31]) were "down-selected" for final evaluations as potential candidates to meet the required design limitations. Yet, remarkably, no consideration was given by either company to the long-term performance of the

candidate materials. Though considerable effort was undertaken to examine the role of bonding on static material performance, the role that this bonding would play on the fatigue process was not explored.

Problem Statement

Eight material systems have been obtained from McAir and six material systems been obtained from Northrop (see the next chapter for details). These material systems are unique in that they have been systematically altered with regard to the fiber/matrix bond. These systems are extremely well characterized with respect to their static mechanical properties. **The object of this work is to study the influence of the fiber/matrix interphase on the static and fatigue behavior of the host laminates.** The present work distinguishes itself from previous studies in a number of ways:

- The quasi-static test specimens utilized to determine the effect of the interphase on the laminate strength are notched with a center hole. Notched strength is a complex function of unnotched strength altered by the presence of a global stress concentrator. How the interphase affects both of these variables *in tension and in compression* constitutes a fascinating study. The strength of a $\pm 45°$ laminate — a "matrix-dominated" laminate configuration frequently used to characterize a material's shear response — provides another interesting chance to exploit interphase effects on material strength.
- This appears to be the first study on the effect of the *carbon* fiber/matrix interphase on fatigue performance. Carbon fibers are extremely important constituents to the structural designers as evidenced by the 40+ carbon fiber systems examined in both Air Force programs.
- The fatigue loading mode, specimen geometry, and laminate configuration are truly representative of actual in-service structural components. Longitudinal, tension-compression fatigue loading of center-holed, cross-ply *laminates* (not unidirectional specimens) permits a wide range of failure mechanisms including (yet, not limited to): fiber microbuckling, tensile fiber

failure, matrix cracking, fiber/matrix debonding, and delamination. The study of the initiation, interaction, and progression of these damage mechanisms as a function of the fiber/matrix bonding is unique.

- The effect of bond strength on the fatigue behavior of $\pm 45°$ specimens is investigated. While others [32] have researched the effect of numerous test conditions on the performance of $\pm 45°$ laminates, this is believed to be one of the first studies attempting to isolate the interphase as a key variable affecting the laminate's fatigue response.
- This investigation employs a new test technique, indentation testing of composite materials [33], to interrogate the fiber/matrix interphase strength. This technique has been found to be very sensitive to differences in the *in situ* bond strength of unidirectional composite laminates. Transverse flexure testing, recently popularized by the results of Madhukar and Drzal [10] and Adams, *et al.* [34], is pursued in addition to the indentation testing. Both test techniques are used to assess the bond strength of composites made with fibers that have received a *gradation* of surface treatment. There is disagreement among the composite community on just how effective changing percentages of surface treatment is at altering bond strengths. This is an ideal chance to help settle this dispute.
- An attempt is made to study the effect the interphase has on altering the strain field in a notched composite. It is conceivable that differences in laminate stiffness brought about by the presence of a third distinct region may influence both the value of the stress concentration at the notch and the manner in which the laminate distributes this stress. A "strip gage" — ten miniature strain gages situated in a row — are positioned along a ligament of a center-holed specimen in the hopes of detecting a gradient in the strain.
- Another new test technique is employed in an attempt to distinguish the presence of differing fiber/matrix interphases on the fatigue process. This technique, called Dynamic Signal Analysis (DSA) [24], monitors the cyclic deformation of a specimen undergoing fatigue loading, and analyzes the relationships between the input (load) signal and the output (displacement) signal. It has been shown [24] that careful analysis of the stored signals can be used to distinguish between different material systems and can indicate the onset of specimen failure.

To complete the study of the role of the fiber/matrix interphase on the static and fatigue performance of composite laminates, a quantity characterizing the bond condition is introduced into mathematical models that predict composite behavior. Introducing the variable of "interphase strength" into micromechanical models is an original and potentially valuable contribution to the technical community.

Experimental Techniques

Material Systems

Fourteen different material systems were investigated in this study. In order to facilitate the explanation of the detail behind each system, the material systems will be divided into two major categories (indicating under which contract the material was made): McAir material and Northrop material. Within each of these major categories, the systems will be further subdivided into those systems sharing a common fiber.

McAir Material Systems

Eight distinct material systems were received from the Dexter Hysol Corporation. The matrix material remained a constant throughout the eight systems; a toughened epoxy marketed by Dexter Hysol and designated as HC 9106-3. Reference [36] lists several properties of the neat resin including glass transition temperature, tensile modulus, fracture toughness, *et al.* Two different fiber types were pre-pregged with the HC 9106-3 resin system: an "XA" fiber and an "Apollo" fiber.

Each fiber — manufactured by Courtaulds Research — will be designated by its respective nominal fiber properties rather than the fiber names just indicated.

Composites Possessing the 32-550 Fiber

The "XA" fiber possesses a 32 Msi tensile modulus and a 550 ksi tensile strength (on the average, as determined by the manufacturer). The cross-section of the fiber is circular and is 7 microns in diameter, nominally. Henceforth, all composites laminated with this particular fiber will be indicated by the number "5" — the first digit of its fiber tensile strength.

McAir chose to investigate how different *levels* of surface treatment and different formulations of fiber sizing affected the composites' performance. All of the "5" fibers (i.e., the XA 32-550 fibers) were *unsized* (i.e., were *not* coated with a very thin layer of epoxy) prior to being pre-pregged with the HC 9106-3 matrix. The interphase, instead, was altered by changing the level of fiber surface treatment. Four surface treatment levels were applied: 20%, 50%, 100%, and 200% of the standard treatment level. The 200% system was not investigated in this study, leaving three distinct systems possessing the 5 fiber. To designate these three systems, the trailing zero of each surface treatment percentage was dropped and the remaining digits were placed behind the "5". Thus, the 20% surface treatment level system becomes "52", while the 50% system becomes "55" and the 100% system becomes "510". This coding system is completed with the indication that each of these three systems received no fiber sizing. This is achieved by adding a "U" for "Unsized" at the end of each designation. Thus, the three McAir systems possessing the 32-550 fiber are the 52U, 55U and 510U systems. This group of material systems will be known as the "5U" series. Table 1 details the materials and coding scheme for the McAir systems.

Table 1. List of the McAir Material Systems.

MATERIAL TYPE ACRONYM	FIBER MODULUS (Msi)	FIBER STRENGTH (ksi)	PERCENT SURFACE TREATMENT	FIBER SIZING	MATRIX TYPE	MATERIAL SERIES ACRONYM
52U	32	550	20	Unsized	T. Epoxy	5U
55U	32	550	50	Unsized	T. Epoxy	
510U	32	550	100	Unsized	T. Epoxy	
82A	45	850	20	"A" sized	T. Epoxy	8A&O
85A	45	850	50	"A" sized	T. Epoxy	
810A	45	850	100	"A" sized	T. Epoxy	
820A	45	850	200	"A" sized	T. Epoxy	
810O	45	850	100	"O" sized	T. Epoxy	

Composites Possessing the 45-850 Fiber

The "Apollo" fiber has a 45 Msi tensile modulus and a 850 ksi tensile strength (again, these numbers are imprecise values used by the manufacturer to characterize the fiber properties). The fiber cross-section is circular and is 5 microns in diameter, nominally. All composites created with this fiber will be designated by the number "8", again, the first number of its fiber tensile strength. Of the five systems delivered containing the 8 fiber, four of the five systems had the fiber sized with an "A" epoxy sizing, while the fifth system was sized with an "O" organic sizing. As with the 5U series, McAir, again, chose to experiment with altering the level of applied fiber surface treatment. The 8 fiber that ultimately received the "O" sizing was treated only at the 100% level (the arbitrarily-chosen standard level). The "A" sized fibers were treated at the 20%, 50%, 100%, and 200% levels. Thus, adopting the earlier code, the five systems possessing the 8 fiber are designated as 82A, 85A, 810A, 820A, and 810O. These systems — as a group — will be referred to as the 8A&O series. Again, these details are summarized in Table 1.

It may be important to note that the nominal fiber strength of the 810O system was updated nearly a third of the way through the McAir investigation. The 850 ksi strength designation, and all such similar strength designations, are imprecise characterizations of an end-product that started out as a fixed precursor and endured a set process. Tests on the raw fiber that eventually went into the 810O systems indicated that its nominal strength was noticeably less than the fibers that were sized with the A sizing. McAir began to refer to the fiber with the O sizing as "45-750" rather than "45-850". It should be mentioned that "fiber-dominated" laminate properties, like unidirectional tensile strength, did not necessarily reflect this difference in fiber strength [37]. Because of this, no effort was made to distinguish the 810O system from the other systems possessing the 45-850 fiber in the adopted coding scheme; the composites created using what McAir calls the "45-750" fiber will be referred to as the 810O system in this study.

Northrop Material Systems

Six distinct material systems were received from the Northrop Corporation. Amoco Performance Products was responsible for creating the material systems. As with the McAir material, the description of the systems will be subdivided into two fiber types — those systems containing Amoco's Thornel T650X-50 fiber and T650-35 fiber.

Composites Possessing the T650X-50 Fiber

The T650X-50 fiber is described as, "a developmental carbon fiber in the 50 Msi modulus class...(having) a filament diameter of 5 microns" [38]. The "650" refers to the nominal tensile strength of the fiber, while the "X" indicates that the fiber is deemed to be at an experimental stage. Since the T650X-50 fiber and the T650-35 fiber (to be discussed below) possess the same nominal strength, the strength value could not be used to distinguish the two fiber types, as was the case with the McAir material. Therefore, for the Northrop systems, the first digit of the value characterizing the *tensile stiffness* of the fiber is used, instead. In other words, henceforth, the first digit in the code that refers to the T650X-50 fiber will be a "5". Though this might lead to confusion with the McAir 32-550 fiber designation, the further development of the coding scheme will prevent any misunderstanding.

All of the T650X-50 fibers were pre-pregged with the Amoco resin system ERLX-1901. This resin is described in Ref. [38] as a "standard aerospace epoxy which is similar to (Hercules's) 3501-6." The interphase was created within each system by choosing one of two levels of surface treatment: 0% (or, untreated) and 100% (standard treatment level). The untreated fibers will be designated by an "N" (for No treatment) and the treated fibers by an "S" (for Standard treatment). These abbreviations will appear after the first digit, which indicates the fiber modulus. Thus, the two systems containing the T650X-50 fiber are the 5N and 5S systems. To complete the coding, a letter is added at the end to indicate the fiber sizing. All systems delivered by Northrop contained

fibers that received *no fiber sizing*. This fact will be designated by adding another "N" (for No fiber sizing) to the end of the code. Therefore, these two systems are known, from this point forward, as 5NN and 5SN (the T650X-50 fiber, with Standard fiber surface treatment and No fiber sizing); this group will be known as the 5N series. It should be mentioned that the abbreviation, "U", used in the McAir 5U series, also refers to a lack of fiber sizing; both U and N appearing as the last character in the code refer to an absence of fiber sizing. Table 2 details the materials and the coding scheme for the Northrop systems.

Composites Possessing the T650-35 Fiber

The T650-35 fiber is described in Ref. [38] as, "a standard-modulus, high-strength carbon fiber with a nominal 7 micron filament diameter." Again, the "650" refers to the nominal fiber tensile strength, while the "35" refers to the nominal fiber tensile stiffness. According to the coding scheme adopted above, the T650-35 fiber will be designated by a "3" (the first digit of its fiber tensile modulus).

Two systems possessing the 3 fiber were pre-pregged with the same epoxy as the 5N series; namely, the ERLX 1901 standard epoxy system. The interphase of these two systems was altered, again, by the presence or absence of a standard level of surface treatment; i.e., 0% or 100%. Thus, adopting the current coding scheme, these systems are designated as 3NN and 3SN (T650-35 fiber that has received Standard surface treatment and No fiber sizing). This group is known as the 3N series.

The two remaining systems were pre-pregged with a thermoplastic resin system, named Radel-X (currently under the new designation Radel-8320 [39]). Radel-X is a "polyarylether thermoplastic resin" possessing a "room temperature Young's modulus comparable to typical epoxy formulations (410 ksi); ... its elongation at break in standard ASTM dog-bone tests is 50% higher than even the recent generation of damage-tolerant epoxies" [38]. To indicate that the resin system was not the ERLX 1901 epoxy, an "R" (for Radel-X) was placed beside the "3" in the coding scheme. As with

Table 2. List of the Northrop Material Systems.

MATERIAL TYPE ACRONYM	FIBER MODULUS (Msi)	FIBER STRENGTH (ksi)	PERCENT SURFACE TREATMENT	FIBER SIZING	MATRIX TYPE	MATERIAL SERIES ACRONYM
3NN	35	650	0	Unsized	S. Epoxy	3N
3SN	35	650	100	Unsized	S. Epoxy	
3RNN	35	650	0	Unsized	T-plastic	3R
3RSN	35	650	100	Unsized	T-plastic	
5NN	50	650	0	Unsized	S. Epoxy	5N
5SN	50	650	100	Unsized	S. Epoxy	

the other Northrop systems, the interphase was created either by the presence or absence of a standard level of surface treatment. Therefore, the two systems that contained the T650-35 fiber and the Radel-X matrix were designated as 3RNN and 3RSN. This group is known as the 3R series. Again, details of the Northrop materials and their coding scheme are given in Table 2.

Laminate Configurations and Test Specimens

Laminate Configurations

The McAir material arrived in panel form in three distinct configurations. Each of the eight material systems was laminated into a single 12″ by 12″ panel, 32 plies thick, with a cross-ply lay-up of $[0/90]_{8s}$. Each of the eight material systems were also laminated into a single 12″ by 12″ angle-ply panel. All of the systems — except the 55U and 820A systems — were laid-up in a 16-ply, $[+45/-45]_{4s}$ configuration. The 55U and 820A systems were received in a 32-ply, $[+45/-45]_{8s}$ configuration. The final configuration received was a 28-ply unidirectional lay-up with the fibers aligned along the six inch dimension of a 6″ by 4″ plate on all but the 52U and 510U panels. In these two systems the 0° fibers ran along the four inch dimension.

The Northrop material arrived in pre-preg form instead of panel form. Two sizes of pre-preg were delivered; twelve inch tape (the 3SN and 5SN systems) and six inch tape (the remaining Northrop systems). The same general procedure was used in the formation of all panels from the pre-preg: the tape was cut by hand into square pieces, the tape pieces were vacuum debulked, the pieces were placed in a vacuum bag prior to positioning them in their respective steel molds and pressed in a hydraulically-driven hot press according to the consolidation cycle set forth by the manufacturer. The Radel-X systems did not require vacuum debulking or placement in a vacuum bag.

Only two distinct configurations were laminated using the Northrop pre-preg. Each material system was laid-up into a 32-ply, $[0/90]_{8s}$ configuration. The size of the panel, and, ultimately, the number of specimens cut from each panel was dictated by the size of the pre-preg tape. Each system was also laid-up into a 6″ by 6″, 32-ply, unidirectional panel.

Each panel to be tested, whether the panel was created at Dexter Hysol or at Virginia Tech, was inspected using an ultrasonic C-scan unit to verify its integrity. Every panel received from Dexter Hysol was deemed acceptable for testing. A few panels created at Virginia Tech did not pass this inspection and were exempted from further testing.

Test Specimens

Every cross-plied panel was cut into two specimen types: notched and unnotched coupons. The notched specimens were used in assessing notched strength, monitoring strain gradients near the notch (only in the 810A and 810O systems), and in a subsequent fatigue study. The *only* purpose served by the unnotched specimens were to provide cross-ply stiffness data for the *McAir material* (unnotched cross-plied strength data were published by McAir and Northrop for these material systems [37,40]). Both coupon types were 6″ long and 1″ wide. The only difference between the two specimen types was a 0.25″ diameter center-hole cut in the geometric center of the notched coupons. All such test specimens were cut with a diamond cut-off saw. Specimen cooling during cutting was achieved using a synthetic lubricant. The holes were cut using either a diamond core drill or a carbide twist drill. Damage caused by the drill was minimized, yet, if drill-induced damage was feared to interfere with the introduction or progression of damage due to the test regimen, the specimen was discarded. At least twenty test specimens were obtained from every 12″ by 12″ panel. Thus, a high level of uniformity was expected between each specimen, provided that the panel passed the C-scan inspection. Only five specimens could be obtained from the 6″ by 6″ panels. Since four panels had to be fabricated from the 5NN, 3NN, 3RNN, and 3RSN pre-preg to equal the number of test specimens from one 12″ by 12″ panel, some non-uniformity between

these specimens was anticipated, even though the integrity of each panel was verified via C-scan inspection.

It is reasonable to ask why the specimens in this fatigue study were notched (with a center hole) instead of unnotched. Quite simply, it is the author's experience that the fatigue performance of unnotched laminates possessing 0° fibers ultimately becomes a study in delamination resistance and/or resistance of damage growth due to failures located at the grip. These problems are not entirely illuminating. By placing a hole in the laminate — which may represent an unloaded bolt hole — one can study the initiation, interaction, and propagation of many competing damage modes, including, but not limited to: fiber failure (either in tension or compression), longitudinal splitting and subsequent notch blunting, delamination, off-axis matrix cracking, etc. One, too, may ask why a cross-plied laminate configuration has been studied rather than a quasi-isotropic or more exotic lay-up. In this case, simplicity is sought both in the interpretation of damage inception and progression, and, in any attempts made to model the performance mathematically. This line of reasoning led to the present specimen geometry.

The decision to test $\pm 45°$ specimens was made for several reasons. First, it is well documented [41,42] that $\pm 45°$ laminate tension tests are an easy and highly effective manner in which to characterize the shear performance of a material system. Suspecting that the interphase plays a large role in defining the shear behavior of a laminate, it was desirable to chose a laminate configuration that would experience considerable shear loading. The McAir $\pm 45°$ material was cut into 6″ long by 1″ wide specimens using the same cutting procedure as detailed above. This material, however, was tested in an unnotched condition.

Several 90° coupons measuring a diminutive 1.25″ long by 0.5″ wide were cut from the unidirectional panels of all fourteen material types to be used as specimens during transverse flexural loading. All unidirectional material was cut using a high-speed diamond wheel cooled with water jets. The Radel-X material (the 3R series) tended to resist cutting with this wheel and had to be cut using a low-speed diamond wheel.

The unidirectional McAir material was also devoted to the formation of several 0° specimens in order to obtain unidirectional compressive data. These specimens measured 6″ in length and 0.5″

in width. End tabs — used to protect the specimen from grip damage — were formed from high-pressure glass/epoxy cross-plied laminates. The tab thickness was 0.1 inches. Prior to adhesion, the unidirectional specimens were sanded with 180 grit sandpaper to "rough up" the surface. The glass/epoxy tabs were lightly sandblasted to provide an attractive surface for bonding. Two end tabs were placed over the specimen such that a central 0.29″ gap remained. The tabs were affixed with a "patch adhesive" manufactured by Hysol (the manufacturer's data sheets quote a lap shear strength of 3200 psi). A bond line of 0.007″ was maintained between the two adherends. The epoxy was a room-temperature cure system. After bonding two tabs on one face of the specimen, the tabs were ground flat to form a surface parallel to the specimen. The other two tabs on the opposite face of the specimen were then applied. These tabs were then ground to a surface parallel to the opposite face. The specimens were post-cured at 140°F for 2.5 hours after all cutting and grinding had been completed. One strain gage was adhered to the gage section of each face of the specimen. The gages (CEA-06-125UN-350 by Micro-Measurements) were aligned to the axis of loading to monitor longitudinal strain; they conform to the ASTM standard for composite compression testing [43]. The strain gages allow the operator to monitor failure strain, compressive modulus, and determine the amount of bending occurring in a loaded specimen. Such assiduous specimen preparation is essential in order to obtain representative and reproducible compressive data.

From each of the fourteen material systems, "chunks" of unidirectional material were cut to be placed in a 1.25″ diameter, cold-mount ring form. Once inside the ring form — after ensuring that the fibers of the composite rested perfectly perpendicular to the free surface — a room temperature-cure epoxy (Epoxide Resin, manufactured by Buehler) enveloped the material in order to provide a metallographic mount. Upon curing, the specimen was polished on a polishing wheel starting with 180 grit sandpaper and progressing through finer grades of grit and powder until reaching the final 0.3 micron alumina powder stage.

Mechanical Testing

Quasi-static Strength and Stiffness Testing

Notched Cross-plied Specimens

All of the notched strength tests were performed on a 20 kip, electro-hydraulic, servo-controlled load frame with hydraulic wedge grips. To minimize grip damage, each specimen end was wrapped in two layers of 60 grit sandpaper with the grit side facing the specimen. The sandpaper was affixed using masking tape. At least 1.5″ of each specimen end was inserted into the gripping region. A right-angle level was used to ensure that the specimen was aligned to the loading axis. A grip pressure was chosen to prevent premature slipping of the specimen. A pressure of 1500 psi was found to be sufficient to hold the specimens enduring the highest loads to failure.

Strain was measured in every notched strength test via an extensometer. Aluminum V-notched tabs measuring 0.5″ long by 0.1875″ wide were placed 1″ apart and centered about the hole. These tabs were adhered to the specimen with a thin layer of silicone rubber. The knife edges of the extensometer were placed in the V-notch of each tab and the extensometer was held in place by rubber bands (see Ref. [44] for a schematic of this set-up). It is important to note that the strain is measured *across* the hole, and, therefore, cannot be used in the characterization of *material* stiffness. Since the extensometer measures a strain reading across the notch, the measurement takes into account both geometric and material responses. Yet, since every specimen possesses an identical geometry, this measure can be used for comparative purposes.

At least two quasi-static tension and compression tests were run to failure for each material type. This is an unusually low number of specimens to use to characterize strength, yet, this is all that could be spared out of the limited amount of material available. More strength tests were performed if the two values did not coincide within an exceptable deviation. No anti-buckling guides

were used during the compression tests; the only precaution taken was to ensure that a region of 2″ remained ungripped (this is called the unsupported gage length). The tests were run in load control at a rate of 1000 lb. per second. This is an unusually high rate of loading, yet, a high loading rate was preferred since the strengths tabulated were used to determine fatigue load levels that would be applied at a frequency of 10 Hz. Every specimen, both in tension and compression, failed through the notch. Buckling did *not* play a role in the final failure of the compressively-loaded specimens.

The strain signal from the extensometer was fed through the load frame's internal amplifier and then fed into a computer-driven data collection system. The load signal from the load cell also left the machine's internal amplifier for the data collection system. Both signals were received as raw voltages. An A/D board converted the analog signals and stored the data at a rate of nearly 5 Hz. The data stored using the data collection software (written in-house by Ahmad Razvan) was input into a spreadsheet, where conversions from volts to strain and stress were performed. A data regression analysis was executed on the linear portion of the resulting stress-strain relationship to determine a modulus. A peak detector enabled the operator to capture the highest load achieved prior to failure. Once converted into a peak stress, this value, along with the modulus, eventually characterized the response of the specimen to its quasi-static strength test. These results will be detailed in the next chapter.

Unnotched Cross-plied Specimens

The only meaningful data collected from the McAir unnotched cross-plied specimens were stiffness measures. Strength data for the unnotched cross-plied configuration for all of the systems studied herein was published by McAir and Northrop [37,40]. In addition, Northrop also measured the stiffness of their systems under tensile and compressive loadings. Since unnotched cross-plied stiffness values were necessary to aid in the modelling effort, these numbers were sought from the McAir material.

The test machine and gripping procedure employed in these tests were identical to the notched strength tests. Axial strain was measured using an extensometer with a 1″ gage length. An attempt was made to monitor transverse strain using an extensometer mounted perpendicular to the direction of the applied load on the side opposite of the axial extensometer. This attempt failed miserably. First, the transverse strains in the cross-plied specimen were too small to monitor precisely using an extensometer. Secondly, mounting the opposing extensometers proved time consuming and impractical. Clearly, transverse strains are monitored more efficiently with strain gages.

The specimens were loaded at a rate of 500 lb./s until reaching 10,000 lb., upon which the specimen was ramped back to zero at the same rate. Load and strain voltages from the machine's internal amplifiers were input into a computer-driven data collection system (the same program used in monitoring the data from the notched strength tests). The stored data was imported into a spreadsheet, where stiffness was computed as the slope of the linear regression of the stress and strain data.

Unnotched ±45° Specimens

The ASTM standardized method, D-3518, for determining the "Inplane Shear Stress-Strain Response of Unidirectional Reinforced Plastics" [45] mandates the use of a balanced and symmetric ±45° composite specimen loaded in uniaxial tension [46]. This test technique was inspired by the work of Petit [47], and was improved upon by Rosen [48]. The specimen dimensions are enforced by ASTM's standard for composite tensile testing (D-3039), yet allow the researcher considerable flexibility; a specimen may possess from 4 to 20 standard-thickness plies. Kellas, *et al.* [46], have shown this to be a potential source for considerable error in obtaining reproducible strengths, since, they maintain, shear strength measured in this manner is highly dependent on specimen thickness. To obtain a "unidirectional" shear strength, one simply loads the $[\pm 45°]_{ns}$ laminate in tension until failure. The shear strength of the material, τ_f, is then calculated from:

$$\tau_f = \frac{P_f}{2wt} \ , \tag{2.1}$$

where,

P_f is the load at failure,

w is the width of the specimen, and,

t is the thickness of the specimen.

The engineering shear strain, γ_{xy}, may be derived from the longitudinal strain and transverse strain measurements according to:

$$\gamma_{xy} = \varepsilon_x - \varepsilon_y \ , \tag{2.2}$$

where,

ε_x is the strain measured in the longitudinal direction, and,

ε_y is the strain measured in the transverse direction.

The shear stiffness is simply calculated by forcing a linear regression through the shear stress and shear strain data derived above.

The gripping procedure developed for the cross-plied specimens was also adopted for the unnotched $\pm 45°$ specimens. All strength tests were performed on the load frame detailed above. Strain, however, was measured with strain gages instead of extensometers. In order to measure the shear strain in a $\pm 45°$ specimen, it is necessary for one gage to be axially aligned while the other gage is aligned transverse to the applied load. Two gages (each designated CEA-06-125UW-350 by the supplier, Micro-Measurements), therefore, were adhered to each test specimen tested for strength. The gage length of each gage was 0.125″. The edge of the transverse gage and the base of the axial gage were positioned to meet at the center line of the specimen. The gages were affixed using a cyanoacrylate adhesive (M-Bond 200, manufactured by Micro-Measurements). It was necessary to sand down the regions where the gages were to be applied in order to get satisfactory bonding of the gage to the specimen.

Only tension tests were performed. Though two of the systems were 32 plies thick (the 820A and 55U systems), the remaining systems were 16 plies thick and would be unable to tolerate a significant compressive load without buckling (without the use of anti-buckling guides). All tests were run in load control. After several trials, a loading rate of 200 lb. per second was chosen for the 32-ply specimens, while 100 lb. per second was deemed satisfactory for the 16-ply specimens. The gages were inserted into a full-bridge configuration. The resulting signal from the external amplifier, along with the load signal, was monitored using the data collection program used during the notched cross-plied strength tests. Manipulation of the stored signals via a spreadsheet led to the computation of the shear modulus value, G. This value was recorded, in addition to the stress calculated from the load peak detector, for each strength test run. These values are displayed and discussed in the next chapter.

Unidirectional Compressive Specimens

All unidirectional compressive tests were performed on a screw-driven, 22 kip-capacity load frame possessing a 20 kip load cell. A Wyoming IITRI test fixture was employed in the compression tests. The IITRI fixture is approved by ASTM in their standard for composite compression testing, D-3410 [45]. One is encouraged to refer to Ref. [45] for details about the fixture, including its critical dimensions. An alignment fixture, supplied by Wyoming Test Fixtures, ensured the alignment of the test specimen within the loading wedges. Strain and load were monitored via the data acquisition software package Global Lab (marketed by Data Translation). A crosshead displacement of 0.05″ per minute was specified in standard D-3410 and adopted in the present testing. Fixture and specimen preparation was optimized to minimize specimen bending. It was determined that the absolute value of the microstrain read from each strain gage never deviated from the other gage by more than 6.9% during testing; this is overt evidence that bending had largely been avoided. Three specimens from each of six material types (all of the McAir material systems except the 52U and 510U systems; they could not be tested because their fiber direction occurred

over a 4″ dimension) were tested. The level of reproducibility between the three specimens in each material type was deemed acceptable.

Transverse Flexure Specimens

Tests were run to determine the transverse (90°) flexural (three-point bending) strength of each of the fourteen material systems. This test has been lauded by Adams, *et al.* [34], and Madhukar and Drzal [10], as being extremely sensitive to differences in fiber/matrix bond strength. While Madhukar and Drzal chose to conform to the ASTM Standard D-790 for three-point flexure testing [49], Adams, *et al.*, experimented with smaller geometries and smaller span-to-depth ratios than the standard specified. They settled upon a 5:1 span-to-depth ratio (a ratio standardized for short beam shear tests) and a specimen geometry of 0.59″ by 0.5″ (15 mm by 12.5 mm). While such a minute span-to-depth ratio would normally be a concern in a three-point flexure test, the inherently low tensile strength of the 90° specimen precludes a midplane shear failure of the specimen. Encouraged by the results of Adams, *et al.*, the present author employed a somewhat larger specimen geometry, confident that reasonable and reproducible values could be achieved.

Specimens measuring 1.25″ in length and 0.5″ in width (as described earlier) were inserted into a three-point bending fixture possessing a 1″ span length. The three-point bending fixture rested at the base of a screw-driven load frame containing a 1000 lb. load cell. The plunger connected to the loading nose travelled at a rate of 0.011 in. per minute. This value was derived from the equation [49]:

$$R = \frac{ZL^2}{6d} , \tag{2.3}$$

where,

R is the rate of crosshead motion, in./min.,

L is the support span, in this case equal to 1″,

d is the depth of the specimen, set at a nominal 0.15″, thus producing a nominal span-to-depth ratio of 6.67:1, and,

Z is the rate of straining on the outer fibers, dictated by ASTM to be equal to 0.01 in./in.min.

Two signals, load and crosshead displacement, were output from the load frame into a data collection program (written in-house by Bob Simonds). As before, the stored voltage values were input into a spreadsheet where they could be converted into stress and strain values according to the equations found in Ref. [49]. Such conversions were often subjective. In particular, though the strain value increased in proportion to the movement of the crosshead, both the inherent compliance of the three-point bending fixture and the interpretation of when a level of zero stress and zero strain occurred simultaneously, forced one to "adjust" the two signals so they could meet at the origin. Values for the maximum stress endured prior to failure, the strain achieved at failure, and the modulus of stress over strain (found by calculating the slope of the linear regression of these values) were recorded for each specimen. Madhukar and Drzal [10] point out that the strain calculated from the crosshead displacement signal is, in fact, less than the strain measured if a strain gage were to be placed on the tensile face of the specimen. Strain measurements from the crosshead displacement fail to take into account shear deformation. Thus, the measured strain is less than the true strain, therefore, the calculated flexural modulus is greater than the actual flexural modulus.

It should be mentioned that *all* failures occurred on the tensile side of the specimen. There was absolutely no indication of the initiation of shear failure in any of the specimens. None of the fracture surfaces emanated from a loading nose.

Fatigue Testing

Notched Cross-plied Specimens

Once the tensile and compressive strength of each of the fourteen material systems was determined, the unenviable task of determining an applied fatigue stress level was approached. In an

attempt to create an equitable means of comparing fatigue performance, two choices were apparent: compare the performance of each by applying the same fatigue stress level, or, compare the performance of each by applying the same *percentage of ultimate strength* as a fatigue level. The virtue of the first choice is simplicity; simplicity in running the tests and in interpreting the results. Yet, there is something inherently bothersome in choosing the former approach: since systems with different fibers (possessing different strengths) were to be compared, by comparing each on the basis of equal applied stress, one might simply be measuring a strength-dominated response instead of a fatigue response. In other words, if system X is 50% stronger than system Y, and each are fatigued at a stress level that is coincidentally 90% of Y's ultimate strength, then it would not be a surprise if X performed much better than Y to this fatigue regimen (since X is being fatigued at only 60% of its ultimate strength). It is well documented — works by Bakis, *et al.* [50], Simonds, *et al.* [51], and Kellas, *et al.* [52], are clear on this point — that the fatigue performance of notched composites is a strong function of the level of applied load (this level is often regulated as a percentage of the specimen's ultimate strength). Due to this ratiocination, it seemed more reasonable to compare the performance of the materials by comparing their response to an applied fatigue stress level equal to a fixed percentage of their respective ultimate strength. This, too, unfortunately, has its pitfalls. In comparing materials in the same group or series (e.g., the 8A&O series), since the fiber and matrix system remain the same within the series, the differences in the ultimate strengths *must* be attributed to statistical variation (perhaps related to the quality of the panel), or, to interphase effects. Therefore, two questions will ultimately have to be addressed: first, why did the interphase alter the materials' strength, and, secondly, was the fatigue performance more a function of the stress level or a function of the effect of the interphase? Perhaps, it would have been more appropriate to keep the applied fatigue stress level a constant *when comparing systems within the same series.* Yet, this would have complicated any attempts to make comparisons or generalizations among all of the fourteen systems studied.

Work performed by Madhukar and Drzal, *et al.* [8], has shown that interphase strength plays a decisive role in the compressive performance of composite laminates. In Ref. [8], three levels of interphase strength correlate to three distinct levels of unidirectional compressive strength which,

in turn, correspond to three distinct failure modes. With this in mind, it was desirable to introduce a compressive load cycle into the fatigue regimen. Tension-compression fatigue was chosen over compression-compression fatigue since it is well established that tension-compression fatigue is the more enervating of the two. Perhaps it is the process of "wrinkling" individual fibers, followed by their subsequent straightening — all of which would tend to degrade interphase strength — or, as in the case of notched fatigue, it is the reversal of the shear stress along longitudinal lines tangential to the hole boundary and parallel to the specimens edge that aids in the degradation of the specimen during tension-compression fatigue more than compression-compression or tension-tension fatigue. For these reasons, a fatigue ratio of $R = -1$ (equal amounts of applied maximum tensile and compressive load) was chosen to be applied using a sinusoidal waveform with a frequency of 10 Hz.

Once the manner in which the comparisons among the fourteen systems had been decided, and the fatigue ratio and frequency had been settled, the remaining issue was the determination of the fixed percentage of ultimate strength to apply. It was obvious from the strength results (to be detailed in the next chapter) that the operative strength from which a percentage would be taken had to be the compressive strength, since, in some circumstances, the notched cross-plied compressive strength was approximately 50% of the material's notched cross-plied tensile strength. The works of Bakis, *et al.* [50], Simonds, *et al.* [51], and Kellas, *et al.* [52], have indicated that an applied stress level exists above which specimens decay rapidly and always exhibit short lives, while, below this level, specimens consistently display a great tolerance to degradation and exhibit long lives. Kellas, *et al.* [52], call this stress level, "the damage transition stress", and believe this level to be a laminate property. It was not the interest of the present author to perform high-load/low-cycle studies nor low-load/high-cycle studies. Hopefully, a percentage could be found that would provide a full spectrum of responses. After trying fixed percentages of 60%, 65%, 70%, and 75% of the materials' ultimate compressive strength (UCS), it was determined that 75% UCS met the imposed criteria wonderfully. A range of lives from 1200 cycles (nearly a full two minutes of fatigue) to 5.1 million cycles (nearly six full days) were achieved by mandating 75% UCS as the applied stress level.

All of the notched cross-plied fatigue tests were performed on a 20 kip, electro-hydraulic, servo-controlled load frame with hydraulic wedge grips. The gripping procedure developed for the strength testing was followed without exception during the fatigue testing. Since the applied loads are 75% less than the compressive failure loads, grip pressures did not need to be as large as those used during strength testing. Strain was measured via an extensometer in the same fashion as during the cross-plied strength testing. Precautions were taken to minimize breakage of the rubber bands used to support the extensometer on the specimen since this leads to extensometer slippage, and, subsequently, erroneous strain readings. This was accomplished by wrapping one layer of masking tape around the sharp specimen edges. It should be noted that sometimes this precaution proved unsuccessful at preventing rubber band breakage.

An attempt was made to measure the notch temperature using a thermocouple (marketed by Omega). The thermocouple was encased in an adhesive film backing to encourage contact with the specimens through these means. This adhesive backing proved insufficient in retaining contact with the specimen. Once the tip of the thermocouple was placed near the longitudinal tangent of the hole (the region of highest axial stress), it was bonded to the specimen by wrapping it with adhesive tape. The main drawback to this scheme was the operator's inability to visually monitor damage around the notch. Because the thermocouple was placed on the side opposite of the extensometer, either the adhesive tape or the extensometer blocked one's view of the loaded specimen.

Once the fatigue test had commenced, it was *never* interrupted unless the decision was made to terminate the test prior to failure, for the purpose of damage analysis. All tests were run in load control, therefore, once the load levels had been finely tuned at the beginning of the test, they remained constant throughout the life of the specimen; perhaps only minor adjustments were needed due to slowly floating electronics. A data collection program ("M-R Phase 3000" written in-house by Ahmad Razvan) gathered five signals from the test: load, strain, temperature, phase lag, and gain (these final two signals will be detailed in the following chapter). Of the first three signals, only the temperature data was kept for future analysis. Applied load (stress) was known, and assumed to remain constant. Strain was monitored visually from the output of the peak detector. The maximum and minimum value of strain measured from the extensometer was manually recorded either

after a set number of elapsed cycles, or, when the numbers changed rapidly and merited recording. This account of the maximum tensile and compressive strain readings throughout the life of the specimen enabled the author to create a "modulus" plot as a function of cycles. By recording the value of strain, ε_o, the moment the load level was set and corrected, one had a value of the initial stiffness, E_o, by dividing the applied stress by ε_o. If one chose to normalize the value of E_o by setting it equal to one, and then compare all subsequent stiffness readings, E_i, to E_o, since the applied stress never changed, this could be accomplished by dividing ε_o by the present strain reading, ε_i. In other words, if one wanted the ratio $\frac{E_i}{E_o}$ this could be simply achieved by calculating $\frac{\varepsilon_o}{\varepsilon_i}$ since:

$$\frac{E_i}{E_o} = \frac{\frac{\sigma_i}{\varepsilon_i}}{\frac{\sigma_o}{\varepsilon_o}}, \tag{2.4}$$

and, since, $\sigma_o = \sigma_i$,

$$\frac{E_i}{E_o} = \frac{\varepsilon_o}{\varepsilon_i}. \tag{2.5}$$

Therefore, for each test, after dictating the applied fatigue stress level, the following data were monitored: cycles to failure (unless stopped prematurely), notch temperature as a function of cycles, maximum and minimum strain as a function of cycles (to be converted into modulus as a function of cycles), and phase and gain as a function of cycles (to be discussed in the next chapter).

Unnotched ±45° Specimens

After the tensile strength of the ±45° McAir specimens had been measured, it was necessary, again, to determine the applied fatigue stress levels. This time, however, the decision was made to keep the stress level constant among the eight systems. The difference between this situation and the previous one (the notched cross-plied systems) is the fact that the matrix type remains constant. Since the response of ±45° laminates is "matrix-dominated" and the matrix *does* remain the same,

keeping the stress level constant seems to be the best manner in which to compare the influence of the interphase on the fatigue performance.

The gripping procedure developed earlier was followed identically. The same 20 kip-capacity load frame used in the above fatigue study was employed. Strain was monitored using a 1″ gage-length extensometer with a 15% strain limit. Temperature of the specimen was again measured via a thermocouple affixed at the center of the specimen's surface. Load, strain and temperature data were collected into the program "M-R Phase 3000", allowing one to monitor the phase, gain, and temperature in real time. All fatigue tests were run at 10 Hz, at a fatigue ratio of R = 0.1 (since six of the eight specimens were only 16 plies thick, a compressive cycle was *not* introduced into the fatigue regimen). The maximum applied stress level was chosen to be 24 ksi. This stress level produced a wide range of fatigue lives, varying from 1200 cycles to 1 million cycles without failure. The data to be analyzed from each test included: cycles to failure, temperature, gain, and phase as a function of cycles.

Indentation Testing

Lesko, *et al.* [33], have investigated the use of a conventional hardness-measurement test technique as a means to differentiate purposely altered interphases in carbon/epoxy composites. They have also experimented with a unique ball-indentation system that allows the researcher to introduce a continuously increasing load and simultaneously monitor the penetration depth. Employing the Continuous Ball Indentation Test (CBIT), they have been able to observe regions of linear behavior followed by transition points that usher in non-linear response. They have correlated these transition points to the appearance of microscopic failure along the fiber/matrix interphase. Once this transition point is inserted into a micromechanical model of Carman, *et al.* [53], this point represents the "shear strength" of the interphase. This test is a very appealing measure of interphase response due to the fact that it avoids the inferences necessary when interpreting single fiber tests

(since it is performed on an actual laminate), and, it loads and monitors deformation at a scale that is much closer to the failure phenomena than most conventional laminate tests.

The test specimen is mounted in metallographic epoxy such that the fiber direction remains perpendicular to the free surface. The mounted specimen is then polished (the reader is referred to the "Test Specimens" section earlier in this chapter for more detail). The indentation is performed with a 1/16″ (0.0625″) hardened-steel ball under displacement control at a rate of ~4 microns per second. The penetration of the indenter is measured via an LVDT sensitive to 0.1 microns. The experimental test frame was developed by Lesko and Armstrong [54].

The test surface consists of three small specimens, each measuring approximately 0.75″ in length (in the "2" direction of the composite) and 0.168″ in width (the "3" direction), surrounded by the cured mounting epoxy. A total of approximately twenty indentations are performed per one sample, spread among the three imbedded coupons. Each indentation is spaced at least 2-5 ball diameters apart, while ensuring that no indentation occurs near material edges or corners.

A computer-driven data collection system (Global Lab, marketed by Data Translation) collects the load signal and the indenter displacement. This data may be reduced — in a manner similar to converting load and displacement to stress and strain — into quantities called the Mean Hardness Pressure (MHP) and the representative strain (d/D). The equations used to perform this conversion are found in Ref. [33]. These data are input into a spreadsheet to facilitate future data manipulation. Erroneous indentation responses that may arise due to inproper specimen placement within the test chamber are discarded. A Weibull analysis is performed on the remaining data to characterize the shape and location parameters of the distribution. To verify that the Weibull distribution "fits" the data, a Chi-squared goodness-of-fit test is performed. The reported mean and standard deviation values are calculated based upon the Weibull distribution.

Measurement of Strain Gradients

An attempt was made to measure a gradient in the longitudinal strain field that arises due to the presence of a center-hole strain (stress) concentrator. One 810A and 810O specimen was chosen for this investigation. The strain field was detected using a "strip gage" (identified as EA-13-020PF-120 by its manufacturers, Micro-Measurements). The strip gage consists of ten individual grids positioned 0.035″ apart. Each individual grid has a dimension of 0.02″ in length and 0.03″ in width. The array of ten evenly-spaced grids created an overall strip length of 0.385″. Since the ligament upon which the gages were placed was only 0.375″ in width, it was necessary to "cut away" one of the gages. This did not affect the performance of the other nine gages. Each gage shared a common tab, creating the need to bond one lead wire per each gage and one wire to the common tab. The gages were affixed to the specimen using a cyanoacrylate adhesive (M-Bond 200, manufactured by Micro-Measurements). It was necessary to sand down the regions where the gages were to be applied in order to get satisfactory bonding of the gage to the specimen. A photograph of a strip gage applied to a specimen is shown in Figure 1.

In the absence of nine amplifier channels, a scheme was developed where only one gage was monitored at a time. The lead wire from the particular gage and the common tab were inserted into a full-bridge configuration. The strain signal output from the external amplifier was monitored via a data acquisition software program at a rate of approximately 5 Hz. For each of the nine gages, a target applied load was approached through ramping over a time period of 15 seconds. The gage nearest the hole was monitored first, followed by the next gage, and so on, until nine ramping functions had been endured. The load versus strain signal was stored during this operation. A load of 1000 lb. was chosen as a means of introducing stress without causing any specimen damage (including longitudinal splitting). This load was applied in tension first, then in compression. Afterwards, the maximum applied fatigue load for the 810A specimen (5752 lb.) served as the target load for the ramping function. This, too, was performed in tension, followed by compression. The specimen was then subjected to 1150 cycles of $R = -1$, 10 Hz fatigue (with a maximum applied load

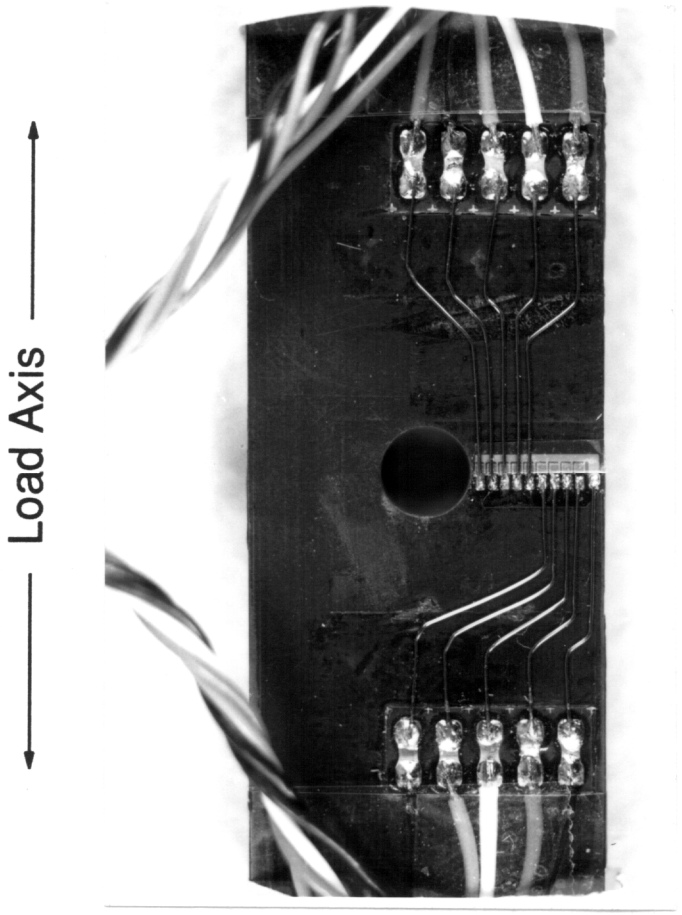

Figure 1. Photograph of a Strip Gage Applied to an 810A Specimen.

equal to 5752 lb.) in an attempt to introduce damage that would serve to blunt the strain (stress) concentration. Unfortunately, high strain concentrations and propagating damage destroyed several gages while leaving others intact. These remaining gages were monitored again by ramping each of them to the maximum applied fatigue load level. This procedure was performed in tension and then in compression. This allowed the investigators to compare the pre-fatigue and post-fatigue strain fields.

Non-destructive Testing

Fiber Volume Fraction Determination

The most common composite properties measured in a lab — strength and stiffness — are strong functions of fiber volume fraction (FVF). Other composite properties, though not tabulated as often, also reveal an intimate dependency on fiber volume fraction. Knowledge of FVF enables one to check the integrity of the panel (since pre-preg is often made with a target FVF in mind) and provides a means of normalizing data. Despite these benefits, FVF is rarely measured, largely due to the unwieldy technique standardized for its measure. Matrix digestion [55] forces one to work with noxious acids which many laboratories are ill-equipped or lack the desire to handle. A technique based upon Archimedes' principle, however, is rapidly gaining popularity due to its outstanding simplicity [56].

The basic equipment for this technique is an analytical balance and a supply of isopropyl alcohol (IPA). It is necessary to configure a small tub that will enable a sample to be submerged in the IPA, yet allow the operator to measure the weight of the sample while submerged. A schematic of the set-up employed to this end is shown in Figure 2.

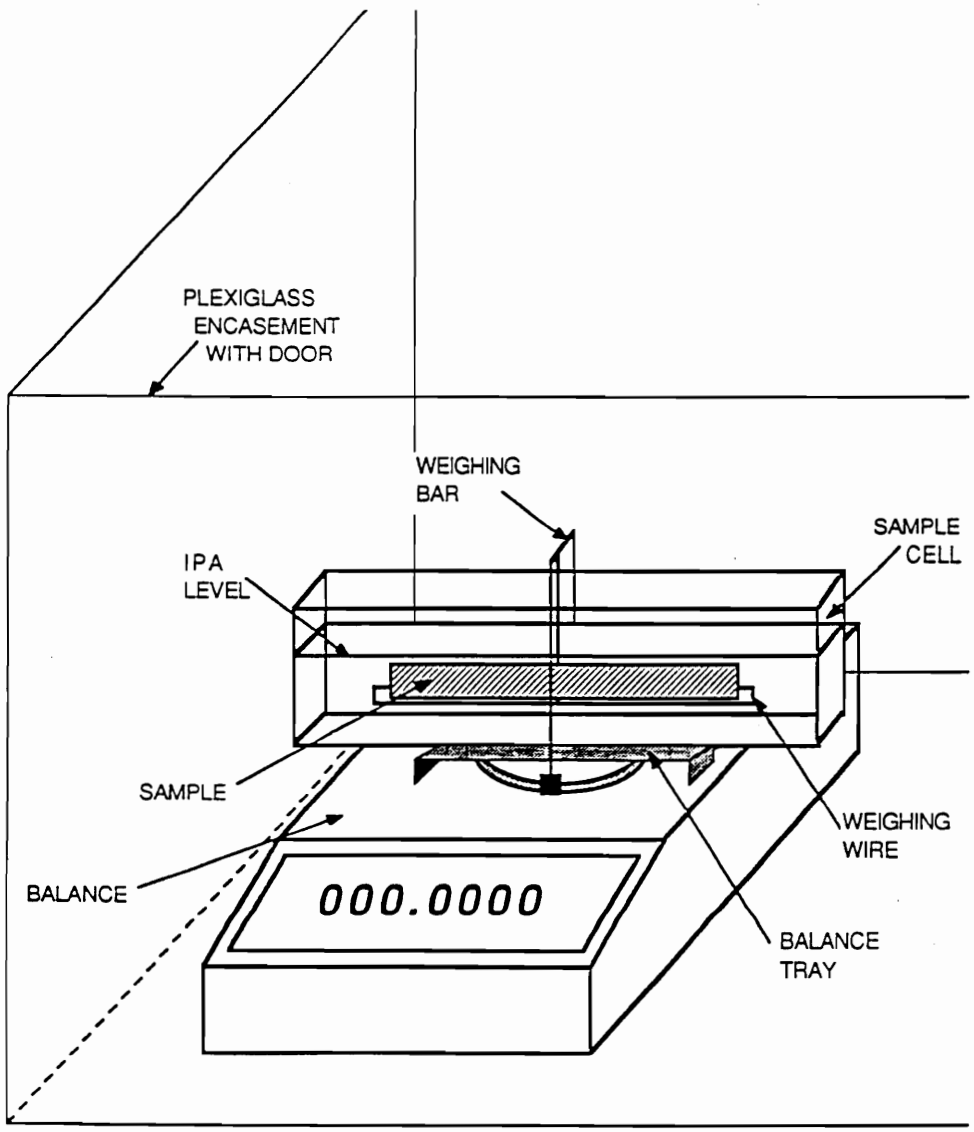

Figure 2. Set-up for Isopropyl Alcohol (IPA) Technique for Measuring Fiber Volume Fraction (taken from [56]).

Prior to positioning the tub, the dry weight of the specimen was taken. After the tub is situated over the balance, the frame used to hold the submerged specimen is put into place in the IPA bath. The balance is then tared. The sample is submerged in the IPA and suspended by the frame. The weight of the submerged specimen is recorded. The procedure is complete once the calculations detailed below have been performed.

The first calculation made is the density of the composite specimen. This is where Archimedes' principle comes into play. Defining W_d as the dry weight of the specimen, W_s as the submerged weight of the specimen, and ρ_I as the density of the IPA, the density of the composite specimen, ρ_c, is calculated according to:

$$\rho_c = \frac{W_d \rho_I}{W_d - W_s} \ . \tag{2.4}$$

In order to calculate the fiber volume fraction, it is necessary to know *a priori* the density of the matrix system, ρ_m, and the density of the fiber system, ρ_f. This is not esoteric information and can be easily obtained from the material supplier. Once this information is known, the FVF is calculated using:

$$\text{FVF} = \frac{\rho_c - \rho_m}{\rho_f - \rho_m} \ . \tag{2.5}$$

Researchers are expressing confidence in this technique, claiming that when run in parallel with the matrix digestion technique, differences between the two techniques average to about $\pm 2\%$ or less. These differences can largely be attributed to the IPA technique's inability to measure *void* volume fraction [57].

Penetrant-enhanced X-ray Radiography

X-ray radiography has proven to be an invaluable tool to the researcher investigating damage in composite laminates. Penetrant-enhanced radiographs possess the sensitivity to allow one to detect damage modes such as fiber failure, kink band formation, matrix cracking, and delamination. Through-the-thickness and through-the-width radiographs enable the researcher to locate damage in three dimensions with reasonable accuracy. Recording damage states via X-ray radiography throughout a specimen's cyclic life is a particularly valuable technique towards understanding the progression of damage.

The procedure for obtaining an X-ray radiograph of a fatigue-damaged specimen begins with the termination of the fatigue test. The specimen, in each instance, was removed from the load frame prior to the application of the penetrant. A zinc iodide solution (60 g of ZnI_2 mixed in 10 ml each of water, isopropyl alcohol, and Kodak Photo-Flo 200) is then liberally applied to the specimen, especially at sites where damage has intersected the free surface. The best results occur after the zinc iodide solution has seeped in for 24 hours or more. The excess penetrant is removed from all free surfaces with acetone; failure to do so will mar the X-ray film.

The X-ray cabinet utilized (Hewlett Packard 43805N Faxitron Series X-ray System) introduces three variables into each radiograph: the distance from the emitting element, the applied X-ray tube voltage, and the exposure time. Each radiograph in this study was produced using Kodak M-5 double-side emulsion film. Based upon this film and considerable experience, all flat-wise radiographs (through the thickness) of the 32-ply specimens were X-rayed under uniform conditions; each specimen was situated 16 in. from the emitting element, a 35 kVp tube voltage was applied, and the exposure time was set for 30 seconds. Edge-wise radiographs (through the width) of the 32-ply specimens were X-rayed under the following conditions: each specimen was placed 40 in. from the emitting element, a 90 kVp tube voltage was applied, and the exposure time was set for 30 seconds. These settings provided for high contrast radiographs.

Scanning Electron Microscopy (SEM)

Due to the absence of a universal technique to measure fiber/matrix bond strength, researchers have relied on the visual interpretation of SEM micrographs to fill this void. Weak bonding is inferred by the preponderance of long, bare, clean fiber segments that have been pulled out from the surrounding matrix. Strong bonding is inferred by short fiber segments that are covered in deformed matrix material. The SEM was employed in the present study towards this end and in an attempt to distinguish the effects of fiber surface treatment and fiber sizing on the size and distribution of the second phase toughener in the composites possessing the HC 9106-3 toughened epoxy system.

Fractured specimens examined for an overt indication of bonding quality were simply cut to size using a water-cooled low-speed diamond wheel and gold sputtered prior to insertion into the SEM's test chamber. The Scanning Electron Microscope utilized was model type SX 40 manufactured by International Scientific Instruments (ISI).

The SEM studies performed on the toughened epoxy specimens required the use of a chemical etch in order that one may distinguish between the epoxy phase and the toughener phase. A formula for an etchant typically used with PEEK matrix materials [58] was found to be effective at removing the toughener phase. The procedure used to etch the samples is detailed here for the sake of completeness. One gram of ground potassium permanganate ($K_2M_2O_4$) was added to 40 ml of 85% orthophosphoric acid (H_3PO_4). This solution was stirred vigorously for 15 minutes. Afterwards, the liquid was decanted off of the remaining potassium permanganate crystals. Ten ml of distilled water was added to the liquid while stirring. Cold-mounted specimens (the same procedure followed to mount the specimens used in the indentation studies) were submerged in this solution at room temperature for five minutes. After time had elapsed, the specimens were vigorously washed with water in an attempt to halt the etching action. Prior to insertion into the SEM's test chamber, the etched specimens were gold sputtered. It should be mentioned that the solution's

effectiveness decayed as a function of time. Though the original reference [58] claimed effectiveness for one hour, the author felt that a half-hour was more reasonable for his usage.

Experimental Results and Discussion

The organization of this chapter will be similar to the last chapter in order to aid in the simplicity and clarity of its exposition. In each section the collected data will be presented in tabular and/or graphical form. A discussion of the data will follow its presentation in an attempt to highlight any salient points and to formulate the interrelationships that exist among the data. This chapter will begin by examining the results obtained in the pursuit of characterizing the fiber/matrix bond strength. This will facilitate the understanding and analysis of all subsequent data, since the object of this work is to identify the role of the interphase in the performance of polymeric matrix composite materials.

The McDonnell Aircraft Company (McAir) and the Northrop Corporation, under contract from the United States Air Force, ran numerous independent tests in an attempt to characterize their respective material systems. These extensive data have been collected into quarterly reports by each company and are available through the Air Force under a limited distribution policy.[1] In order to fully comprehend the data collected during this investigation, it often was necessary to refer to the data found in these quarterly reports. To protect proprietary information from each company and the Air Force, all discussion of these data is restricted to comparative evaluations. In

[1] Interested readers should write: WL/MLBC, Attn: Lt. S. Guihard, WPAFB, OH 45433-6533, for information on how to obtain these reports.

other words, data taken from these reports will not be presented on an absolute scale; instead, the data will be "normalized" by the value of one point with respect to another point, either by setting one value to "1" and scaling the next point accordingly, or by comparing the value of one point as a percentage of the other. In light of the present study, it is the opinion of the author that the absolute values of the data provide only limited information; studying how the response of these systems deviates from one another clues one in on the essential variables that enter into the equations that govern performance.

Characterization of Interphase Strength

Transverse Flexure Testing

It is important to re-emphasize the purpose for undertaking this test regimen. The results from two independent research teams, Madhukar and Drzal [10] and Adams *et al.* [34], strongly indicated that Transverse Flexural Strength (TFS) is an extremely effective gauge for characterizing interphase strength. The material systems investigated were the same in both studies. The systems within each investigation were altered *only* with respect to their bonding characteristics; i.e., three fiber interphase conditions were studied: non-surface treated/unsized, surface treated/unsized, and surface treated/sized. The fiber type and matrix were kept constant in all three materials. Thus, any changes found in the TFS could be directly attributable to chemical and/or physical changes brought about within the interphase. Their results force one to consider TFS to be a viable monitor of interphase strength. In the present investigation, however, the fiber and matrix systems are altered in addition to the degree of fiber surface treatment and the presence (or absence) of fiber sizing. Therefore, it is quite possible that differences in TFS could be attributable to, say, matrix strength, since the material cleaves through both the matrix and the interphase. Throughout this

section, however, if it is discovered that TFS is a function of the bond condition, it will be tacitly assumed that this strength reflects the strength of the interphase. Any alteration of the fiber and matrix will be assumed to vary the chemical and/or physical nature of the interphase region; it will be necessary, however, to critically assess the role of these constituents beyond this scope.

Figure 3 presents the average strength measured from each of the fourteen material systems while under transverse (90°) flexure (three-point bending) loading. A schematic of the failure strain and flexural stiffness data obtained from these tests is located in Figure 4. All of these data are collected and tabulated in Table 3.

The most obvious conclusion from Figure 3 is that the transverse flexural strength *is* sensitive to the bond condition. It is especially noticeable when comparing the strengths of the non-surface treated Northrop material with their surface treated counterparts. The very presence of the surface treatment causes the transverse flexural strength (TFS) to increase by 135% in the 5N series, 48% in the 3N series, and 146% in the 3RN series, on the average. These large differences are not entirely unexpected. Madhukar and Drzal [10] report an increase in TFS of 135% when going from non-surface treated/unsized AU4 fiber ("U" representing, in this case, Untreated) to surface treated/unsized AS4 fiber ("S" representing Surface treated) in an Epon 828 mPDA epoxy matrix. Adams, *et al.* [34], report an increase of 136% (on the average) for the exact same systems investigated by Madhukar and Drzal. Adams, *et al.*, indicate, however, that the results from transverse flexure testing are strongly influenced by fiber volume fraction, a point taken up later in this discussion.

It is interesting to compare these remarkable differences with those seen in the systems that have received a gradation of surface treatment. With the only exception being the 55U system, it is clearly seen that an increase in the level of surface treatment corresponds to an increase in the TFS in these systems. It is somewhat surprising that increasing the surface treatment from 20% to 100% only causes an increase of 14% in the 8A&O series and an increase of 12% in the 5U series. The 8A&O strengths seem to "level off" as the level of surface treatment increases, with no great gains witnessed between the 810A and 820A specimens. This result echoes the finding of other researchers who report significant gains in "matrix-dominated" properties (as opposed to "fiber-

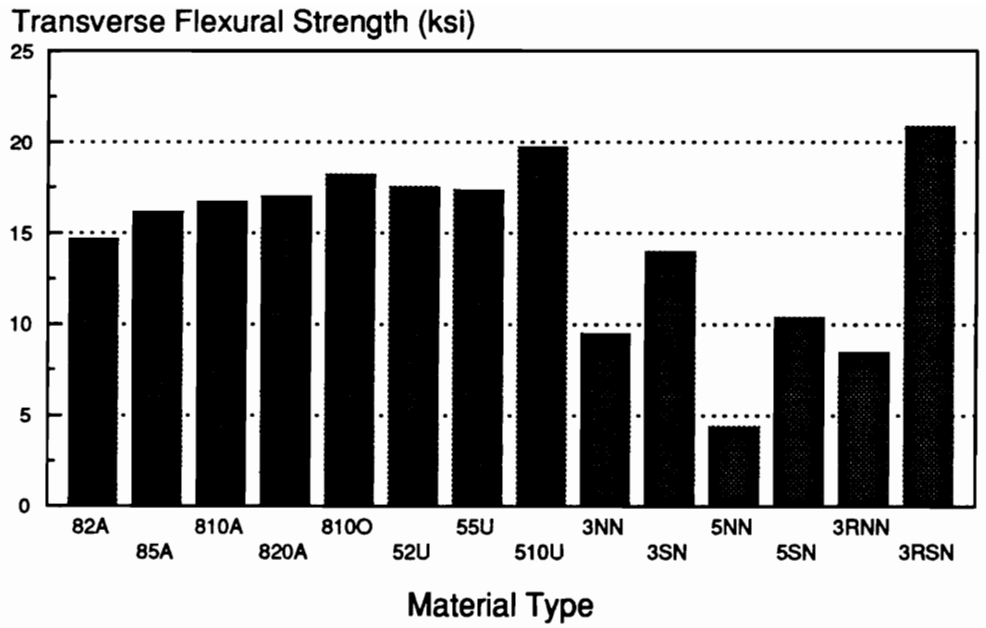

Figure 3. Average Transverse Flexural Strength of the McAir and Northrop Materials.

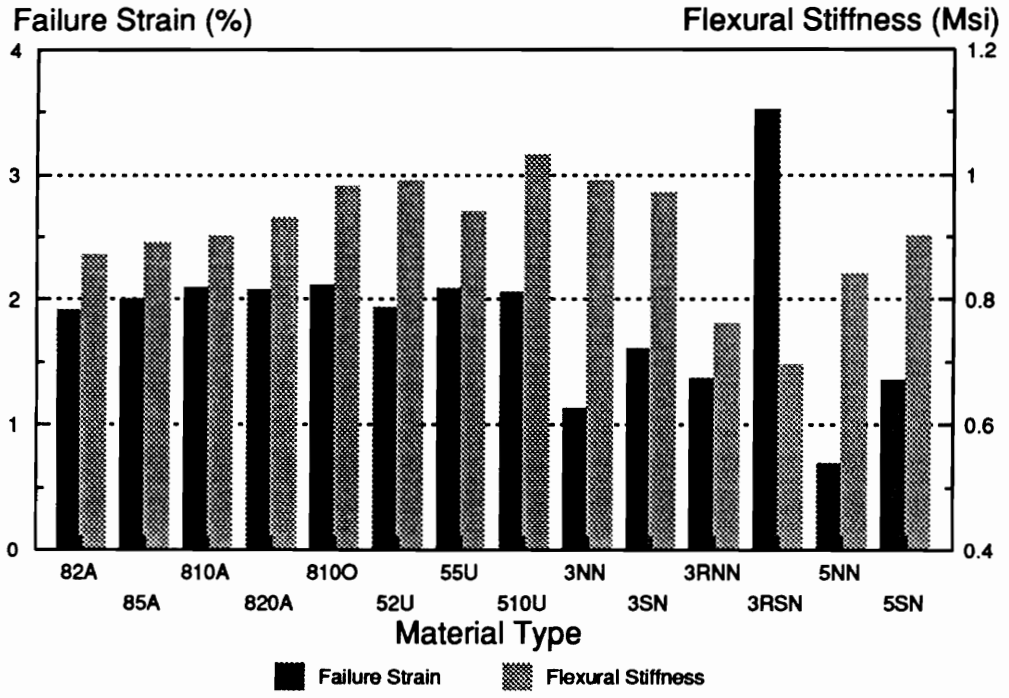

Figure 4. Average Transverse Flexural Failure Strain and Stiffness of the McAir and Northrop Materials.

Table 3. Averaged Data from the Transverse Flexure Testing.

MATERIAL TYPE	DATA PTS.	AVG. STRENGTH (ksi)	COV (%)	AVG. FAILURE STRAIN (%)	COV (%)	BENDING STIFFNESS (Msi)
82A	5	14.68	11	1.915	12	0.87
85A	5	16.19	6	2.001	5	0.89
810A	5	16.75	2	2.085	2	0.90
820A	4	17.00	5	2.071	4	0.93
810O	5	18.21	3	2.110	4	0.98
52U	5	17.56	5	1.934	5	0.99
55U	5	17.38	3	2.080	5	0.94
510U	5	19.70	6	2.050	4	1.03
3NN	5	9.48	9	1.128	9	0.99
3SN	5	13.99	13	1.604	12	0.97
3RNN	5	8.48	10	1.361	8	0.76
3RSN	5	20.89	6	3.514	8	0.70
5NN	5	4.40	5	0.692	5	0.84
5SN	5	10.35	18	1.354	17	0.90

dominated" properties) as the fiber surface treatment goes from the 0% level to as little as the 10% level, yet a quick "leveling off" (and in some instances, decay) as the surface treatment level exceeds 100% [11,14,16,19,59].

Other variables in addition to surface treatment seem to affect to bond strength. The difference in the 810A and 810O strengths leads one to believe that sizing formulations contribute to the strength of the bond. In this case, both fibers have been treated at the 100% level, yet, the "O" sizing appears to produce a composite system whose TFS is 9% higher than the "A" sized system's TFS. The strength results of the 3N and 3RN series clearly indicate that the matrix influences the bond strength. Though the non-surface treated strength of each is relatively close in value, the surface treated strength differs enormously. Bear in mind that the fiber and level of surface treatment are exactly the same in these two systems. Therefore, the matrix material is somehow responsible for the difference in the TFS between the 3SN and 3RSN systems. A first attempt at explaining this behavior might take into account the residual stresses at the interphase due to laminate consolidation. The thermoplastic Radel-X material is processed at 650°F, compared to the cure temperature of 350°F for the ERLX 1901 resin composites. This 300°F difference should certainly translate into a considerable difference in thermal contraction, and as a result, residual stresses. Surely, the Radel-X composites possess a higher compressive residual stress at the interphase. While this line of reasoning may explain the large disparity between the 3SN and 3RSN strengths, it fails to explain why the strength of the non-surface treated specimens are similar. Since other variables are intimately involved, it is imprudent to make any comparisons between the toughened epoxy systems (the McAir materials) and the standard epoxy systems (the 3N and 5N series).

Though it is not surprising that the matrix material strongly influences the interphase strength, it is interesting to note that the fiber type may affect the bond strength. There are two sets of comparisons from which to draw conclusions. The first is between the 3N and 5N series. In this instance, the levels of surface treatment (and, for that matter, the cure conditions) are identical. The "3" fiber enjoys a much higher TFS in both the surface treated and non-surface treated condition. One variable that could possibly explain this difference is fiber volume fraction. The fiber

volume fraction of each test specimen type (unidirectional, cross-plied, and $\pm 45°$) was measured using the IPA technique detailed in the previous chapter. These values are located in Table 4. Adams, *et al.*, after witnessing a decrease of TFS attending an increase in FVF, hypothesized that this may occur due "to increases in stress concentrations in the matrix coincident with increasing fiber volume (closer spacing)" [34]. The results from Table 4 indicate that no large differences in FVF exist between the 3N and 5N series in their unidirectional configuration. At least three distinct mechanisms may contribute in varying extent to this observed behavior:

- The reader is reminded that the "3" fiber is a 7 micron diameter fiber while the "5" fiber is a 5 micron diameter fiber. Therefore, since the FVF of the two series is similar, and the fiber diameter of the "5" fiber is approximately 70% smaller than the "3" fiber, obviously the total amount of interfacial area has increased significantly. If one assumes that the interphase region is the "weak link" in the transverse flexure loading case, then having a larger amount of interfacial area would enhance the potential for weak sites and premature failure.

- Another difference in the two fibers is the fiber tensile modulus. The "3" fiber has a longitudinal stiffness of approximately 35 Msi, while the "5" fiber has a longitudinal stiffness of approximately 50 Msi. It is well established that carbon fibers are anisotropic, therefore, the longitudinal stiffness of the fiber is not necessarily a reliable indication of the value of its transverse stiffness. Nevertheless, if the transverse moduli of the two fibers were to differ, then one could expect a difference in the interfacial response under transverse loading. The argument for this entails the value of the stress concentration around the fiber. The higher the transverse modulus, the more the fiber resembles a rigid inclusion; this encourages high stress concentrations around the fiber at diametrical positions parallel to the applied load. Following this analogy, as the fiber modulus decreases, tending to the modulus of the matrix in the limit, the stress concentration obviously decreases. The problem with this argument is that both fibers — though perhaps having differing moduli — surely possess moduli that are much greater than the fiber. Therefore, it is purely speculative whether variations in the transverse moduli would manifest themselves as proportional variations in stress concentrations, and, ultimately,

Table 4. Fiber Volume Fraction Measurements of the Test Specimens under Investigation.

MATERIAL TYPE	$[0/90]_n$ (%)	$[0]_n$ (%)	$[+45/-45]_n$ (%)
82A	59.7	59.3	58.1
85A	61.8	62.0	61.8
810A	60.2	59.2	62.8
820A	62.7	64.6	62.9
810O	58.7	62.6	60.9
52U	66.1	63.4	63.3
55U	61.8	63.6	61.2
510U	63.3	63.4	64.5
3NN	68.1	63.1	-
3SN	57.9	60.0	-
3RNN	62.3	63.1	-
3RSN	60.7	60.7	-
5NN	59.5	60.8	-
5SN	56.4	59.3	-

transverse strengths. Also, in order to be applicable to the present data, the transverse moduli of the "3" fiber must be less than the transverse moduli of the "5" fiber. No data exists at this time to verify this supposition.

- The difference in fiber moduli can affect the TFS in another manner. In the creation of higher-modulus fibers (like the "5" fiber), it is necessary to process the fibers at higher temperatures and greater tow tensions. This produces a fiber in which the graphitic (and, in general, carbonized) layers possess a greater degree of orientation and larger crystallite sizes. As Robinson [37] describes it: "it is well established that as crystallite size increases, and the ratio of basal plane area to edge area increases, the more severe the conditions required to achieve a given level of interlaminar shear [strength]." In other words, according to Drzal and Rich [37], "the structure of the fiber near the surface and its changes with increasing fiber modulus are a potentially limiting factor in increasing the fiber interfacial strength...." Since the "5" fiber possesses a higher longitudinal modulus, one may assume that the surface of the fiber is inherently less receptive to forming (and maintaining) bonds.

Any or all of these scenarios supports the difference in transverse flexural strengths witnessed between the 8A&O series and the 5U series. For the most part, the 5U series (possessing 7 micron diameter fibers) are stronger than the 8A&O series (possessing 5 micron diameter fibers). What makes this result all the more surprising is that the fibers in the 5U series are unsized. The work of Madhukar and Drzal [10] has shown that the presence of a sizing in addition to the (100%) surface treatment causes the TFS to increase by 51% over the surface treated/unsized laminate. This result would lead one to believe that the "A" sized fibers (8A&O series) would create interphases that would be considerably stronger than the interphases created by unsized fibers (5U series), if the fibers were the same.

The failure strain results displayed in Figure 4 closely mirror the strength results with only a few exceptions. This finding concurs with data of Madhukar and Drzal [10]. In the present case, both the 510U and 820A systems fail to increase their failure strain over the 55U and 810A systems, respectively. Yet, this is accounted for in the flexural stiffness data displayed in Figure 4. Both the

510U and 820A show moderate increases in their flexural stiffness that apparently cause the slight lowering of the failure strain (assuming a strength-based failure criteria).

The flexural stiffness data found in Figure 4 deserves some comment. Madhukar and Drzal indicate that flexural stiffness is a poor indicator of the bond condition, remaining nearly constant for their three systems (non-surface treated/unsized, surface treated/unsized, and surface treated/sized [10]). The Northrop materials provide the best comparison to their material systems. In the present data, the flexural stiffness decreases as the surface treatment is applied in the 3N and 3RN series, while in the 5N series, the flexural stiffness increases noticeably once the surface treatment is applied. One is cautioned from drawing any conclusions from the bending stiffness data, D, since these values are strongly dependent on the thickness, t, of the individual laminate ($D \propto t^3$). In the 8A&O series, the flexural stiffness increases as the level of treatment increases. Notice, too, the large difference between the 810A and the 8100 systems. Yet, the trend of increasing stiffness with increasing surface treatment level breaks down with the 55U system. Again, though it is desirable to speculate about the interphase's contribution to the flexural stiffness, it is likely that geometric parameters affect the results more than material parameters do.

A few key observations are in order. It was interesting to note that failure of the surface treated systems was *always* accompanied by complete fracture of the specimen. Yet, the untreated systems (the 5NN, 3RNN, and 3NN materials) *always* remained intact upon failure. Surely, this simply reflects the release of strain energy. Yet, this truly provided an infallible test for determining whether the specimen was surface treated or not. Finally, because of the imprecise manner in which strain was measured (via the crosshead displacement) and, therefore, the flexural stiffness was obtained, henceforth, only the strength values obtained from the transverse flexure test will be used to characterize the bond condition; i.e., while the failure strain and flexural stiffness data may have added insight, they will no longer be used towards the characterization of the interphase. Therefore, if one simply regards the material series *on the basis of their 100% surface treated material*, then the ordering of TFS, from the weakest to the strongest, is: 5SN, 3SN, 810A, 810O, 510U, and 3RSN.

Prior to leaving this section, one necessary and important question should be asked and answered: Is TFS a good measure of fiber/matrix interphase strength? The test is a global test —

taking an actual laminate and putting it under load – in order to measure a *very* local property (interphase strength). For this to be a true representation of the interphase strength it would be necessary for the failure of the interphase to initiate the laminate's failure, *not* fiber failure or matrix failure. *If* this indeed occurs, and no attempt was made to ascertain this fact in this study, then one could feel fairly confident that this is a good measure. Perhaps some readers will be disturbed that constituent behavior seemed to influence the TFS results. This should not be bothersome, since it is the marriage of the constituents that produces the interphase. Verpoest, *et al.* [18], astutely point out, "as final fracture occurs only when the matrix fails, it can be expected that matrix properties and the matrix volume fraction can play a role." A reasonable objection is that the TFS only characterizes the response of the interphase to *transverse tensile loading*, and, therefore, only measures the tensile strength of the interphase. It could be possible that the *shear* strength of the interphase is a more important variable to the ultimate performance of a laminate than is the tensile strength of the interphase. In an attempt to address this objection, another method of interrogating interphase strength was performed. In this instance, the interphase is loaded both in compression and shear and a strength number is derived. The results from the indentation testing are detailed below.

It is somewhat illuminating to compare the results of the TFS tests to other common measures (inferences) of interfacial "strength". One would suspect TFS to correlate extremely well with transverse tensile strength (TTS); the comparison is made for only the six Northrop systems [39] (since McAir did not publish TTS data) in Figure 5. One is hard-pressed to form a relationship between these data. This assessment is not without precedence, however. Both Madhukar and Drzal [10], and Adams, *et al.* [34], found that while higher TTS corresponded to higher TFS, the relationship was not one-to-one. Adams, *et al.* [34], observed that the TFS results were always higher than the TTS results for the same material system, leading them to postulate that TTS data was flaw sensitive, and, therefore, an inferior method of probing interfacial strength. Only one data point, the 5NN result, deviates from the observation of TFS > TTS. This may be attributable to fluctuations in fiber volume fraction, among other things.

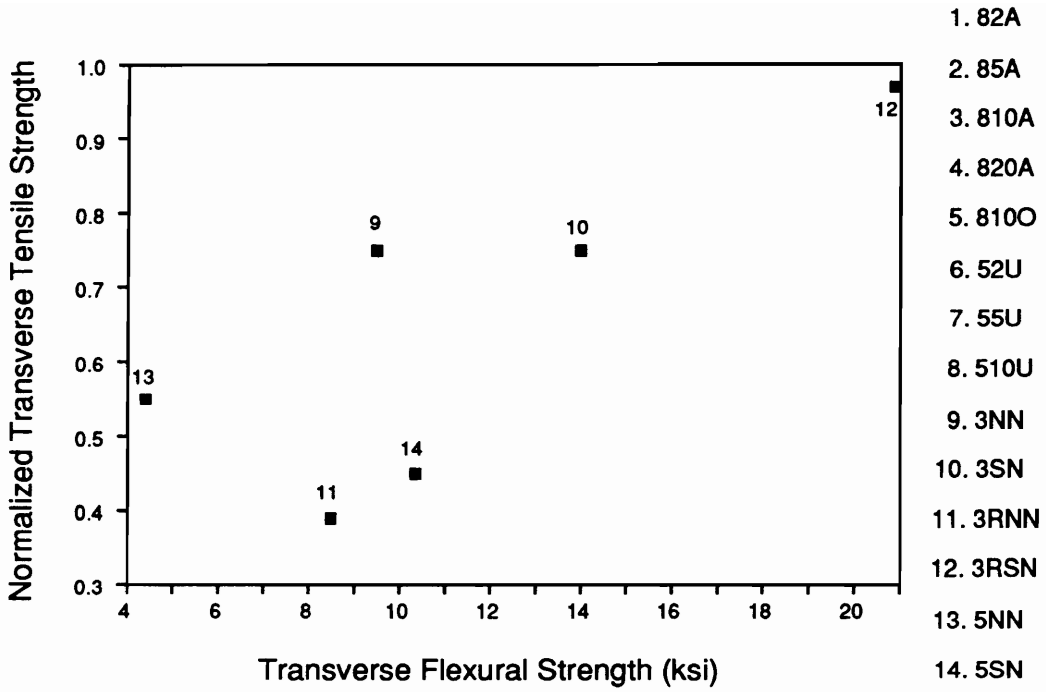

Figure 5. Normalized Transverse Tensile Strength versus Transverse Flexural Strength of the Northrop Materials [39].

Short Beam Shear Strength (SBSS), a very popular method for assessing the fiber/matrix bond strength, is plotted against the TFS results in Figure 6. Clearly, one data point, the 3RSN value, falls *way* off an impressive linear correlation. This small-scale correlation is somewhat surprising since serious criticisms may be levelled at the SBSS test as a method of interrogating interphase performance. Yet, if one routinely expresses confidence in SBSS as a tool for characterizing interfacial strength, then Figure 6 might convince one to adopt the simple and straightforward TFS test.

Indentation Testing

A typical record of load vs. indentation depth for one of the fourteen material systems (in this case, a 55U specimen) is located in Figure 7. The specimen has been loaded from zero pounds to an arbitrary load beyond the transition point — defined as the depth at which the load noticeably drops — and then returned to zero. A measurable amount of residual penetration depth is usually present; in this case the residual depth is approximately 0.0003 inches. Lesko [54] has observed that the quantity of residual depth can often indicate the degree of bond strength; minimal depths often correspond to weak bonding, while large residual depths connote strong bonding. In Figure 7, the transition point is clearly seen to occur near 0.001 inches (or 23 lb.). It has been hypothesized that this point indicates the occurrence of sub-surface damage, especially the formation of kink bands [33]. The response from zero to the transition point is termed the "linear region" though some non-linearity is present. It has been observed that the "linear region" delineates the elastic response of the specimen; i.e., load that is removed prior to reaching the transition point results in an absence of residual penetration depth.

The data that created Figure 7 is inserted into equations (provided in Ref. [33]) that convert load to mean hardness pressure (MHP) and penetration depth to representative strain (d/D). This converted data is plotted and shown in Figure 8. A gap located near the beginning of the plot represents discarded erroneous data. The data in this regime is "noisy", reflecting a lack of sensitivity

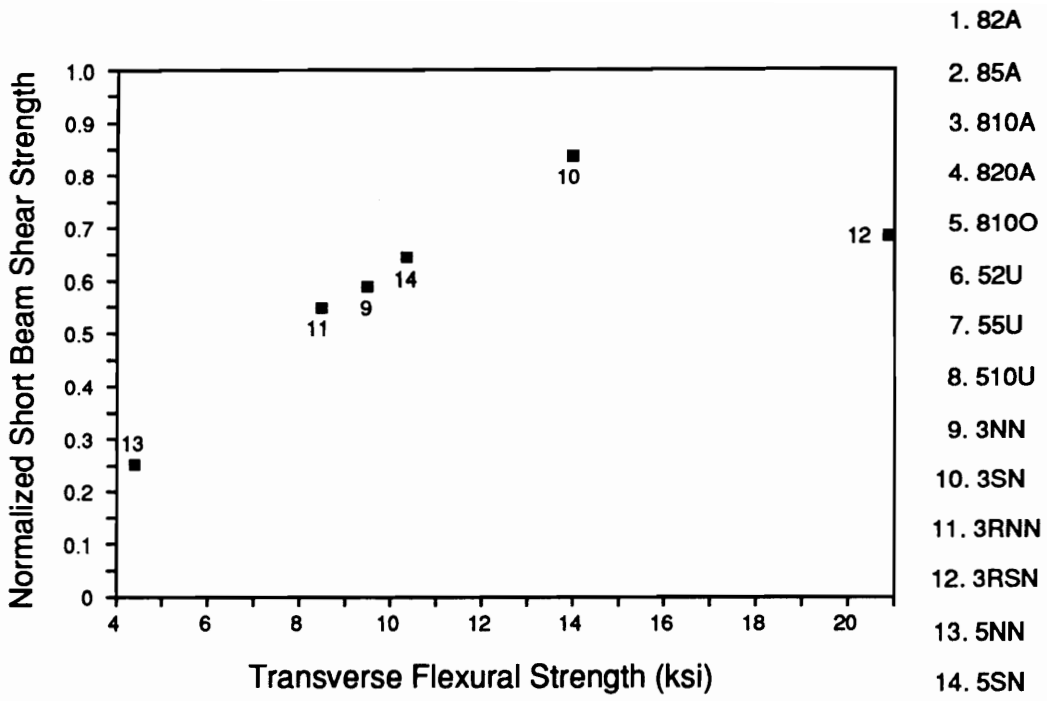

Figure 6. Normalized Short Beam Shear Strength versus Transverse Flexural Strength of the Northrop Materials [39].

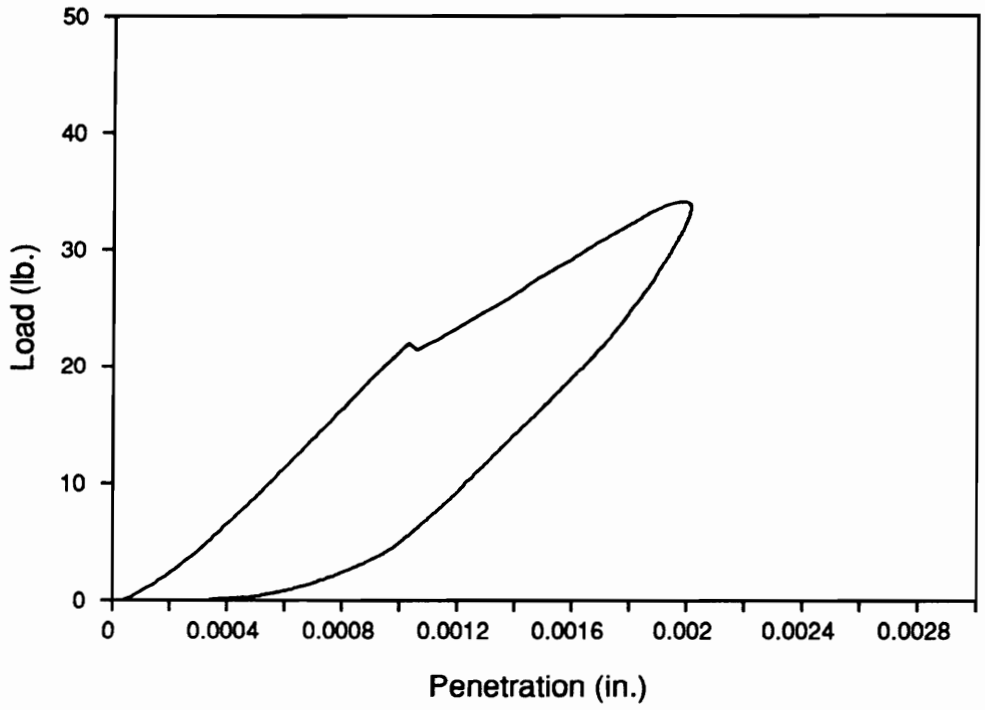

Figure 7. Applied Load versus Indentation Depth on a 55U Specimen using the CBIT.

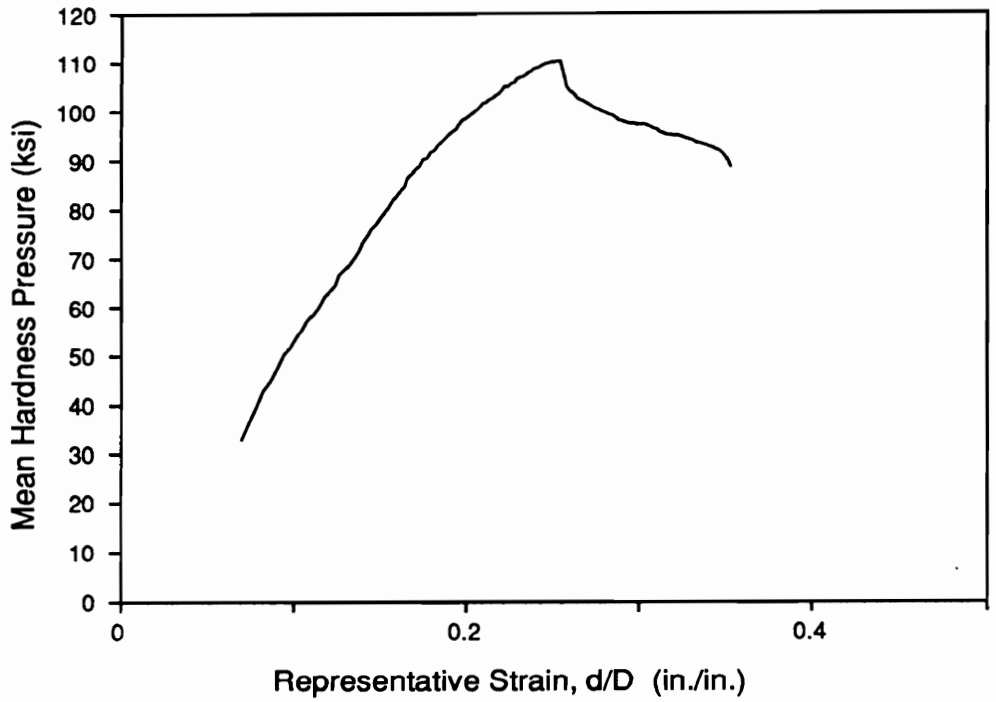

Figure 8. Mean Hardness Pressure versus Representative Strain for a 55U Specimen using the CBIT.

in both load and displacement transducers. The remaining data is subjectively adjusted until the slope of the linear region appears to go through the origin. This is necessary because an arbitrary amount of displacement may occur prior to making contact with the specimen. The Maximum Mean Hardness Pressure (MMHP) is simply defined as the maximum pressure that is achieved during the penetration; in Figure 8 this value is approximately 113 ksi. The representative strain value corresponding to the MMHP is recorded as a value reflecting "the strain to failure". It is these two values (MMHP and d/D at MMHP) that are characterized using a Weibull distribution. After ascertaining that a goodness-of-fit has been achieved using this distribution, the mean value and the standard deviation of the distribution is quoted for each material system. A schematic of the mean MMHP and d/D (at the MMHP) for all fourteen material systems is located in Figure 9. The actual mean values, along with the coefficients of variation, are displayed in Table 5.

Examining the response of the 8A&O material in Figure 9, there is no clear trend apparent in the data. At first, it seems that the MMHP values decreases as a function of surface treatment level, since the MMHP slopes down from the 82A specimen to the 810A specimen and remains nearly constant for the 810O specimen. The 820A specimen is remarkably uncharacteristic of the other systems in the series, however. There is no obvious reason why the response of this system is so different. It has been generally observed by Lesko [54] that the MMHP is a sensitive indicator of bond strength; i.e., the higher the MMHP, the stronger the interphase. One *possible* explanation — and this will serve as a guiding hypothesis throughout the interpretation of these results — is that the MMHP reflects a *shear* phenomena. Carman, *et al.* [53], have approximated the actual stress field of an indented half-space using a cellular-model approach. The results from this model indicate a substantial shear region below the surface of the indentation and less than a ball radius away from the center of the indentation. Sub-surface damage has been observed to occur in and near this region [54]. Given these observations, it is possible that the MMHP best represents the material's resistance to shear failure. The data discussed below can only provide proof of this hypothesis through inference. Clearly there is a need to further investigate the mechanisms that control the indentation response.

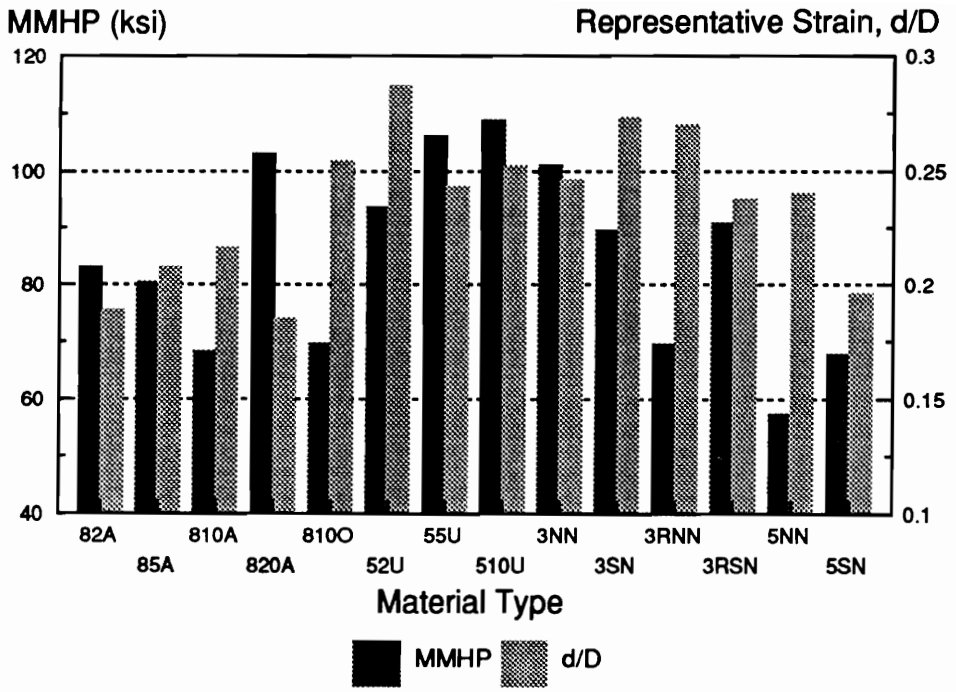

Figure 9. Average Maximum Mean Hardness Pressure and Representative Strain of the McAir and Northrop Materials.

Table 5. Maximum Mean Hardness Pressure and Representative Strain Data from the McAir and Northrop Materials.

MATERIAL TYPE	MMHP (ksi)	COV (%)	d/D	COV (%)
82A	83.2	14.9	0.189	4.6
85A	80.4	9.5	0.208	7.2
810A	68.4	12.9	0.216	8.3
820A	102.8	10.5	0.185	3.5
810O	69.6	7.3	0.254	4.3
52U	93.6	12.7	0.287	6.6
55U	106.1	17.8	0.243	9.3
510U	108.8	20.9	0.252	8.5
3NN	100.9	5.9	0.246	7.9
3SN	89.6	8.9	0.273	9.0
3RNN	69.4	11.4	0.270	5.4
3RSN	90.8	11.1	0.237	7.0
5NN	57.3	6.6	0.240	8.4
5SN	67.8	9.1	0.196	8.3

Returning to the discussion of the 8A&O response, the first three surface treatment levels display a continual rise in the representative strain (d/D at MMHP). The 820A specimen, again, deviates considerably from the response of the other systems. Lesko [54] has observed that, in general, low d/D values accompanied by high MMHP values often suggest a "brittle" quality of the material, with high values of d/D and low values of MMHP implying a "ductile" nature. This behavior has been observed in the fracture surfaces of notched specimens failed in tension (discussed in detail further below — see Figures 14 and 15). Obviously, the 810O material reveals a "compliant" response, deforming excessively under very moderate load levels.

The three 5U series materials ascend in MMHP as the level of surface treatment increases, in stark contrast to the 8A&O systems possessing the same level of treatment. If one ascribes to the notion of strong bonding/higher MMHP, these results are more satisfying. It should be noted that the differences between the systems are not subtle, which could be considered a virtue of this method, provided it does truly characterize the bond condition. The d/D response of these three materials does not admit to a definite trend, though it is obvious that these systems "give" much more than the 8A&O systems do; perhaps this reflects the stiffness of the laminate, since rule-of-mixtures would predict the composites containing the 32 Msi fibers (the 5U series) to be more compliant than those possessing the 45 Msi fibers (the 8A&O series).

If the indentation test *is* sensitive to the bond condition, then the responses from the Northrop material systems should indicate this quality (since distinct differences were seen in the TFS of these systems). The 3N series is the only Northrop series *not to show* an increase in MMHP as the level of surface treatment was increased from 0% to 100%. The MMHP and d/D values of the 3NN material seemed so inconsistent with the other Northrop data that a new indentation sample was created and re-tested, only to corroborate the previous data. With the exception of the 3NN specimen, though, the other Northrop systems reveal a larger d/D in the untreated material than in the treated material. Combining this observation with the MMHP trends, the untreated systems should appear more ductile than the treated systems. This presumption will be verified by the data discussed in a later section.

It is only fair to ask the same question of the indentation test as was asked of the transverse flexural strength test: Is the indentation test (or, more precisely, the Continuous Ball Indentation Test) a good measure of the fiber/matrix interphase strength? Many factors indicate that it *should* be a good test method for interrogating the bond strength. It tests real laminates (instead of model systems), it introduces load and monitors deflection at a scale approaching the scale of the interphase (though not as efficiently as single fiber indentation tests do [60]), while providing a natural means to "smear out" highly local incongruities by testing over a large number of fibers all at once. The drawback — as in the case of the transverse flexure test — is one's ability to trace a failure "strength" back to the interphase. In the flexure test, it was necessary to assume that the interphase formed the "weak link" of the system, and that failure of this link equated to failure of the system. The path from the interphase strength to the failure strength is not as straightforward in the CBIT. The indentation clearly produces a stress state that is compression- and shear-dominated. Hence, material failure will occur as a result of either of these stresses, or, more likely, as a result of the combination of these stresses. It can be unequivocally stated that shear failure is intimately related to compressive failure; the analysis of unidirectional (0°) compressive strength is *frequently* reduced to an analysis of *shear support* provided to the load-carrying fibers. Batdorf and Ko [61] have shown that the compressive strength of a composite is lowered tremendously once shear loading is also introduced. So the question remains: does the MMHP reflect a shear failure or a compression failure or both? Though Lesko has observed kink band failures below the surface of his indentation specimens, it is unknown whether interphase shear failure instigated these kink bands. If one combines the findings of Batdorf and Ko, along with the approximated indentation stress state of Carman, *et al.* [53], it seems quite reasonable to assume that shear *is* responsible for sub-surface failures, and, therefore, the Maximum Mean Hardness Pressure value. If the CBIT *does* represent the *shear strength* of the interphase (as opposed to the transverse strength measured during transverse flexure testing), this would be an extremely valuable characterization tool. The results in Figure 9 provide very little verification of the MMHP/shear failure relationship; this is not to say that the data *disproves* the hypothesis, it simply is unable to prove it.

The transverse flexural strength (TFS) of each material system is displayed next to the material's Maximum Mean Hardness Pressure (MMHP) in Figure 10. A different viewpoint for these two data sets is provided in Figure 11, where MMHP is plotted versus TFS. In general, it appears that MMHP increases as TFS increases, yet, no obvious relationship between the two measures is seen. Several systems reveal widely different responses. While the TFS for the 3NN material is third from the weakest, its MMHP is fourth from the strongest. The 810O material, on the other hand, has the third largest TFS, yet its MMHP is one of the lowest. This would suggest that the failure phenomena producing these "strengths" is entirely different. It should be re-affirmed, however, that as one strength increases, it is generally observed that the other strength increases also.

The Maximum Mean Hardness Pressure is plotted against the normalized $\pm 45°$ tensile strength — a common measure of shear performance — in Figure 12. With the exception of a few points, there seems to be a nearly linear relationship between these two measures. This would normally lend considerable credence to the claim that MMHP characterizes the shear behavior of the composite system (it will be shown later, however, that the $\pm 45°$ tensile strength correlates remarkably well with the transverse flexure strength — see Figure 23). Figure 12 was partly responsible for the indentation re-testing that was performed on the 3NN material system. Surprisingly, the two average MMHP values were nearly the same in each trial.

Quasi-static Strength and Stiffness Testing

Notched Cross-plied Specimens

The notched strength tests fulfilled two purposes: first, it was necessary to measure the tensile and compressive strengths in order to determine the applied fatigue load levels. Secondly, one of

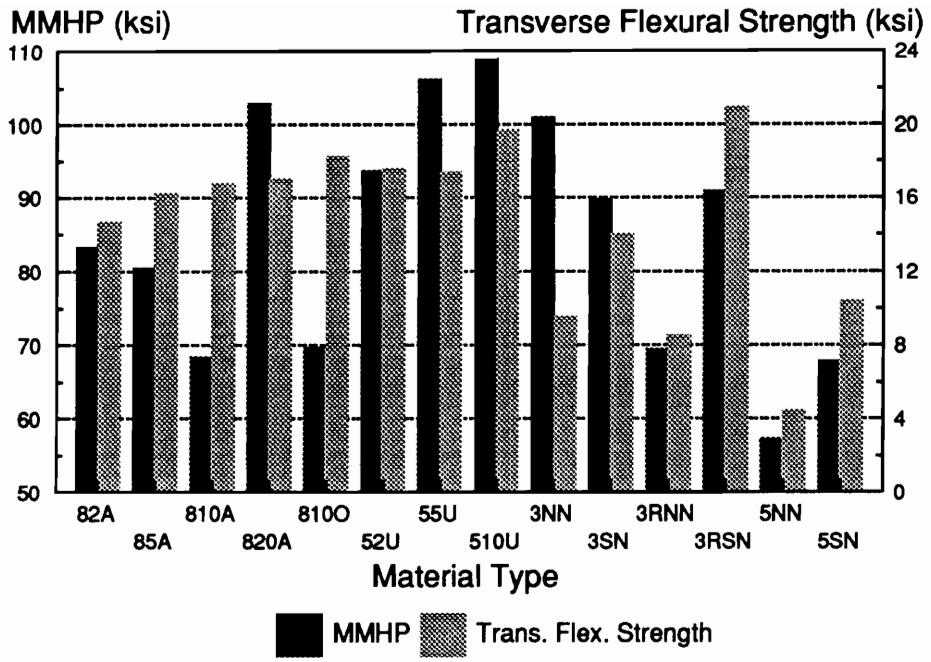

Figure 10. Maximum Mean Hardness Pressure and Transverse Flexural Strength of the McAir and Northrop Materials.

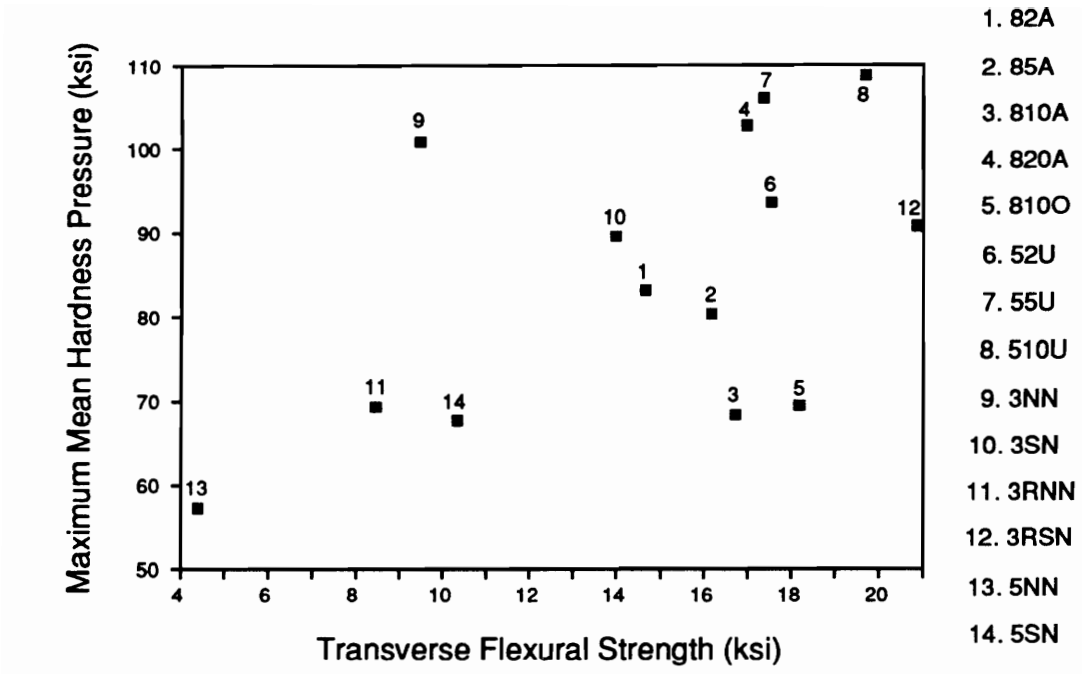

Figure 11. Maximum Mean Hardness Pressure versus Transverse Flexural Strength of the McAir and Northrop Materials.

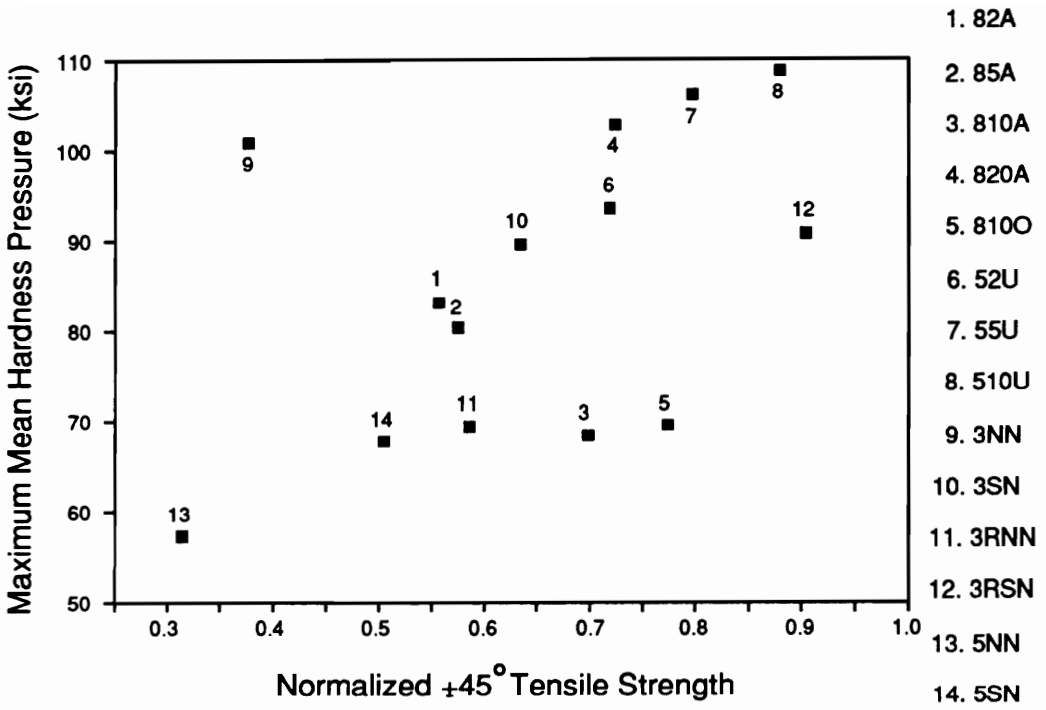

Figure 12. Maximum Mean Hardness Pressure versus Normalized ±45° Tensile Strength of the McAir & Northrop Materials [37,39].

the objectives of this research was to investigate the role of the interphase in the static strength of an engineering laminate; i.e., it was highly relevant to study how bond strength influenced the damage mechanisms, which, in turn, dictated the strength of these center-holed, cross-plied specimens.

Strength Results

The notched tensile and compressive *gross-section* strengths (found by dividing the ultimate load by the average cross-sectional area located away from the notch) of the McAir and Northrop material systems are displayed in Figure 13. Owing to the wealth of data in Figure 13, the tensile strength of the systems will be discussed prior to the compressive strength.

Tensile Strength: The most striking aspect of the 8A&O series data is the large variability in the strength values, ranging from 71.9 ksi for the 820A system to 91.7 ksi for the 85A system. Contemporary thinking on notched strength focuses on two parameters: unnotched strength and the hole-to-width ratio. Since the specimen geometry remains a constant, the first explanation for the differences in the strength would naturally lead to the variability in the unnotched strength of the respective systems. The ordering of the unnotched data [37] follows the ordering the notched data *exactly*; i.e., the strength values read 820A < 810A < 82A < 810O < 85A. This led the author to suspect that the two data set correlated with one another. This suspicion proved to be true for four of the five points; the notched strength of the 820A specimen was considerably less than the unnotched data would have predicted. This leads one to conclude that the material was flawed, or, that another mechanism — likely the hole effect — enters the problem.

Given the condition of equal unnotched strengths, the general claim is made that the stronger the bonding, the weaker the material in the notched condition. All tensile (and compressive specimens, for that matter) specimens tested in the notched condition, failed through the center hole. This hole concentrates the stress around the hole, especially the stress applied along the longitudinal

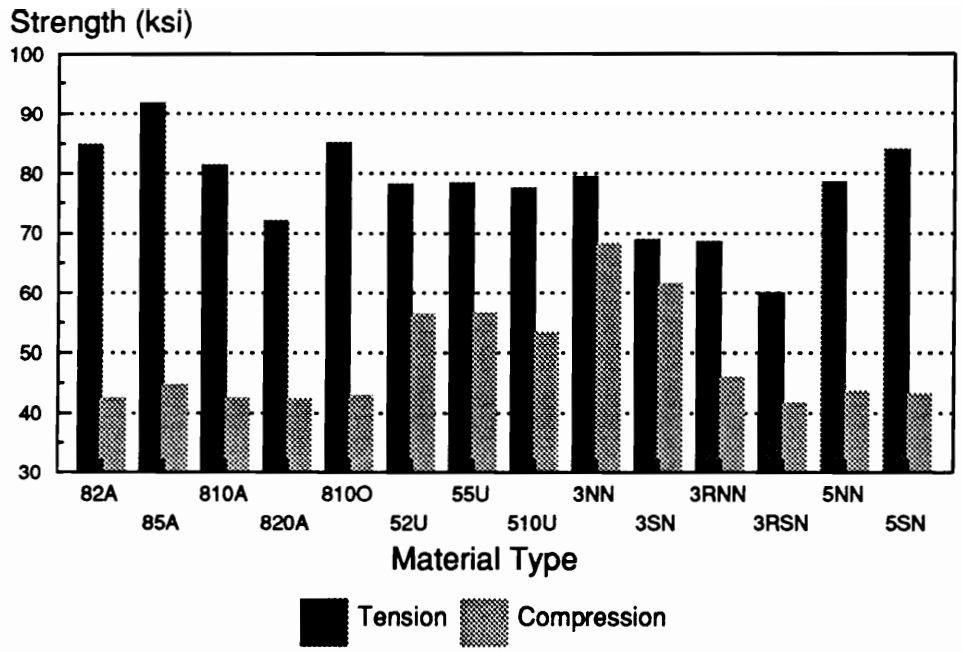

Figure 13. Average Gross-section Tensile and Compressive Strengths of the Notched Cross-plied McAir and Northrop Materials.

axis of the specimen. This stress, σ_{xx}, peaks along the longitudinal lines tangent to the hole and decays as one moves away from the hole in a direction perpendicular to the applied load. It is this large stress concentration that drives the failure of the notched laminate. Fibers near the hole boundary progressively fail, creating a local stress concentration (that becomes superposed with the global stress concentration) that quickly enervates the laminate. In addition to a concentration of σ_{xx} stresses, there exists formidable shear stresses, τ_{xy}, along the longitudinal lines tangent to the hole. If 0° plies exist in the laminate, they will usually fail in shear along the hole boundary prior to the occurrence of axial fiber failure. This failure, called "longitudinal splitting", serves to "blunt" the global stress concentration caused by the hole. In the extreme case, this causes a center-holed specimen to behave as a specimen possessing two isolated and symmetric ligaments (perfect notch insensitivity). Kress and Stinchcomb [62], Wagnecz [63], and Kortschot and Beaumont [64] (among a multitude of others) have shown that by encouraging these splits, one can lower the stress global stress concentration and allow the specimen to endure much greater applied stresses prior to laminate failure. Kortschot and Beaumont [64] claim that the length of these splits and the intrinsic strength of the unnotched material are the *only* variables that enter into the notched strength equation. Therefore, it follows to reason that by decreasing the bond strength (and, in turn, encouraging longitudinal splitting) the notched strength will increase *provided that the unnotched strength is not diminished as a result of weak bonding*. This is the justification of the general claim that strong bonding lowers notched tensile strength. In the next chapter, "Modelling Considerations," the foundation for introducing interphase strength into the equations of notched strength will be put into place.

If the MMHP values from the indentation tests are accepted as a reasonable characterization of the *shear* strength of the interphase, then those results help explain, at the very least, the unusually low notched strength for the 820A specimens. According to Figure 9, the MMHP of the 820A material is 50% greater than 810A's value. According to the above reasoning, the higher the shear strength of the 0° lamina, the greater the resistance to form longitudinal splits, and, subsequently, the weaker the notched specimen. If the specimen can exploit its weak bonding by providing avenues for damage to occur (and strain energy to be dissipated), then it can endure more

load to failure. Proof of this is seen in Figures 14 and 15. Figure 14 is a photograph of a failed 82A tensile specimen. Notice the fairly extensive fiber pull-out, the numerous longitudinal splits, and the delaminated regions revealing the first sub-surface 90° ply. Compare Figure 14 with Figure 15, a photograph of a failed 820A tensile specimen. In this case, no fiber pull-out is apparent and no delaminated regions are seen. One should be reminded that these two laminates possess the *same fiber and matrix*. On just the basis of this, many would be satisfied in believing that these two systems are really the same material. Clearly, this is not the case.

The average notched tensile strength values for the 5U series are remarkable in their *lack* of variability. The values are nearly indistinguishable if one accounts for experimental spread. The *unnotched* data [37] orders itself as 52U < 510U < 55U, with an increase of only 5% from the weakest to the strongest. Thus, in this instance, unnotched strength seems to be a strong indicator of notched tensile strength. Were it not for the 820A specimen, the ratio of the notched strength over the unnotched strength was, on average, 3% greater in the 8A&O series than in the 5U series. Apparently, then, the 5U series possesses a slightly greater notch sensitivity than does the 8A&O series, and, therefore, utilizing previous reasoning, possess greater interfacial shear strength. The MMHP results reinforce this notion.

An interesting fact to consider is that the "8" fiber represents a *fiber* tensile strength of 850 ksi compared to the 550 ksi strength listed for the "5" fiber. It is apparent that improvement in fiber strength has not translated into an improvement in the unnotched (and notched) cross-ply laminate strength.

Both series containing the "3" fiber exhibit a *drop* in notched cross-plied tensile strength when going from the untreated to the surface treated condition. Yet, in this particular instance, the *unnotched* cross-plied strength [40] *increases* with the application of the surface treatment. These data are compelling indications that bonding plays an important role in the notched tensile strength of cross-plied laminates. The MMHP data fails to verify these trends in the case of the 3N series, however. The MMHP value for the 3NN specimen is noticeably higher than its surface treated counterpart.

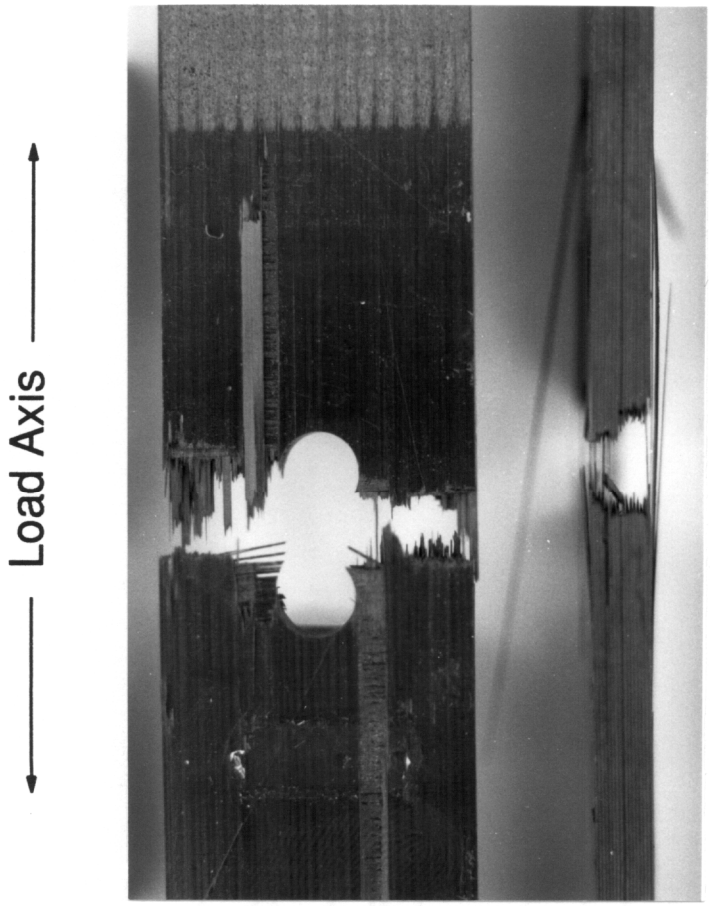

Figure 14. Photograph of Failed 82A Tensile Specimens.

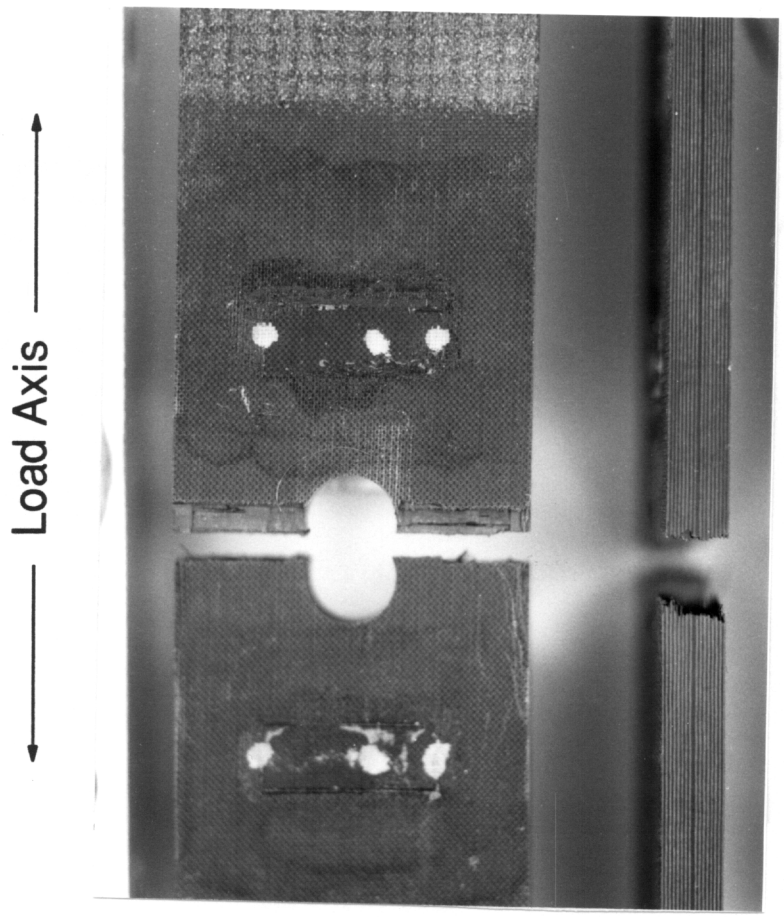

Figure 15. Photograph of Failed 820A Tensile Specimens.

The 3RN series indentation data confirm the high MMHP/low notched strength trend seen in all the systems thus far. It is also important to recognize that the 3RNN specimens were only as strong as the 3SN material, leading one to infer that the thermoplastic resin forms stronger bonds than the epoxy resin. Unfortunately, again, the MMHP values to not corroborate this claim, yet, one must be mindful that the indentation results may be sensitive to matrix properties in addition to interphase properties. Since the matrix changes from an epoxy to a compliant thermoplastic, it is possible that the indentation response is altered accordingly. This may not be surprising since, by simply changing the matrix (and *keeping the fibers the same*), the *unnotched* cross-plied tensile strength (a "fiber-dominated" property) of the 3RSN system is 16% less than the 3SN system [40].

This same argument applies to the comparison between the 3SN and 510U notched and unnotched cross-plied tensile strength. The "3" fiber is reported to possess a strength of 650 ksi while the "5" McAir fiber displays a strength of 550 ksi. Yet, perhaps due to the different binding matrices, the unnotched tensile strength of the 510U system exceeds that of the 3SN system by 13%.

Perhaps the most overt deviation from the "weak bonding/strong notched strength" hypothesis is the 5N series. The bonding in the 5NN system is clearly the weakest of any the material systems under investigation; TFS results (Figure 3) and MMHP results (Figure 9) concur with this assessment. Yet, the 5NN specimens possess a noticeably weaker notched tensile strength than their 5SN counterparts. It may be that the preponderance of other failure modes (90° cracking, gross delamination, 0° splitting, etc.) tend to weaken the material and change the failure mode from one driven solely by the presence of the global stress concentration. Figure 16 captures the fractured surfaces of two 5NN tensile specimens. An *extreme* amount of "critical" and "sub-critical" damage has attended the final failure. The long pull-out lengths are especially obvious. The fractured surfaces of failed 5SN specimens are shown in Figure 17. In these 5SN specimens, many of the same damage modes are present, but not to the same degree or extent as in the 5NN specimens.

It is interesting to note that the notched cross-plied tensile 5SN specimen is 22% stronger than the 3SN specimen, despite only showing an increase of 5% over 3SN's *unnotched* cross-plied tensile

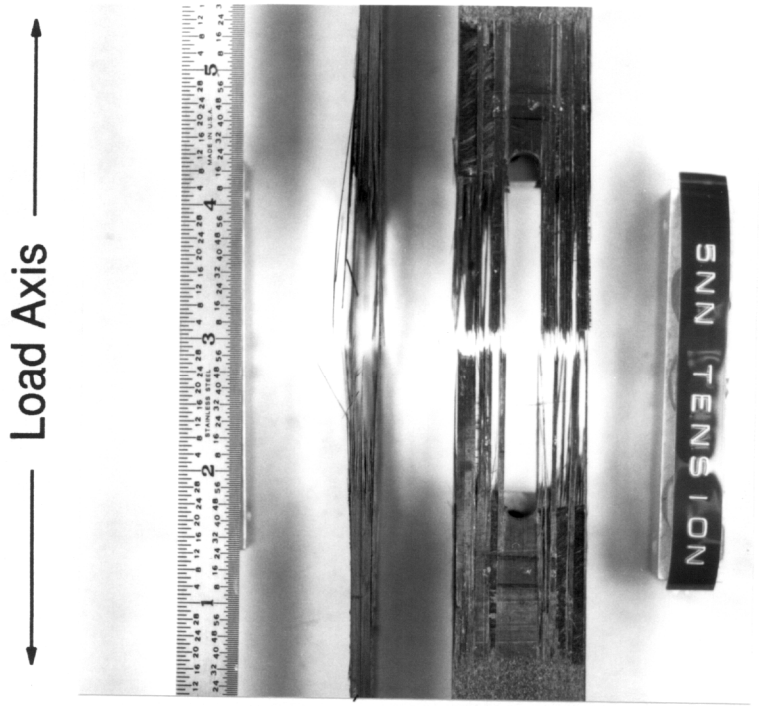

Figure 16. Photograph of Failed 5NN Tensile Specimens.

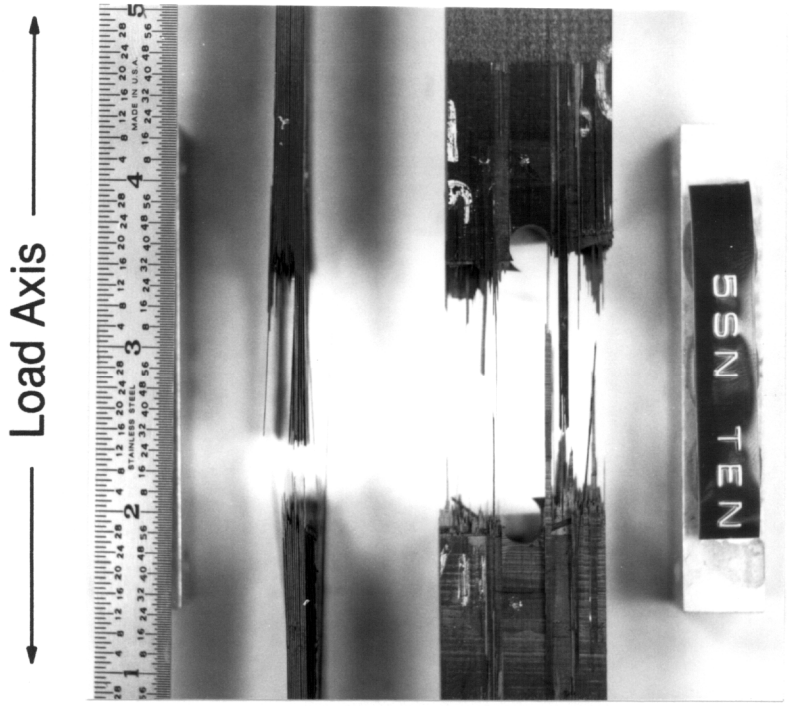

Figure 17. Photograph of Failed 5SN Tensile Specimens.

strength [40]. The MMHP of the 3SN material is 32% greater than the 5SN material. Surely bonding is somewhat responsible for this jump in comparative notched tensile strength.

Compressive Strength: The reason the compressive results were not separated from the tensile results in Figure 13 is so the reader could get the immediate sense of how much weaker the material was in compression than in tension. In the 85A material, for instance, the average compressive strength was less than *50%* of the tensile strength. The first thought that may enter one's mind is that the compressive values did not correlate to material properties, i.e., they were more a measure of Euler buckling than of material strength. Each specimen tested was 32 plies in thickness and was positioned in the grips such that only 2″ of material were ungripped. Failure analysis did not reveal bending-type failures; in most instances the failure surfaces resembled pure crushing. Therefore, this does not seem to be a plausible reason to explain the unusually low compressive strengths.

Whereas the tensile response of the 8A&O material was highlighted by the large variability in the strength values, the compressive response is remarkable in its repeatability. With the possible exception of the 85A material, by taking into account statistical spread, the compressive strengths of the remaining 8A&O specimens were indistinguishable. If the tensile data discussed above had convinced one that bonding played an important role in notched strength, then this data may be perceived as counter-intuitive. Yet, one should recall *how* bonding enters the notched tensile strength scenario. In the tensile test, the lack of strong bonding enables longitudinal splits to grow relatively easily, thus helping to reduce the global notch concentration, and allow the specimen to endure higher applied tensile loads until local fiber fracture initiates and proceeds to failure. It is not to be expected that bonding will enter the compressive scenario in the same fashion, since tensile and compressive failures rely on different damage sequences. This is substantiated in the micromechanical models used to predict these respective strengths (see the following chapter). Tension models rely on careful characterization of the fiber strength, and must account for local stress concentrations caused by broken fibers [65-67]. Compression models focus primarily on analyzing the *support* given to the fibers by the surrounding matrix system [65]. In models of

unidirectional (0°) tensile strength, the interphase enters through two competing effects; the determination of the "bundle strength" of the fiber, and the manner in which stress concentrations caused by broken fibers are perceived by neighboring fibers [68]. In models of unidirectional compressive strength, the interphase naturally enters those models that incorporate initial fiber misalignment. As the misaligned fibers increase their local curvature due to the applied compressive load, support failure is assumed to occur by shear in the matrix, thus failing to support the fiber and precipitating failure, or fiber failure is assumed to occur at the regions of maximum bending stress. A lack of bonding fails to support the fiber in its role as a load-carrying column and the fiber buckles. The gross deformations associated with this buckling are transferred to neighboring fibers causing a buckling "domino effect" that is manifested into a "kink band". So, while it will be necessary to determine if and how bonding enters notched compressive strength, it is *not* altogether discouraging — and should be expected — that bonding does *not* affect notched compressive strength the way it does notched tensile strength.

The strength results from the 5U series concur with the 8A&O results in regard to a lack of strength variability as a function of bond strength. Again, it can be concluded that the strength results among the systems possessing a gradation of surface treatment levels were largely indistinguishable. The 5U compressive strength values do differ from the 8A&O values, however, in terms of their absolute value. On the average, the 5U series (550 ksi *tensile* fiber strength) displays a 29% larger notched cross-plied compressive strength than 8A&O series (850 ksi *tensile* fiber strength). The *unnotched* cross-plied compressive strength [37,40] of the 5U series is, on the average, 36% larger than its 8A&O counterparts. Neglecting any effect due to bonding (which, as of yet, none has been indicated), there are at least two reasons why the 5U systems are stronger than the 8A&O systems in compression: fiber diameter and intrinsic fiber strength. The larger the cross-section of a (round) fiber is, the larger its moment of inertia, I, is ($I \propto r^4$, where r is the radius of the fiber), and, hence, its bending stiffness. This increase in bending stiffness tends to resist bending and buckling. This realization has lead to a very intense study of proposed fiber shapes that exploit high moment of inertia geometries [38,69]. Therefore, it is possible that the 7 micron diameter of the 5U fibers plays a major role in ensuring higher compressive loads than does the 5 micron fiber in

the 8A&O systems. Another variable to consider is intrinsic fiber compressive strength. It is well established that improvements in fiber moduli are nearly always at the expense of the fiber's compressive strength. Increases in fiber modulus come about by aligning the orientation of the graphitic crystallites. Yet, this is not necessarily the culprit responsible for the low fiber compressive strength, as indicated by Robinson [37]. Instead, he claims, crystallite *size* — which also increases during the process of making a higher modulus fiber — may be the cause of low compressive strength fibers. The fact of the matter remains that fiber diameter and intrinsic fiber strength may be the key variables in the explanation of the improvement in compressive performance in going from the 8A&O series to the 5U series.

The 3N and 3RN series results are the first to possibly indicate a bonding/strength relationship. Even so, the differences in 0% surface treatment strength and 100% surface treatment strength are not very dramatic; the 3NN notched compressive strength is 11% greater than the 3SN strength, while the 3RNN compressive strength is 10% greater than the 3RSN strength. Perhaps the comparison between the strengths associated with the respective matrix systems is more important than the comparison between the strengths associated with the respective surface treatment levels. In this instance, the fiber compressive strength and fiber size remain fixed (since the fiber is identical in the two systems), allowing one to investigate the matrix's role in the compressive response. Comparing the standard surface treatment levels, the system possessing the epoxy matrix (3SN) enjoys an increase in notched cross-plied compressive strength of 48%, an increase in unnotched cross-plied compressive strength of *79%*[40], and an increase in unidirectional compressive strength of 65% over its thermoplastic (3RSN) counterpart [39]. Though the shear moduli of the respective matrix systems were not available to the author, the axial moduli were. The ERLX 1901 epoxy maintains an axial stiffness that is 30% greater than the axial stiffness of the Radel-X thermoplastic [70]. If one makes the broad assumption that shear stiffness of the isotropic matrix scales with the axial stiffness (i.e., the Poisson's ratio of the two systems are comparative), then the respective shear stiffness of each system could be so ordered. Obviously, other factors must be taken into account to explain the differences in compressive strength between the epoxy and thermoplastic systems.

These differences may come into play when one compares 3SN strength with 510U strength. In this case, the matrix systems differ (an epoxy and a toughened epoxy, respectively), yet, so do the fiber *shapes*. All of the Northrop systems contain Thornel fibers which assume a "kidney bean" shape due to their fabrication conditions. Though both fibers are reported to be 7 micron fibers, it is unknown to the author if this number represents the largest dimension on the kidney-bean shaped fiber. Thus, fiber moment of inertia may affect the differences in performance, yet, these differences (in shape) should not be expected to exhibit the same magnitude of difference as seen between the 7 and 5 micron fibers. Likely, the disparity in shear moduli between these two systems plays some part in this, yet, the differences in axial modulus between the toughened epoxy and the standard epoxy are approximately 1% [29,70]. If one maintains that higher-modulus fibers inherently possess lower compressive strengths (as addressed above), then one might conclude that the intrinsic strength of the 35 Msi Thornel ("3") fiber is less than the 32 Msi ("5") fiber. If this were, in fact, true (and the author has no data to support or deny its veracity), then one would be forced to conclude that laminate compressive strength it not as strong a function of intrinsic fiber strength as it is of other variables.

The 5N series upholds the finding that notched cross-plied compressive strength is not *highly* dependent on bond strength. The strength value of each system is equivalent, within statistical spread. It is interesting to compare the absolute strength of the 5N series with the other series' strengths. The strength of the 5N systems is dramatically less than the strengths in the 3N series. This may be attributable to the fact that the "5" Thornel fiber is a 5 micron fiber while the "3" Thornel fiber is a 7 micron fiber. With this in mind, it is curious to find that the 5N series strength is virtually equivalent to the 8A&O series strength, despite the fact that each series involves a different binding matrix. It will be necessary to introduce many of the micromechanical variables mentioned in this section into a model to attempt to predict compressive strength. Once such a model is in place, one could perform sensitivity studies to assess the role of these variables on notched cross-ply compressive strength.

Stiffness Results

In this section the value called "stiffness" is not a true material stiffness. It will be more appropriate to replace it with the word "modulus", since the number reported is simply the stress applied divided by the strain measured *across the center hole* of each specimen. Therefore, this measure incorporates both material and geometric responses rather than purely material responses. Since the geometry is kept constant among all specimens, this measure will indicate how the central ligament (that region above and below the center hole) displaces once a stress is applied. This amount of displacement will clearly reflect the intrinsic material axial stiffness, yet, it will also monitor how easily the hole is permitted to deform, which is obviously a function of a number of the material's stiffness properties. It will be interesting to see if the different surface treatment/sizing combinations alter the measured moduli of the materials under investigation.

Tensile Modulus: The tensile and compressive moduli data (both as-measured and normalized with respect to fiber volume fraction) from the fourteen material systems are found in Figure 18. Examining the 8A&O series data, it is apparent that the modulus values are a positive function of surface treatment level; i.e., as the level of surface treatment increases the modulus value increases (yet, in considering the normalized values, a "leveling off" or slight decay occurs after the 100% surface treatment is reached). One is tempted to explain this behavior by coupling the stiffness and strength of the interphase region. In other words, if the bonding is weak, premature failure will occur in the 90° plies and in high stress regions (under the influence of the global stress concentration). This "subcritical" damage results in a lack of specimen integrity and increases the specimen's compliance.

The *net-section* stress vs. strain (measured across the hole) response of two systems in the 8A&O series is found in Figure 19. It is seen that the two sets of curves diverge at approximately 1000 $\mu\varepsilon$, with the 820A specimens possessing a higher slope. By approximately 4000 $\mu\varepsilon$ one can see a distinct "glitch" in all four responses; this may be either 90° failure or longitudinal splitting at the hole boundary. Both curves reveal obvious non-linearity after 4000 $\mu\varepsilon$; it is arguable if non-linearity

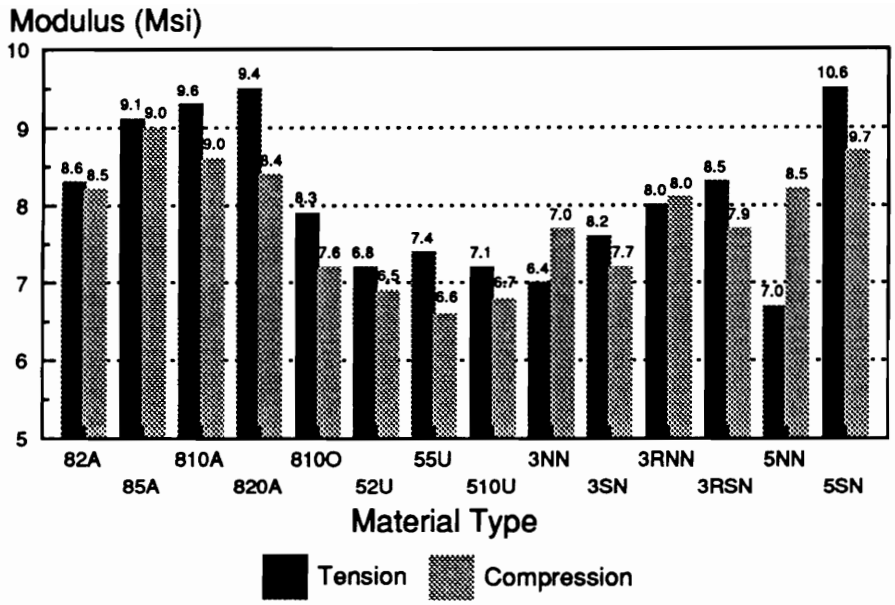

Column height represents measured value

Numbers above column represent values adjusted by fiber volume fraction

Figure 18. Average Gross-section Tensile and Compressive Moduli of the Notched Cross-plied McAir and Northrop Materials.

occurs prior to this point. In all truthfulness, because the linear region is ill-defined, and because subcritical damage can occur at low loads due to the presence of the global stress concentration, the modulus data shown in Figure 18 may simply reflect the specimens proclivity towards inelastic response.

Another possible explanation could involve the elastic properties of the interphase region itself. Given that interphase regions are distinct phases with the potential of possessing both tensorial strength and stiffness unique to their region, it is conceivable that by altering the level of surface treatment and adding a fiber sizing, one is altering the axial modulus (among others) of this third phase. If this were the case, then one would expect to see the unidirectional unnotched tensile stiffness, E_{xx}, to change as a function of the surface treatment level. No distinguishable change is seen in the McAir data, with the 82A, 85A, 810A, and 820A values (normalized to equal amounts of fiber volume fraction) deviating from one another by less than 1% [37].

It appears from Figure 18 that sizing formulation is a major influence on the notched cross-plied tensile modulus. In this case, however, this trend also appears in the value for the unnotched unidirectional tensile stiffness, E_{xx}. The normalized stiffness of the *unnotched* 810O system [37] drops by 17% from the 810A value; again, this drop cannot be traced back to the fiber modulus. It is very surprising that a 100-500 nm fiber coating [21,22] can influence the axial stiffness — a "fiber dominated" property — that profoundly. From this result one may infer that the "O" sizing contributes to an interphase that is more compliant than the one in which the "A" sizing appears.

The normalized tensile modulus values of the 5U series reveal an increase in modulus when going from the 52U to the 55U material, yet, this increase turns downward for the 510U material. In this instance, however, the normalized *unnotched* unidirectional tensile stiffness, E_{xx}, climbs steadily, with the 55U value larger than the 52U value by 8%, and, with the 510U value larger than the 55U value by 13% [37]. The unidirectional tensile stiffness data seems surprising in light of the lack of variability in the 8A&O series data and in the fact that the 5U series fibers are unsized. One would normally not expect changes in surface treatment alone to have such an effect on the axial stiffness of a unidirectional specimen.

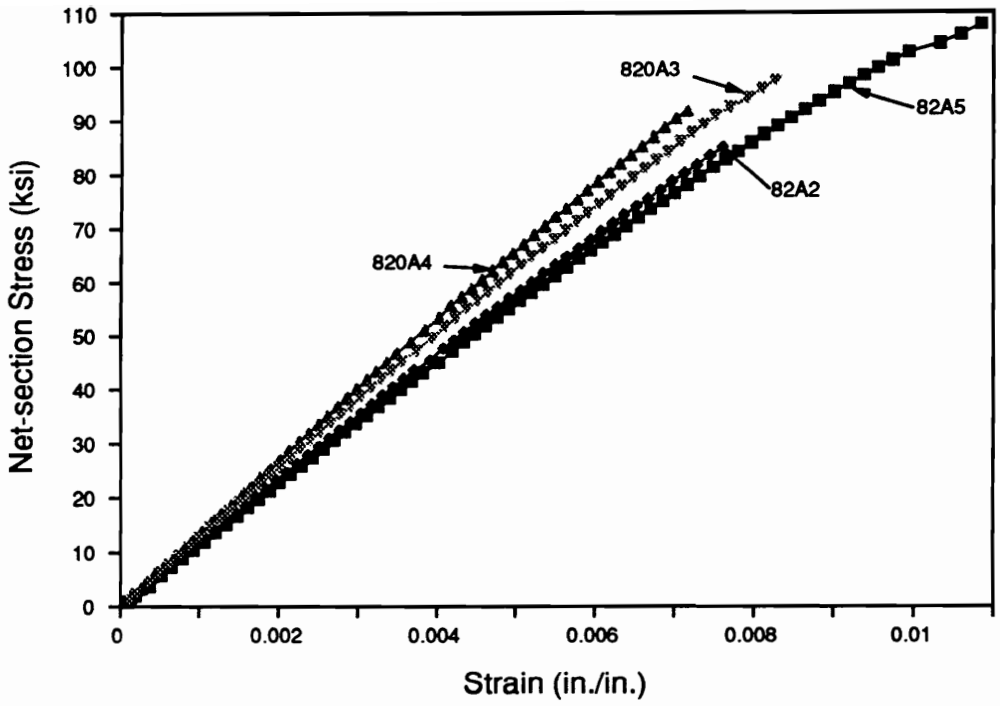

Figure 19. Net-section Tensile Stress versus Measured Strain for Two 82A Specimens and Two 820A Specimens.

The untreated and surface treated Northrop material systems provide another example of the effect of surface treatment on modulus values. In each of the three series, the as-measured and fiber volume fraction-normalized moduli increase as surface treatment is added to the fiber. In no instance is this point more obvious than between the 5NN and 5SN systems. The *net-section* stress vs. strain response for two specimens of each material type are shown in Figure 20. The responses from the two materials diverge at approximately 2500 $\mu\varepsilon$. This strain value appears to be a linear limit for the two 5NN specimens. Again, this probably indicates the presence of longitudinal splitting and/or 90° cracking at the hole boundary. Notice, however, the greater degree of toughness displayed by the 5NN systems *simply on account of fiber surface treatment.* What makes this result more astonishing is the fact that this is a "fiber-dominated" laminate.

The *unnotched* unidirectional stiffness data from Northrop [39] reveals an increase in modulus with the presence of surface treatment in only one of the three material series; the 5N series. Yet, it should be noted that their results indicate that all three systems differ by less than 1 Msi in modulus, indicating a veritable insensitivity to the surface treatment. Because this conflicts with the 5U data, one is forced to speculate on the role of the matrix in interacting with the surface treated fiber. Perhaps certain matrix formulations are more susceptible to changes in fiber chemistry than others.

Compressive Modulus: The compressive *net-section* stress vs. strain response of two systems in the 8A&O series is shown in Figure 21. This data clearly indicates the degree of non-linearity of the response. Because of this, the modulus values recorded are difficult to correlate to any one (or more) physical property of the material. In addition, no unidirectional unnotched compressive stiffness data was collected. These two observations combine to make any and all trends ascribed to this data set purely speculative. Therefore, only obvious relationships will be brought forth.

Except for the specimens possessing the weakest bonding (ordered by TFS as 5NN, 3RNN, and 3NN), the tensile modulus of each system is higher than the compressive modulus. The 5NN *tensile* response found in Figure 20 obviously diverges from linearity due to subcritical damage occurring at low levels of applied stress. Once this specimen (and the other weakly-bonded systems)

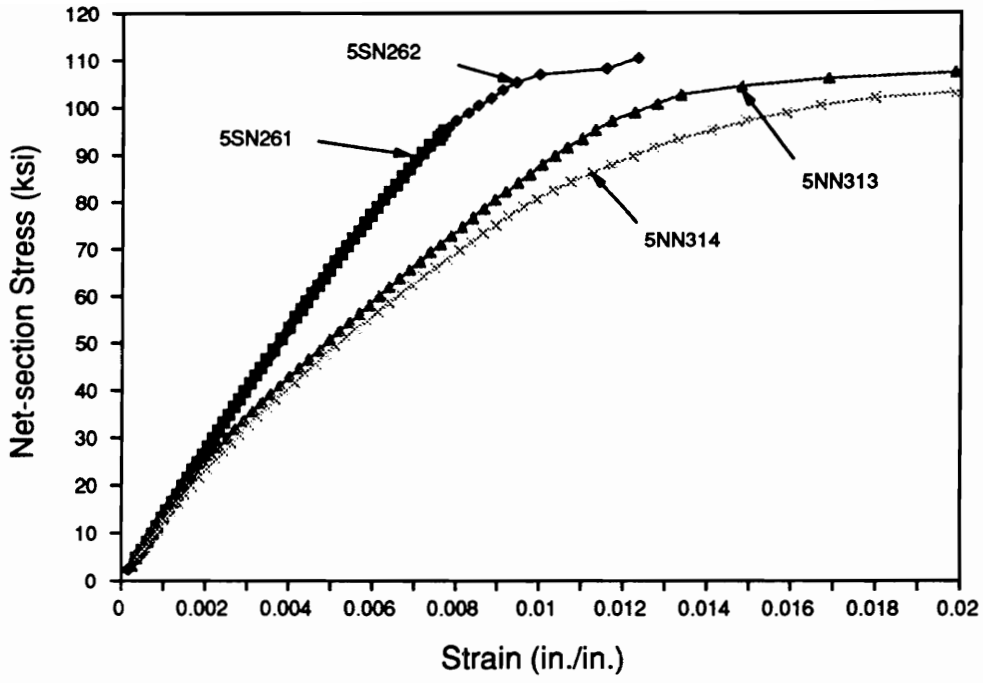

Figure 20. Net-Section Tensile Stress vs. Measured Strain for Two 5NN Specimens and Two 5SN Specimens.

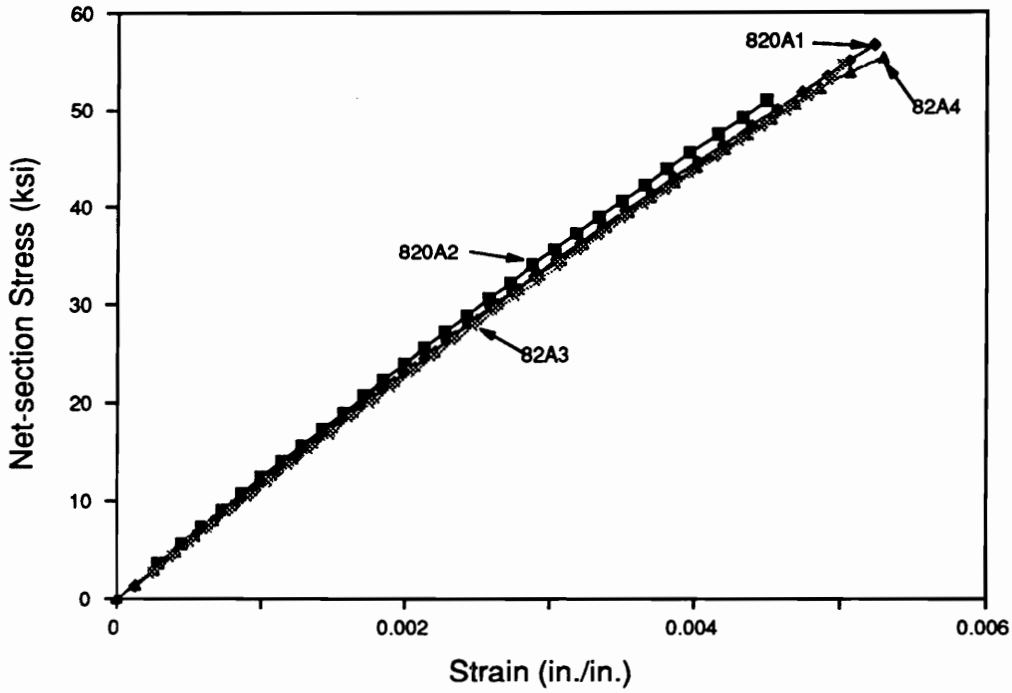

Figure 21. Net-Section Compressive Stress vs. Measured Strain for Two 82A Specimens and Two 820A Specimens.

is loaded in compression, it is possible that these damage modes are suppressed until higher applied loads, allowing for a larger compressive, rather than tensile, modulus. One obvious damage mode that would behave in such a way is 90° matrix cracking. It is well known that 90° lamina are much stronger in compression than in tension, a point illustrated in the transverse flexure tests. The author *did not* isolate the damage modes that were responsible for this disparity between the tensile and compressive modulus responses.

Unnotched Cross-plied Specimens

Stiffness Results

It was necessary to determine the unnotched cross-plied tensile stiffness of the McAir material in order to aid in the modelling effort detailed in the next chapter. A schematic of these stiffness data (as-measured values and values normalized by fiber volume fraction) for the McAir material is shown in Figure 22. In complete contrast to the notched cross-plied tensile moduli, the 8A&O specimens appear to *decrease* in stiffness as the level of surface treatment increases. The 810O stiffness is noticeably lower than the other 8A&O systems; this is in complete agreement with the tensile moduli discussed above. The 5U series data displays no definite trends. The normalized stiffness value for the 55U system appears disproportionately large; it is felt that this reflects differences in fiber volume fraction more than differences in the nature of the material.

Unnotched $\pm 45°$ Specimens

Prior to collecting strength data from these specimens, a strong suspicion concerning the performance of $\pm 45°$ laminates was confirmed. Since the response of $\pm 45°$ laminates is a "matrix-

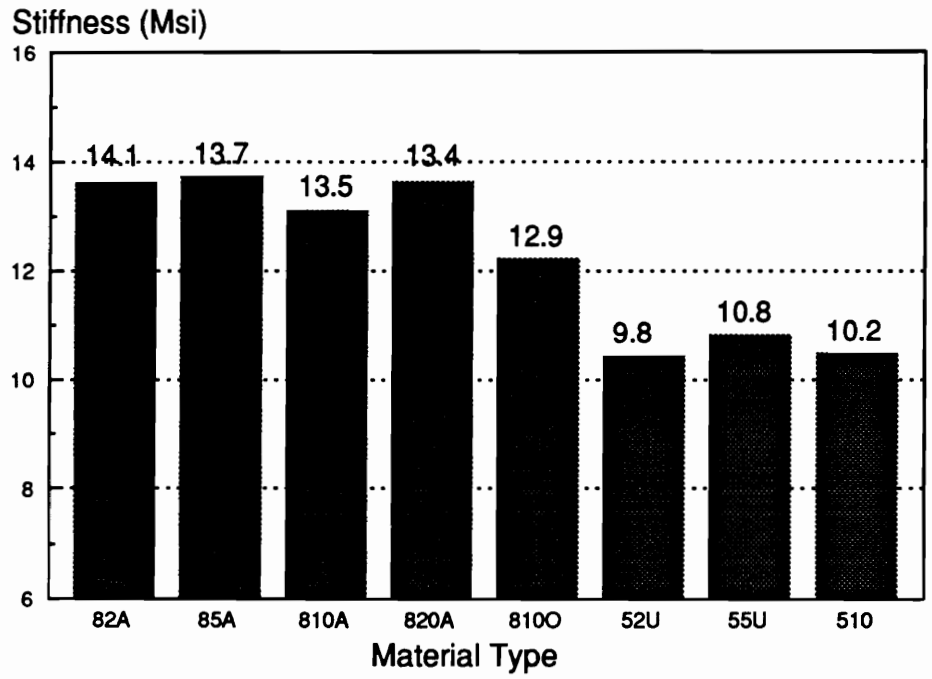

Column height represents measured value

Numbers above column represent values adjusted by fiber volume fraction

Figure 22. Tensile Moduli of the Unnotched Cross-plied McAir Materials.

dominated" response, it was felt that a relationship between its performance and the performance monitored by the TFS test may exist. To this end, normalized Northrop [39] and McAir [37] $[\pm 45]_{ns}$ ($n=2$ in the Northrop tests, $n=4$ in the McAir tests) tensile strength data (45TS) was plotted against the TFS data collected by the author; this is presented in Figure 23.

With the exception of experimental scatter that would naturally occur in comparing data taken from three *independent* laboratories, it is amazing to find a nearly linear relationship between these two sets of data. Contributing to the profound surprise of this result is the fact that the $\pm 45°$ test is supposed to be a *shear* test, while the TFS data could *never* be interpreted as a shear test (unless one made the claim that polymer failure is *always* a shear failure no matter what the state of stress [71]). Though this is the first data to the author's knowledge that correlates the results from these two different test techniques (fully realizing that Madhukar and Drzal [9,10] have collected both sets of data on their well-characterized material systems), others have hinted that $\pm 45°$ tensile strength could reflect some degree of transverse strength. Kellas, *et al.* [46], observed that the first failure that occurs in $\pm 45°$ laminates loaded in tension is trans-fiber matrix cracking on the two outer faces. While most conclude that this failure is due to shear, they conclude that it is due to the presence of transverse stresses in the angle-plies. Thus, if first-ply failure was equated to specimen failure in these laminates (instead of ultimate strength), then, they surmise, fiber/matrix interphase strength could definitely affect these results.

Figure 23 seems to strongly indicate that transverse interphase strength and $\pm 45°$ tensile strength are intimately related. Yet, this is *truly* surprising if one considers the process that leads to ultimate failure in the $\pm 45°$ laminates. The reader is reminded that the data normalized in Figure 23 is *ultimate* stress; i.e., the maximum load endured by the laminate prior to fracture. During a ramp load, these specimens will transition through a visible "yield point"; i.e., they will sustain *large* deformations and still possess the ability to maintain stress. These deformations occur due to the well-known "scissoring effect", where the original 90° angle between two plies is severly reduced even though the laminate remains integral. A photograph of two $\pm 45°$ specimens is shown in Figure 24. One specimen has yet to receive any loading; the other was fatigued until test termi-

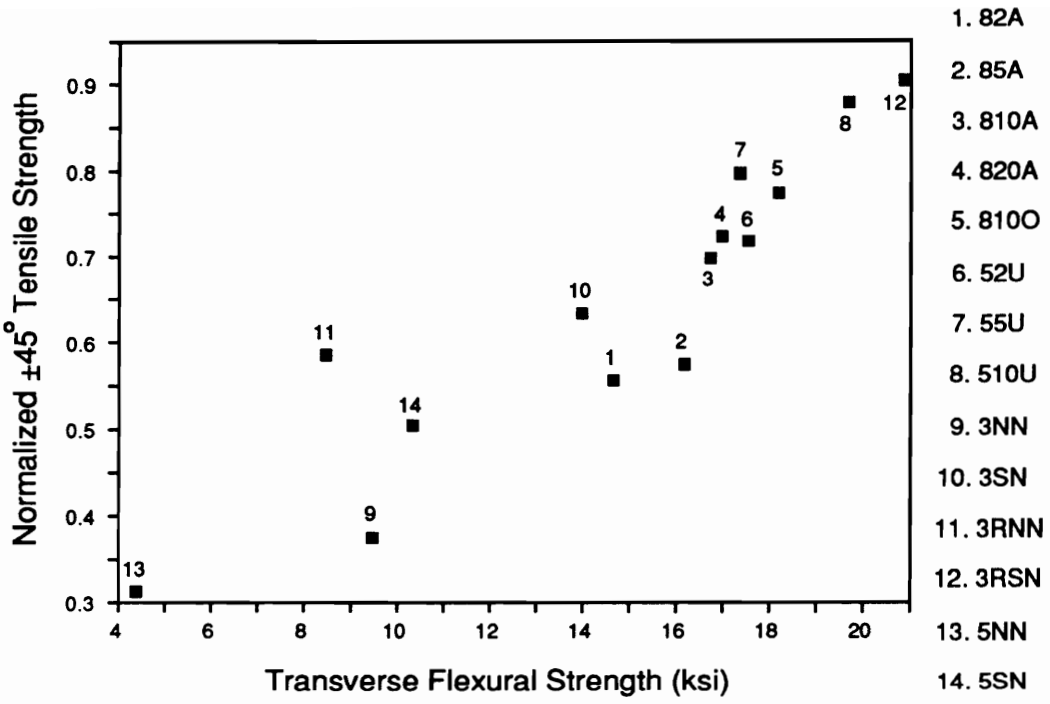

Figure 23. Normalized ± 45° Tensile Strength versus Transverse Flexural Strength of the McAir and Northrop Materials [37,39].

nation. One can see from Figure 24 how severely the cross-section of the specimen changes and how long the specimen becomes.

Once the plies yield, the fibers become more aligned with the load axis and the laminate becomes *stiffer*. The aligned fibers can carry a great deal of load beyond this yield point. Thus, ultimate strength largely reflects a measure of the degree of alignment, since, as the fibers become more aligned, the laminate becomes stronger. With this in mind, it is really quite surprising that the ultimate strength of the $\pm 45°$ laminates correlates at all with the TFS. Perhaps a first-ply failure strength, or, the stress at which gross yielding occurs would be a more valid parameter to compare to the TFS. One would be fortunate, however, to replicate the same degree of correlation seen in Figure 23.

As a result of this serendipitous finding, the 45TS data collected by Northrop [39] was plotted against other common measures of interphase strength. Normalized Northrop 45TS data plotted against their normalized Short Beam Shear Strength (SBSS) data [39] is shown in Figure 25.[2] Certain points seem to form a linear relationship, while others scatter about. These data fail to correlate as cleanly as the 45TS and TFS do.

Another test measure that is noted for measuring "matrix-dominated" effects is the Edge Delamination Strength (EDS) test [72]. Normalized 45TS data is plotted as a function of normalized EDS data [39] in Figure 26. Again, an astonishing level of correlation is seen between these two seemingly distinct test methods. One is tempted to ascribe pure coincidence to the correlation between these results since the tests purport to measure such different responses. Yet, perhaps a common thread runs between all of these test results. It is hypothesized that the thread is, indeed, the interphase. If one could accept the proposal that 45TS behavior is strongly affected by transverse interphase strength, then the leap to EDS is not that great. The EDS test primarily monitors a laminate's resistance to interlaminar Mode I cracking, or, in a more crude sense, out-of-plane interlaminar strength. If TFS is an effective means of gauging transverse interphase strength, then

---

[2] This figure (along with several to follow) displays the normalized results obtained from Northrop's twenty different material systems. These systems are described as a fiber/matrix/surface treatment/sizing in the figure's legend. The coding scheme adopted for the fourteen material systems studied herein is *not* replicated in the legend. Readers who are interested in a more detailed description of these twenty systems are encouraged to contact the Air Force in order to obtain copies of Northrop's quarterly reports.

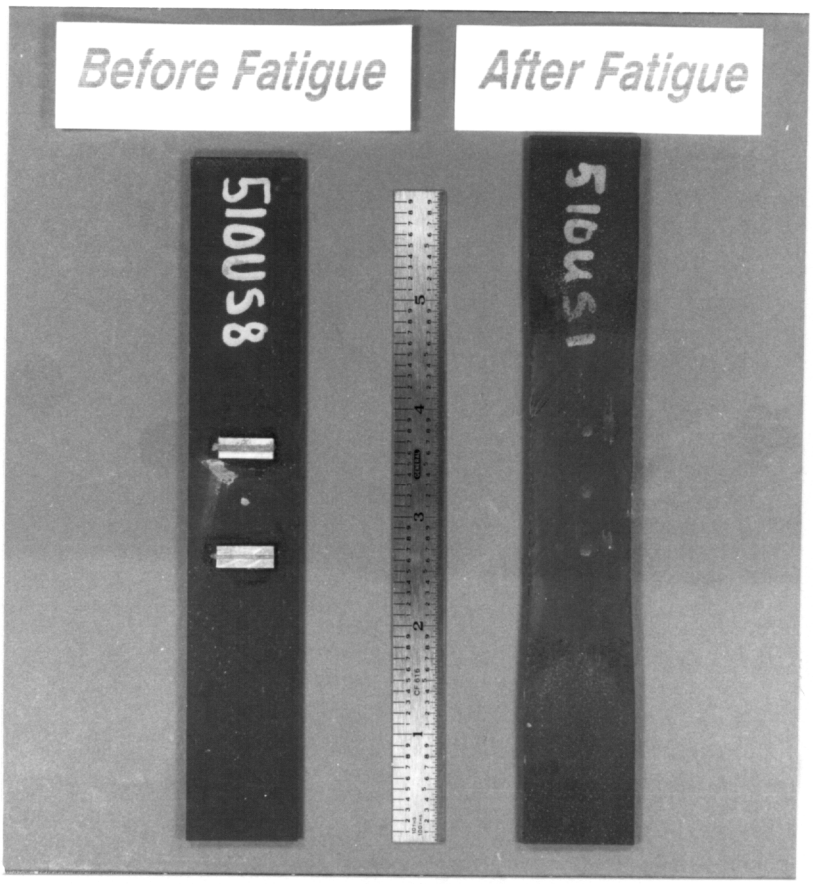

Figure 24. Photograph of Two ±45° Specimens; a.) A Virgin Specimen, b.) A Fatigue Specimen that has Yielded.

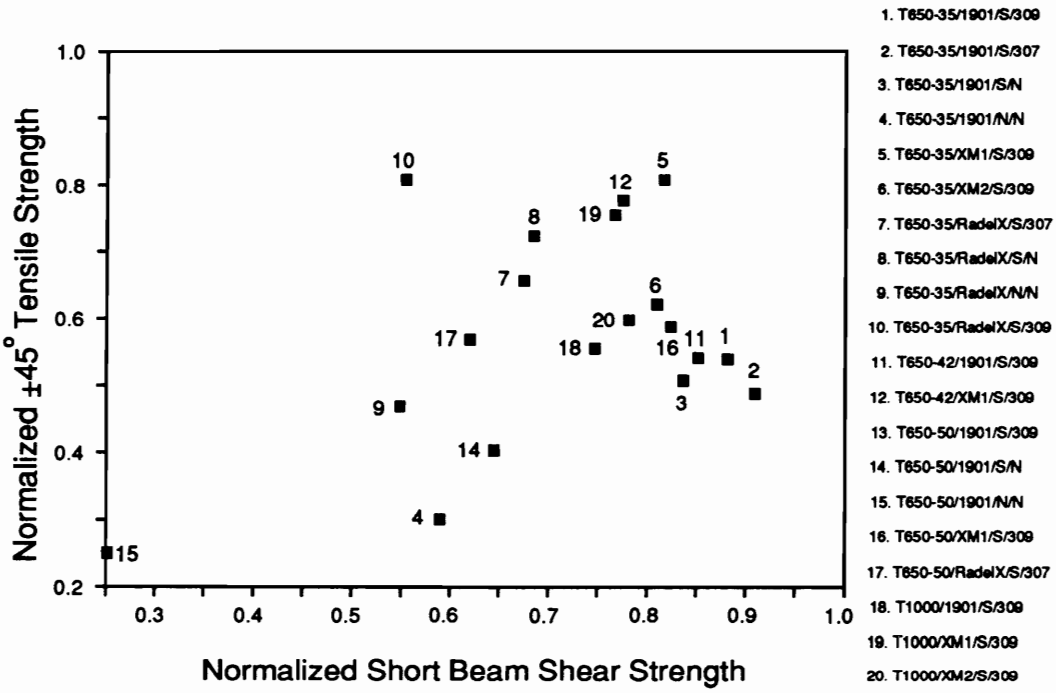

Figure 25. Normalized ± 45° Tensile Strength versus Normalized Short Beam Shear Strength of the Northrop Materials [39].

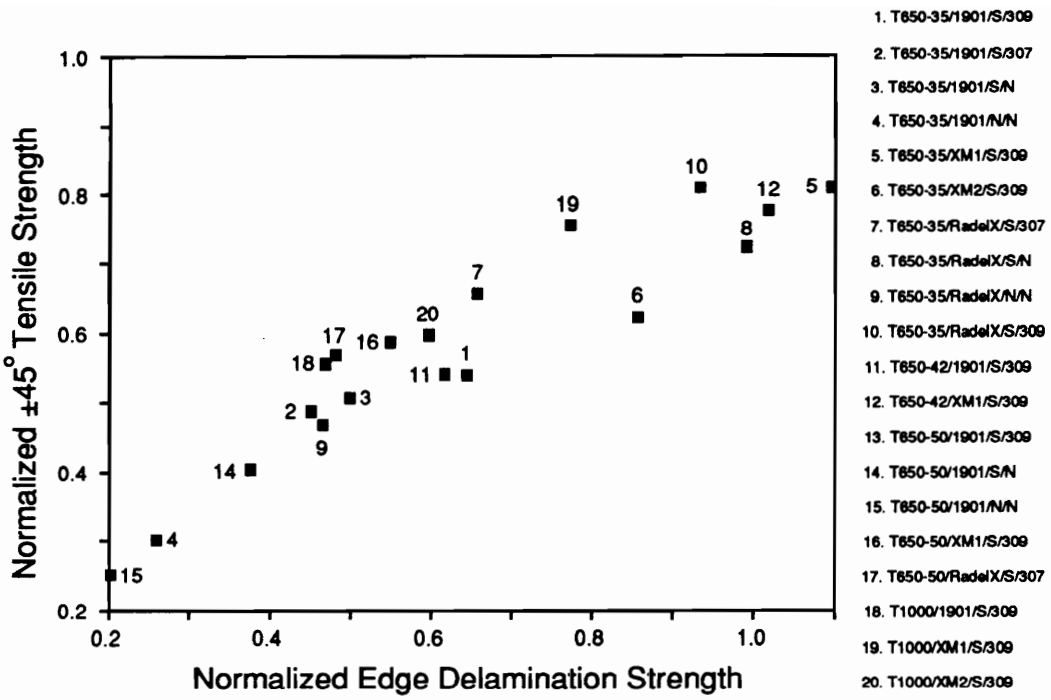

Figure 26. Normalized ± 45° Tensile Strength versus Normalized Edge Delamination Strength of the Northrop Materials [39].

shouldn't the EDS also show similar trends? In the TFS case, the interphase is being stressed perpendicular to the fiber axis, and in the EDS case, the same is true. Yet, the obvious difference between the two cases is that one is an *intra*laminar response, the other an *inter*laminar response. One could easily argue that failing the resin-rich zones in between each ply is *not* a measure of interphase behavior. One could reply, however, that the fiber/matrix interphase is the weak link in that simulated chain of constituents. Such a claim could easily be proved by performing careful surface analysis tests on EDS fracture surfaces, to determine if the failure surface is cohesive or adhesive. Such tests are left for future work.

Tensile and Shear Strength Results

The focus of this sub-section now shifts from the analysis of data collected primarily outside of this institution to data collected internally. The average $\pm 45°$ tensile strength (45TS — which is simply double the calculated "unidirectional" shear strength) and the average shear stiffness for the McAir and Northrop material systems under investigation are presented in Figure 27 and collected in tabular form in Table 6. It is apparent that the trends seen in the 45TS data are very similar to the data collected during the TFS tests; i.e., increasing the level of surface treatment increases the strength. One also must be reminded that the 820A and 55U specimens were 32 plies thick. It has been shown that the 45TS obtained from the 32-ply specimens is routinely greater than the 45TS obtained from 16-ply specimens [46]. It is apparent that certain disparities exist between the 45TS and TFS data sets. First, the 45TS is higher in the 82A system than in the 85A system, defying the established trend of the higher 45TS/higher TFS. Secondly, whereas the 810O material displayed a noticeable increase in TFS over the 810A material, the 45TS of the two materials are nearly indistinguishable. The difference in the 45TS data between the 8A&O series and the 5U series is quite obvious, more than in the TFS results. In general, however, the 45TS data supports the trends established in Figure 23; i.e., there is a positive correlation between 45TS and TFS.

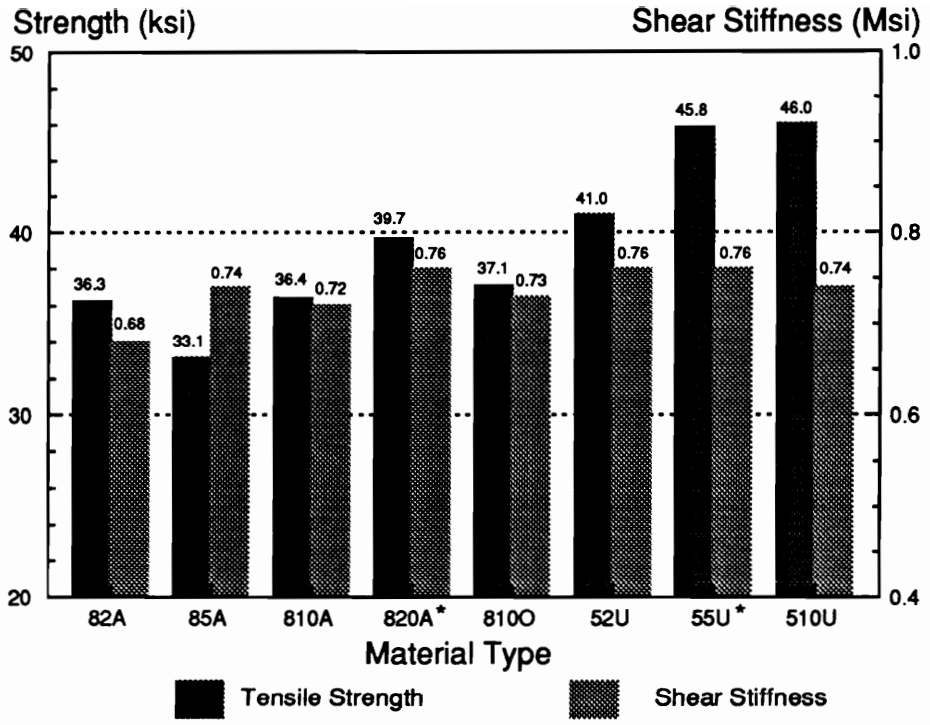

Numbers above column represent actual value

* 32-ply specimens

Figure 27. Average ±45° Tensile Strength and Average Shear Stiffness of the McAir Materials.

Table 6. Average Tensile Strength, Shear Strength, and Shear Stiffness Data Obtained from the ± 45° McAir Specimens.

MATERIAL TYPE	DATA PTS.	AVG. TENSILE STRENGTH (ksi)	COV (%)	AVG. SHEAR STRENGTH (ksi)	SHEAR STIFFNESS (Msi)
82A	3	36.26	2.3	18.13	0.68
85A	3	33.14	2.5	16.57	0.74
810A	3	36.44	2.4	18.22	0.72
820A	3	39.71	0.3	19.86	0.76
810O	3	37.10	2.5	18.55	0.73
52U	3	40.99	3.6	20.49	0.76
55U	3	45.81	0.9	22.91	0.76
510U	3	46.01	1.4	23.00	0.74

One troubling aspect of this strength data, however, is that it is consistently higher than the data collected by McAir on the same systems having the same laminate configuration [37]. The first conclusion reached upon this realization was that McAir was quoting an ultimate strength that was achieved by reading the stress level that accompanied the onset of gross non-linear behavior. Since the strength recorded in the lab in which the author worked represented the maximum stress achieved prior to fracture, this might explain why the McAir strength was lower. Consultation with scientists at McAir disproved this theory, since they, too, measured the maximum stress achieved prior to fracture [73]. Differences in specimen geometry could possibly explain these differences, yet, it was ascertained that both sets of specimens were 16 plies in thickness (though the 820A and 55U specimens were 32-ply specimens). This discrepancy will remain an unknown and cast a shadow of uncertainty on one data set or the other (or both).

It is quite illuminating to see the actual shear stress versus shear strain response of the material systems. The shear stress-strain diagram of the five 8A&O specimens is shown in Figure 28, while the three 5U specimens are shown in Figure 29. Figure 28 gives the reader an appreciation for the amount of "yielding" that takes place within the $\pm 45°$ specimens. Each specimen undergoes a change in shear strain of approximately 20% while the stress level remains constant. The stress level at which this occurs is probably a truer measure of shear response than the ultimate tensile strength is. The yield response of the 82A specimen is unseen in Figure 28 due to the fact that the extensometer tabs loosened during yielding and invalidated the strain measurement. The remaining specimens order themselves such that the 85A yields at the lowest stress, followed by 810A, 820A, with the 810O yielding at the highest shear stress. Notice from Figures 27 and 28 that this ordering is not necessarily replicated in the ultimate strength results.

It is interesting to note how the 510U specimen shear stress-strain response distances itself from its 5U counterparts (see Figure 29). The stress level that initiates the gross yielding in the 510U specimen is nearly 2000 psi greater than either the 52U or the 55U specimen. The stress level at gross yielding for these latter two specimens is nearly equivalent to the yield stress level for the 820A specimen seen in Figure 28.

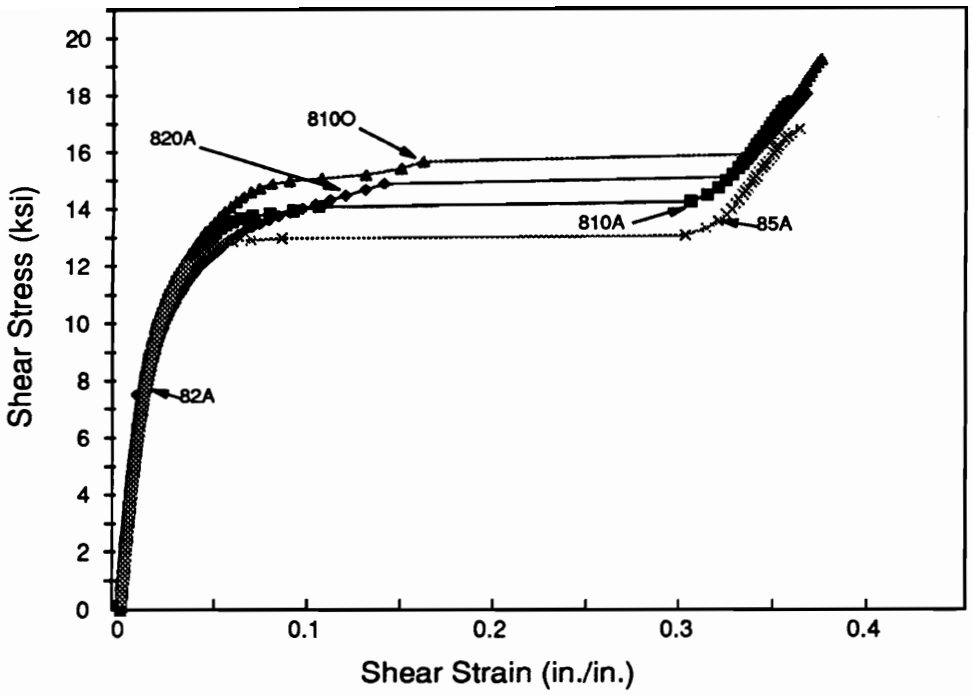

Figure 28. Shear Stress versus Shear Strain for Five Specimens in the 8A&O Series.

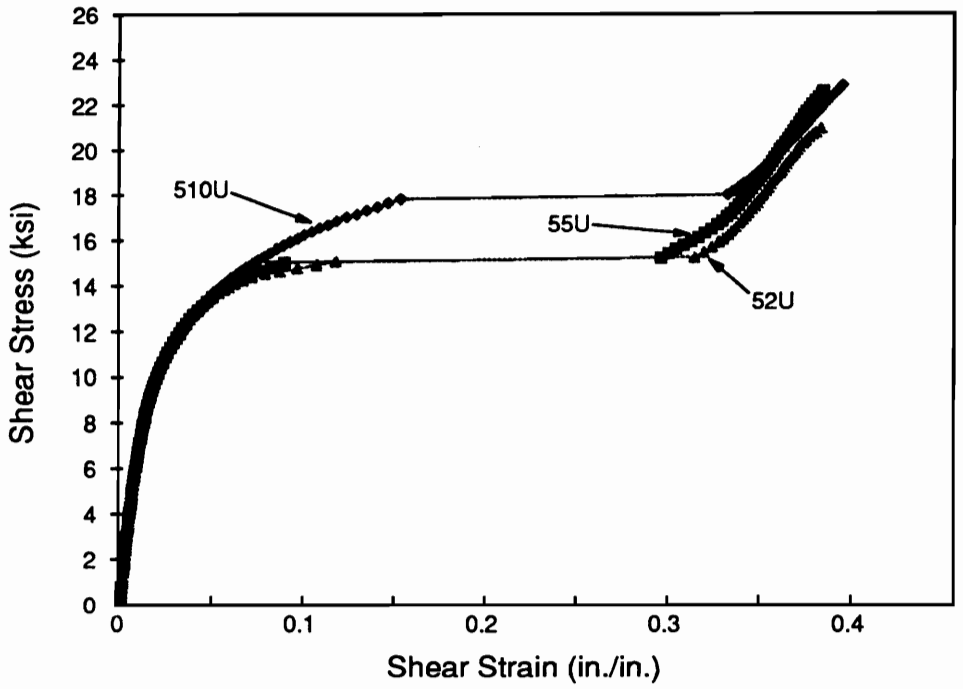

Figure 29. Shear Stress versus Shear Strain for Three Specimens in the 5U Series.

Shear Stiffness Results

With the exception of the 82A specimens, which exhibit the lowest shear stiffness of the eight specimen types, the values of the remaining seven specimens are nearly indistinguishable given experimental scatter. Madhukar and Drzal [9] found that, in general, the shear modulus *decreased* as the level of bonding increased. They attributed this behavior to the scissoring effect described earlier, wherein the rotation of the fibers cause a "stiffening" of the laminate. Hence, strong-bonded systems restrict fiber rotation, and therefore, reveal lower shear stiffnesses.

Unidirectional Compressive Specimens

The unidirectional compressive strength of the McAir material was determined for use as a comparative measure of material performance and for potential use in the modelling work detailed in the next chapter. These tests were not performed on the Northrop material systems since these data had already been published [39]. A schematic of the average compressive strength is shown in Figure 30, while the failure strain data and stiffness data are located in Figure 31. These data are collected and listed in Table 7.

Strength Results

It should be noted that the data seen in Figures 30 and 31 and Table 7 have *not* been normalized with respect to fiber volume fraction (listed in Table 4). The fiber volume fraction of the six specimens did not deviate by more than 5.5%, and, therefore, it did not seem imperative to normalize the measured values. Judging from Figure 30, it does not seem that there is any definitive relationship between interphase strength and the IITRI compressive strength. Though large differences in strength are apparent, they do not seem to correlate with bond strength as conventional

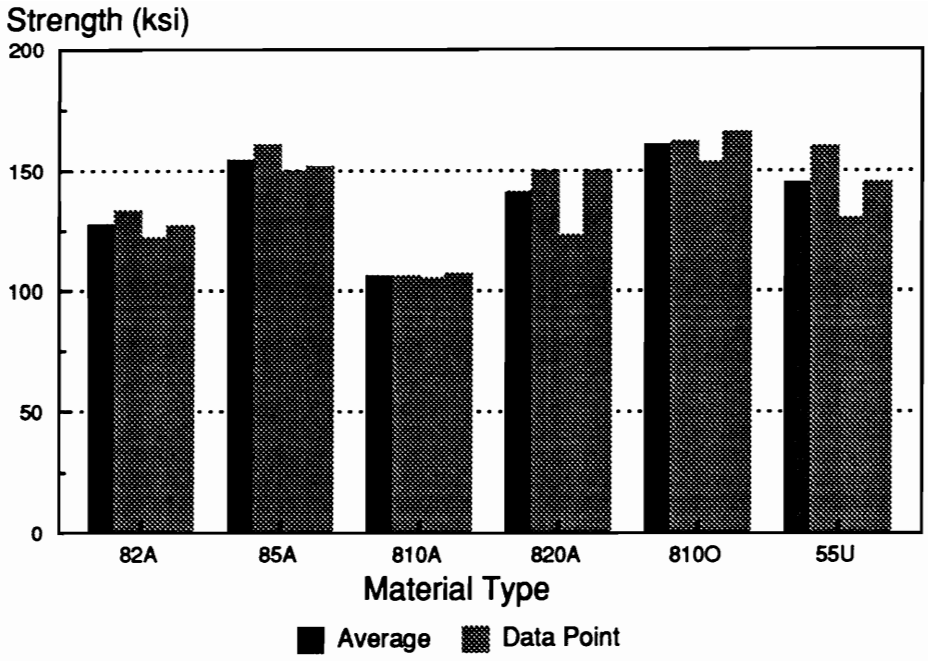

Figure 30. Average Strength and Strength of Individual Unidirectional Compressive Specimens from the McAir Materials.

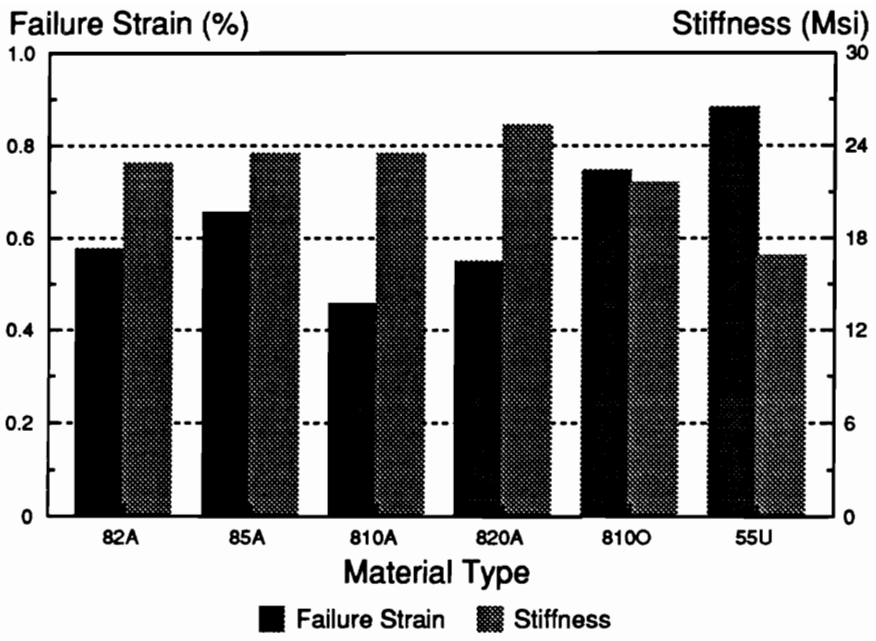

Figure 31. Average Failure Strain and Average Stiffness of the Unidirectional Compressive Specimens from the McAir Materials.

Table 7. Strength, Failure Strain, and Stiffness of the McAir Unidirectional Compressive Specimens.

MATERIAL TYPE	AVERAGE STRENGTH (ksi)	AVERAGE FAILURE STRAIN (%)	AVERAGE STIFFNESS (Msi)
82A	127.4	0.576	22.8
85A	153.9	0.653	23.5
810A	105.8	0.456	23.5
820A	140.8	0.547	25.3
810O	160.2	0.746	21.6
55U	144.8	0.883	16.8

wisdom would have desired. One data point that is especially troubling is the 55U strength. Both notched cross-plied compressive strength and unnotched cross-plied compressive strength [37] indicate that the 5U series has, on average, a higher compressive strength than the 8A&O series specimens by approximately 30%. The explanation for this finding centered on the larger fiber diameter in the 5U material systems, and the subsequent resistance this fiber would have to buckling and bending. In the present data, however, the unnotched unidirectional compressive strength of the 55U material is nearly indistinguishable from its 8A&O counterparts. This strength value is viewed suspiciously, especially in deference to the unnotched cross-plied compressive strength values published in Refs. [37,40].

The strength values displayed in Figure 30 seem to be unusually low when compared to the results published by Northrop on similar material systems [39]. Perhaps this disparity reflects the manner in which the values were obtained. Northrop chose to test a tabbed version of the ASTM D695 standard ("A Standard Test Method for the Compressive Properties of Rigid Plastics" [74]) and described their specimens in this manner [39]:

> The test specimens were 8 plies thick, three inches long, with adhesively bonded unidirectional tabs (of the same material as the specimen). There was a 0.185 inches space left between each tab at the center of the specimen. This specimen was mounted in the ASTM D695 cruciform fixture to provide buckling support during testing. For thermoplastic test coupons, thermoset tabs were used.

This specimen is to be contrasted to the McAir specimens tested in the present investigation. In this case, the specimens were 28 plies thick, 6″ in length, with an unsupported gage section of 0.29″. Strains were monitored on each side of the specimen to invalidate any test that exhibited excessive bending. Different failure modes were observed, ranging from "in-plane shear", to "out-of-plane shear", to crushing. Nearly all failures were located in the tabbed region or at the tab/material juncture.

It is possible that the test method adopted by Northrop constrained the material into limited failure modes or reduced the volume of material that could possibly fail in compression. ASTM warns that standard D695 "should not be used for highly oriented fiber composites." [75]. Due to this caveat and the disparity seen between the present strength values and those obtained by Northrop, there is an uncertainty which values represent true material properties.

Comparing the present 8A&O results to the notched cross-plied compressive strength results, if one completely ignores notch sensitivity, then the large strength of the 85A material is a common factor between the two sets of data. On the other hand, the notched cross-plied compressive strength of the other four systems in the series are nearly equal; this cannot be said of the unnotched unidirectional strength. This may indicate the presence of notch sensitivity, yet, it is curious that the notch tends to "homogenize" the strengths. These issues will be re-examined in the next chapter.

Prior to leaving this sub-section, it is important to establish whether unidirectional compressive strength is dependent on interphase strength. Due to the discrepancies that exist between the McAir unidirectional compressive strength values and the Northrop unidirectional compressive strength values, the two sets of data will not be placed on the same plot. If a trend exists, it should exist for all material systems. Therefore, the normalized Northrop unidirectional compressive strengths [39] are plotted against their respective TFS values in Figure 32. The epoxy systems seem to form a linear relationship that bears no resemblance to the thermoplastic response. One is unable to make any conclusions regarding the thermoplastic behavior since only two data points exist. Yet, the epoxy composites seem to reveal an intimate relationship between unidirectional compressive strength and TFS values; as bonding gets stronger, the strength value increases. This would concur with the findings of other researchers [8,11,14], who have witnessed similar trends.

Failure Strain and Stiffness Results

The failure strain of the 82A, 85A, and 810A systems (see Figure 31) differ from their respective strengths by a nearly constant factor, that factor being a virtually identical compressive stiffness. The 810O system reveals a slightly smaller modulus than the other systems in this series, reaffirming the trends seen in the notched cross-plied modulus data. The average modulus of the 55U specimen is approximately 70% of the modulus of the 82A, 85A, and 810A specimens. This is — perhaps coincidentally — the same ratio as the two fiber tensile moduli, 32 Msi over 45 Msi.

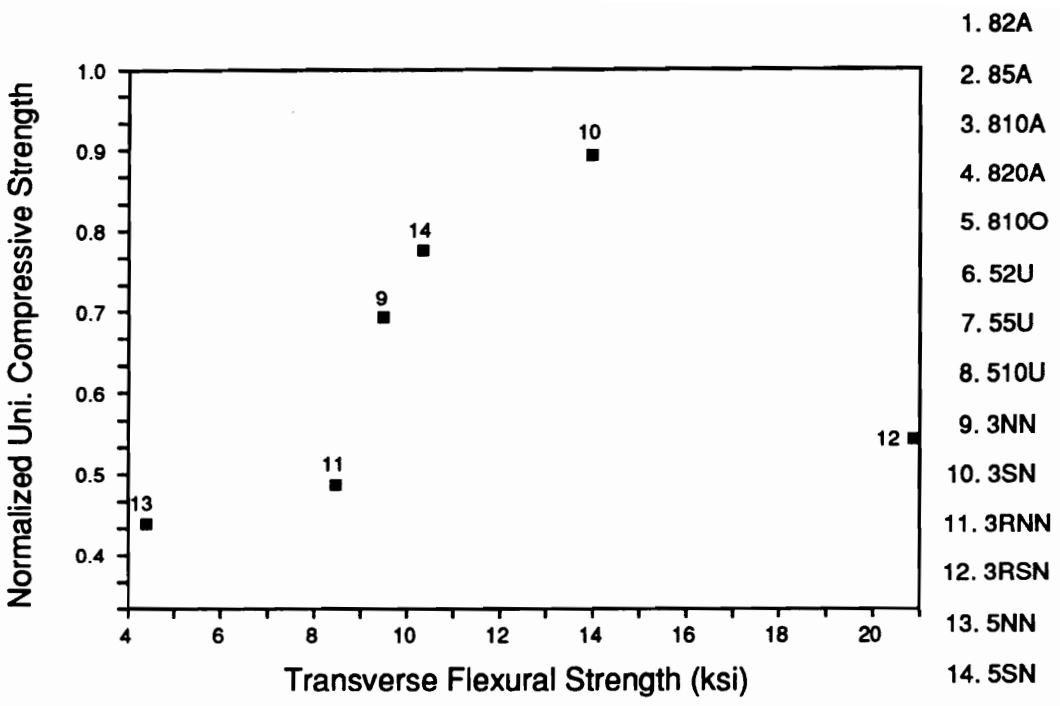

Figure 32. Normalized Unidirectional Compressive Data versus Transverse Flexural Strength of the Northrop Materials [39].

Fatigue Testing

The format of this section will deviate only slightly from the previous section. In performing the quasi-static strength and stiffness tests, usually only these two variables were measured and presented. Yet, during fatigue testing, several variables were monitored, including: cycles to failure, modulus as a function of cycles, specimen temperature as a function of cycles, and phase and gain data collected via the "M-R Phase 3000" program. Thus, just as in the previous section, a sub-section will be devoted to presenting and analyzing each of these data sets. To help focus the presentation, each sub-section will be broken down into three smaller sections representing the results from the 8A&O series, the 5U series, and the Northrop material systems. It is hoped that this structure will assist the reader in assimilating the information presented.

Notched Cross-plied Specimens

Comparing cycles to failure between different specimens of the same material type is, under normal circumstances, very straightforward. Distinct systems possessing different strengths, however, complicate the interpretation of cycles-to-failure data. As indicated in the section, "Mechanical Testing", located in the previous chapter, the decision was made to compare every specimen on the basis of their fatigue performance under an applied fatigue stress level equal to a set percentage (75%) of their respective ultimate compressive strength. The reasons for this were detailed in that section. One of the drawbacks in choosing the present scheme is the ability to perform a comparative analysis, especially in the instances where the quasi-static compressive strength between two systems is vastly different (e.g., the 3NN and 3SN specimens). Therefore, throughout this section, one must look upon the fatigue results with a critical eye and ask the following question: Does the presence of the interphase have more to do with determining the quasi-static compressive strength (and, therefore, the fatigue stress levels) or does it, indeed, influence the fatigue

behavior by affecting the fatigue process? Fortunately, because the notched compressive strength was often times found to be largely insensitive to variations in the bond condition, one can claim, with a certain level of confidence, that the resulting fatigue performance was attributable to the interphase. Such subtleties will hopefully be addressed.

Cycles to Failure

At least two specimens of each system were fatigued to failure in order to monitor the number of cycles to failure. With few exceptions, the data displayed a remarkable degree of reproducibility. This was wholly unexpected, since a *large* spread in the data (perhaps even several orders of magnitude) usually accompanies the cycles-to-failure data during composite fatigue testing. If the results from two tests did not coincide within the same order of magnitude, another specimen would be tested. Some may criticize that the dearth of fatigue data precludes the ability to make any true assessments. The data displayed in this sub-section is *not* just the "best data", i.e., only the data that showed the least spread; it is presented as characteristic of the performance — a sampling, if you will. As it were, several more specimens were fatigued (to perform X-ray analysis) that used these cycles-to-failure data as a strict guideline. In other words, if it was characteristic of the system to fail around 10,000 cycles, specimens in this group were often taken to 80-90% of this cyclic life, in order to introduce damage. The bottom line is that *every* attempt is made to represent the actual performance of these material systems. There would be little doubt in some of these results if the author had had access to unlimited quantities of material. Since this was not the case, the data is displayed and analyzed in the best manner deemed possible.

The 8A&O Series: The cycles to failure for the first two specimens from each material type, tested at a maximum stress level of 75% of their respective ultimate compressive strength (UCS), are displayed in Figure 33. The data located in this figure represents one of the major findings of this research. The foremost conclusion to form upon inspecting this data is that the interphase plays a

primary role in the fatigue performance of these notched cross-plied specimens. Due to the fact that the notched compressive strength of the systems in this series revealed little to no dependence on the interphase, the applied stress levels remain nearly the same for each material; this tremendously facilitates a one-to-one comparison.

One of two trends can be inferred by examining the response of the first three systems (82A, 85A, and 810A). One may conclude that an increase in the level of surface treatment causes a slight increase in the cycles to failure. This conclusion would be very speculative, however. A more conservative opinion would consider these first three indistinguishable, since there are many factors to consider, the least of which is data spread. This assessment is bolstered by the fact that all six data points presented fall within the same order of magnitude.

A noticeable leap in performance occurs upon increasing the surface treatment level from 100% to 200%. The cyclic life of the 820A specimens increases an by an order of magnitude over the three previous systems. This increase is overshadowed, however, by the performance of the 810O specimens. As of this writing, an 810O specimen has *never* been failed at an applied stress level equal to 75% of its compressive strength. One 810O specimen was allowed to run until 5.1 million cycles (nearly six days of 10 Hz cycling) before a run-out was declared. This performance is noted despite that fact that the applied stress level (32.1 ksi) was *slightly* larger than its 810A counterpart.

The obvious question is: Why? Why should an increase in the surface treatment level from 100% to 200% cause an increase in the fatigue life by an order of magnitude? Why should a different sizing formulation cause the fatigue life to increase by *at least two orders of magnitude*. An attempt will be made to answer these questions, however, the answer may be incomplete until all of data collected has been analyzed. In other words, the remaining part of this "8A&O Series" section will be devoted to examining the results of damage analysis and previously-discussed data. It should be stated that, for the most part, the data that remains to be discussed mainly serves to complete the understanding of the interphase/fatigue relationship. Thus, most of the data needed to form any judgments (not including the damage analysis) has been presented.

Figures 34-36 show X-ray radiographs of damaged 82A, 85A, and 810A specimens, respectively. The 82A specimen shown in Figure 34 has sustained 2550 cycles. Three distinct damage modes

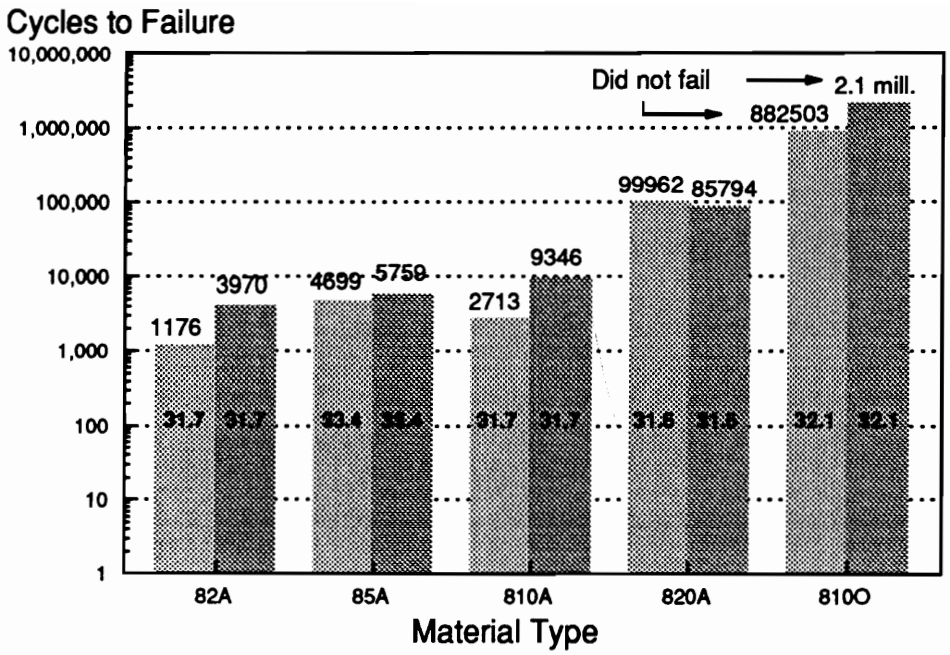

Numbers above bar: actual cycles

Numbers inside bar: applied stress level (ksi)

Figure 33. Cycles to Failure of the Notched Cross-plied Specimens in the 8A&O Series; Max. Applied Stress = 75% UCS; R = -1 at 10 Hz.

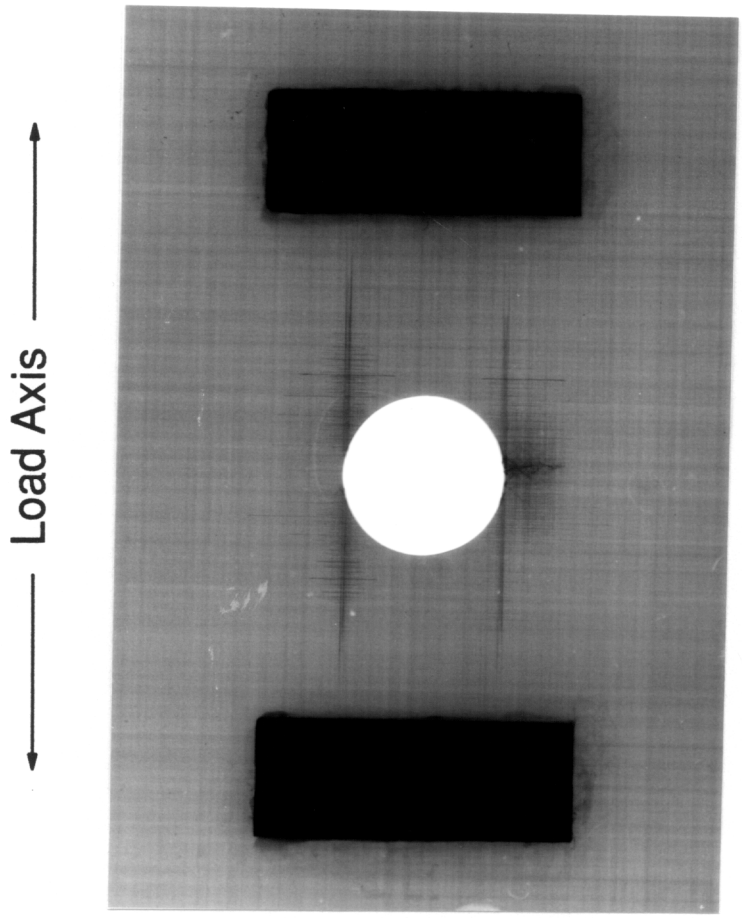

Figure 34. X-ray Radiograph of an 82A Specimen after 2550 Cycles.

are present in Figure 34. Longitudinal splitting has occurred tangent to the hole on each side. Intersecting these splits are 90° matrix cracks. The position of these 90° cracks indicate the mechanism responsible for their formation. It is the responsiblity of the 90° plies to transfer the stress between the two 0° ligaments separated by the longitudinal crack. The primary mechanism through which this transfer occurs, is shear across the 90° plies. Therefore, the presence of these cracks along the longitudinal splits indicates that the cracking is due to a combination of shear and tensile loading (and, perhaps compressive loading). It is very surprising that this is the *only* region in which 90° cracking occurs. The extensometer recorded a value 4500 $\mu\varepsilon$ prior to test termination. Recall from the 82A quasi-static tensile stress vs. strain plot (Figure 19) that damage caused a visible change in the response around 4000 $\mu\varepsilon$. Since 90° cracking only occurs along the longitudinal splits, one may conclude that the damage that caused the perturbation in the stress-strain response was probably not 90° cracking.

The third damage mode present in Figure 34 is compressive (microbuckling) failure of the 0° plies. This "self-similar" crack, resembling a tensile crack in metal structures, has been identified by a number of researchers [76,77]. Confirmation of the compressive nature of the failure is seen in the edge radiograph shown in Figure 36b. One can see broken 0° plies beginning at the surface and progressing into the interior of the laminate This is characteristic of a compressive failure since the laminate will fail in the regions which provide the least support, i.e., at a free surface. This distinguishes itself from a tensile failure, since the latter failure displays no real preference in location of initiation. Once a compressive failure has occurred on either face of the specimen, this region no longer carries any load or provides any stiffness. This tends to unbalance the laminate and creates a "domino effect", with subsequent compressive failures working their way towards the other face of the laminate. Referring back to Figure 34, notice the density of matrix cracking that has occurred in the vicinity of the microbuckle. Microbuckling is a locally catastrophic failure mode, causing neighboring material to experience locally high levels of shear and axial stress. In addition, the tip of the microbuckle acts as a stress concentrator, tempting the surrounding material to fail in a compressive manner. Because of this tip-induced stress concentration, the laminate seeks a way to relieve this focused and local strain energy. The options include compressive failure of the

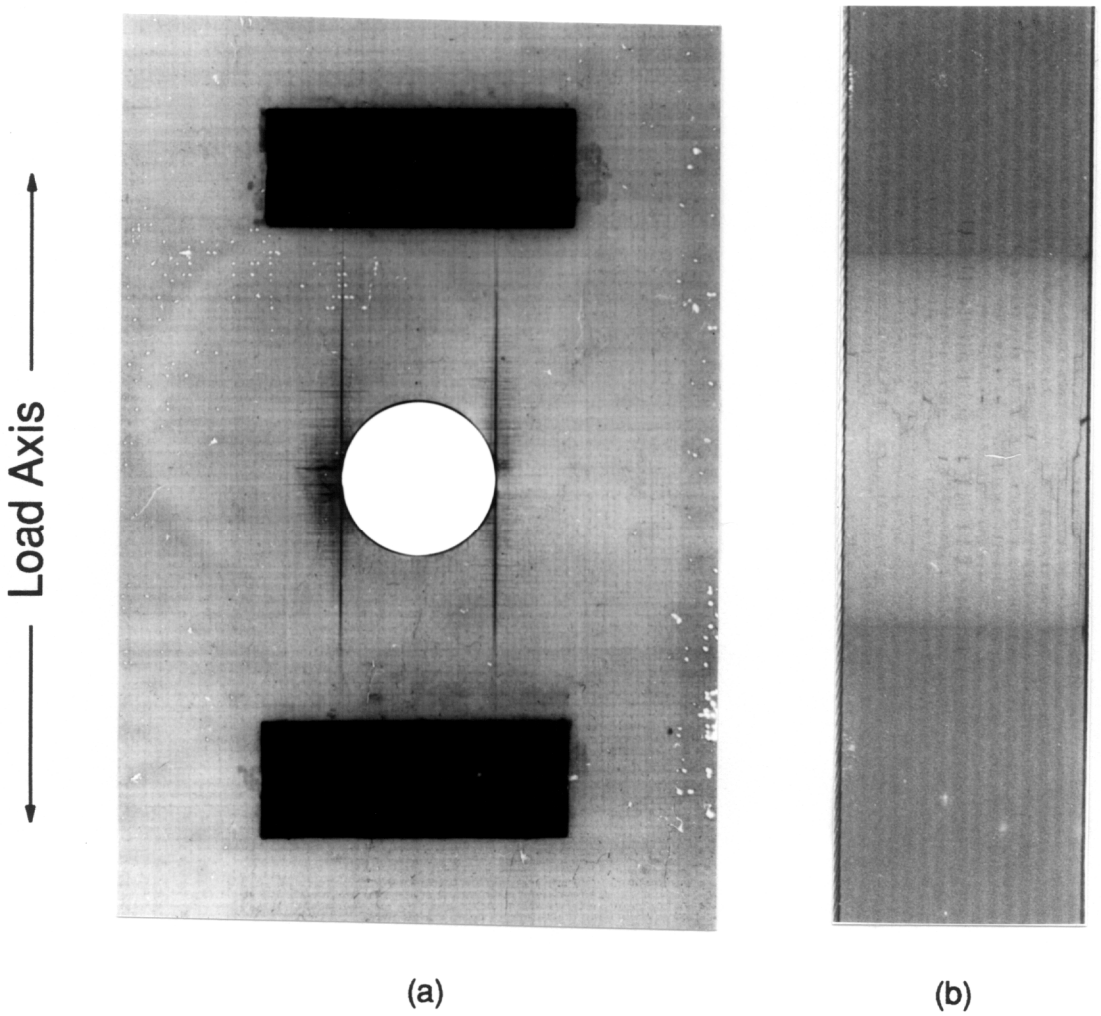

Figure 35. X-ray Radiograph of an 85A Specimen after 2870 Cycles; a.) Front View, b.) Edge View.

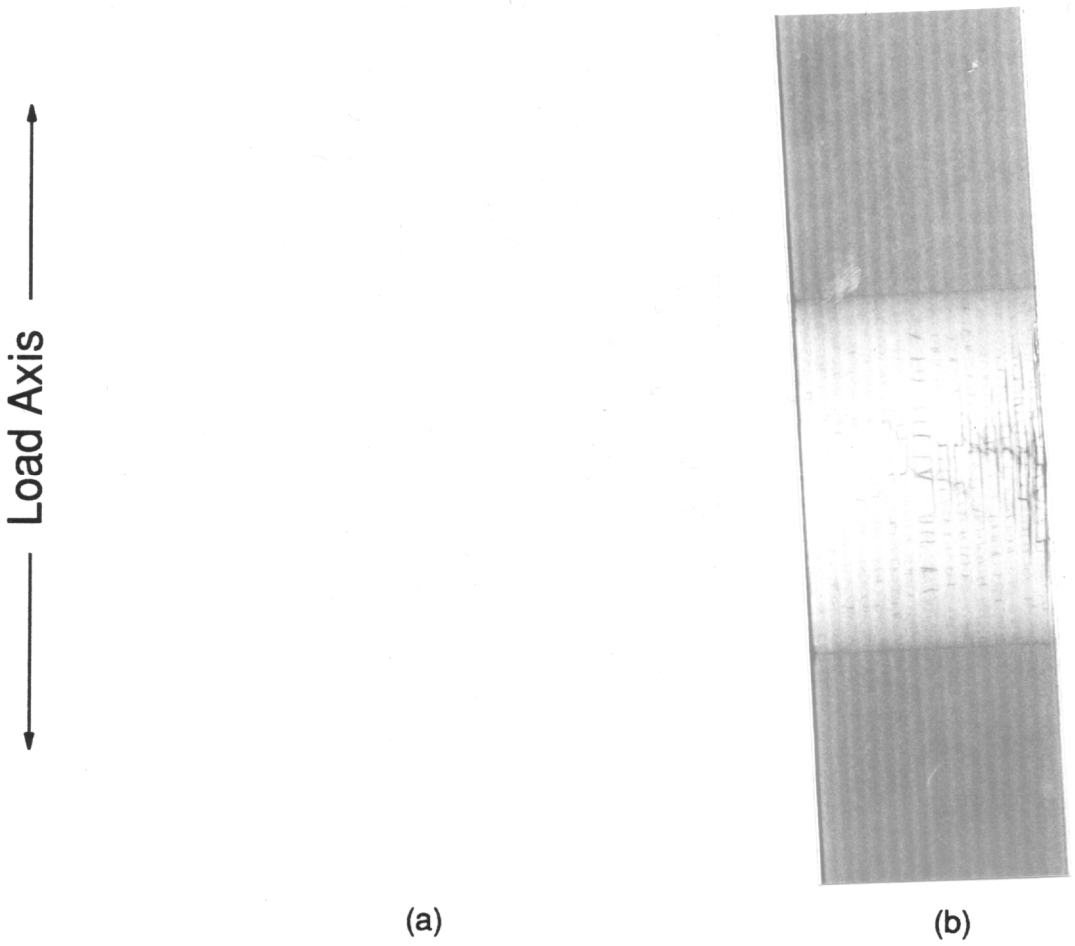

Figure 36. X-ray Radiograph of an 810A Specimen after 3000 Cycles; a.) Front View, b.) Edge View.

adjacent fibers, or, longitudinal cracking along the fiber/matrix interphase, if that region is weak. Though it appears that longitudinal cracking accompanied the growth of the microbuckle (producing the dense grid of cracks that envelop the microbuckle), this cracking was never sufficient enough to blunt the microbuckle. Soutis and Fleck [78] have hypothesized that the microbuckle will grow in a controlled fashion as a function of cycles, until it reaches a critical length dimension that ushers in unstable growth — this cyclic point is equated with specimen fatigue failure. The specimen seen in Figure 34, having exceeded the life of other 82A specimens, reveals a microbuckle length that is probably very near its critical dimension.

It is surprising that delamination is largely absent from this laminate. Both Kortschot and Beaumont [79] and Spearing and Beaumont [26] (who followed Kortschot and Beaumont's work) indicate that delamination is among the list of damage modes present when loading a notched cross-plied laminate quasi-statically [78], or in fatigue [26]. In their studies, delaminations emanate from the tips of their sharp notches and form right triangles whose one side runs coincident with a longitudinal split. Kortschot and Beaumont [79] reason that the delaminations are a result of the shear deformation cited above as the cause of the 90° matrix cracks.

The 85A specimen shown in Figure 35 has endured 2870 cycles. The radiograph seen in Figure 35a is very similar to Figure 34. Two differences are readily apparent, however. The first difference is the extent of the microbuckle length. It also seems that two, perhaps three, microbuckles have formed. It is interesting to note that they appear to emanate at the point where the longitudinal crack intersects the hole. If the hole were cut perfectly round, this juncture would be at only one point on each side of the hole. In reality, however, the holes "flatten out" where the 0° plies form the boundary. Thus, the four places where the circular arc of the hole intersects with the 0° plies appear to be potential sites for microbuckle growth. Three of these potential four sites seem to have sprouted microbuckles, the dominant one being in the upper left-hand quadrant. The difference in the microbuckle length of the 82A and 85A specimens may indicate that this 85A specimen would have had a longer cyclic life than its 82A counterpart.

The second difference seen between the damage modes in Figures 34 and 35a is the extent of the longitudinal splitting. Kortschot and Beaumont [64] considers this length to be of primary

importance in the determination of quasi-static notched strength. Basically, the longer the longitudinal splits, the lower the axial stress concentration adjacent to the notch. The lower the stress concentration, the higher the applied stress endured before local failure occurs at the notch and spreads to the laminate's edge. In the previous section, this philosophy was improved by introducing the interphase strength as a variable that may dictate the laminate's ability to grow these splits. This line of reasoning is applicable to the fatigue scenario only in a limited sense. Clearly, if split growth is encouraged by weak bonding, then specimens *should* benefit in one of two ways. First, since the longitudinal splits tangent to the hole occur prior to the onset of critical damage modes (i.e., fiber failure), the unabated growth of these splits will reduce the magnitude of the stress concentration (which is primarily responsible for creating the critical damage modes). The second beneficial aspect of weak bonding comes in the ability to blunt the microbuckle crack tip.

Soutis, *et al.* [78], present convincing data correlating the presence of a penetrant consisting of a zinc iodide solution (used in present study, too) with an increase in longitudinal split growth rate in their laminates. They tested $[(\pm 45/0_2)_3]_s$ specimens with two holes spaced symmetrically about the longitudinal axis at a distance of one radius apart. Under conditions of compression-compression fatigue (R = 10), at an applied stress level of 90% of the specimen's ultimate compressive strength, failures were observed after approximately 10^5 cycles, when run — without interruption — to failure. They identified microbuckling growth as the life-limiting failure mechanism in this case. In instances when they stopped the specimen and applied the penetrant solution (for X-ray analysis), then resumed fatigue loading, they found that ultimate failure occurred after more than 10^5; shockingly, the failure was reported to have occurred *in the grips* — not through the hole. They felt that the zinc iodide solution encouraged longitudinal split growth that served to blunt any and all microbuckling growth. While the microbuckle length remained small and near the global stress concentrator, enough stress magnification was present to stimulate further growth. A point is reached, they feel, after which a blunted microbuckle will grow no further and other damage mechanisms will ultimately be responsible for the laminate's final failure.

It is the opinion of the present author that the "beneficial" aspects of weak bonding purported above may be counter-acted by an enervating effect of weak bonding. It is obvious from the

radiographs in Figures 34 and 36 that compressive (microbuckling) failure is to be avoided in order to prolong the life of the laminate. In thinking about the micromechanics of compressive failure, one realizes that the study of compression boils down to, in most cases, a study in support provided by the binding material. Madhukar and Drzal [8] have shown that weak bonding leads to weak unidirectional (0°) compressive strength. The reason that this did not manifest itself when notched cross-plied compressive strength was studied, had a lot to do with the *process* that brought the notched laminate to failure. In any event, specimens with a weak interphase region will probably be highly susceptible to local compressive (microbuckling) failure. The veracity of this hypothesis still needs to be proved by examining the remaining data.

A radiograph of an 810A specimen fatigued to 3000 cycles is shown in Figure 36. The most noticeable feature of Figure 36a is the prominent microbuckle emanating from the hole. It is arguable whether this microbuckle is one large region or the coalescence of two growths emanating from previously-identified locations. Attending the growth of the microbuckle is the dense network of longitudinal splits that likely arose from the tip of the microbuckle, as it grew. On the side opposite of the largest microbuckle is visual proof of the point established above. It appears that microbuckling growth emanating from the upper right-hand quadrant of the hole has been blunted by a long longitudinal split. Yet, it appears (and this is speculative) that the microbuckle formation is re-establishing on the other side of the split. Notice, also, how few 90° cracks intersect the two main longitudinal splits. Perhaps this is an indication of a higher shear strength (which may ultimately be a higher interphase strength) in the 810A material over the 82A and 85A material (a trend that is not confirmed in the MMHP results). The edge radiograph of the 810A specimen confirms the compressive nature of the damage. One surface 0° ply has failed and delamination has formed in the interface between the 90° ply and the adjacent outer 0° ply. As the compressive failures work their way towards the center of the laminate it is interesting to note how the delaminations surrounding each broken ply form a "cone" whose base is the surface ply and whose point is near the center of the specimen.

Figures 34-36 detailed the damage states of the material systems that exhibited nearly indistinguishable fatigue lives. The discussion now turns to the two specimen types that displayed a larger

resistance to fatigue failure. A front and edge radiograph of an 820A specimen that has endured 30,000 cycles is found in Figure 37. These radiographs are very similar to those seen in Figure 35 (the 85A specimen). The length of the 90° cracks and the longitudinal splits are longer in the 820A specimen than in the 85A specimen. The microbuckle growth in Figure 37a is similar in length to the microbuckle growth in Figure 35a. It is important to realize that these two radiographs are taken at an order of magnitude apart in cyclic life. Given this, it is somewhat surprising that the damage states of these two specimen types are so similar. One might expect that the differences in cyclic life are due to the occurrence of different damage modes. Apparently this is not the case.

It remains a mystery how the 820A is able to delay the progression of these identical damage modes. One possible explanation leads back to the argument concerning compressive stability. Perhaps it is the higher strength of the 820A interphase (seen in the MMHP and TFS results) that precludes premature compressive failures. It seems reasonable to assume that interphase strength degrades. Since low interphase strength should encourage compressive failure, perhaps a level of interphase strength exists below which the surrounding media can no longer support the fibers. The higher cyclic life attained by the 820A specimen may simply reflect the (cyclic) time involved in *degrading* the interphase. Plans had existed to test this hypothesis using the indentation testing scheme. It was felt that the cross-ply laminate inhibited the execution of the present indentation test method. This is left for future work.

Another damage state of an 820A specimen is displayed in Figure 38. This specimen characterizes the imprecise nature of using fatigue cycles as a measure of expended life; the specimen in Figure 38 has endured only 19,000 cycles. Obviously — and rapidly-changing stiffness measurements confirmed this — this specimen is very close to failure. The changes that bring the damage state from the one shown in Figure 37 to the damage state shown in Figure 38 are readily apparent. A major microbuckle has continued to grow further towards the specimen edge. Delamination has now become manifest, yet it is confined laterally by the longitudinal cracks that have emanated from the tip of the microbuckle. The edge radiograph (Fig. 38b) shows that the laminate is replete with failed 0° plies.

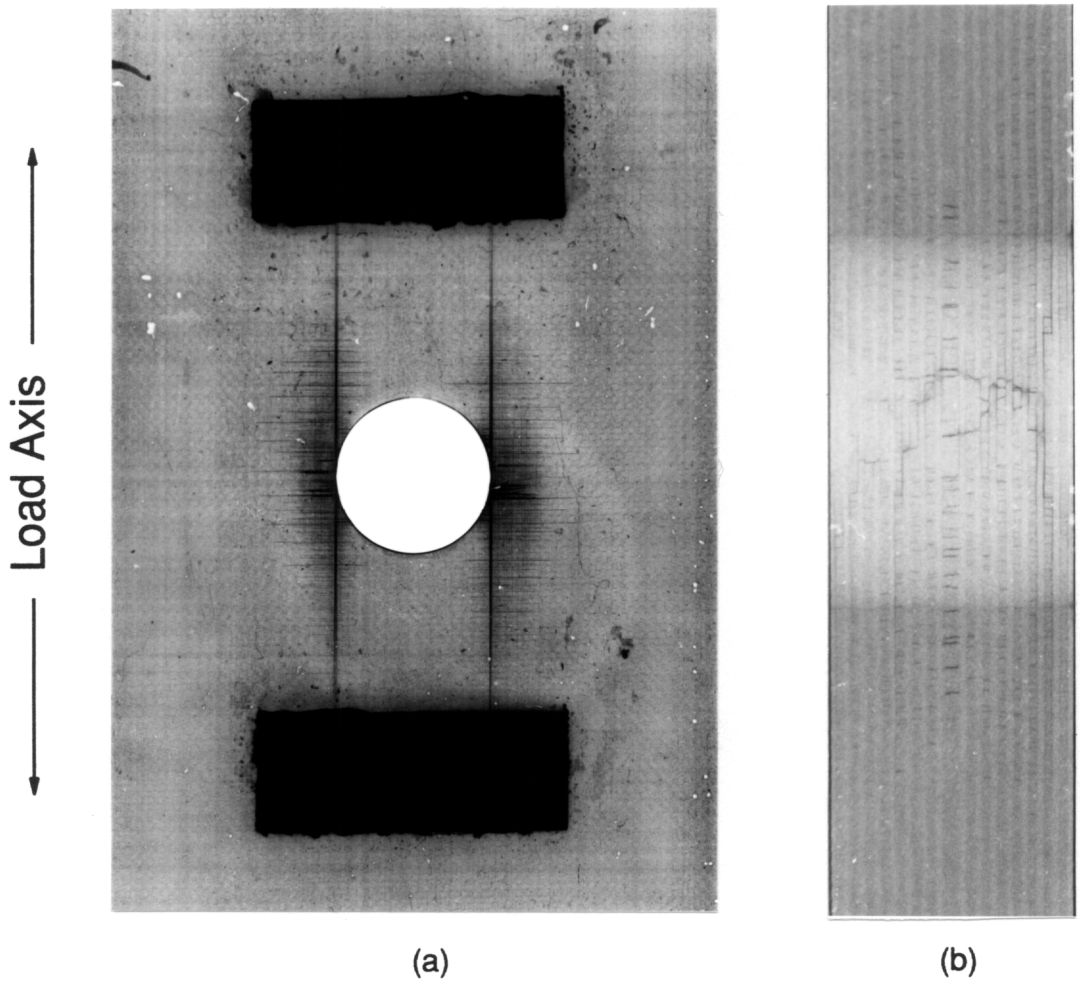

Figure 37. X-ray Radiograph of an 820A Specimen after 30,000 Cycles; a.) Front View, b.) Edge View.

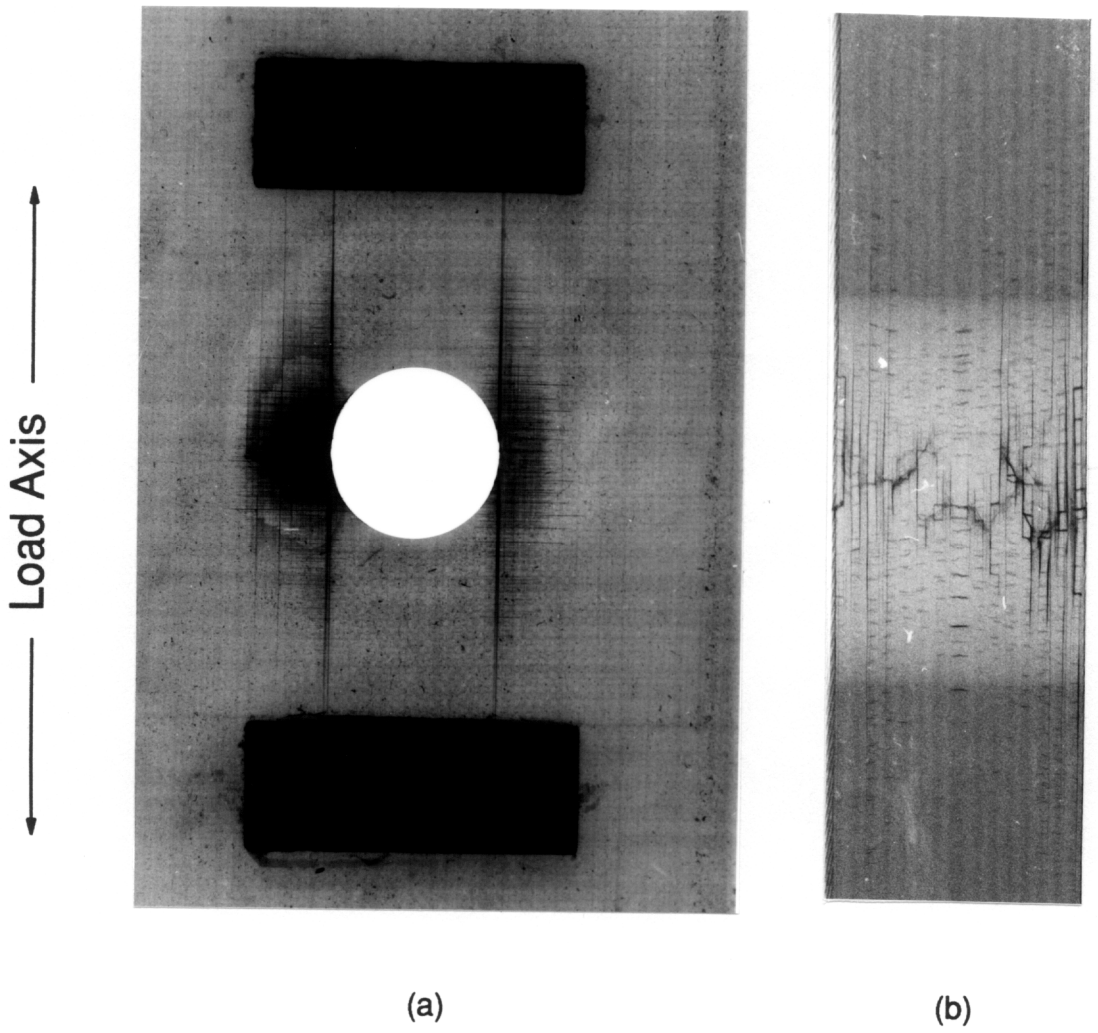

Figure 38. X-ray Radiograph of an 820A Specimen after 19,000 Cycles; a.) Front View, b.) Edge View.

An X-ray radiograph of an 810O specimen that has endured 2.1 million cycles is shown in Figure 39. This is the first instance where no obvious microbuckle failures can be detected on either side of the hole (this is confirmed in the edge radiograph). It is arguable whether the 90° crack in the upper right-hand quadrant of the hole that has spawned a longitudinal split is a microbuckle; if it is, it has been effectively blunted. The longitudinal splits extend all the way to the grips, and the 90° matrix cracks that originally intersected these splits have grown to the edge of the specimen. Delaminated regions appear in areas that have the highest density of cross-cracking. It appears that delamination would have to ultimately separate this specimen into sub-laminates before it would fail.

The damage state in Figure 39 is to be contrasted to the damage state seen in Figure 40. In this instance, an 810O specimen has endured 882,500 cycles prior to the test being terminated due to circumstances beyond the operator's control. It appears that microbuckling formations exist encased between longitudinal splits near the hole. For the most part, these microbuckles have been blunted. One major crack formation exists near the top of the hole and runs in the 90° direction towards each specimen edge. The edge radiograph reveals that the outer plies have failed and delaminated.

The results of the X-ray radiography study indicate that the critical damage mechanism for all specimens except 810O is the growth of microbuckling failure. In the 82A, 85A, and 810A specimens, the microbuckling grew quickly and the laminate failed in fatigue after very few cycles. The 820A specimen somehow has been able to delay the growth, either by delaying the initiation of compressive failure or by slowing its growth. It was hypothesized that the stronger interphase of the 820A material — confirmed by both the TFS, $\pm 45°$ tensile strength, and MMHP data — may have played a key role in stunting this growth. Yet, only the results of the TFS could be used to justify this theory when applied to the fatigue life of the 810O specimens. The MMHP and 45TS results do not detect a difference in the bonding condition between the 810A and 810O materials. The TFS does indicate a difference in the interphase strength, yet, the difference is not even as large as the difference seen between the 82A and 810A specimens (which did not manifest itself in dramatically different fatigue lives). Prior to leaving this chapter, an attempt will be made to identify

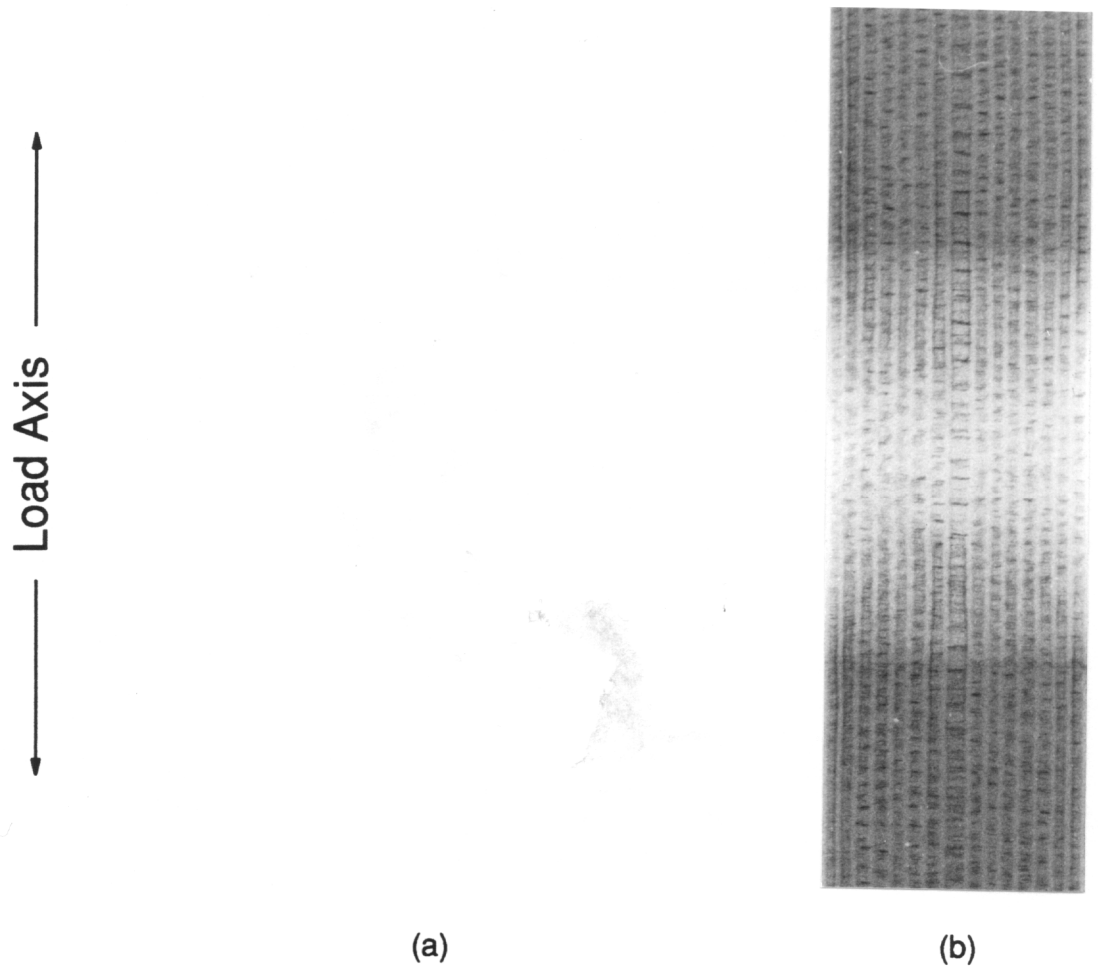

Figure 39. X-ray Radiograph of an 810O Specimen after 2.1 Million Cycles; a.) Front View, b.) Edge View.

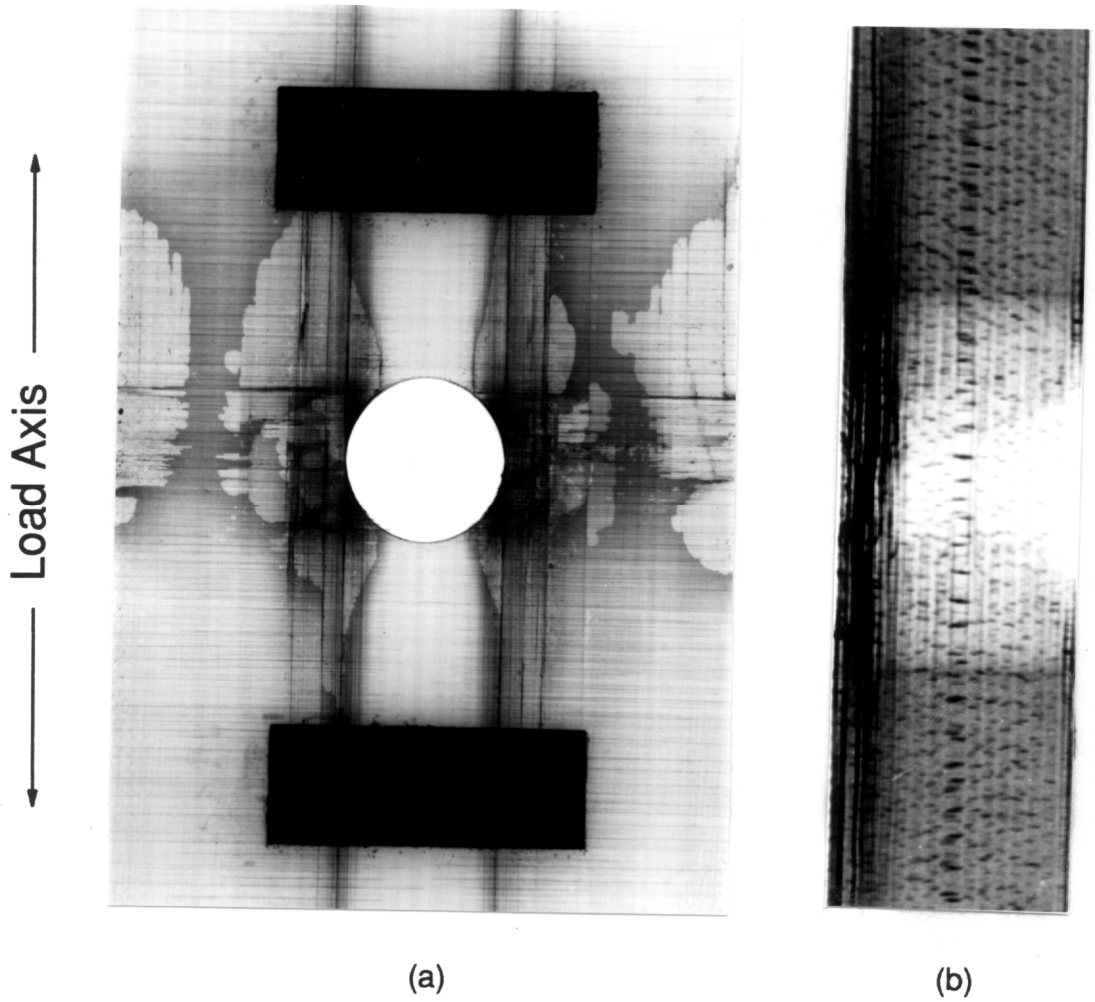

Figure 40. X-ray Radiograph of an 810O Specimen after 882,500 Cycles; a.) Front View, b.) Edge View.

other mechanisms that may be responsible for the staggering differences in the fatigue performance between the 810A and 810O specimens. To this end, other tests have been run in the search to find new clues. The results of these tests and the conclusions drawn will be presented later in the chapter, so that other data may be presented from the other material systems that may also provide answers to these mysteries.

The 5U Series: The cycles to failure for the first two specimens from each material type tested at a maximum stress level equal to 75% of their respective ultimate compressive strength (UCS) are shown in Figure 41. There, again, seems to be a relationship between the cyclic performance of these specimens and their respective levels of surface treatment (or, bond strength). Yet, these differences are not as dramatic as in the 8A&O series. One might infer a slight increase in life, essentially a doubling, when going from the 52U to the 510U specimens. This viewpoint is subject to further scrutiny, however. The increase in life between the 52U and 55U specimens may simply reflect the small sample size. The increase in life between the 55U to 510U specimens could be attributed to the fact that the 510U specimen endures a lower applied stress, due to its lower notched cross-plied compressive strength. Overall, though, one should be alerted to the fact that these materials have displayed lives in the 100,000 to 200,000 cycle range, despite sustaining higher applied stresses. The 510U specimens (carrying the lowest applied stress in the 5U series) must endure an increase of 26% in the applied stress over the 8A&O specimen that displays a similar magnitude of life (the 820A specimen). Thus, as a general rule, the 5U series materials perform better under an applied load equal to 75% of its ultimate compressive strength than the 8A&O series materials that are surface treated at levels of 20%, 50%, and 100%. An appeal is made to the damage states to help explain this trend.

Figures 42-44 display the damage state of a 52U, 55U, and 510U specimen, respectively, fatigued to approximately equal stages of life (as determined by stiffness drop or temperature rise — see later sections detailing this procedure). The radiograph of a 52U specimen found in Figure 42 was taken after 70,000 cycles (hence, around 70% of expended life). The longitudinal splits have grown well beyond the 1″ gage length. Transverse (90°) matrix cracks have grown off of the longitudinal splits

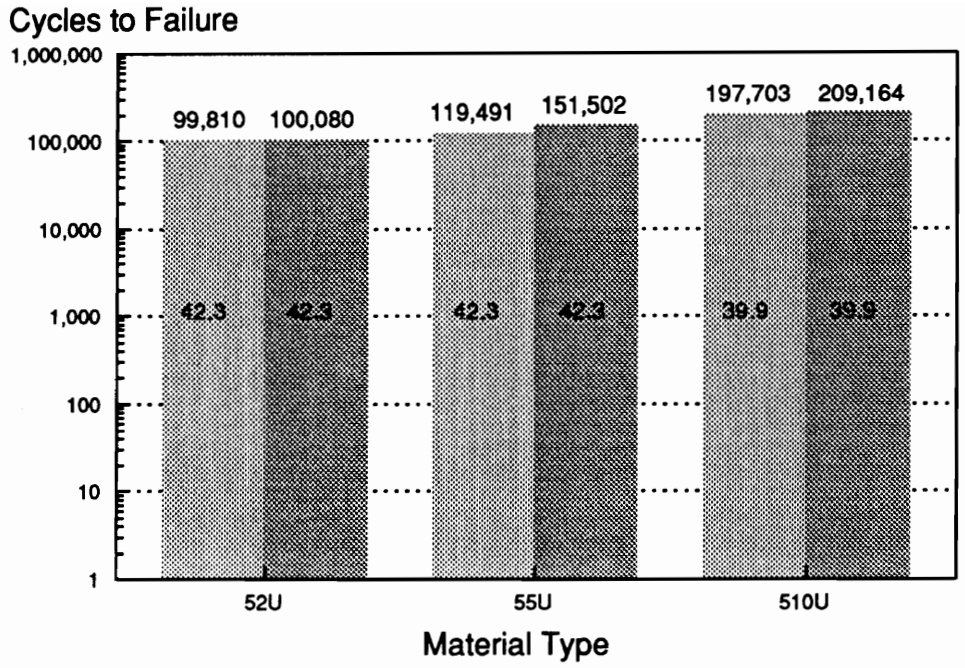

Figure 41. Cycles to Failure of the Notched Cross-plied Specimens in the 5U Series; Max. Applied Stress = 75% UCS; R = -1 at 10 Hz.

and, in some cases, have reached the edge of the specimen. The grids formed by the longitudinal splits and transverse cracks have spawned delaminated regions. No microbuckles are apparent anywhere in the radiograph. It is unclear what damage mechanism is responsible for the final failure of this specimen.

The damage state of a 55U specimen cycled to 100,000 cycles is shown in Figure 43. This radiograph is nearly indistinguishable from the radiograph of the 52U specimen shown in Figure 42. The only obvious difference exists in the of the amount of transverse matrix cracking. It appears in the 55U specimen that a number of 90° cracks have initiated from the edge and end up joining cracks that have initiated from the longitudinal splits. The damage state from the 510U specimen is seen in Figure 44. This specimen had reached 136,100 cycles before this radiograph was taken (again, nearly 70% of its cyclic life). As before, there is nearly no detectable difference between this damage state and the previous two. Perhaps a higher density of transverse cracks may be present. Yet, it is unlikely that anyone could identify the specimen type solely by the record of its damage state. This partially explains the relative agreement in cyclic life between these three systems. It also indicates the fundamental difference between the performance of the 8A&O and 5U material series (when compared at equal levels of applied surface treatment): the 5U series, possessing the higher notched cross-plied compressive strength of the two series, performs better under an applied load level equal to 75% of it UCS, due largely to the absence of microbuckling failure. In an earlier section, it was hypothesized that differences in fiber diameter and, possibly, intrinsic fiber compressive strength, led to differences in the notched and unnotched cross-plied compressive strengths between the 5U and 8A&O material series. These claims are applicable to the present argument. Given the same matrix system serving as support to the fibers, the larger fiber diameter serves to resist bending and buckling. If the fibers are assumed to be initially misaligned, a higher compressive strength fiber will survive greater deformation, and, therefore, higher loads prior to failure.

Before leaving this sub-section, a question may linger as to what is the predominant damage mechanism that ultimately causes failure in the 5U materials. The radiograph in Figure 45 shows a 510U specimen at 183,400 cycles. This specimen was interrupted just prior to final failure. A

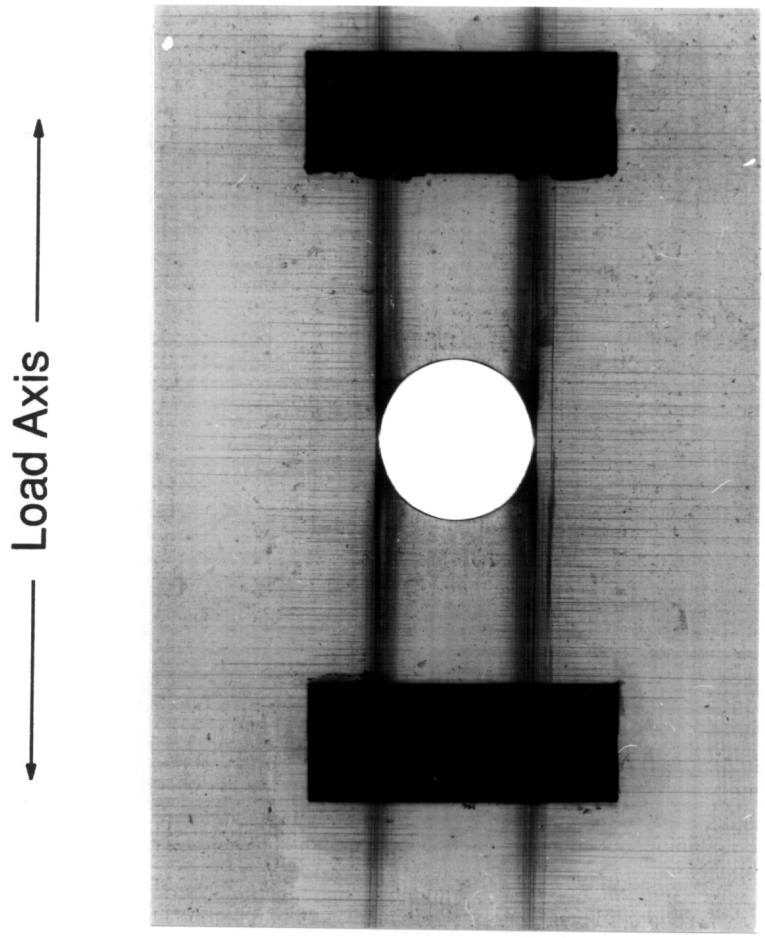

Figure 42. X-ray Radiograph of a 52U Specimen after 70,000 Cycles.

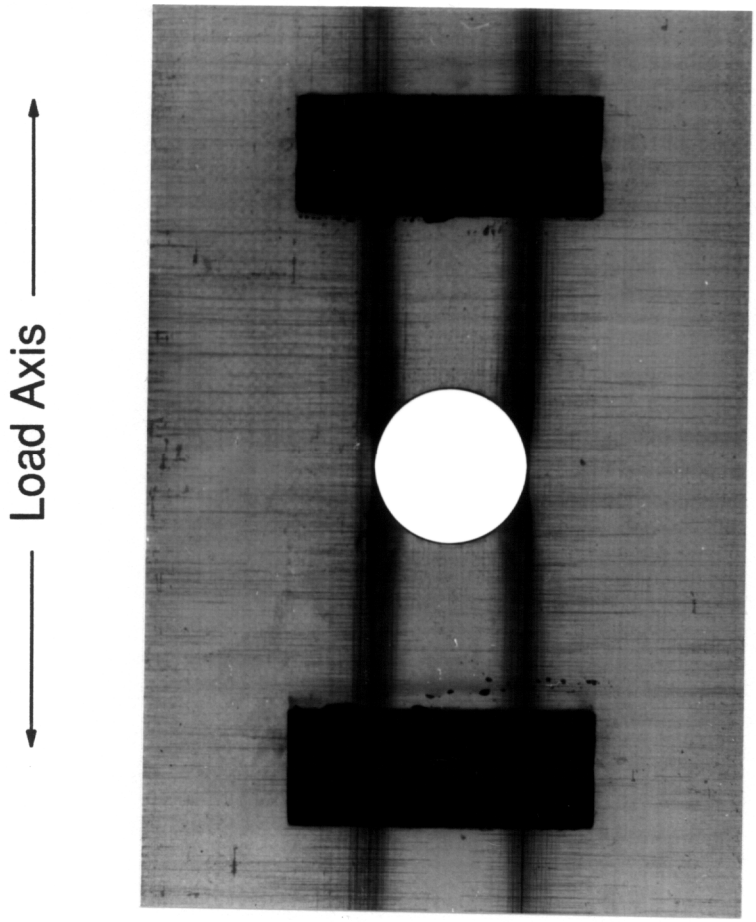

Figure 43. X-ray Radiograph of a 55U Specimen after 100,000 Cycles.

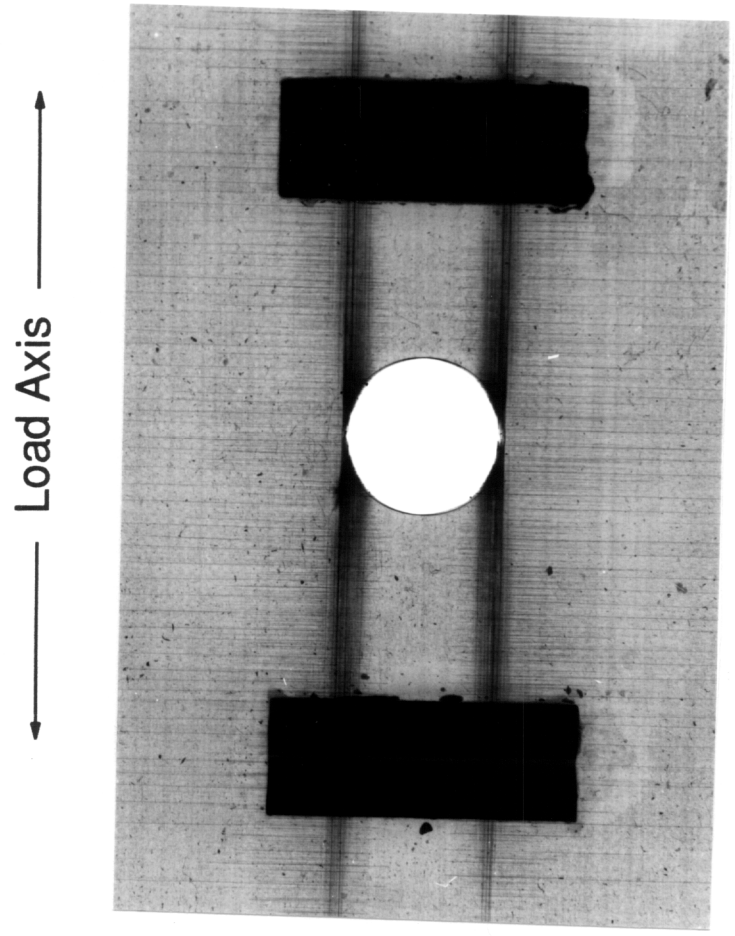

Figure 44. X-ray Radiograph of a 510U Specimen after 136,100 Cycles.

large band of compressive damage has grown across the specimen. One can see the progression of the growth by the presence of the longitudinal splits near the origin of the growth. Delamination has encased the area. It appears that the microbuckle grew off of a longitudinal split rather than from the hole. This is not that surprising, since no microbuckle growth has been seen near the hole in the three previous radiographs. The long longitudinal split growth seen in the three previous radiographs tended blunt the global stress concentration, creating two parallel ligaments separated by material above and below the hole. This failure scenario lends credence to the hypothesis that steady degradation of the compressive support (which may be the interphase) limits the life of these (generally strong-bonded) composites. Material with extremely weak bonding will be addressed below.

The Northrop Material Systems: The representative fatigue life for each material type supplied by Northrop is shown in Figure 46. Each specimen was cycled at a maximum stress level equal to 75% of their respective ultimate compressive strength (UCS). Each material series will be addressed sequentially, making necessary comparisons where appropriate.

One's immediate reaction to the short fatigue lives of the 3NN specimens is that this material is clearly inferior to its surface treated counterpart. Yet, this assessment deserves further scrutiny. The 3NN material endured the highest maximum stress level of *any* of the fourteen material systems, meaning, of course, that it possessed the highest notched cross-plied compressive strength. Its applied stress level is 11% higher than its counterpart, also the largest disparity among all of the material systems. The two cyclic lives were longer than one of the 82A specimens, even though the applied stress was *61% higher* than the 82A's stress level. This is the most obvious instance where choosing to fatigue at a percentage of ultimate compressive strength complicated the interpretation of the results. Fatigue performance is a function of how the stress level compares to the ultimate stress of the material *and* (at the very least) a function of the *absolute* stress level. If one wishes to simply compare the 3NN material vs. the 3SN material on the basis of their response to an applied stress equal to 75% of their respective UCS, then, clearly, the 3SN performs better. It might be (as could be said for all fourteen systems) that the 3NN's notched cross-plied compressive strength was

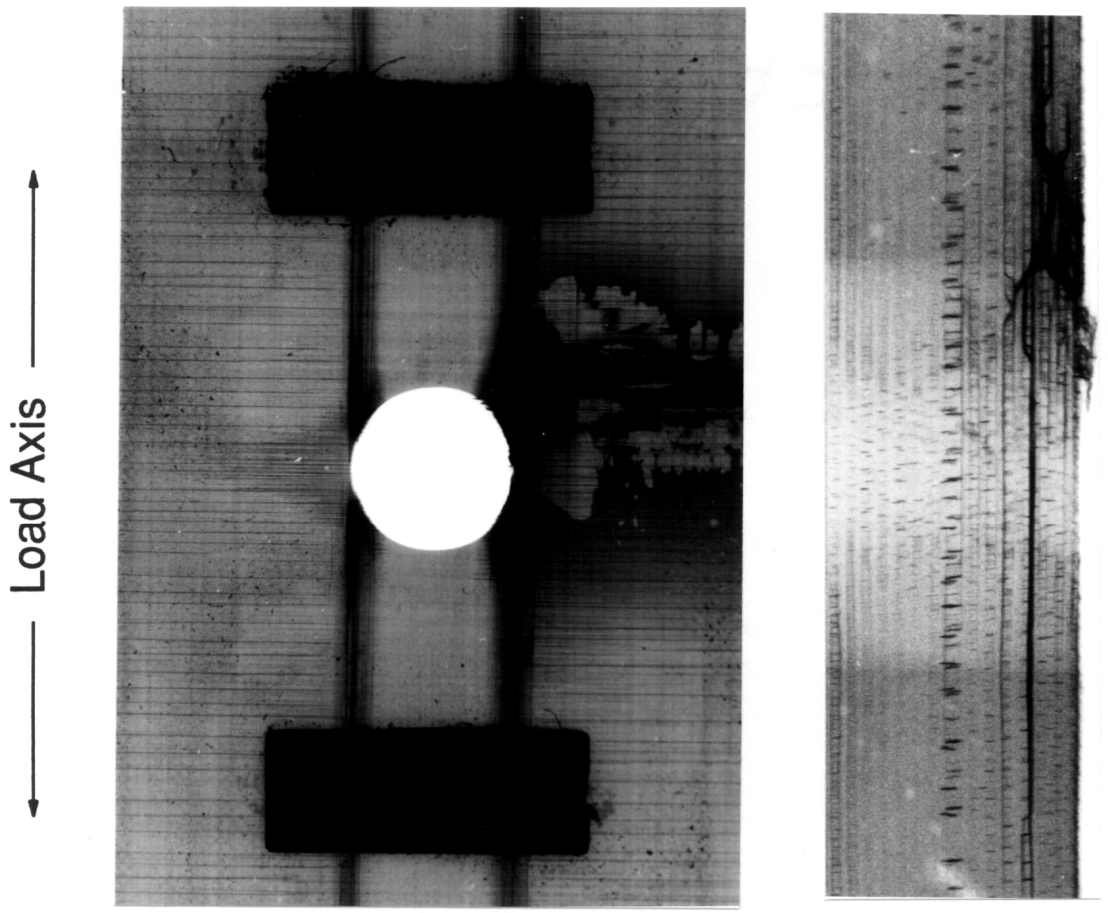

Figure 45. X-ray Radiograph of a 510U Specimen after 183,400 Cycles; a.) Front View, b.) Edge View.

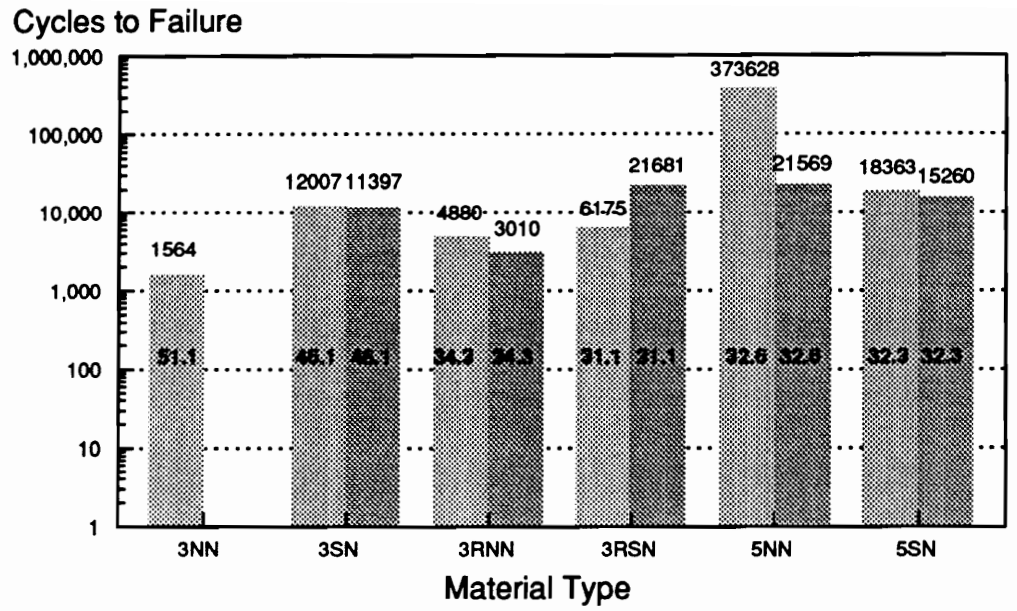

Figure 46. Cycles to Failure of the Northrop Notched Cross-plied Specimens; Max. Applied Stress = 75% UCS; R = -1 at 10 Hz.

not well characterized. There might be some truth to this, even though the two 3NN specimens tested to failure had strengths that deviated less than 5% from one another. When each of the fourteen specimens had their notched cross-plied compressive strength divided by their unnotched cross-plied compressive strengths, the 3NN system had the largest ratio by far, leading one to believe that the notched strength was unusually high (or, the unnotched strength was unusually low). In an attempt to remedy the difficulty in getting a direct comparison between the 3NN and 3SN systems, several 3NN specimens were run at the same applied stress level used in the 3SN tests. A sampling of three specimens yielded lives of 7778, 25,994, and 14,867 cycles. Due to the spread in this data, these points indicate that this performance is comparable to the performance of the 3SN specimen. It should be mentioned that the lack of agreement between these three points may be attributed to the fact that these specimens came from different panels. Though the cure cycle was followed indentically for each panel, subtle differences do exist, especially in the amount of resin flow and bleeding. If these differences are detected in the C-scan inspection, then further comparison is avoided by discarding the inferior material. Yet, differences caused by such parameters as resin flow, etc., may go undetected and, ultimately, introduce spread in the data. The 3SN and 5SN systems were the two material types produced from 12″ tape; therefore, all of the specimens tested from these material types came from the same panel. Notice in Figure 46 how little spread these two systems revealed. Unfortunately this must be considered when interpreting the results of materials made with the 6″ tape. Every precaution was taken to minimize these effects, however.

Despite these caveats, it is still surprising that the 3NN and 3SN systems displayed similar fatigue lives. It is obvious from the TFS and MMHP data that the bond condition is very different between the two. Perhaps the applied stress level is so high (even at 46.1 ksi — the second highest applied stress level in this study) that the mechanisms that would normally separate the response of these two systems cannot come into play. To test this hypothesis, the damage states of each material type were examined via X-ray radiography (under equal applied stress levels). Figure 47 shows a front and edge X-ray radiograph of a 3NN specimen after 7000 cycles of fatigue, while Figure 48 shows a front and edge radiograph of a 3SN specimen after 6900 cycles of fatigue. While the two radiographs look very similar, interesting differences should be noted. The length of the

longitudinal splits in the 3NN material are noticeably longer. Since the 3NN bond strength (as determined by TFS) is weaker, this result is not surprising. Notice, also, the presence of microbuckling on both sides of the hole in Figure 47. These microbuckles, as in the late-life 510U specimen (Figure 45), apparently originate off of longitudinal splits. Yet, both microbuckles have been blunted by longitudinal splits that have emanated from the tips of the microbuckles. No such formations are seen in the 3SN radiograph located in Figure 48a.

A radiograph of a 3NN specimen (under the same applied stress level as the 3SN specimens) near failure (in this case, 12,300 cycles) is shown in Figure 49. This damage state is similar in many ways to the final damage state of the 510U specimen (see Figure 45). A band of compressive failure has reached an edge of the specimen, indicating imminent demise. The main difference between the two late-life damage states (Figure 49 and Figure 45) is the extent of delamination accompanying the compressive failure. One of the findings in the present study is that weak bonding manifests itself as poor delamination resistance. In Figure 45, the band of compressive failure has produced only a modicum of delamination. Yet, in Figure 49, the growth of the compressive failure has produced delamination that runs the length of the specimen. This is definitely a detriment to the life of the weak-bonded specimens; delamination is a bane to compressively-loaded structures.

It appears from Figures 47 and 48, and other radiographs of these two materials, that the main difference in the response lies in the initiation and growth of microbuckling failure. The 3NN specimen seems to grow microbuckles early and have them blunted by longitudinal splits. Apparently, initiation of microbuckles occur late in the life of the 3SN material, and quickly grow to catastrophic proportions. The growth of the existing microbuckles in the 3NN material seems to occur more gradually due to its ability to blunt the growths. This brings up an important point. In these two systems, having this laminate configuration possessing the center-hole geometry (under these applied stress levels), compressive failure is the life-limiting damage mechanism. *At another applied stress level* it is likely that another damage *sequence* takes place (this, of course, would be the case if the lamination configuration and/or the specimen geometry changes). Thus, while it just so happens that the 3NN and 3SN materials reveal similar lives under these circumstances, it may be purely coincidental. In other words, if the applied stress level was lowered, there is good reason

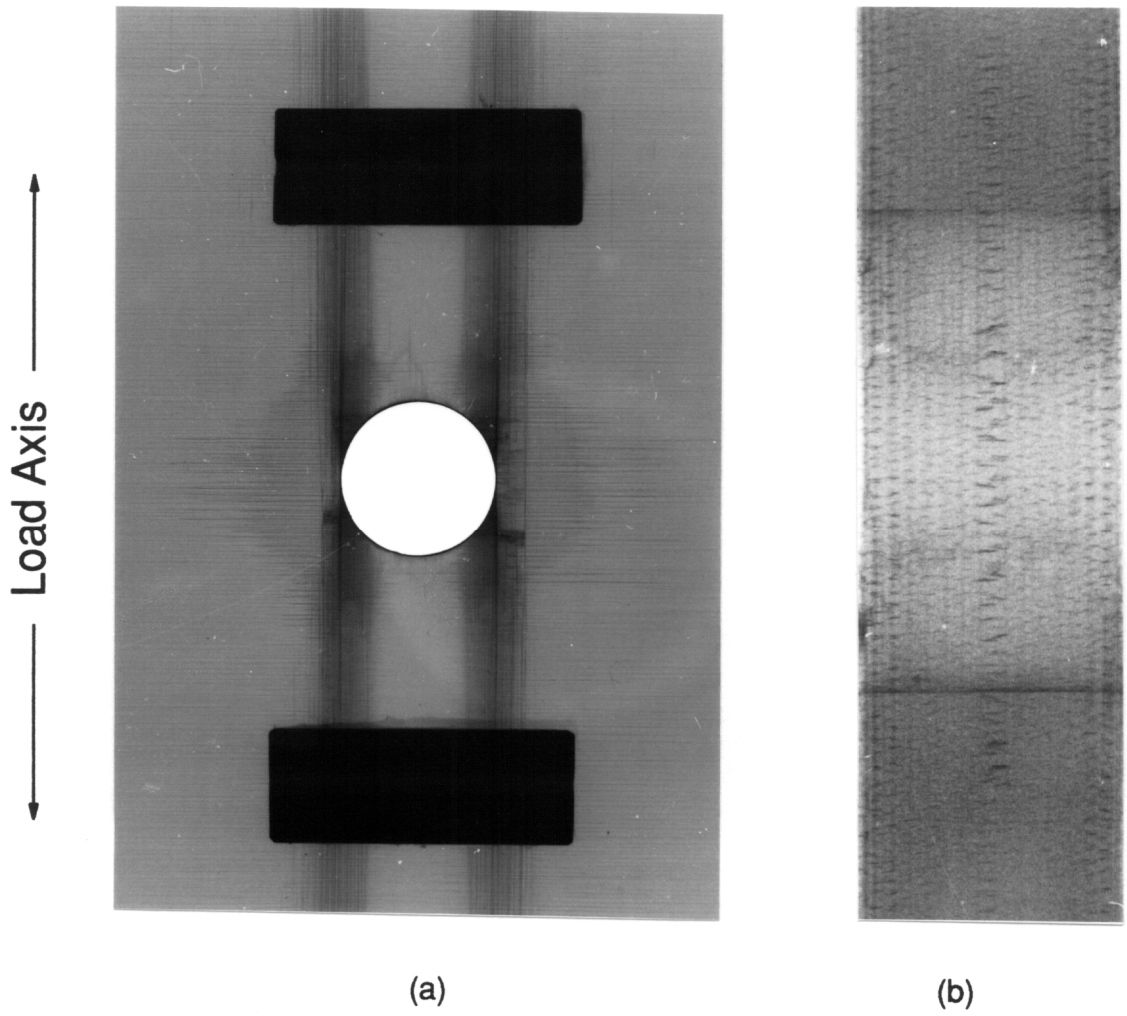

Figure 47. X-ray Radiograph of a 3NN Specimen after 7000 Cycles; a.) Front View, b.) Edge View.

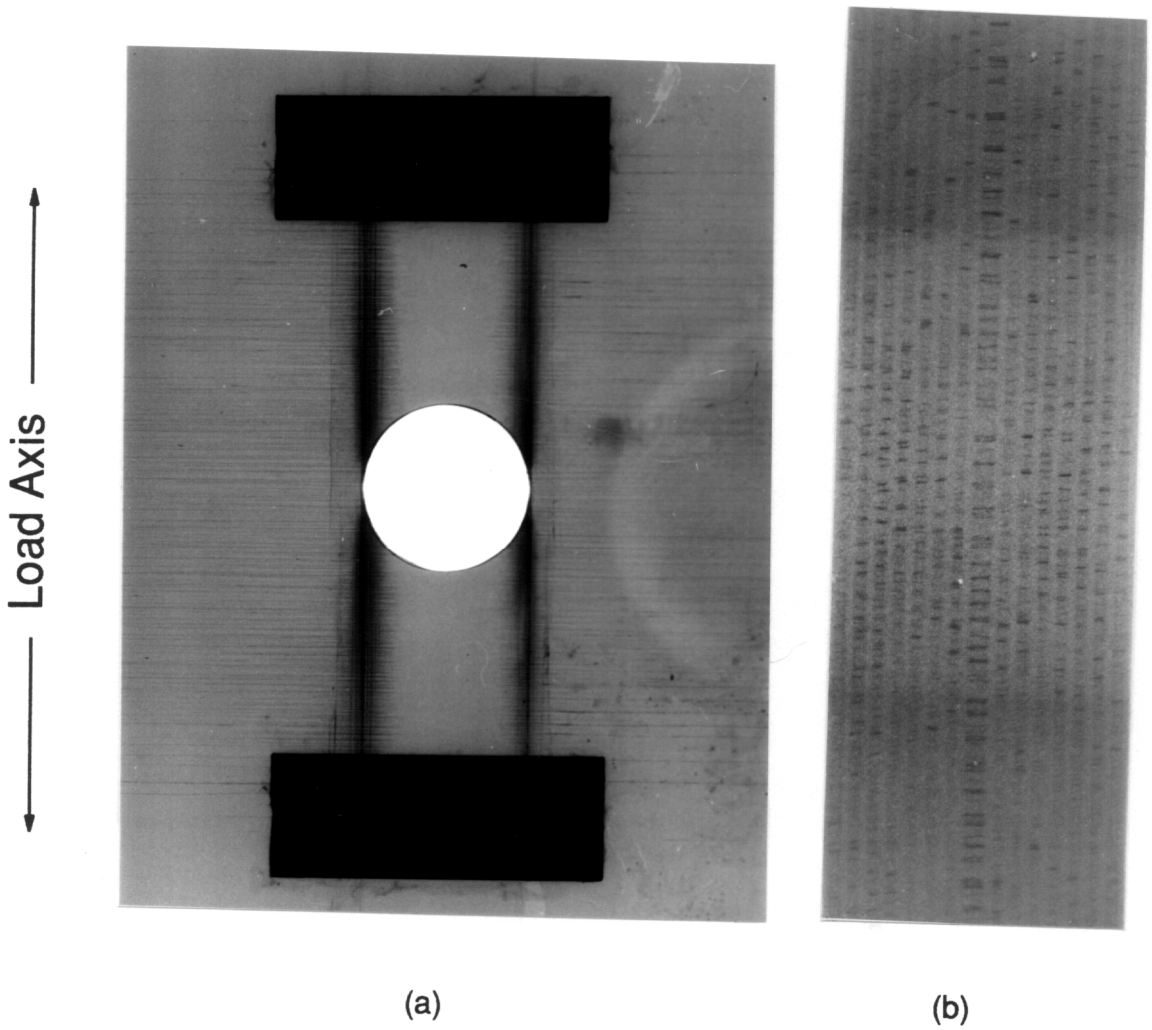

Figure 48. X-ray Radiograph of a 3SN Specimen after 6900 Cycles; a.) Front View, b.) Edge View.

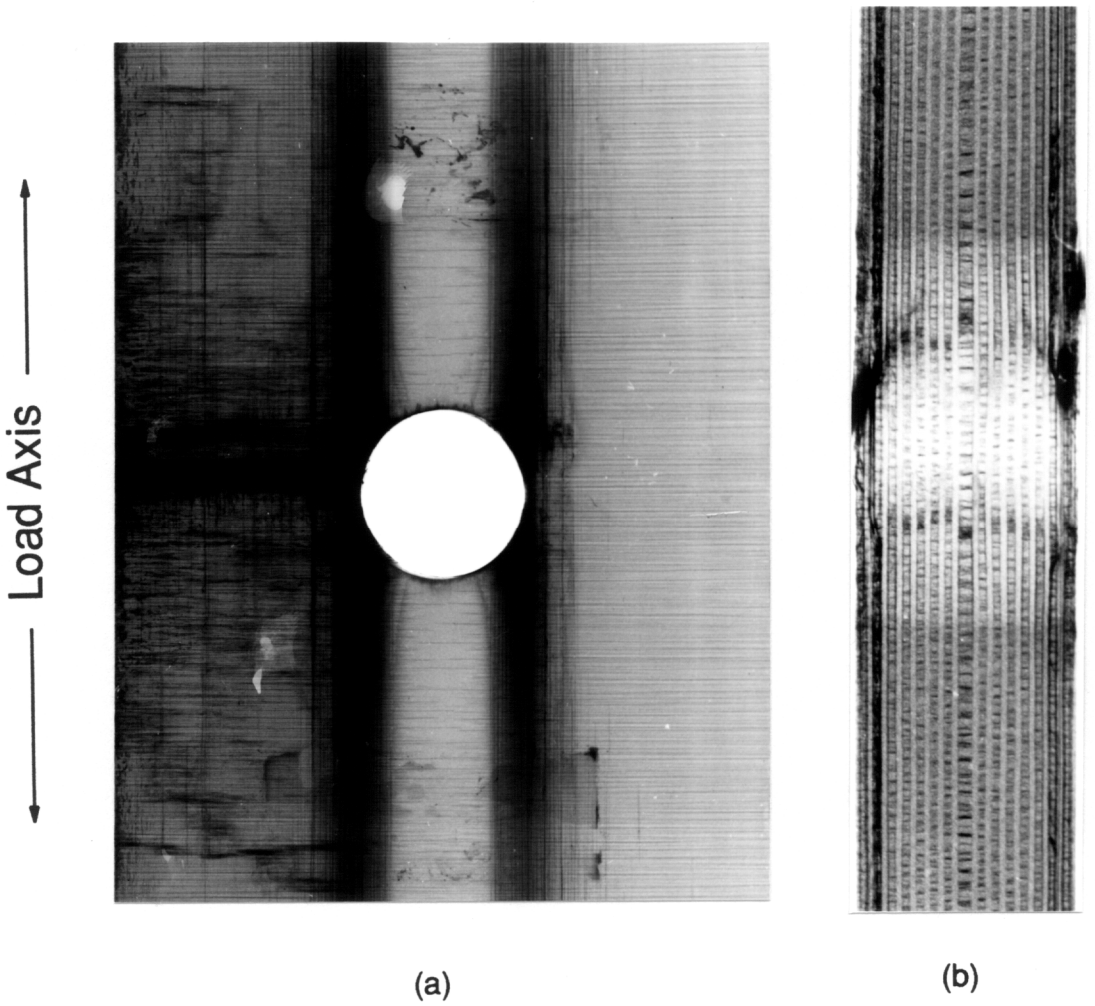

Figure 49. X-ray Radiograph of a 3NN Specimen after 12,300 Cycles; a.) Front View, b.) Edge View.

to believe that the performance of these two materials would diverge. This generalization applies to all of the materials studied in this investigation.

In trying to compare the fatigue lives of the 3RNN and 3RSN (the systems possessing the thermoplastic matrix), one again suffers from differences in the applied stress level (as a result of differences in the notched cross-plied compressive strength). The applied stress level of the 3RNN material is 10% higher than its surface treated counterpart. Another unfortunate result that hampers a direct comparison between the two fatigue lives, is the noticeable spread in the 3RSN data. In order to represent the material system fairly, one specimen was taken from two panels (true, also, for the 3RNN material). This may explain *some* of the discrepancy.

Front and edge radiographs of a 3RNN specimen fatigued to 2200 cycles are shown in Figure 50, while front and edge radiographs of a 3RSN specimen fatigued to 5500 cycles are shown in Figure 51. These comparative damage states are somewhat reminiscent of the 3NN-3SN damage states. The most striking feature of the two radiographs is the high density of cross-cracking. It is argued that this cracking is *not* a result of mechanical loading, but rather, the result of thermal loading. Recall that the thermoplastic composites were processed at 650°F. If this is considered the stress-free temperature of the laminate, then the laminate experiences a change in temperature of nearly 580°F. The contraction that would be associated with such a dramatic change in temperature is constrained in both directions by the cross-ply laminate. As a result of this constraint, tensile cracking occurs along the length of the fibers, likely at the fiber/matrix interphase (this phenomena has been observed for other composite material systems [80]). One must wonder if this damage has degraded the interphase prior to the introduction of load. Realize, also, that the measures of bond strength quoted in this study were obtained from unidirectional material. This unidirectional laminate configuration will not possess the same propensity for thermal cracking, since no off-axis lamina exist that might resist the transverse thermal contraction. For that matter, one would expect large *compressive* radial stresses at the interphase (in the unidirectional material) due to the effects of thermal contraction. This may explain, in part, the huge TFS strength in the 3RSN material (but fails to explain the low strength of its 3RNN counterpart).

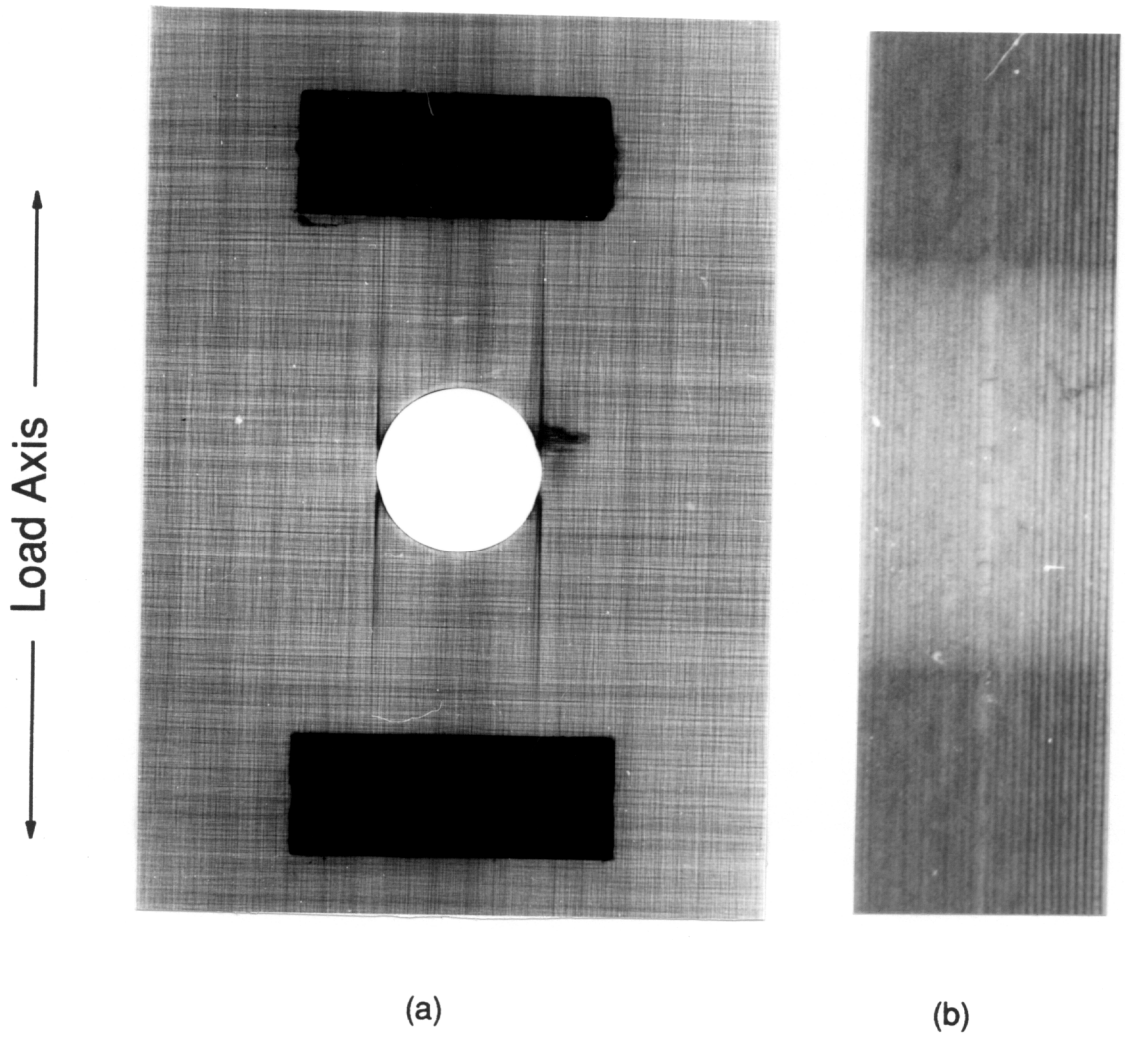

Figure 50. X-ray Radiograph of a 3RNN Specimen after 2200 Cycles; a.) Front View, b.) Edge View.

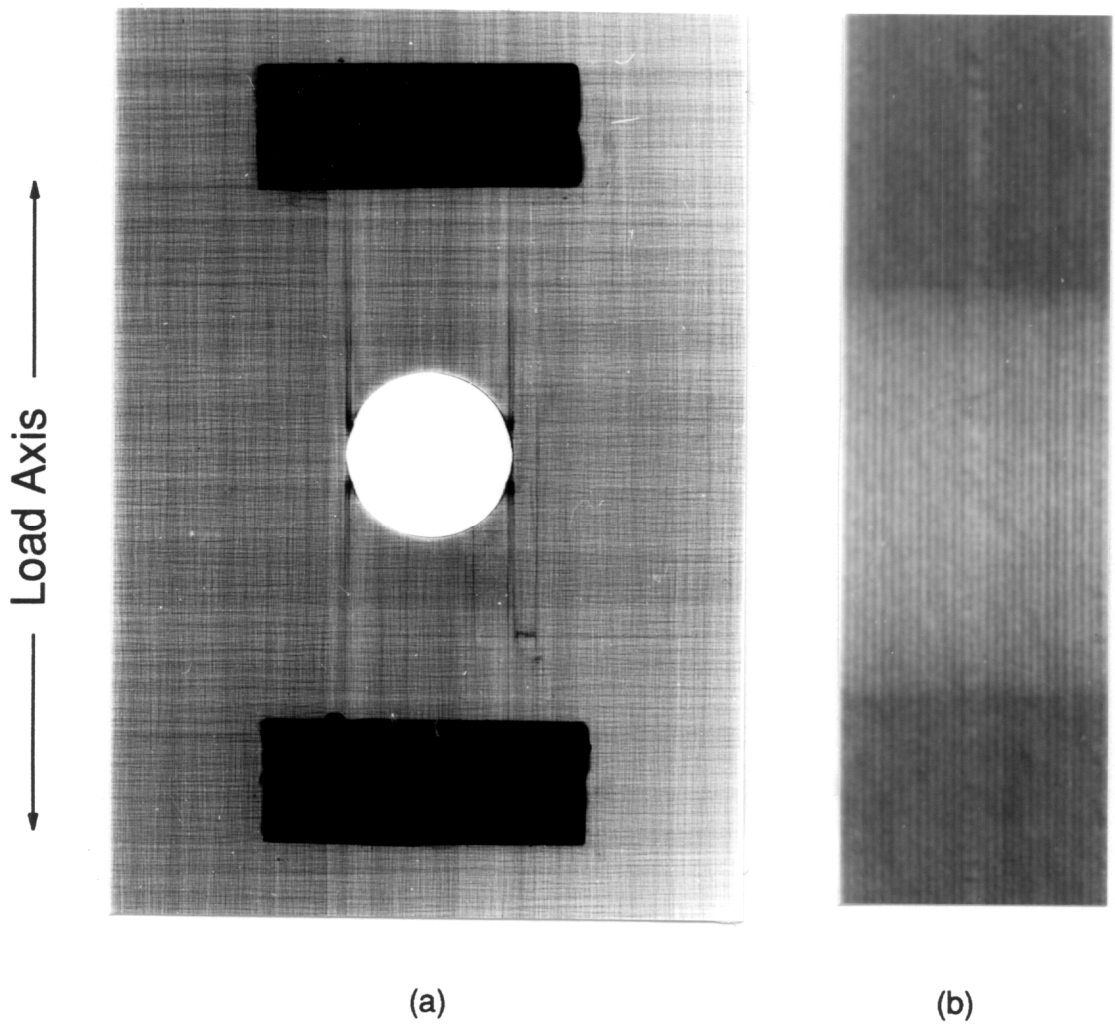

Figure 51. X-ray Radiograph of a 3RSN Specimen after 5500 Cycles; a.) Front View, b.) Edge View.

Referring back to the radiographs, there is an obvious resistance to longitudinal splitting, apparent more in the 3RNN specimen than in the 3RSN specimen. A microbuckle has formed in the upper right-hand quadrant of the hole in the 3RNN specimen. This formation is clearly seen, via visual inspection of the specimen, as a "puckered" line of material on the outer surface. In contrast to the 3NN material, there seems to be no tendency for this 3RNN specimen to form longitudinal splits off of the tip of the microbuckle. This is somewhat unexpected, since both TFS and MMHP results categorize the interphase of the 3RNN material as weaker than the 3NN material. The 3RSN radiograph (Figure 51) reveals a small region of microbuckling that has formed off of the longitudinal split. Unlike the 3RNN specimen, though, a split has formed off of the tip of the microbuckle. Since these materials have displayed the greatest disparity in bond strength (according to the TFS) results, it is surprising that the 3RSN material displayed a propensity to form longitudinal splits, yet, because of the thermal cracking, it is unknown what the nature of the interphase is in this material system.

The most noteworthy aspect of the 3RNN and 3RSN data is their relatively poor cyclic performance as compared to the other systems studied thus far. It was obvious that the 5U system performed better than the 8A&O material (comparing equal applied surface treatment levels), since it displayed longer lives under considerably higher applied stresses. One explanation for this behavior focused on the role of the larger fiber in the 5U series as a means of delaying microbuckling failure. The 3N series was found to have a a shorter life than the 5U series (at an applied stress level of 75% UCS), yet, the applied stress level was 15% higher in the 3N series. It stands to reason that the performance of the two systems possessing the 7 micron fiber (the 5U and 3N series) was somewhat similar. The 3RN series, on the other hand, though comparable in its response to an applied stress level of 75% UCS, performs in the same league as the 100% surface treatment level-and-below systems in the 8A&O series *despite having a 7 micron fiber.* The applied stress level of the 3RSN material is comparable to the 810A material, while the applied stress level of the 3RNN material is comparable to the 85A material. Both sets of cyclic lives are also comparable. This realization establishes the role of the matrix material within the fatigue process. It is unclear what specific property of the thermoplastic matrix is responsible for the poor performance (or, what

combination of properties are responsible). It is likely that the thermoplastic matrix provides less shear support to the fiber than would an epoxy. This theory receives some validation in the unnotched unidirectional compressive data obtained by Northrop [39]. The 100% surface treated/unsized "3" fiber in the Radel-X matrix displayed a compressive strength that was 61% of the compressive strength of the composite made using the same fiber in the ERLX-1901 epoxy matrix.

The fatigue lives of the two 5NN specimens are an order of magnitude different. This would be extremely troubling if these two specimens had come from the same panel; they did not. Yet, it is bothersome that such spread is seen in the same material system since this tends to cast doubt on the quality of the other data. Other specimens were run from the same panel that produced the specimen displaying the long life. One such specimen was terminated at 112,000 cycles in order to record the radiograph seen in Figure 52. The 5NN system is an exceptional system due to its extremely low interphase strength. It is unknown if this contributes to its difficulty in creating panels with uniform properties, or, if this was clearly the fault of the material processors. One can seek some solace in the realization that this material serves only as a laboratory oddity and not as an marketable product. While the spread of data is unfortunate, it *must* be considered within the context of this highly specialized and highly unpredictable material system.

Fortunately, the 5SN specimens' fatigue lives reveal a good degree of reproducibility. Despite the large spread in the 5NN material, it still remains true that the 5SN lives are shorter. It will be necessary to appeal to the radiographs in an attempt to explain this behavior.

The most striking feature of the radiograph seen in Figure 52 is the preponderance of longitudinal splits away from the hole boundary. These splits arise due to mechanical loading, not thermal loading (this was verified by taking a radiograph of a virgin specimen). The presence of these splits is convincing proof of how truly weak the bonding is. These splits occur due to the transverse stresses that arise in the 0° plies as a result of their inability to experience Poisson's expansion and contraction (because of the presence of the 90° plies). One can see multiple regions of microbuckle formation on each side of the hole. In each case, these microbuckles have been blunted by longitudinal splits that have formed at their tips. It is likely that the gross delamination

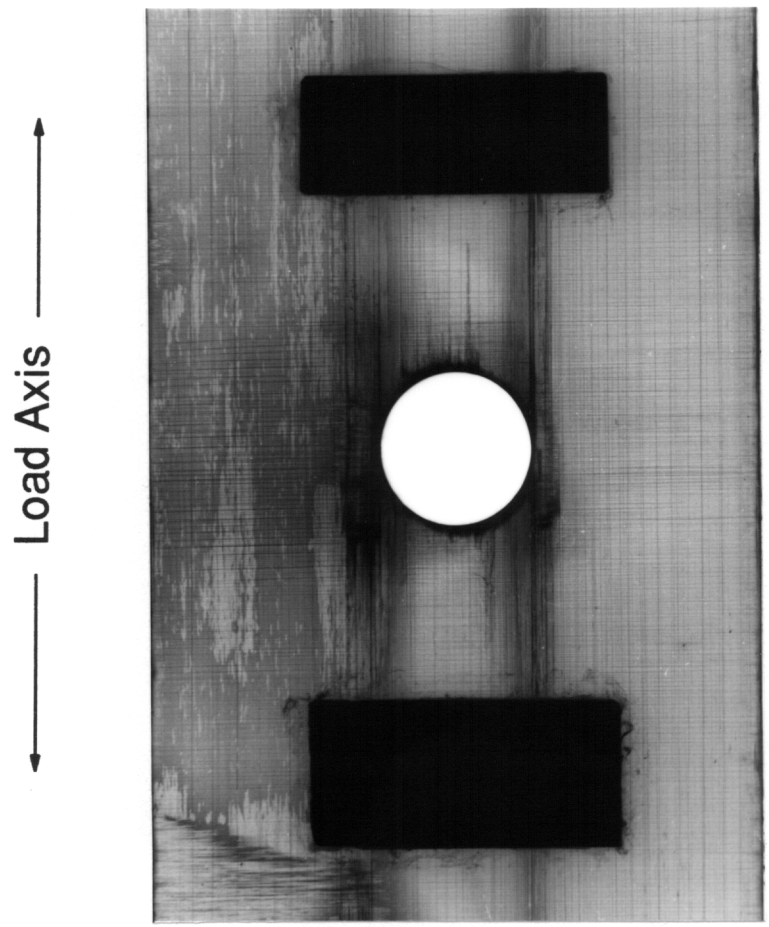

Figure 52. X-ray Radiograph of a 5NN Specimen after 112,000 Cycles.

seen on the left side of the specimen is the result of the microbuckle formation. It is probable that the delamination will cause the outer 0° plies to become very susceptible to buckling.

The radiograph seen in Figure 52 is to be contrasted to the radiograph of a 5SN specimen that has failed after 15,200 cycles of fatigue (see Figure 53). An interesting feature of this damage state is the delamination region that surrounds the compressive failure. It appears that the shape of the delamination has been dictated by the length of the longitudinal splits. The splits were probably produced at the tip of the microbuckle. As the microbuckle(s) grew, new splits formed while existing longitudinal splits increased in length. It seems that the upper and lower boundary of the delamination "connects" these split ends. The right-hand longitudinal boundary of the delamination may signify the length of the microbuckle prior to unstable growth towards the specimen's edge. It should be noted that outside this delaminated region, no longitudinal splits occur except for the two splits tangent to the hole. Microbuckles grew in this specimen just like in several of the 8A&O specimens. The 5SN radiograph looks very similar to the late-life 820A radiograph (Figure 38) — only nearer to failure. It appears, however, that the damage occurring in 820A specimen has been intensified; few transverse cracks are apparent beyond the immediate region of the hole. Bakis, *et al.* [50], have indicated that, within a notched structure, resin toughness tends to concentrate damage onto critical elements. The 82A, 85A, and 810A specimens tended to have slightly shorter lives than the 5SN specimens (under comparable applied stress levels). By considering the differences in bond strength (from the TFS and MMHP tests), it may be that the pattern of damage intensification attributed to resin toughness should be, instead, attributed to interphase strength.

Normalized Modulus versus Normalized Life

Plots of normalized modulus versus normalized life served two functions in this investigation. The first function has already been utilized, yet never credited. Experience in composite testing has taught researchers that stiffness monitoring during fatigue loading is an extremely useful tool in estimating a specimen's fatigue life. As damage is introduced into the laminate, certain damage modes

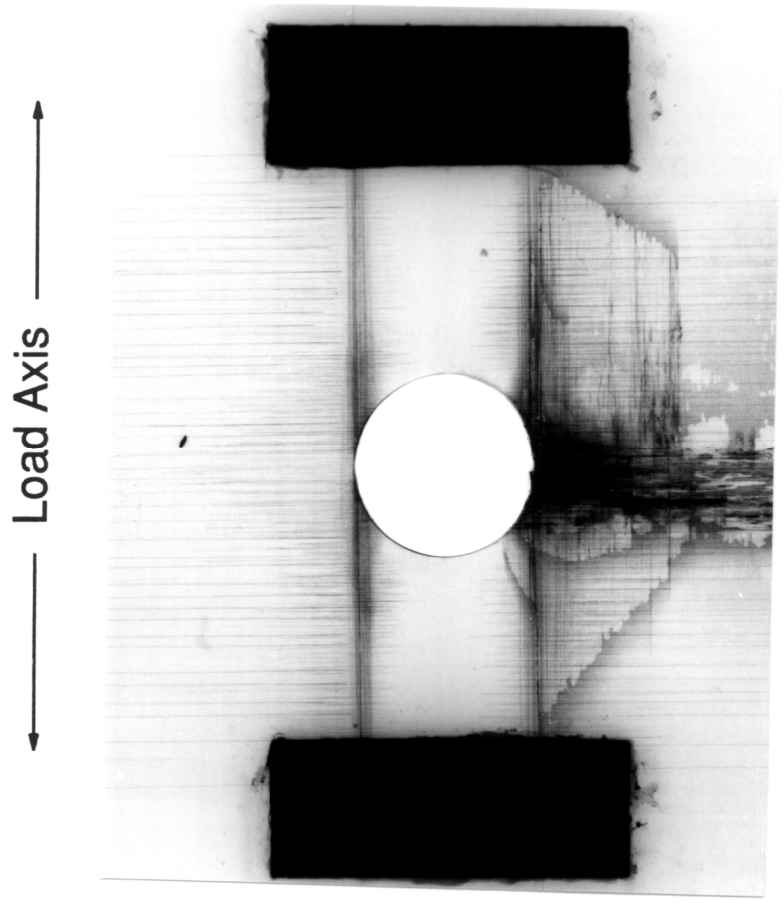

Figure 53. X-ray Radiograph of a 5SN Specimen after 15,200 Cycles.

appear. Each damage mode has an effect on the stiffness. If one has a record of how damage affects the stiffness throughout the life of one specimen, this record will be a fairly accurate predictor of future tests, since the progression of damage — from intiation to final failure — rarely deviates from specimen to specimen (provided the laboratory conditions remain constant). In other words, if one records a total drop of 30% in laminate stiffness just prior to final failure, this number represents the effect of a particular pre-failure damage state on the laminate's stiffness. In most circumstances, another specimen of the same specimen type will experience the same damage mechanisms and arrive at the same damage state as its predecessor, resulting in a total stiffness loss of around 30%.

Proof of this is shown in Figure 54, where the normalized modulus (differentiated from stiffness, since the strain was measured across the hole) versus normalized life for two distinct 510U specimens run under identical conditions is shown. The normalized tensile and compressive modulus of each material was recorded as a function of cycles (details of this procedure are found in the previous chapter). Instead of plotting these results as a function of cycles, the results are normalized by the number of cycles to failure. As shown in Figure 54, the corroboration between distinct specimens is remarkably good. Once such a plot is developed, the test operator can designate a certain "stage of life" that she would prefer to terminate the test. Using Figure 54 as an example, if one wanted to X-ray a specimen after it had expended 70% of its life, she would stop the test after the tensile (or, in this case, compressive) modulus had dropped by approximately 20%. Tests were terminated following this procedure in nearly every instance. In many cases, the author sought to examine the damage state of the material at approximately 70% of its life, in an attempt to record how damage had initiated, and in what form it had progressed. The reader may have noticed that on several occasions radiographs were compared that showed damage states of specimens that had been fatigued to vastly different cyclic times. Hopefully, though, the reader also noticed that the two damage states were comparable. That was the important goal, yet, the detail behind this goal was omitted until now.

The second function served by the normalized modulus vs. normalized life plots will be addressed in this section. Basically, the hope was that this record could reveal information that would separate the responses of the fourteen different systems. In other words, by monitoring modulus,

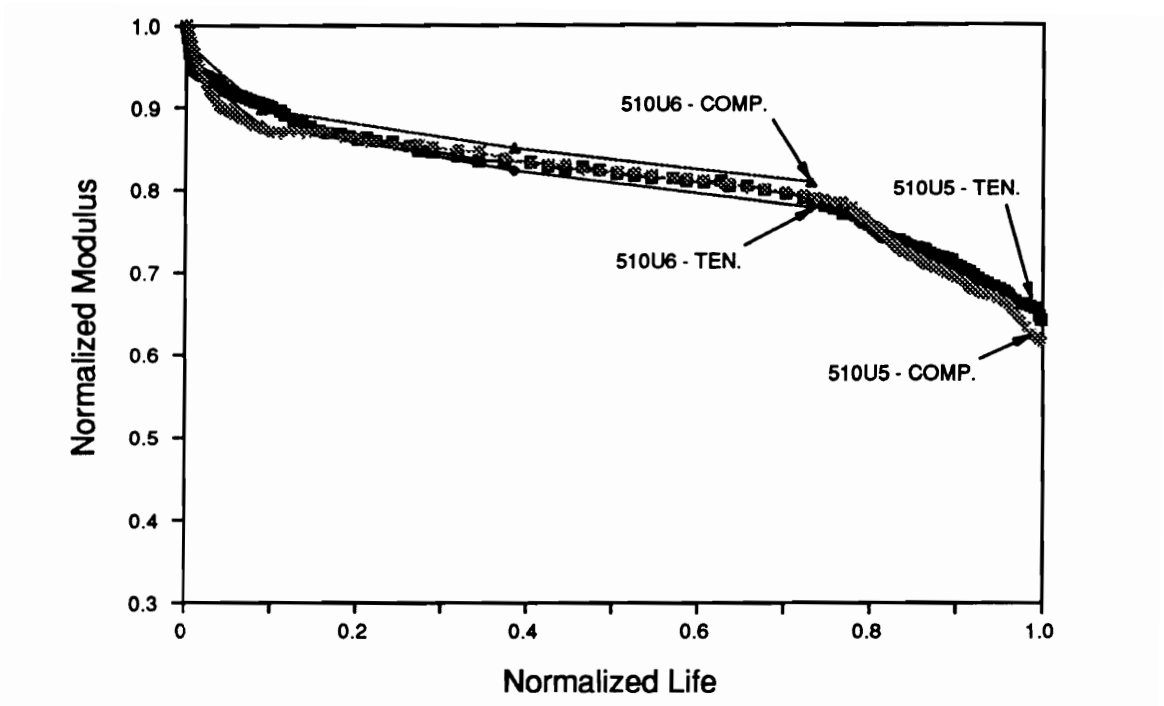

Figure 54. Plot of Normalized Modulus versus Normalized Life for Two 510U Specimens; Max. Stress = 75% UCS; R = -1 at 10 Hz.

one might discern, in a non-destructive manner, subtleties in behavior that had yet gone undetected. Instead of printing each normalized modulus versus normalized life plot, only those plots that add to the understanding of the material behavior or re-affirm an important point will be discussed.

The 8A&O Series: The normalized modulus versus normalized life plot for two distinct 810A specimens is shown in Figure 55. Again, it is important to notice the general agreement seen in the two responses; this helps to justify using this technique as a predictor of composite life. In this case, the corroboration between the two curves is not commendable prior to a normalized life of 0.7. The tensile modulus drops noticeably more than the compressive modulus does. The claim is made that this is a result of the microbuckling growth. One would think that such compressive failures would "open up" under tensile load, providing no local tensile stiffness. During the tensile half-cycle the microbuckle behaves like a large crack. Yet, during the compressive half-cycle, the microbuckled material *does* provide resistance to further crushing. This scenario may explain the difference in the compressive and tensile responses. A normalized modulus vs. normalized life plot of two 85A specimens (not shown) possessed the same steep down turn in the tensile curve towards the end of life, and, of course, shared the same tendency to fail quickly by microbuckling. A similar plot for two 82A specimens (again, not shown) had too few points (since both tests were relatively quick) to make any judgments. Despite this, the normalized modulus results of the first three systems agreed with each other nicely, bolstering the conviction that their responses were quite similar. In all of the systems in the 8A&O series, except the 810O material, the tensile modulus decayed to a greater extent than the compressive modulus. A general rule-of-thumb for these systems had the tensile modulus decreasing by 30% just prior to fracture. The tensile and compressive modulus of the 810O specimens decayed equally throughout the life of the material.

The 5U Series: The normalized modulus versus normalized life plot for two 55U specimens is shown in Figure 56, complementing the plot of the two 510U specimens in Figure 55. The two plots are similar in many ways. Both reveal an approximate 12% decay in compressive and tensile modulus prior to 20% of the normalized life. In each case, the tensile and compressive curves de-

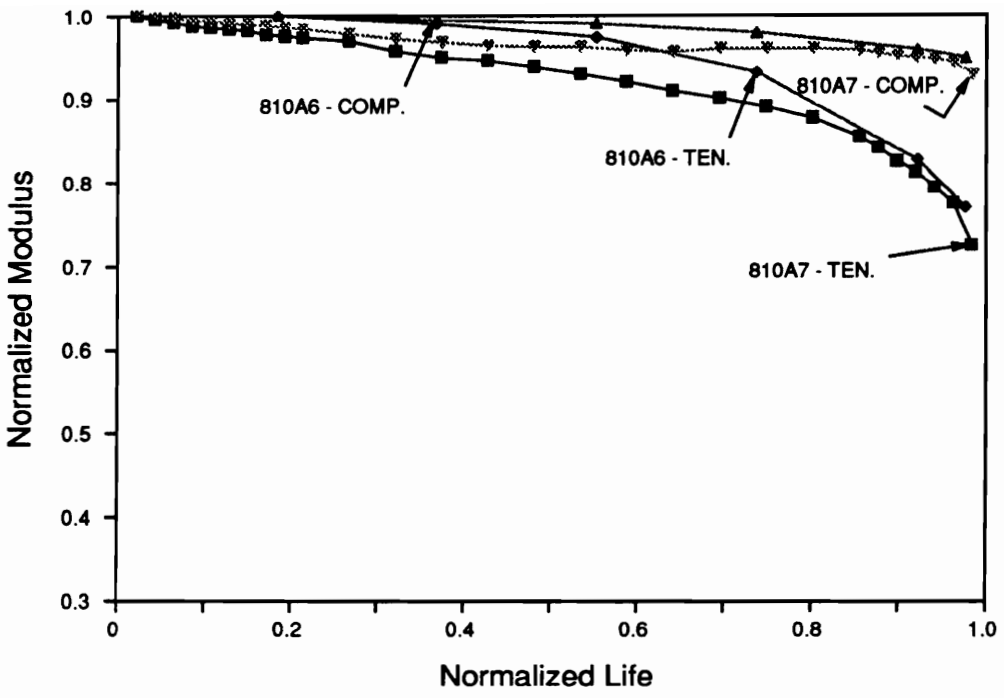

Figure 55. Plot of Normalized Modulus versus Normalized Life for Two 810A Specimens; Max. Stress = 75% UCS; R = -1 at 10 Hz.

grade at nearly the same rate. The only distinguishing facet among these plots is the steady and marked decay in the signals monitoring the 510U5 specimen. It appears that the compressive modulus has dropped more than the tensile modulus, at the very end of this specimen's life (this was true in the 52U response, too). The one 55U specimen had a somewhat greater decay in tensile modulus than in compressive modulus. These responses are to be contrasted to the 810A (and, for that matter, 82A and 85A) responses. In the case of the 810A specimens, the tensile modulus dropped rather precipitously while the compressive stiffness decayed gradually. The 5U series response does not follow that pattern. It may be that the failure of the 5U specimens is more sudden. Yet, it may be that the critical damage mode (microbuckling) takes the same amount of (cyclic) time to fracture the specimen as in the 100% surface treatment-and-below 8A&O specimens, but since it occurs over the final, say, 500 cycles of life, it is virtually undetectable via stiffness monitoring. In the 82A specimen, 500 cycles was nearly one-third to one-half of its life. In the 5U series, where the shortest life lasted around 100,000 cycles, it would simply be fortuitous to record the final modulus signals.

The Northrop Material Systems: The normalized modulus versus normalized life plot for two 3NN specimens is shown in Figure 57 while the plot for two 3SN specimens is shown in Figure 58. The contrasts are quite stark. The compressive response of specimen 3NN3 decays dramatically and steadily throughout the life of the specimen. This curve converges with the tensile curve from the 3NN3 specimen and the compressive curve of the 3NN4 specimen during the final 10% of life. The three curves display a final degradation of nearly 40% of their initial value. The 3SN responses seem very controlled, in comparison. Two tensile curves and one compressive curve remain closely grouped throughout the life of the specimens. These three curves reveal a degradation on the order of 17%. It appears that the two tensile signals drop about 5% in the last 5% of life. This is somewhat reminiscent of the 810A response, although, not of the same magnitude. The 3NN and 3SN plots point out the contribution of sub-critical damage to the damage development. Extensive longitudinal splitting and subsequent delamination, not unlike that seen in Figure 49, dramatically affect the strain measurement by disrupting the continuity the extensometer tabs have with the

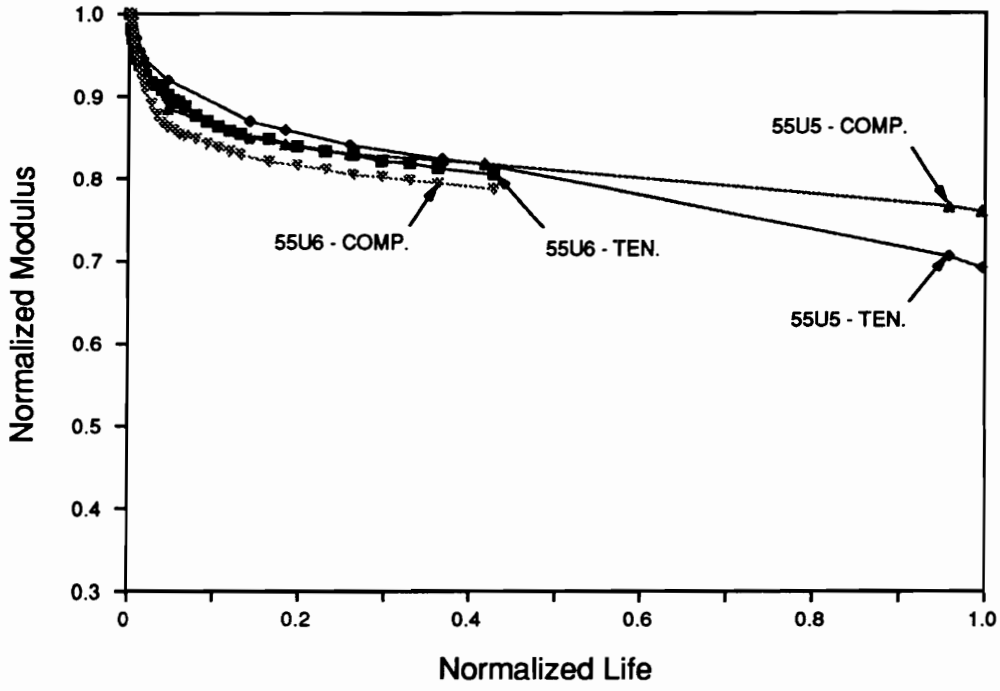

Figure 56. Plot of Normalized Modulus versus Normalized Life for Two 55U Specimens; Max. Stress = 75% UCS; R = -1 at 10 Hz.

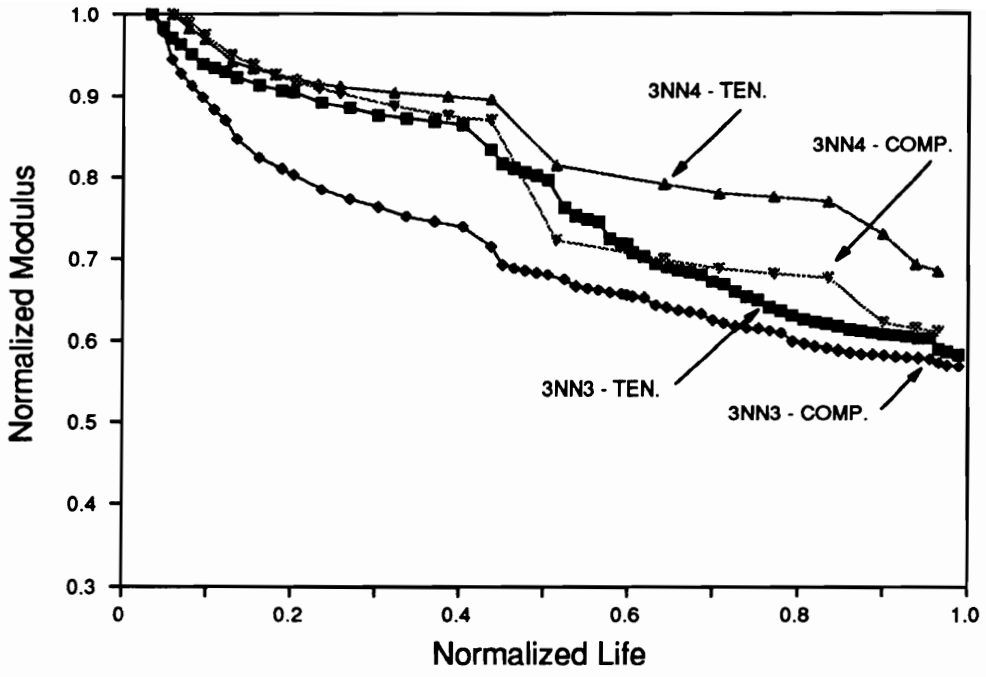

Figure 57. Plot of Normalized Modulus versus Normalized Life for Two 3NN Specimens; Max. Stress = 75% UCS; R = -1 at 10 Hz.

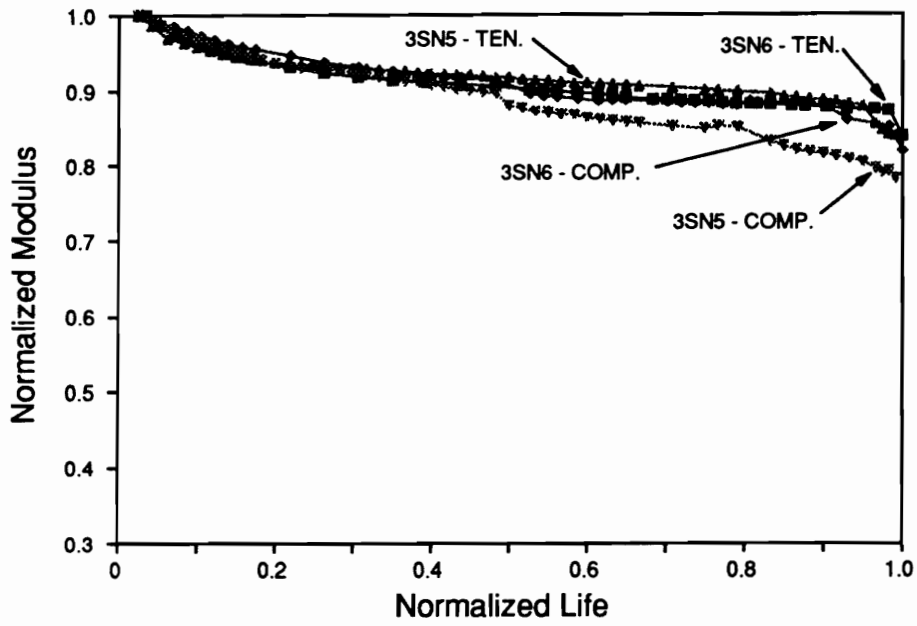

Figure 58. Plot of Normalized Modulus versus Normalized Life for Two 3SN Specimens; Max. Stress = 75% UCS; R = -1 at 10 Hz.

specimen. This is a clear example of the efficacy of using normalized stiffness versus normalized life as an indicator of the degree and nature of damage within a composite.

Notch Temperature

The measurement of the local temperature near the notch served at least two functions. Monitoring specimen temperature as a function of cycles has been shown to be a reproducible measure of material degradation, comparable to using stiffness monitoring to gauge the same response [81]. An example of its utility is shown in Figure 59. The temperature of the specimen surface measured in the region of highest axial stress (due to the presence of the global stress concentrator) is shown for two distinct 820A specimens as a function of normalized life. The two signals are remarkably close, deviating by no more than a few degrees through the first 80% of life. Due to the reproducibility, the signals can be used in the same manner as the modulus degradation plots. In other words, using Figure 59 as an example, if one wanted to capture the damage state of the specimen after 80% of its life had been expended, then one would cycle the specimen until the notch temperature reached approximately 107°F. This technique was used in conjunction with the monitoring of stiffness degradation to create an "either/or" scenario; a test would be stopped for damage analysis if either the modulus dropped by X % or the temperature reached Y°F. This marriage of the two techniques formed a "safety net"; i.e., if one signal deviated from the norm, chances were the other measurement was able to predict a specimen's stage of life.

Relating the notch temperature measurement to the nature of the interphase was the second aspect of this particular study. It was felt that weak bonding might contribute to an excess of dissipative energy since it was expected that such bonding would contribute to damage and a general lack of continuity. Conversely, strongly-bonded composites, by minimizing — at the very least — frictional energy created during slipping between the fiber and matrix, would create its own unique temperature signature that would be distinct from weakly-bonded composites. The results provided by the fourteen material systems are discussed below.

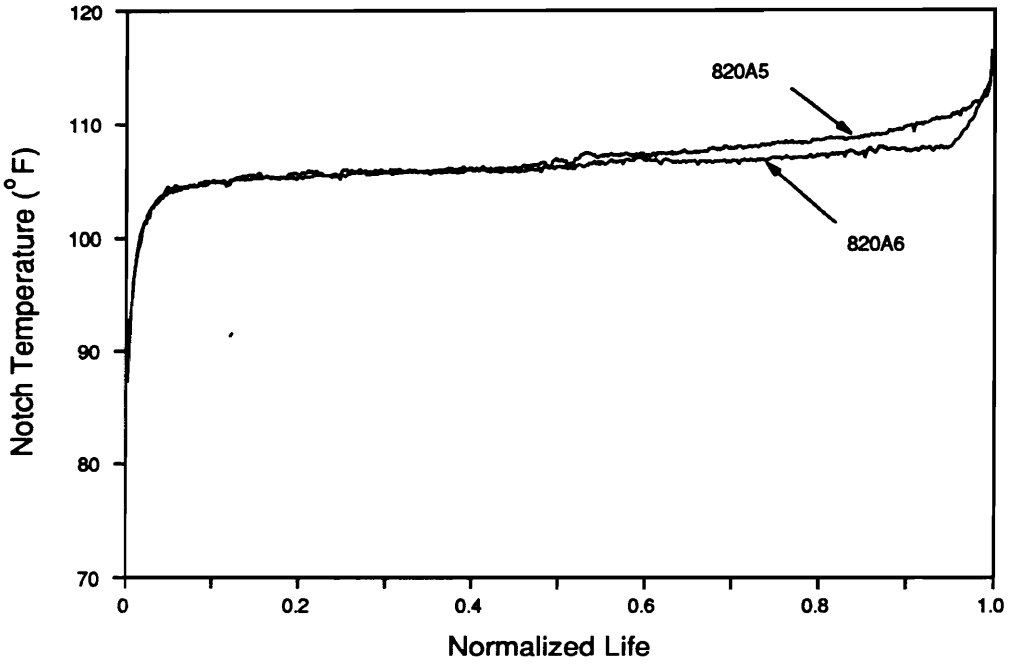

Figure 59. Plot of Notch Temperature versus Normalized Life for Two 820A Specimens; Max. Stress = 75% UCS; R = -1 at 10 Hz.

The 8A&O Series: A plot of the notch temperature versus normalized life for two 85A specimens is shown in Figure 60. This figure provides a nice contrast to the results for the two 820A specimens found in Figure 59. As will be discussed in detail later in this section, two temperatures, the "equilibrium" and "maximum" temperatures, were ultimately saved from each test to serve as a comparative measure. In nearly every plot an "equilibrium" temperature was determined by subjectively viewing the temperature record. In Figure 59, this temperature is easy to distinguish as the value where the two curves "level off"; the average value for the 820A specimens was judged to be 106°F. The average equilibrium value for the 85A specimen is more difficult to discern, in this case; a value of 105°F was chosen. The second temperature reading used to quantify the effect of specimen heating was the maximum (or final) temperature. This value could be obtained by referring to the stored temperature data taken from the "M-R Phase 3000" data acquisition program. In reality, the maximum values obtained from several specimens were averaged to give the quoted result. The average maximum temperature for the 820A specimens was 116.5°F; it was 112.5°F for the 85A specimens. A schematic of the average equilibrium and maximum temperature for all fourteen material systems is located in Figure 61. These values are collected and presented in Table 8.

The 5U Series: A plot of the notch temperature versus normalized life for two 52U specimens is found in Figure 62. The difference in temperature between the two specimens is approximately 10°F for most of the normalized life. These two signals appear to be excessively "noisy". For some unknown reason, every temperature measurement taken from material in the 5U series revealed this behavior. There seems to be some degree of periodicity to the noisy signal in Figure 62, however. It is possible that this is due to the cooling effects of a powerful air conditioner in the laboratory when this test was performed. An amazing result from the 52U specimens (and all of the 5U series specimens) is the magnitude of heating that takes place. The average maximum temperature for the 52U specimens was 202°F. It also appears that each specimen in Figure 62 had a point in its normalized life where the slope of the temperature curve changed noticeably. This point occurred around 50% of the normalized life in the 52U6 specimen and around 60% of the normalized life

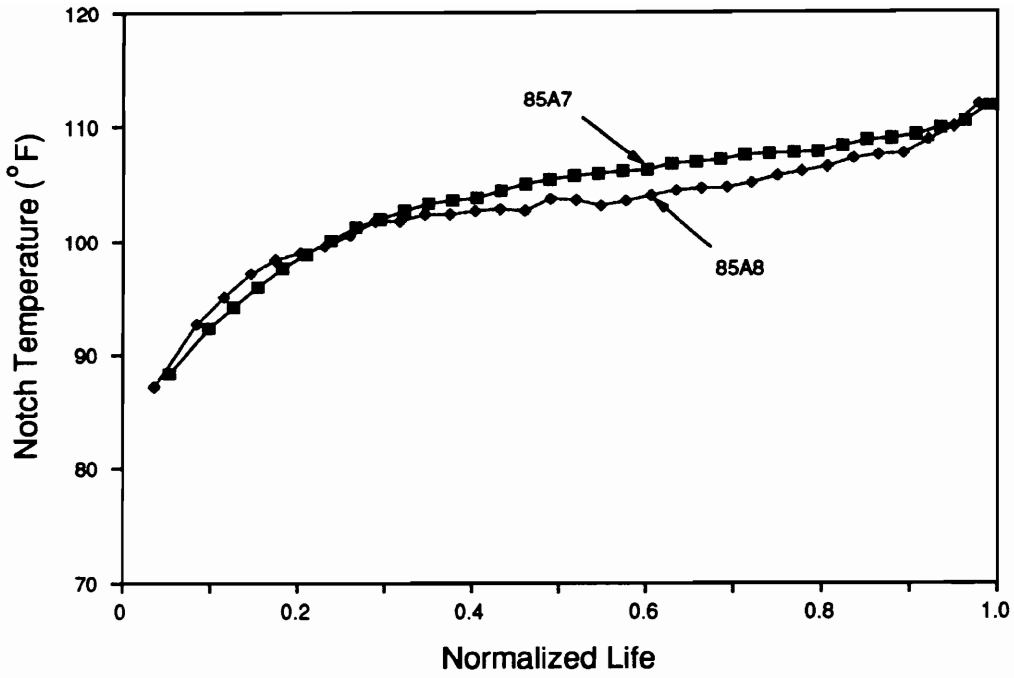

Figure 60. Plot of Notch Temperature versus Normalized Life for Two 85A Specimens; Max. Stress = 75% UCS; R = -1 at 10 Hz.

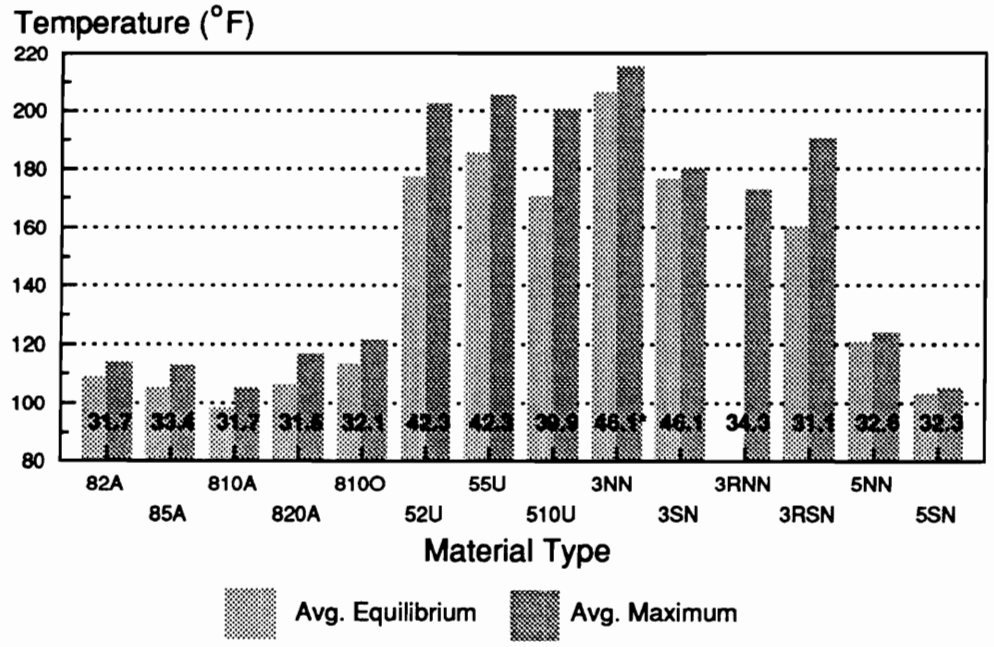

Numbers in bars: applied stress level (ksi)

* Actually less than 75% UCS

Figure 61. Average Equilibrium Temperature and Maximum Temperature of the McAir and Northrop Materials during Fatigue Loading.

Table 8. Average Equilibrium Temperature and Maximum Temperature of the McAir and Northrop Materials during Fatigue Loading.

MATERIAL TYPE	AVERAGE EQUILIBRIUM TEMPERATURE (°F)	AVERAGE MAXIMUM TEMPERATURE (°F)
82A	108	114
85A	105	112
810A	98	105
820A	106	116
810O	113	121
52U	177	202
55U	185	205
510U	170	200
3NN	206	215
3SN	176	180
3RNN	-	172
3RSN	160	190
5NN	120	124
5SN	103	105

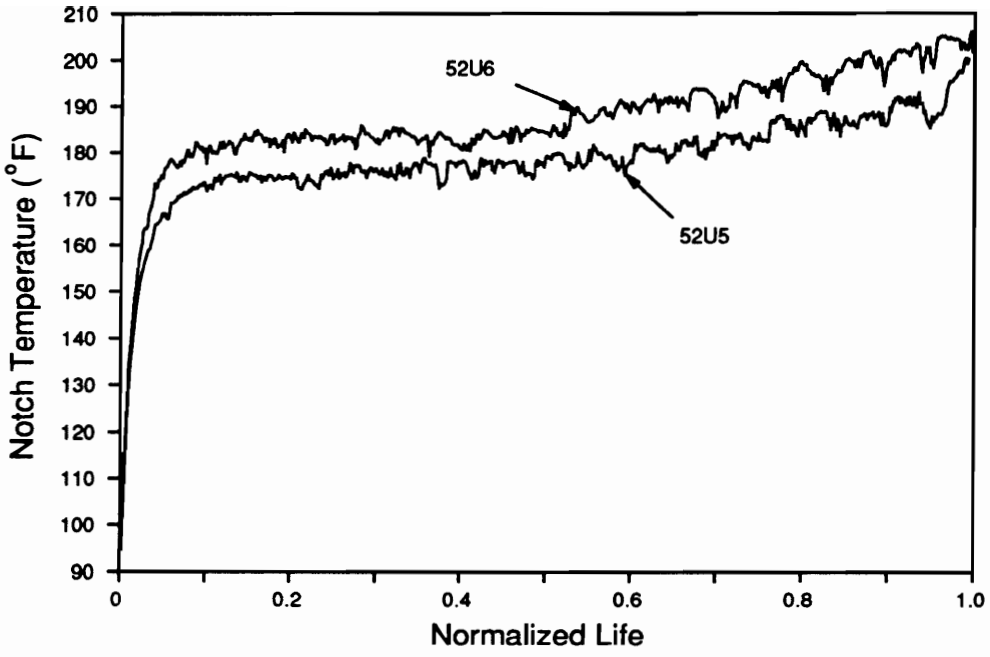

Figure 62. Plot of Notch Temperature versus Normalized Life for Two 52U Specimens; Max. Stress = 75% UCS; R = -1 at 10 Hz.

in the 52U5 specimen. This change may indicate the initiation of a damage sequence that brings the specimen to final failure.

The Northrop Material Systems: A plot of the notch temperature versus normalized life for two 5SN specimens is seen in Figure 63. The agreement between the two signals is exceptional. A distinguishing characteristic of this figure is the lack of temperature rise during the last half of normalized life for both specimens. This lends credence to the notion that failure in the 5SN specimens tended to be catastrophic, never revealing a protracted period in which critical damage grew stably. The average maximum temperature of these two signals is 105°F, nearly *100°F less than* the maximum temperature recorded for the 52U specimens. An attempt at explaining these disparities follows.

Analysis of the Temperature Results: Upon examining Figure 61, the most striking aspect is the dramatically high "maximum" temperatures recorded from the 5U series and the 3NN series specimens. The distribution of the maximum temperatures was very reminiscent of the distribution seen in the quasi-static notched cross-plied compressive strengths of the fourteen material systems (see Figure 13). In that instance, all of the 8A&O series and the 5N series specimens revealed similar, low notched cross-plied compressive strengths, while the 5U and 3NN series specimens displayed considerably higher strengths. The first impulse was to see if a relationship could be forged between these two observations.

According to Reifsnider and Williams [82], "there are two basic classes of material response associated with fatigue that are commonly assumed to generate heat: rate-dependent (viscous) behavior and rate-independent behavior." The rate-dependent behavior is best understood in terms of material viscoelastic behavior. The viscoelastic response of a material may be represented by a complex modulus that may be further separated into two components: the storage modulus and the loss (dissipative) modulus. Perfectly elastic materials possess no loss modulus component, only a storage modulus component. The ratio of the loss modulus over the storage modulus leads to the definition of tan δ, where δ is the phase angle in which strain "lags" behind stress in a stress-

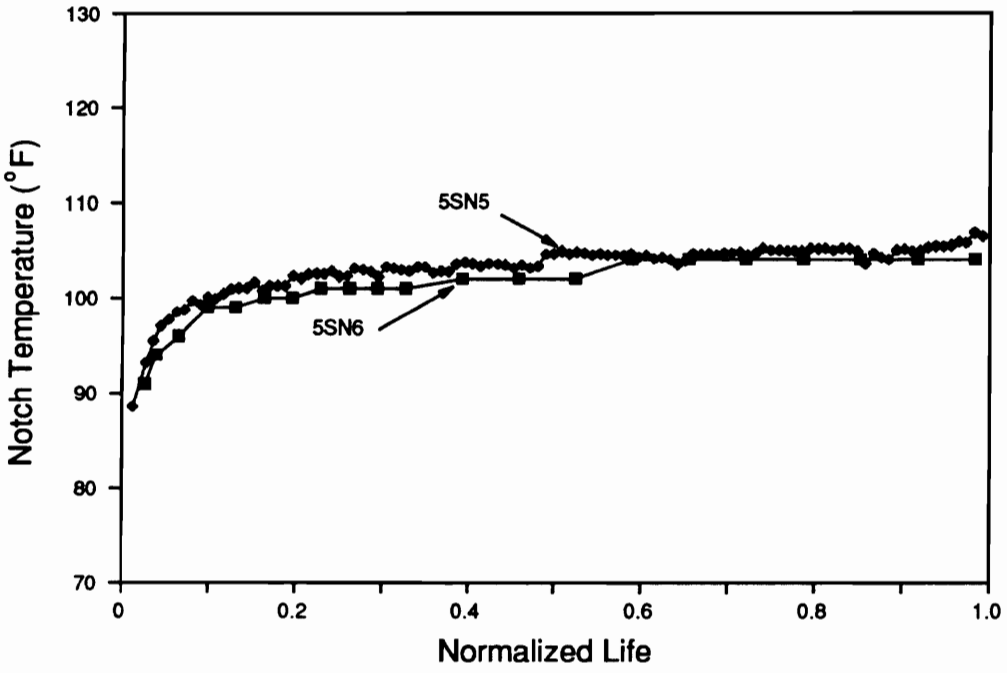

Figure 63. Plot of Notch Temperature versus Normalized Life for Two 5SN Specimens; Max. Stress = 75% UCS; R = -1 at 10 Hz.

controlled test [82]. It may be shown that the rate-dependent contribution to the heat generation per unit volume per unit time may be written as [82,83]:

$$Q_r = \sigma_a \varepsilon_a \omega \sin\delta \,, \tag{3.1}$$

where,

Q_r is the heat generated per unit volume per unit time,

σ_a is the applied stress amplitude,

ε_a is the resulting strain amplitude,

ω is the cyclic frequency, and,

δ is the phase lag.

If one assumes that the analysis of the temperature distribution in a cycled composite specimen reduces to a one-dimensional heat conduction problem, then [84]:

$$k \frac{d^2\theta}{dx^2} + Q_r = 0 \,, \tag{3.2}$$

where,

k is the composite thermal conductivity (through the thickness),

θ is the temperature difference between any internal point, x, and the specimen surface, and,

Q_r is found in equation (3.1).

The temperature distribution resulting from equation (3.2) is parabolic in shape with a maximum at the center of the composite equal to [84]:

$$\theta_{max} = \frac{Q_r a^2}{2k} \,, \tag{3.3}$$

where,

a is the thickness of the specimen.

Substituting equation (3.1) into (3.3) produces an expression that is proportional to the surface temperature, T_s. To simplify this analysis, the phase lag, δ, will be assumed constant for all of the material systems studied herein (in reality, a poor assumption, but not critical to the point of this analysis). It is also assumed that the thickness is approximately equal for all the specimens (not a bad assumption) and that the through-the-thickness thermal conductivity is a constant for *materials possessing the same matrix material.* Since the actual stress and strain amplitude are unknown at the point where the temperature is measured, and since the strain is only known across the 1″ gage length, the final form relating the measured surface temperature to the applied stress amplitude and measured strain amplitude is:

$$T_s = C\sigma_{ap}\varepsilon_m , \tag{3.4}$$

where,

T_s is the temperature measured at the surface,

σ_{ap} is the globally applied stress amplitude,

ε_m is the strain amplitude measured by the extensometer, and,

C is a constant that embodies the thickness, frequency, heat conduction, phase lag, ratios of the local stress and strain to the applied stress and measured strain, and the ratio of surface temperature to the maximum temperature in the specimen center.

For each specimen type, the average applied stress (which, recall, is a function of the notched cross-plied compressive strength) and the average maximum measured strain (just prior to failure) were multiplied together and served as the abscissa in a plot where the corresponding maximum temperature (found in Table 8) served as the ordinate, to see if a linear relationship — predicted by equation (3.4) — resulted. Such a plot is shown in Figure 64 for the McAir material systems. It is comforting to see that the difference in maximum temperatures between the 5U and 8A&O series specimens corresponds to a positive difference in $\sigma_{ap}\varepsilon_m$ between the respective series. Yet, it would be presumptuous to conclude a linear relationship between the two sets of data. The plot of

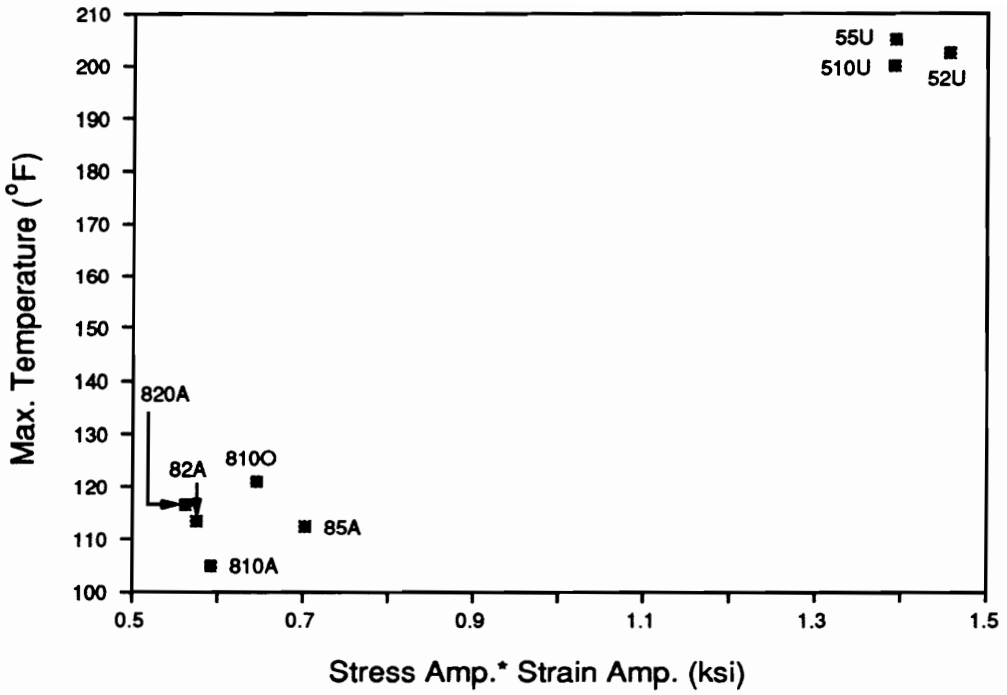

Figure 64. Plot of Maximum Specimen Temperature versus Specific Energy Term for McAir Materials; Max. Stress = 75% UCS; R = -1 at 10 Hz.

maximum temperature versus $\sigma_{ap}\varepsilon_m$ for the Northrop material systems possessing the epoxy resin is shown in Figure 65. These results are very encouraging, and lead one to conclude, with moderate confidence, that the large differences in the maximum temperatures seen in Figure 61 have been accounted for within this simple analysis. One could use the above analysis to attempt to differentiate the temperature response of systems with differing interphases by quantifying the effect that these interphases have on the phase lag response of the material. The discussion of this quantification follows; the incorporation of the measure phase lag values into a temperature-predicting scheme is left for future work.

Phase and Gain Measurements using M-R Phase 3000

Elahi, *et al.* [35], have published research on the development of a testing scheme that enables an operator to measure dynamic properties of a specimen while it is undergoing cyclic fatigue in a servo-hydraulic test frame. The software, entitled "M-R Phase 3000", manipulates the load and displacement signals output from a testing machine into two performance metrics: phase lag (shortened to "phase" in Ref. [35] and in this discussion) and gain. The signals used and the equations employed to arrive at these measures are detailed in Ref. [35]. Simply put, gain is a signal that resembles the dynamic compliance of the specimen, while phase resembles the phase angle in which measured strain lags behind applied stress (in the test machines used, however, stress lags behind strain, or, displacement). This test method seemed well suited to this investigation since it was felt that differences in interphase properties could be detected by careful measurement of the composite's dynamic response. Several researchers [85-87] have reported success in being able to infer interphase bonding by performing small-scale Dynamic Mechanical Analysis (DMA) tests. Others [88] have used the DMA to detect changes in the thermomechanical properties of laminates that have been damaged by fatigue loading. The present test technique combines the analysis of the DMA without the need to "scale down" the specimen size or loading conditions. Thus, typical

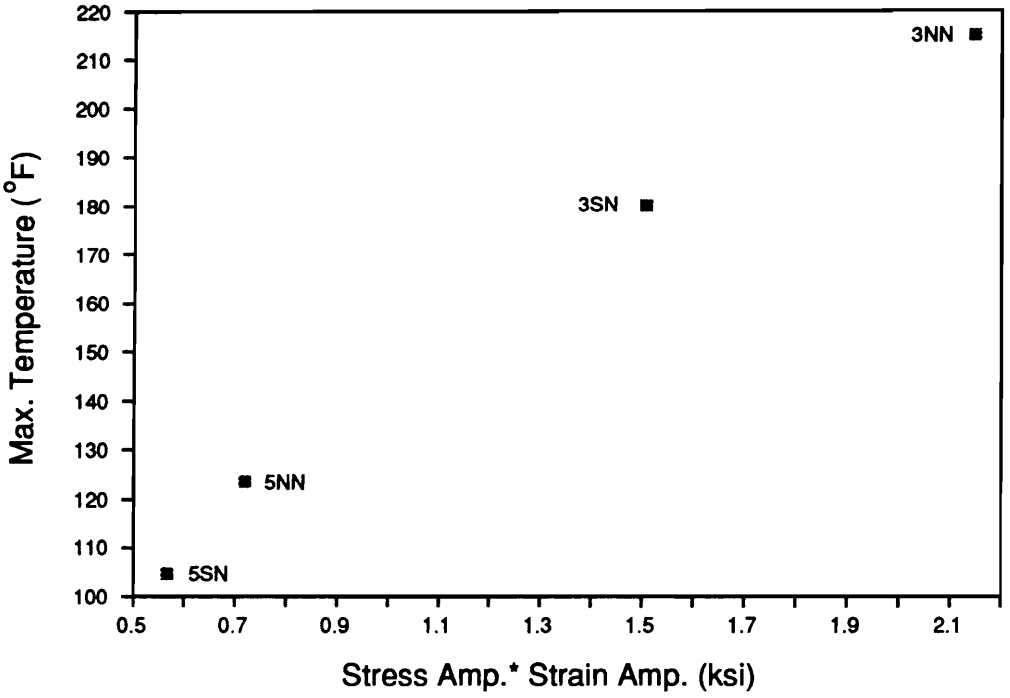

Figure 65. Plot of Maximum Specimen Temperature versus Specific Energy Term for Northrop Materials; Max. Stress = 75% UCS; R = -1 at 10 Hz.

fatigue testing benefits from the ability to analyze the specimen as a dynamic component in a forced vibration problem.

Every fatigue test run in this study was performed in conjunction with the Dynamic Signal Analysis (DSA) software. Nearly eighty fatigue tests in total were run while collecting phase and gain data. Unfortunately, despite the large number of trials, the researchers were unable to use the phase and gain data to conclusively draw comparisons between materials and their respective performance. There are several reasons for this, yet, it is important to point out, none deal with the philosophy behind the test technique. It turns out that these specimens (and several more in the future) were needed to try to "iron out the wrinkles" in the test method. Several sources of error in the collected signals were identified during these tests and removed. One, for instance, had to do with the position of the crosshead during testing. It turns out that the actuator was forced to travel into its inherent non-linear realm during fatigue cycling. The displacement signal output from the machine then became routinely non-linear. This was interpreted as non-linear material behavior instead of non-linear machine behavior. Other errors crept into the test technique. It was determined that the software interpretation is highly dependent on the correct level of signal amplification. Amplification is needed in highly stiff materials, yet, not needed in compliant materials (like the $\pm 45°$ specimens discussed below). This process of identifying problem areas and correcting them left little room for collecting "good" data.

Collected data split itself between "good" data — values that are physically reasonable and well-behaved — and "bad" data — values that reflect inherent flaws in the test set-up and/or data processing. It was disappointing to find that the analysis of "good" data did not often lend itself to reproducibility. In other words, reasonable and well-behaved signals often began and ended with phase and gain signals that differed noticeably from data collected from previous specimens; this was true for phase more than gain. This, combined with the dearth of "good" data, prevented the author from making any meaningful assessment of the influence of the interphase on fatigue behavior using this particular test technique.

This is not to say that the DSA technique was worthless to the present investigation; that would be completely untrue. Several virtues of the technique were confirmed during this study. The first

one that comes to mind is its ability to detect imminent laminate failure. While both signals are useful for this purpose, the gain signal can be depended upon to alert the operator of impending laminate failure. Since the gain signal reflects the material's dynamic compliance, damage that initiates (and is part of) the cascade of subcritical and critical failures prior to specimen fracture is detected. Only in the rare instance of instantaneous and sudden fracture does the gain signal prove insensitive to a failing laminate. The gain signal's ability to detect damage (through changes in dynamic compliance) is certainly not limited to a near-failure time frame. Just as the stiffness measurement has become an effective tool in monitoring damage progression and in estimating stages of life (as was used earlier in this chapter), DSA measurements are capable of doing the same. The benefit of the DSA technique, however, is that it is "non-contact"; i.e., it uses the movement of the load frame's actuator to sense changes in the material's performance. This virtue will be highly attractive to those investigators who are prevented from using extensometers to monitor dynamic composite stiffness due to demanding environmental conditions (high temperature or cryogenic applications), laminate configurations (specimens that undergo extensive surface matrix cracking), etc.

It is simply a matter of time before the DSA technique is exploited for all it's worth. By allowing the specimen to become integral into the dynamic system, one will eventually be able to detect subtle changes in the material performance that were once previously undetectable (progress has already been achieved in detecting fiber failure during fatigue using DSA [89]). Yet, there is a need to build up considerable experience in running the algorithm in order to test and correct its deficiencies. The knowledge acquired in running DSA was directly used towards improving the test method. This will benefit future users and the composite community.

SEM Investigation of the 810A, 820A, and 810O Specimens

At this point, it is still unknown why the 810O's notched cross-plied fatigue life was remarkably longer than its 810A counterpart. The *only* apparent difference between the two materials was their

sizing formulation; the 810O received an "organic" size, while the 810A received a time-tested standard epoxy size. It was anticipated that such large differences in fatigue behavior were simply manifestations of large differences in interphase properties that could be easily discernible. Yet, this was not the case. In addition to the notched cross-plied compressive strength being nearly identical, the MMHP and the $\pm 45°$ shear (tensile) strength and stiffness of the two were virtually indistinguishable. The transverse flexural strength of the 810O material was 9% higher than the 810A material, however, the 510U's TFS was 13% higher than the 55U's TFS, yet, there was not a corresponding leap in fatigue life. The only parameters that revealed a considerable disparity in measured values between the two systems were the representative strain value (d/D at MMHP) quantified during indentation testing and the notched cross-plied tensile and compressive modulus. These two parameters are somewhat akin to one another. The representative strain measures the amount of deformation the material can absorb prior to the onset of inelastic behavior. If one assumes a linear elastic indentation response until damage occurs, then the ratio of the MMHP over the representative strain resembles an indentation (compressive) stiffness. Since the MMHP of the 810O and 810A materials are nearly the same and the d/D value for the 810O material is larger than its 810A counterpart, the "indentation modulus" is greater in the 810A material than in the 810O material.

It should be justifiable to attribute the disparity in stiffness (or, modulus) between the 810O and 810A materials to the interphase. Both parameters quoted above — the indentation response and the notched modulus response — are measures of "fiber-dominated" properties. This is especially true with the indentation response. Conventional wisdom would claim that only the fiber and matrix contribute to the material's resistance to indentation, with the fiber carrying virtually all of the load. Yet, the fibers, and, for that matter, the matrix, are identical in the 810A and 810O systems. Due to a lack of knowledge of any other variable that might differentiate these two systems, it is natural to attribute the disparity in performance to the only known variable: fiber sizing. It does not seem reasonable that a coating estimated to be 100-500 nm in thickness [21,22] could influence the unidirectional, uniaxial stiffness that much, *unless the sizing instigated a change in the matrix material.* Albertsen and Peters [90] will soon present research showing that surface treatment

affects the *stiffness* of the interphase. They observe that an increase in fiber surface treatment corresponds to a decrease in the stiffness of the interphase. They attribute this decrease (and the observation that moisture uptake increases with surface treatment) to an increase in the mean molecular mass of the interphase. Therefore, they conclude, the increase in fiber surface treatment which produces an increase in fiber surface chemical species must interact with the polymerization of the interphase. This same reasoning could be applied to the sizing instead of the surface treatment. Perhaps the formulation of the sizing affects the polymerization of the interphase region, creating a region whose physical size and properties affect not only the stiffness of the composite, but *dramatically* affects the fatigue performance. This provides the motivation in using the Scanning Electron Microscope (SEM) to investigate any differences in the interphase region between the 810A and 810O materials that might be visually detected.

The inspiration for pursuing this avenue was given to the author by P. W. M. Peters. He, along with Albertsen [59], have presented a study on a composite system consisting of Courtaulds's 43-750 fiber (either the same fiber as the 45-850 fiber studied in this investigation, or a nearly indistinguishable variant) sized with an "A" sizing (identical to the sizing used in this study) and surface treated to levels of 0%, 10%, 50%, and 100% of the industry standard; the composite's matrix system was Hysol's HC 9106 resin (likely the same toughened epoxy system studied herein). They performed a chemical etch on the composite in an attempt to identify the interphase under a SEM. They observed a two-phase system in which the thermoset phase serves as a continuous phase that surrounds both the fiber and the discontinuous phase (the thermoplastic toughener). They claim that the surface treatment level affects the coarseness of the discontinuous phase.

Prior to seeing those specific results, the present author etched the polished surface of the 810A, 820A, and 810O specimens mounted in a metallographic epoxy (the details of which were given in the previous chapter). The etchant chosen was a published formula used expressly for etching PEEK composites [58]. Trials were conducted to determine the optimum etching time; five minutes was chosen as the time producing the greatest contrast between the two separated matrix phases. Two new specimens, an 810O and an 820A specimen, were etched at five minutes apiece in order

to the compare them to the 810A specimen that had been etched for five minutes during the etching-time trials. The SEM images are located in Figures 66-68 and discussed below.

The SEM micrograph of the 810A specimen is shown in Figure 66. As a point of reference, two 5 micron fibers appear, one dominating the left-hand portion of the micrograph, the other, the upper portion of the micrograph. The two-phase matrix morphology is very clear. The thermoplastic toughener has been etched away leaving voids where the globules once resided. Unlike the findings of Peters and Albertsen, it does not appear that the thermoset phase surrounds the fibers. Actually, it is difficult to discern any gradients in the structure; i.e., the etched matrix appears to be relatively homogeneous in its structure. This is to be compared to the SEM micrograph of the 820A specimen found in Figure 67. In this case, fewer "voids" are seen *except near the fiber surface*. There is some suspicion that this "smoother" structure may be an artifact of the etching technique. When the trials were conducted to determine the optimal etching time, the longer the etching time, the more the structure looked like the one seen in Figure 67. Though a five minute etch was executed and great care was taken to replicate the etch formula exactly, this suspicion still remains.

The SEM micrograph of the 810O specimen is shown in Figure 68. It is obvious that the nature of the interphase region *is* different from the previous two. In this case, a continuous region does appear to surround the fiber creating a distinct *interface* between this phase and the two-phase region. Because these two regions are so dramatically different (visually), one must wonder if they possess different properties. The structure of the interphase in the 810O system seems to follow the description of the materials examined in Ref. [59]. Yet, their composites were all "A" sized, instead of "O" sized; none of the "A" sized specimens investigated above displayed a "continuous phase" around the fiber. These findings beg for more attention in order to determine the structure/property relationship that seems to exist with these composites. At this point, one may speculate that the *physical* change of the interphase that accompanies the 810O material and contributes to its lower stiffness somehow enters into the fatigue problem, thus creating a notched cross-plied specimen with a longer fatigue life. An investigation into how this interphase may have entered the fatigue problem is presented in the next section.

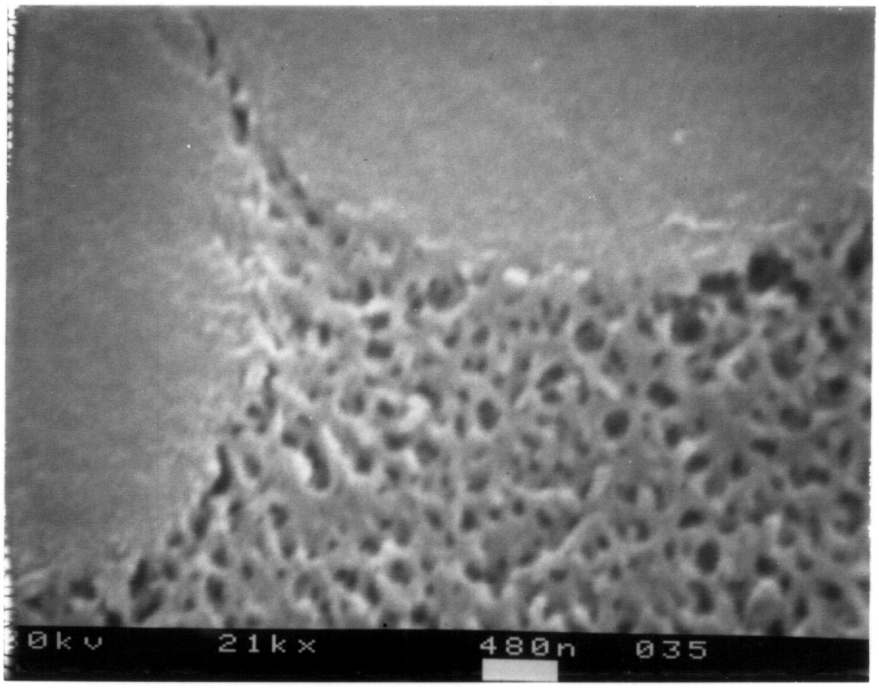

Figure 66. SEM Micrograph of an Etched 810A Specimen (x 21,000).

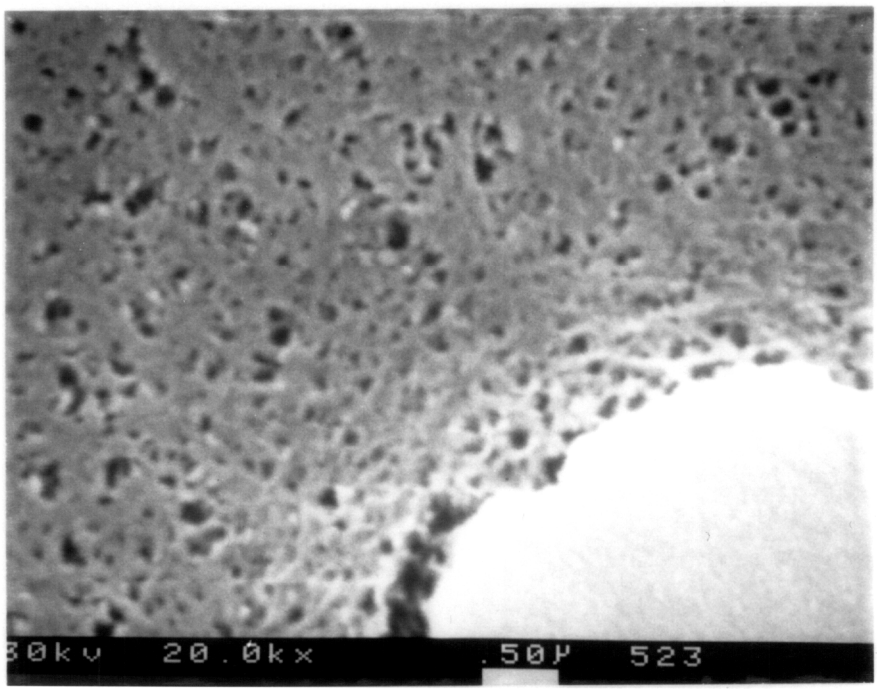

Figure 67. SEM Micrograph of an Etched 820A Specimen (x 20,000).

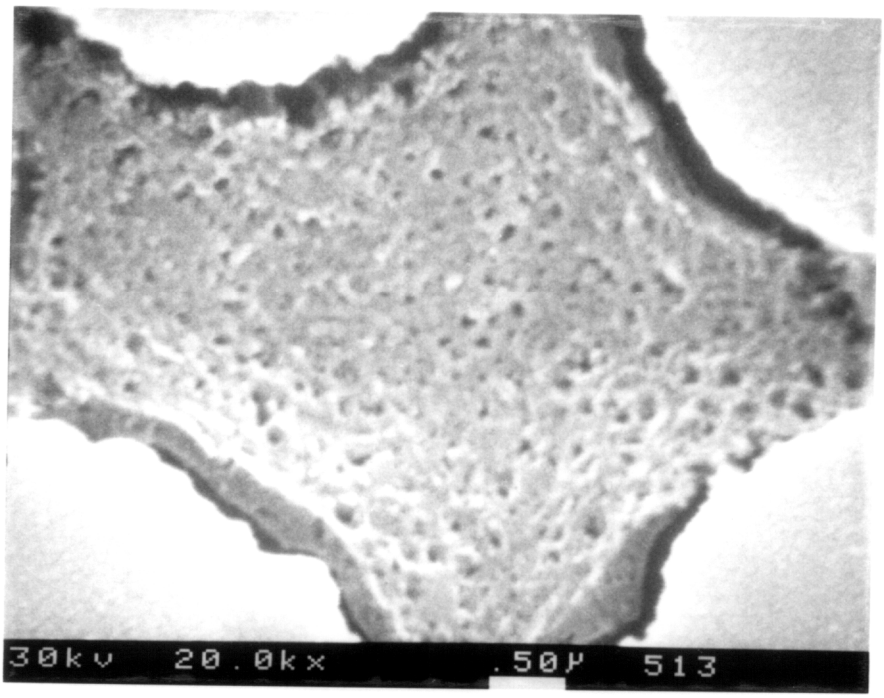

Figure 68. SEM Micrograph of an Etched 810O Specimen (x 20,000).

Prior to leaving this section, another SEM study is presented. A common technique used to qualify the degree of bonding involves examining the fracture surfaces of broken specimens. Clean, bare fibers indicate a lack of bonding, while matrix-covered fibers and matrix failures point to strong bonding in the interphase region. This analysis was pursued using the fractured remains of two notched cross-plied tensile strength specimens — one 810A specimen and one 810O specimen. The SEM micrograph of the failed 810A specimen is located in Figure 69. This figure shows a failed 90° ply with one broken 0° fiber in the foreground. The quality of bonding, judging from this figure, seems fairly strong. No bare fiber surfaces are visible; matrix residue appears to be clinging onto the fibers tenaciously. Compare this to the SEM micrograph of the failed 90° ply in the 810O specimen shown in Figure 70. The fibers surfaces are, again, covered with matrix; in this instance, however, no "powdery" residue is apparent. Applying the findings of the previously-discussed SEM study, one might conclude that the residue seen on the 810A specimen represents fractured regions of the homogenous structure seen spread evenly around the fibers. On the other hand, the lack of residue on the 810O fibers might indicate failure along the interface between the continuous phase and the two-phase region, or, for that matter, between the fiber and the continuous phase. Such ideas are purely speculative until a more thorough analysis has been performed.

Strain Gradient Measurements on 810A and 810O Specimens

The immense difference in fatigue lives between the 810A and 810O specimens occurred because the 810A system developed microbuckling early in its life and the 810O specimen *never* developed microbuckles, despite being loaded at a higher stress level. This would be reasonable behavior if the notched cross-plied compressive strengths of the two systems were accordingly different; essentially, they were not. Attempts at attributing this behavior to the strengths of the respective interphases were largely unsuccessful. The SEM investigation revealed that the two interphases appeared physically different — a difference that *is* being detected in stiffness-based measurements. Perhaps this difference in stiffness is responsible for producing dissimilar values of stress concen-

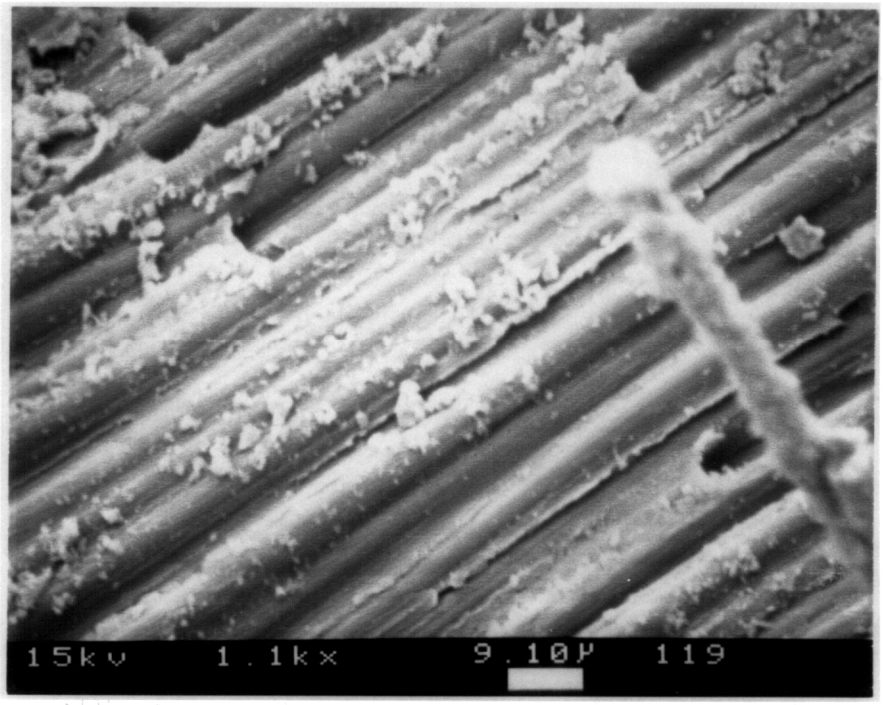

Figure 69. SEM Micrograph of a Failed Notched Cross-plied 810A Tensile Specimen (x 1100).

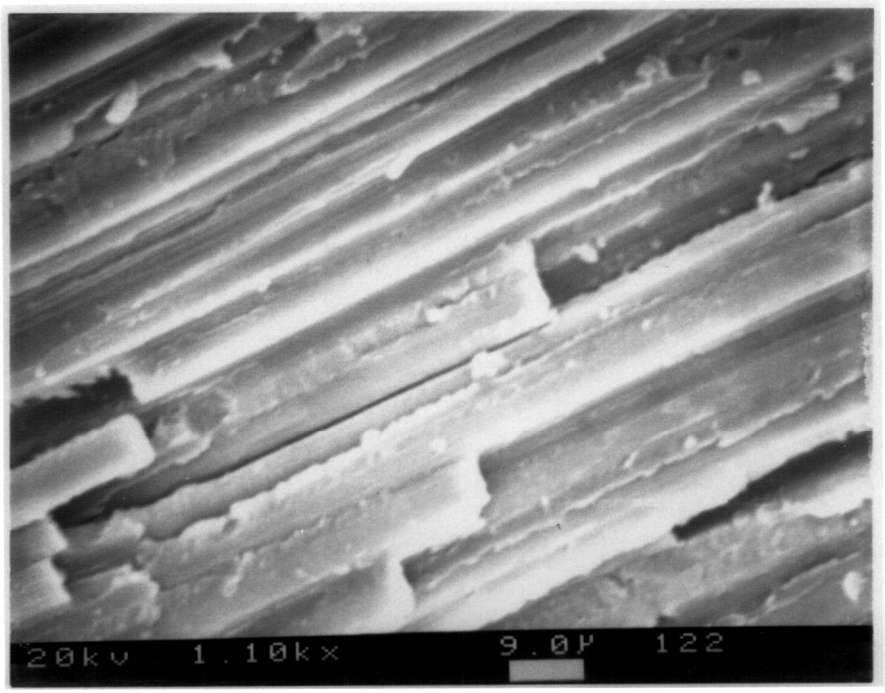

Figure 70. SEM Micrograph of a Failed Notched Cross-plied 810O Tensile Specimen (x 1100).

tration at the hole boundary. The stress concentration factor for an infinite, homogeneous, anisotropic plate containing a center hole has been shown by Lekhnitskii [91] to be a function *only* of the material's elastic constants. It is conceivable that the discrepancy between the two systems' moduli could lead to differences in the respective local notch stress concentrations. One would think that if this were the case, it would become manifest in the values of notched strength. This does not have to be the case, however, because of the complex process a composite must endure between initiation of failure and fracture.

To test the stiffness/stress concentration hypothesis, one 810A specimen and one 810O specimen were affixed with a "strip gage" — ten miniature strain gages aligned in a row — in order to detect gradients in the strain field as one walks perpendicular to the load axis from the center hole to the specimen edge (details about the strip gage and the procedure used to obtain strain readings are located in the previous chapter). The first test compared the materials' response to an applied load of 1000 lb. and -1000 lb. A plot of the 810A and 810O response to these loads are found in Figure 71. The 810O strain response is consistently higher at the given load level, indicating, as has been seen throughout this study, a greater material compliance. If the local compressive strength were a *strain-critical* failure phenomena, one would likely conclude that an 810O specimen would fail at a smaller applied load than an 810A specimen. Several other subtleties exist in Figure 71. Notice in the curves for each specimen that the (absolute value of the) compressive strain is higher than the tensile strain. This indicates that either the fiber compressive modulus is intrinsically lower than its tensile modulus, or, that initial fiber waviness may be present that would create an inequity in the tensile and compressive elastic response (or, that both factors contribute to the difference). The difference between the tensile and compressive strain seems to increase as the measurement is taken nearer to the hole. This may suggest that these moduli are stress-level (or, strain-level) dependent.

The next step in this trial was to ramp-load the specimens to their respective maximum (and minimum) applied fatigue load level. For the 810A specimen, this was calculated to be 5752 lb. For the sake of comparison, the 810O specimen received the exact same level (though this would be *slightly* less than its applied fatigue load level). The results of this trial are plotted in Figure 72.

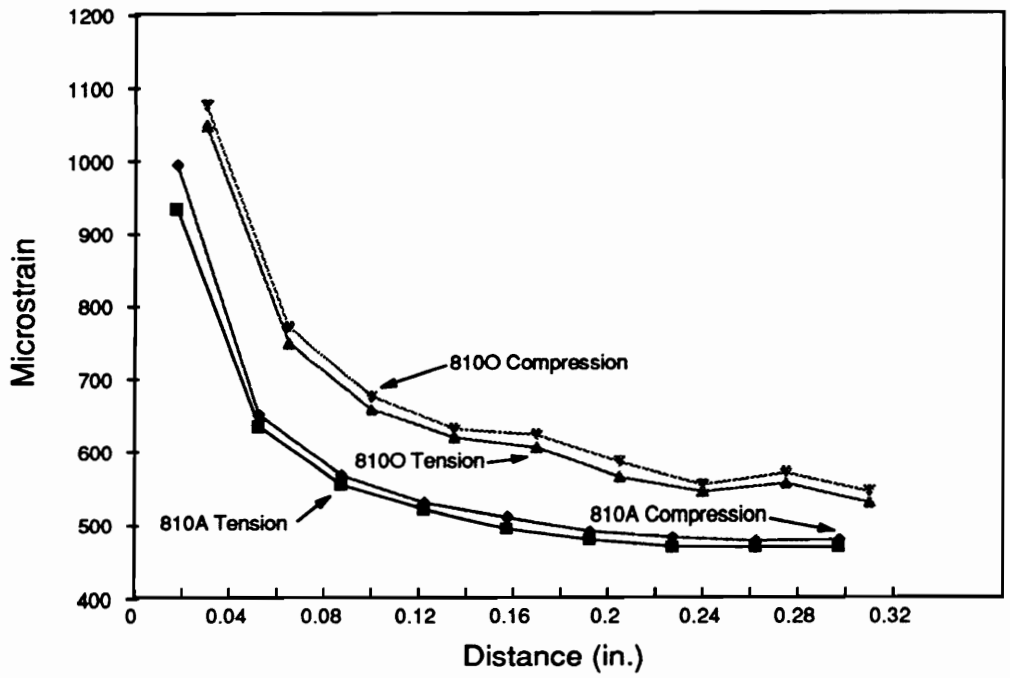

Figure 71. Longitudinal Strain Measurements as a Function of Distance from the Hole; 810A and 810O under 1000 & -1000 lb.

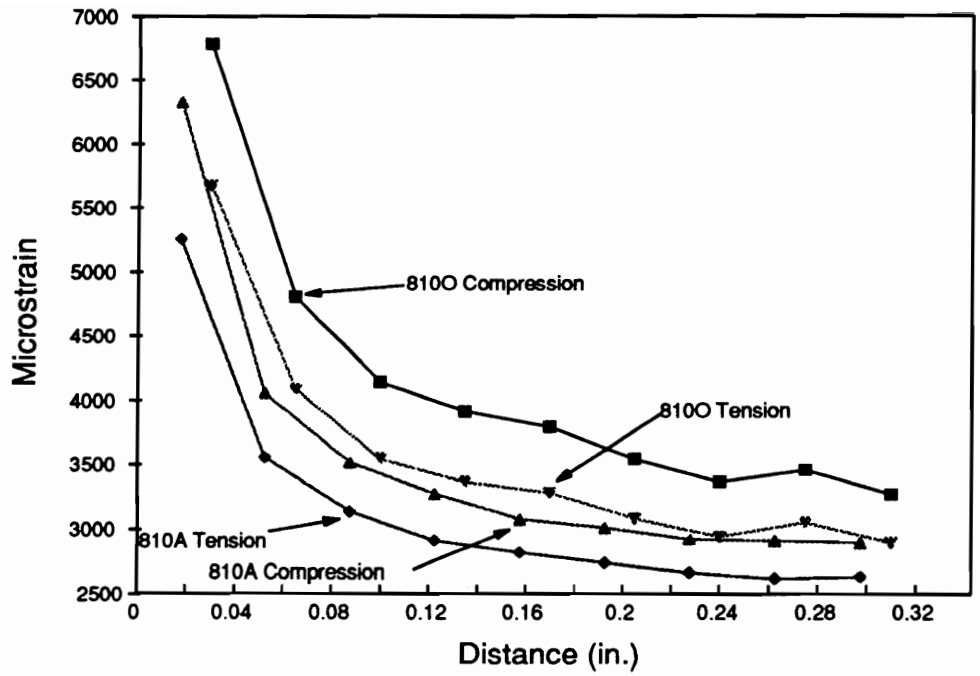

Figure 72. Longitudinal Strain Measurements as a Function of Distance from the Hole; 810A and 810O under 5752 & -5752 lb.

The most interesting change in the curves upon increasing (decreasing) the load level is the degree of separation that now exists between the tension and compression responses within each system; this is especially true with the 810O. The tendency for this disparity in the responses to increase as the local stress (strain) increases (as one gets closer to the hole) is confirmed in Figure 72. If one multiplies the *tensile* strain value obtained from the gage furthest from hole under 1000 lb. loading by 5.752 (the ratio of the two load levels) this overpredicts the actual strain reading at 5752 lb. by 2% for the 810A specimen and 5% for the 810O specimen. If this procedure is followed for the compressive strain, the predicted strain value *underestimates* the actual strain by 5% for the 810A specimen and 4% for the 810O specimen. These data confirm the observation that the tensile response "stiffens" while the compressive response becomes more compliant. Initial fiber misalignment is a plausible explanation for this behavior; compressive loads would tend to exacerbate any out-of-plane fiber deformation, while tensile loads would tend to straighten out the fibers. This does not explain, however, why the disparity between the compressive and tensile responses is greater in the 810O specimen than in the 810A specimen.

The final phase of this trial was to expose each specimen to fully-reversed (R = -1) fatigue loading at 75% of the 810A's ultimate compressive strength (resulting in an applied load level of ± 5752 lb.). The test was terminated after only 1150 cycles, since this had proven (through X-ray analysis of previous 810A specimens) to be enough cycles to cause local damage in the 810A specimens. The plan was to compare the strain field for the as-damaged specimens (again, ramped to 5752 lb.) to the strain field measured prior to fatigue (displayed in Figure 72). The strain field of the 810A specimen before and after fatigue is shown in Figure 73. The fatigue regimen damaged the gage nearest to the hole rendering it inoperable. This was disappointing, since this would have been very indicative of the change in the stress concentration near the hole. Yet, in damaging the gage, one suspects that an unusually high strain value has occurred near the hole. Studying Figure 73, it is surprising how little the strain field changes. This bears testament to how localized the damage is, due to the stress concentrator; the two far-field strains are virtually indistinguishable. It is recognized, however, that as one approaches the hole, the post-fatigue strain levels do appear larger than their pre-fatigue values.

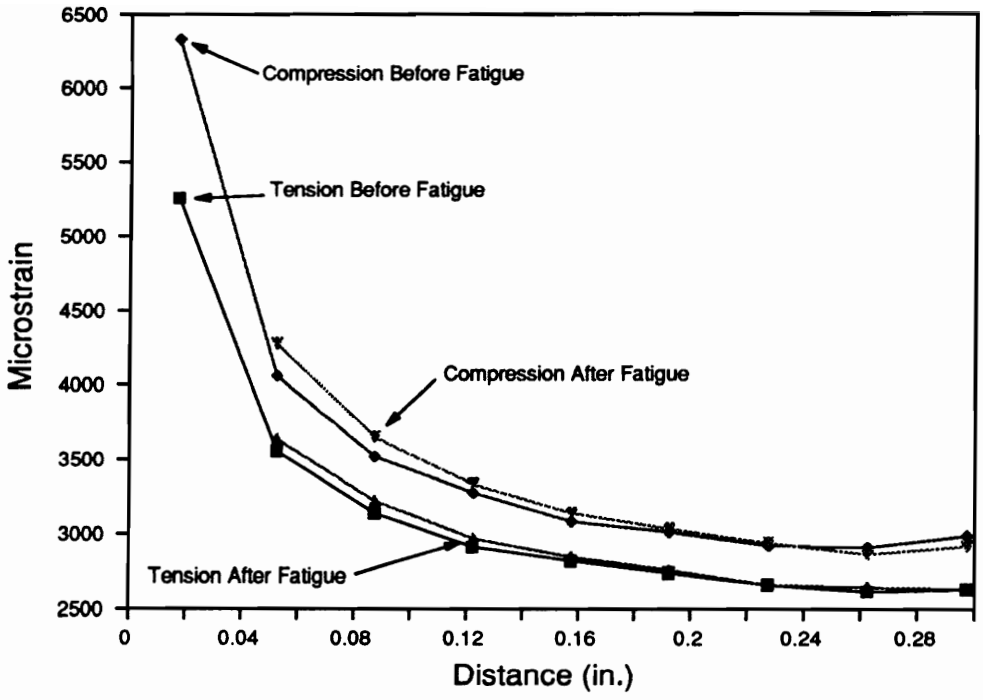

Figure 73. Longitudinal Strain Measurements as a Function of Distance from the Hole; 810A Before and After Fatigue.

The strain field of the 810O specimen before and after fatigue is shown in Figure 74. Unfortunately, strain data was not recorded in the first three gages near the hole because the fatigue cycles *disabled the gages*. While this precludes any assessment of the near-field strain, it does suggest that the strain level was severe enough to impair the gages. This occurred in only the first gage in the 810A specimen, not in the first three gages. This finding would lead one to believe that the 810O specimen was in more serious danger of failing than the 810A specimen. If the damage done to the gages was caused by excessive strain and *not laminate damage* (as previous X-ray experience would dictate), then the 810O response is nearly reminiscent of local plasticity in metal fatigue.

One obvious conclusion from this study is that strip gages are very effective at monitoring the strain field gradient due to a center-hole stress concentrator. The strain values were stable and reproducible. This study also verified the difference in stiffness between the 810O and 810A material. If was felt that this difference may influence the stress (strain) field of the respective specimens. The results were surprising in that the 810O specimen seemed, by all indications, to be more vulnerable to local microbuckling (if a strain-critical failure is assumed). After fatigue loading, the first three gages of the strip gage were disabled in the 810O specimen; in the 810A specimen, only the gage nearest to the center hole was damaged. Previous X-ray analysis indicates that the damage in the 810O specimen is not related to microbuckling. If the response of the near-field strain gages is only related to the magnitude of strain sustained by the specimen, it is *very* surprising that the 810O specimen tolerates it without failure. This may reflect this laminate's ability to "spread out the stress concentration" instead of localizing it. Yet, without the ability to detect the near-field strains in both specimens, this hypothesis was not tested.

Unnotched $\pm 45°$ Specimens

The purpose behind the fatigue study of the $\pm 45°$ specimens is readily apparent: this would provide a good contrast to the notched cross-plied fatigue study since the present laminate is unnotched, displays a "matrix-dominated" response, will *not* receive any compressive loading, and,

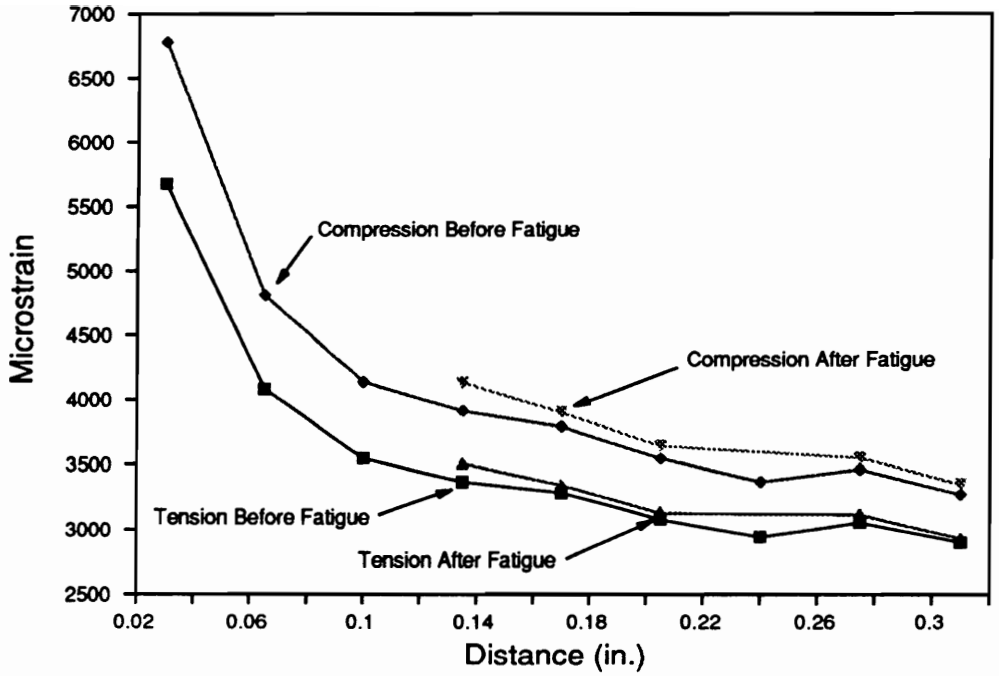

Figure 74. Longitudinal Strain Measurements as a Function of Distance from the Hole; 810O Before and After Fatigue.

in general, serves as another "test case" in this investigation. The intent is *not* to replicate the detail behind the notched cross-plied fatigue study, but rather to quickly assess the role the interphase has on the cyclic performance of the unnotched $\pm 45°$ laminates. Therefore, the only parameters examined in this brief study will be cycles to failure, and specimen temperature. A short word concerning the phase and gain data for these systems will be voiced, in addition.

A subtle point should be re-emphasized prior to examining the data. Only McAir material was available for fatigue testing in the unnotched $\pm 45°$ laminate configuration. Thus, having the luxury of keeping the matrix the same for this "matrix-dominated" laminate configuration, it was not necessary to fatigue the specimens at a percentage of their respective strengths; instead, an applied maximum fatigue stress level of 24 ksi was kept *constant for all eight systems.* This facilitates the comparison between systems, since one is simply interrogating the performance of each material type *under identical conditions.* All fatigue was performed with a fatigue ratio of $R = 0.1$ at 10 Hz. With the exception of the 55U material, each system had at least three specimens cycled to failure under an applied fatigue stress level of 24 ksi.

Cycles to Failure

The results of the three specimens (two for 55U) and their average response is detailed in Figure 75. Perhaps the most interesting aspect of these data is that no great difference was seen between the 810O system and the rest of the 8A&O series. The *average* response of the 8A&O series (with the obvious exception of the 85A specimens) is surprisingly identical. This is nearly incomprehensible if one considers the *process* that each specimen undergoes towards fatigue failure. Soon after the specimen begins cycling, it begins to "yield"; i.e., the $\pm 45°$ fibers begin to change their angle and align themselves towards the load axis. Most specimens withstand this yielding early in their lives and then "settle down" for several thousands of cycles. Their degradation after this initial "yield" is slow, but steady. In most cases, when the strain (measured with a 1″ extensometer capable of detecting 15% strain) reaches approximately 10.5%, the degradation of the specimen be-

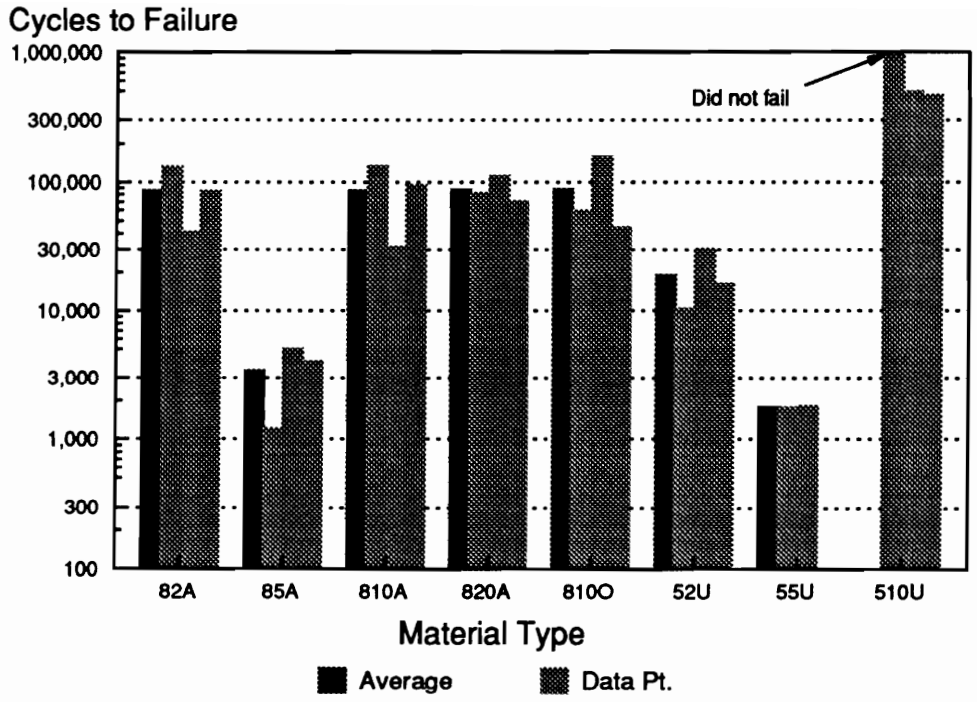

Figure 75. Cycles to Failure of the ± 45° McAir Specimens; Max. Stress = 24 ksi; R = 0.1 at 10Hz.

gins to accelerate towards failure. In a few instances (the 55U and 85A systems), the specimens never "settle" after yielding; they simply keep degrading until failure occurs.

Perhaps the only indication that the 85A specimens would behave so differently from their 8A&O counterparts was the 85A specimens' uncharacteristically low $\pm 45°$ tensile strengths. In Figure 27, the strengths of the 82A, 810A, and 810O systems are nearly equal; thus, 24 ksi represents nearly the same percentage of ultimate strength. The 820A tensile strength is slightly higher; this could be attributed to its thickness, since thickness has been shown to increase the $\pm 45°$ laminate tensile strength [46]. One would think, however, that the increase in 820A strength would be reflected in an increase in cyclic life. Since the 820A is double in thickness, its applied maximum load level is also doubled with respect to its 8A&O counterparts. Fatigue response, as it has already been mentioned, is a function of the *absolute stress level* as well as the ratio of applied stress to ultimate strength. It is also possible that specimen heating played a role in the 820A not achieving a greater average life than its counterparts (see the following section).

While the difference in the fatigue lives of the 8A&O material was generally (in 4 out of 5 cases) unspectacular, the 5U series response varies dramatically among its different systems. If a correlation between higher $\pm 45°$ tensile strength and longer fatigue lives is postulated, then only one of the three systems follows this trend. The 510U material had the highest $\pm 45°$ tensile strength among the eight McAir materials, and its specimens displayed the longest fatigue lives by nearly an order of magnitude. It is very surprising, however, that the 55U material does not behave similarly in terms of cyclic life. The only aspect that separates the two materials (besides surface treatment level) is the thickness of the specimens. Yet, one may claim that the shear stress vs. shear strain plot of the three 5U systems (see Figure 29) anticipated that the 510U material will behave differently from its counterparts.

An X-ray radiograph was taken of a 510U specimen that ran to one million cycles without failure (see Figure 76). There was hope that the radiograph would indicate the predominant damage modes that are present during the late life of many of the $\pm 45°$ McAir systems. To the author's profound amazement, the only damage present in the gage section of the specimen (the region shown in Figure 76) is surface matrix cracking and some edge delamination; *very few cross-*

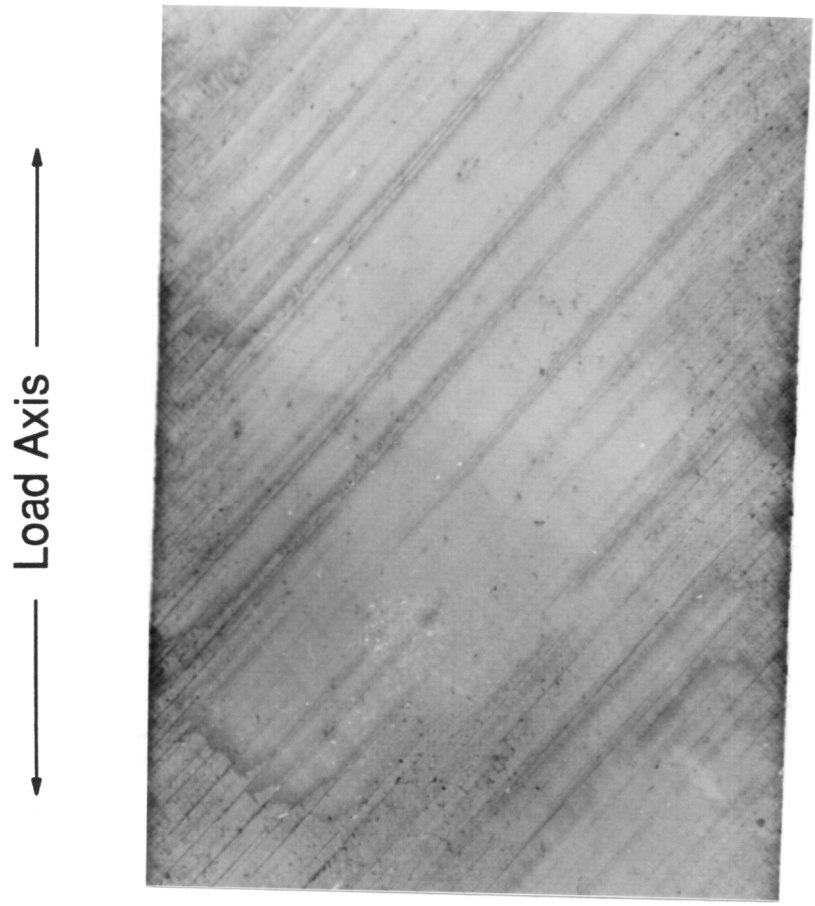

Figure 76. X-ray Radiograph of a ±45° 510U Specimen after 1 Million Cycles; Max. Stress = 24 ksi; R = -1 at 10 Hz.

cracks are located in the mid-section of the laminate. The first explanation of this was that the zinc iodide solution had not penetrated the specimen thoroughly. Yet, if one looks closely, dense cross-cracking is apparent near the grip regions. This indicates that the laminate endured its "yielding" (recall Figure 24) without the contribution of considerable matrix cracking. It is necessary to conclude that this deformation is truly a reflection of matrix behavior. If debonding were responsible for yielding, then one could have anticipated seeing matrix cracking — the product of debonding and one million cycles. Without the matrix cracks (perhaps equivalently, without debonding), the matrix is held responsible for the gross yielding of the material. One could only wonder how the epoxy or thermoplastic systems studied herein would have performed in this instance. This would constitute a fascinating study.

It could be argued that the 32-ply thickness of the 55U specimen caused its virgin tensile strength to appear higher than its 16-ply counterparts. Yet, with the general trend of higher $\pm 45°$ strengths corresponding to higher levels of surface treatment, if the 55U material had been available in a 16-ply configuration, one would not expect its $\pm 45°$ tensile strength to be smaller than the 16-ply 52U $\pm 45°$ tensile strength. The 52U specimens reveal a greater fatigue life than the 55U specimens, however. One might claim that specimen heating contributed to the short lives of the 55U specimens (see below), yet, if this were the case, the 820A specimens should have also possessed unusually short lives.

The cyclic life of the 52U is also difficult to explain when compared to the responses of the 8A&O series systems. This is another instance where an increase in $\pm 45°$ tensile strength *did not* ensure a longer fatigue life. One is tempted to try to attribute the differences in fatigue performance to one of the measures of bond strength, TFS or MMHP. Such a correlation proves to be entirely unsuccessful, in this case.

The fatigue study of the $\pm 45°$ specimens raises more questions than it answers. Differences in fatigue life *are seen*, yet, the reason behind these differences cannot easily be traced to any one or two variables. For the 8A&O series, it seemed that $\pm 45°$ tensile strength was a good basis upon which to rank the fatigue life. This begs the question of how the interphase influences the $\pm 45°$ tensile strength. To make matters worse, this higher strength/longer life philosophy does not apply

to the 5U series. Attempts at correlating cyclic life with bond strength appear unsuccessful. It appears that a key performance variable is eluding description in this study. Specimen temperature is examined below, in the hopes that some light may be cast on this enigma.

Specimen Temperature

Having shown in the notched cross-plied fatigue study that temperature is sensitive to dissipative processes, it was felt that measuring surface temperature could be an effective way to monitor the shear dissipation that accompanies the fatigue of $\pm 45°$ specimens. To this end, the specimen temperature was recorded during the fatigue testing of all eight McAir systems. The average failure temperature, along with the actual values obtained from three specimens from each material type (two specimens for the 55U material) is shown in Figure 77.

The two points that grab one's attention are the average results of the 820A and 55U specimens. These two are the only 32-ply $\pm 45°$ specimens; the others are 16-ply specimens. It was shown in the section detailing the temperature response of the notched cross-plied fatigue specimens that the temperature difference between the center and the surface of the specimen is proportional to the square of the thickness (see equation (3.4)). Thus, it is no surprise that these materials display a much greater maximum surface temperature at failure.

It is interesting to note that the 52U and 510U materials display a noticeably higher failure temperature than their 8A&O counterparts (at least 40°F higher). Disparity between the 8A&O and 5U series' temperatures were seen in the notched cross-plied case, yet, this was attributed mainly to the increase in applied stress that accompanied the higher-strength 5U materials. In the present case, the applied stress remains constant. In order for the temperature difference to be explained by equation (3.4), it would be necessary for the strain amplitude at failure to be consistently larger in the 5U materials than in the 8A&O materials. In the present case, it was not. It is possible that differences in bonding are responsible for the disparity in temperatures between the two series. If this were the case, however, one would strongly suspect that such differences in bonding would

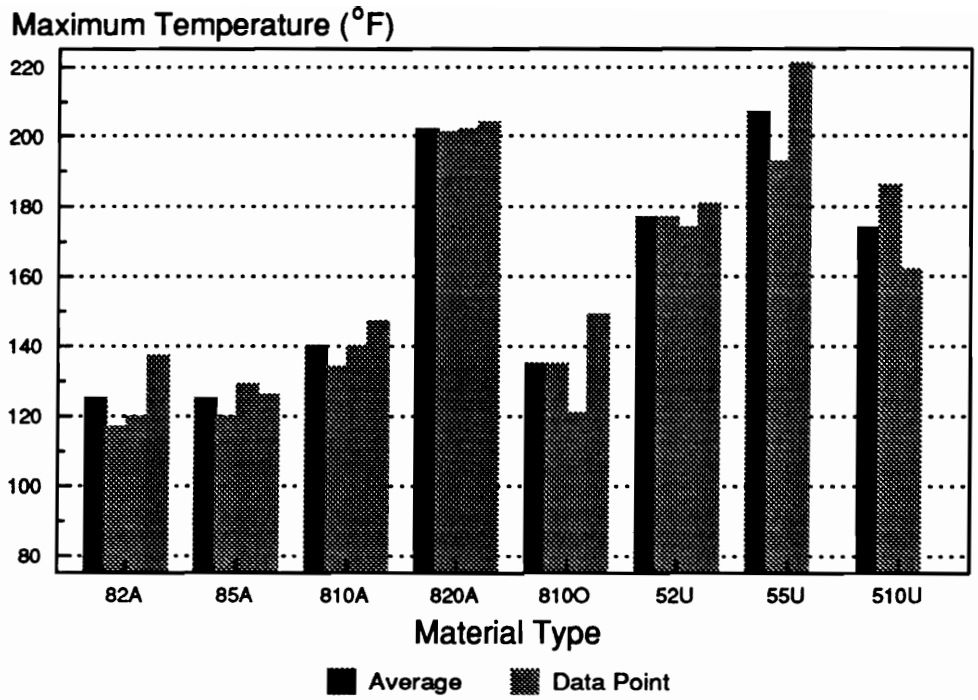

Figure 77. Temperature at Failure of the ±45° McAir Specimens; Max. Stress = 24 ksi; R = 0.1 at 10Hz.

influence the fatigue behavior more than it would the heating behavior. In other words, if bond condition was responsible for the difference in temperature between the 52U and 510U specimens with regard to the 82A and 85A specimens, then one would expect to see similarly ranked differences in fatigue performance. A possible explanation for this behavior may lie in the two opposing fiber systems. One property that could definitely influence the heating behavior of the two systems is thermal conductivity. Despite the matrix system being the same, it is possible that the 5U fibers are more thermally conductive than the 8A&O fibers. In this respect, one would benefit from a micromechanical analysis of thermal conductivity within a composite laminate, cf. [92], for example.

One must openly wonder how dissipative heating contributes to the degradation of a material's performance. Unfortunately, no studies were undertaken in the present investigation to explore the thermomechanical properties of the toughened epoxy. One could envision a scenario in which the thermoplastic phase sustains a transition due to the internal heating. Such speculation is left for future research.

Phase and Gain Measurements using M-R Phase 3000

As was the case in the notched cross-plied fatigue study, though there were a number of reasons to believe that phase and gain data could illuminate the understanding of the fatigue behavior, inconsistent data collection marred any chance of making meaningful comparisons between the systems.

The positive aspects of this system bear repeating, however. In nearly *every* instance, a noticeable increase in the slope of the two signals near the end of a test signified imminent failure. These signals can be likened to a drop in stiffness as measured with an extensometer. Yet, the major advantage to the present system is that the test is a non-contact scheme. This test method allows the operator to monitor the progress of the test in situations and environments where extensometers could not be used. In the $\pm 45°$ fatigue study, specimens late in life were usually replete with surface matrix cracks. This extensive cracking would deteriorate the bond line between the extensometer

tabs and the extensometer, creating erroneous strain information. This is just one instance where DSA monitoring transcends the use of extensometers as a means of evaluating degradation of the material system during fatigue testing.

Modelling Considerations

The input into the ideal composite performance simulation model would be the mechanical and physical properties of the constituents and information detailing in what manner these constituents were brought together. Having this input, the ideal model would be able to predict the performance of a complex-shaped composite structure while under a time-dependent set of loading and environmental conditions. A contemporary and realistic performance simulation code, entitled MRLife 6™ [93], is transforming from a model that demanded input data describing the *lamina* properties of a composite to a model accepting input data that describes properties of the constituents that comprise the lamina. Until recently, only two "constituents" were typically considered: the fiber and the matrix. The main point of this work is to convince the reader that the description of a third constituent is absolutely necessary in order to successfully characterize composite performance. That third constituent is, of course, the interphase.

The purpose of this chapter is to discuss and demonstrate how the interphase may be inserted into models describing composite behavior. Having shown that the interphase can influence the fatigue behavior of composites, the ultimate challenge would be to introduce interfacial properties into a model of fatigue performance. This, however, is a daunting task. Thanks to Reifsnider and Stinchcomb and co-workers, the technical community has been given a clear framework from which one may approach such a task. The "critical element philosophy" of Reifsnider and

Stinchcomb reduces the analysis of the fatigue process into the study of "sub-critical elements" and "critical elements". The initiation, interaction, and growth of damage in "sub-critical elements" causes changes in the local geometry and the local stress state. This altered stress state is inserted along with the residual state of the "critical elements" (those elements whose failure defines specimen failure) into an appropriate failure criteria. The *evolution* of those states as a function of time (or exposure, etc.) define the process known as "fatigue". There are several avenues through which a variable characterizing the interphase may enter this framework. One obvious path lies in the description of the residual state (or — in the case of composite responding to an applied fatigue load — residual strength) of the material. In the past, in an attempt to verify the efficacy of the critical element philosophy in a performance simulation code, the evolution of the residual strength was modelled using a "strength reduction equation"; i.e., a polynomial expression that reduced the initial strength as a function of cycles. The initial desire to base this reduction relationship upon the foundation of mechanics is beginning to be realized. The first step in this realization has been to replace the phenomenological description of material strength with the micromechanical prediction of strength. This is exactly where the interphase may enter the problem, and it is at this juncture where the ensuing discussion will embark.

Composite scientists and engineers have often appealed to micromechanics to predict composite stiffness. This is seen as a mature practice that yields accurate predictions quickly and easily. The use of micromechanics in the prediction of strength, however, has met with considerable resistance and skepticism. Early micromechanical model of strength, though mathematically elegant, often failed to predict strength within engineering accuracy. The value of these models has been in their identification of essential variables within the problem of strength prediction. The seminal work of Rosen [65] stands as a hallmark upon which most treatments of micromechanical strength modelling base themselves. Noticeably absent from a great majority of these models, however, is a variable that quantifies how the fiber and matrix *interact*. This variable — the interphase — is beginning to find its way into contemporary micromechanical models of strength. Recently Gao and Reifsnider [67] have introduced the interphase into a micromechanical model of tensile strength. Experimental work by Madhukar and Drzal [8] show unidirectional compressive behavior to be

intimately related to the bond strength; as bonding became stronger the compressive failure modes changed and the composites became stronger. In the present investigation, definite relationships were seen between bond strength and notched tensile strength. While notched compressive seemed somewhat inured to changes in interphase strength, published unidirectional compressive strength data on the same material systems investigated herein [39] displayed a definite sensitivity to this variable.

With this in mind, an attempt will be made to introduce the interphase into the prediction of notched cross-plied tensile and compressive strength. Prior to solving a notched strength problem, one is forced to reckon with an *unnotched* strength problem. Since the composite to be modelled is cross-plied, this demands an analysis of an unnotched cross-plied laminate. Basing this approach on micromechanics, however, necessitates the formulation of unidirectional strength as a function of the *three* constituents. Therefore, the plan of attack begins with the micromechanical prediction of unidirectional strength, proceeds from there to unnotched cross-plied strength, and then from there to notched cross-plied strength. The first section will deal with the tensile case.

Introducing the Interphase into Predictions of Notched Cross-plied Tensile Strength

According to the plan detailed above, the first step would be to insert the interphase into a model of unidirectional tensile strength. This will not be pursued in this work since considerable headway has been made on this problem [67]. Instead, the starting point for this problem is the same starting point for the majority of analyses dealing with notched laminate tensile strength: the unnotched laminate strength.

The popularity of this starting point is due, in part, to the notched tensile strength model of Whitney and Nuismer [94]. They proposed two failure criteria for notched composites under tensile loading: the "point-stress" criteria and the "average-stress" criteria. In the point-stress criteria, failure of the laminate is predicted to occur when the local stress, σ_x, over some distance, d_o, is equal to or greater than the unnotched strength of the laminate, σ_o; i.e. [94,95]:

$$\sigma_o = \sigma_x(y, 0)_{|y = R + d_o}, \tag{4.1}$$

where,

R is the radius of the center-hole,

x is parallel to the loading direction, and y is perpendicular to the loading direction.

In the average-stress criteria, failure of the laminate is predicted to occur when the stress, σ_x, when *averaged* over some distance, a_o, equals the unnotched strength of the laminate, σ_o; i.e. [94,95]:

$$\sigma_o = \frac{1}{a_o}\int_R^{R+a_o} \sigma_x(y, 0)dy\,. \tag{4.2}$$

One implements the above two criteria by making, at the very least, two measurements: the unnotched strength of the laminate, σ_o, and the applied stress at failure for the laminate, σ_∞, given a fixed hole size, R. Once σ_∞ is known, the *elastic* stress distribution away from the hole can be *approximated* using the expression of Konish and Whitney [96]:

$$\sigma_x(y, 0) = \frac{\sigma_\infty}{2}\{2 + (\frac{R}{y})^2 + 3(\frac{R}{y})^4 - (K_T^\infty - 3)[5(\frac{R}{y})^6 - 7(\frac{R}{y})^8]\}\,,\ y > R\,, \tag{4.3}$$

where,

K_T^∞ is the stress concentration factor of an anisotropic, infinite plate, and can be calculated from the unnotched laminate properties according to [91]:

$$K_T^{\infty} = 1 + \{2[(\frac{E_x}{E_y})^{\frac{1}{2}} - \nu_{xy}] + \frac{E_x}{G_{xy}}\}^{\frac{1}{2}} , \tag{4.4}$$

where,

E_x is the effective laminate elastic modulus along the axis of loading,

E_y is the effective laminate elastic modulus perpendicular to the axis of loading,

G_{xy} is the effective laminate shear modulus, and,

ν_{xy} is the effective laminate Poisson's ratio.

Inserting the stress distribution found in equation (4.3) into the failure criteria (4.1) or (4.2) allows one to calculate the respective distance that produces an equality on each side of the equation. Having measured σ_∞ and σ_o, and having calculated K_T^∞ (from (4.4)) using measured values of the laminate elastic moduli or approximate values from lamination theory, the point-stress distance, d_o, may be calculated from equations (4.3) and (4.1) according to:

$$\frac{\sigma_\infty}{\sigma_o} = \frac{2}{\{2 + \xi_d^2 + 3\xi_d^4 - (K_T^\infty - 3)(5\xi_d^6 - 7\xi_d^8)\}} , \tag{4.5}$$

where,

$$\xi_d = \frac{R}{(R + d_o)}.$$

The average-stress distance, a_o, is calculated via equations (4.2)-(4.4) according to:

$$\frac{\sigma_\infty}{\sigma_o} = \frac{2(1 - \xi_a)}{\{2 - \xi_a^2 - \xi_a^4 + (K_T^\infty - 3)(\xi_a^6 - \xi_a^8)\}} , \tag{4.6}$$

where,

$$\xi_a = \frac{R}{(R + a_o)}.$$

Once d_o or a_o is calculated according to equations (4.5) and (4.6), respectively, this value is said to be *a property of the laminate*, that does not change with hole size or stacking sequence. While few

argue that d_o or a_o is useful in predicting the change in laminate strength as the hole size changes, many have shown that the two parameters do *not* successfully predict notched strength once the stacking sequence of the laminate changes [97]. This led El-Zein [98] to apply the criteria at the ply level instead of the laminate level. Having met with success in this approach, he hypothesized an invariant equation for calculating the average-stress parameter, a_o, for all stacking sequences, once the parameter had been calculated for an arbitrary stacking sequence; the form of this equation is:

$$\left[\frac{a_o v_{xy}}{K_T^{\infty}}\right]_1 = \left[\frac{a_o v_{xy}}{K_T^{\infty}}\right]_2 , \tag{4.7}$$

where,

a_o is calculated for an arbitrary laminate configuration (denoted "1" or "2").

Kortschot and Beaumont [79] openly question the philosophy upon which notched strength models such as point-stress and average-stress criteria are based. According to their reasoning, the use of anisotropic elasticity to predict the stress distribution in a composite just prior to failure is erroneous. Notched laminates, they argue, undergo sub-critical damage that alters the local stress state dramatically, thus invalidating the use of "elasticity". Instead, one should utilize the realistic, as-damaged stress state of the composite just prior to failure (the so-called "terminal state") in an appropriate failure criteria. In their study of double-edge notched (notched with triangular cuts) cross-plied laminates, they found that the terminal stress state could be accurately approximated simply by accounting for the length of the longitudinal splits next to the notches. As the splits grew, the stress concentration due to the notches decreased. Therefore, the longer the splits, the higher the applied stress that could be carried prior to failure. Failure in the laminate occurred when the strength of the 0° ply (the critical element), σ_{0f}, was met or exceeded by the local stress expressed simply as the applied stress, σ_{∞}, multiplied by the stress concentration (which is a function of split length), K_T, or:

$$\sigma_{\infty f} = \frac{\sigma_{0f}}{K_T} \ . \tag{4.8}$$

For the particular material system employed in their study, they determine a phenomenological expression for K_T as a function of the ratio of split length to notch size, l/a. Therefore, the value on the left side of equation (4.8) is a function only of the 0° intrinsic strength (which they calculate using Weibull strength modelling) and the ratio, l/a. They then appeal to energy arguments in an attempt to predict the length of the split (and, therefore, the ratio, l/a) as a function of the applied stress, arguments that ultimately depend on the value of the strain energy release rate for *delamination* (see Ref. [99] for these details). Having gone through these manipulations, they arrive at an expression for notched strength that *only* varies as a function of the notch size, or, for their particular material system and geometry:

$$\sigma_{\infty f} = Ca^{-0.188} \ , \tag{4.9}$$

where,

a is the notch size, and,

C is a constant incorporating all of the material properties that enter into the problem.

It is the present author's contention that these two analyses (the Whitney and Nuismer analysis and the Kortschot and Beaumont analysis) should be reconcilable. Proof of this lies in the data below.

Discussion of Data

As promised earlier, the starting point in the discussion of how the interphase could enter the notched cross-plied tensile strength problem will begin with the unnotched cross-plied tensile strength. A small digression is in order, however. If one were to begin by introducing the inter-

phase into the micromechanical expression for unidirectional tensile strength, the present data indicates that a considerable challenge lies in waiting. The normalized unidirectional tensile strength of the fourteen systems under investigation (culled from published reports by McAir and Northrop [37,39]) is plotted against their respective transverse flexural strength in Figure 78 and their respective values of MMHP in Figure 79. Unfortunately, no *obvious* relationship between unidirectional tensile strength and interphase strength is apparent from these data. Yet, when one compares the normalized unnotched cross-plied tensile strength [37,40] with the transverse flexural strength (see Figure 80), the data "cleans up" somewhat (though cross-plied tensile strength vs. MMHP does not). This may indicate the importance that *in situ* 90° strength has on the specimen strength of a cross-plied laminate.

With the unnotched cross-plied tensile strength of these fourteen material systems known (from published accounts [37,39]) and the notched cross-plied tensile strength measured during this study, the only piece of information needed to perform the Whitney and Nuismer analyses detailed earlier (equations (4.5) and (4.6)) is the stress concentration factor, K_{f^∞}. Examining equation (4.4), since the laminates are cross-plied, $E_x = E_y$, thus leaving E_x, G_{xy}, and ν_{xy} to be determined. The effective laminate axial modulus, E_x, and effective laminate shear modulus, G_{xy}, of the McAir material was measured in this investigation (see Figure 22 and Table 6, respectively) and collected from a published Northrop report [39]. This leaves ν_{xy} as the only unknown. Using the considerable data published by Northrop [39], ν_{xy} could be approximated via lamination theory. For the McAir material, attempts at measuring ν_{xy} using front and back mounted extensometers proved entirely unsuccessful. Without the knowledge of basic lamina properties, ν_{xy} could not be calculated using lamination theory. Instead, after examining the effective laminate Poisson's ratio values for the Northrop material systems, it was decided to fix the value of ν_{xy} for the McAir material (possessing the same toughened epoxy matrix) at 0.02. Careful analysis of equation (4.4) reveals that moderate changes in ν_{xy} are not critical in the calculation of K_{f^∞}. These pertinent data were inserted into equations (4.5) and (4.6).

Solving equations (4.5) and (4.6) for ξ would, in the past, have been challenging, requiring a computer sub-routine that could find the roots of an eighth-order equation. The author, however,

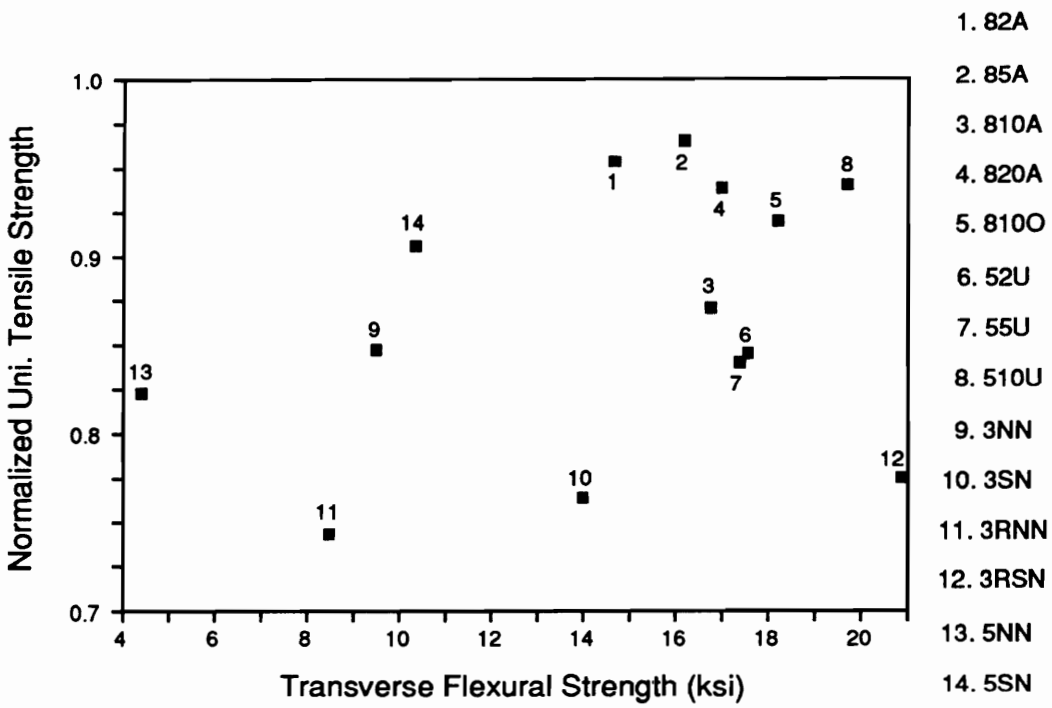

Figure 78. Normalized Unidirectional Tensile Strength versus Transverse Flexural Strength of the McAir and Northrop Materials [37,39].

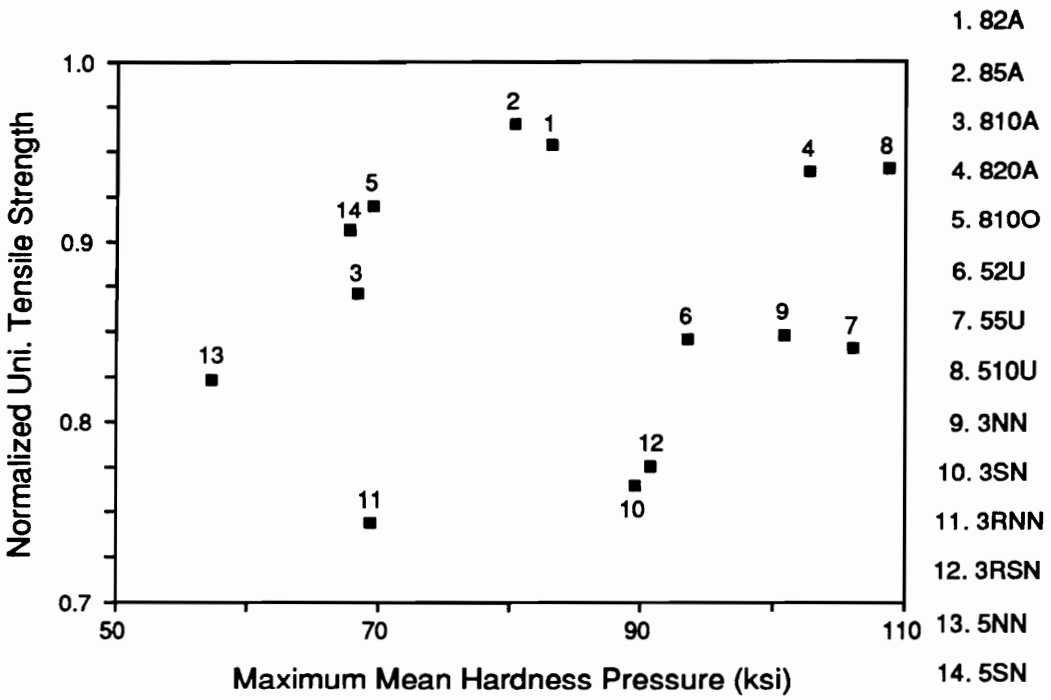

Figure 79. Normalized Unidirectional Tensile Strength versus Max. Mean Hardness Pressure of the McAir and Northrop Materials [37,39].

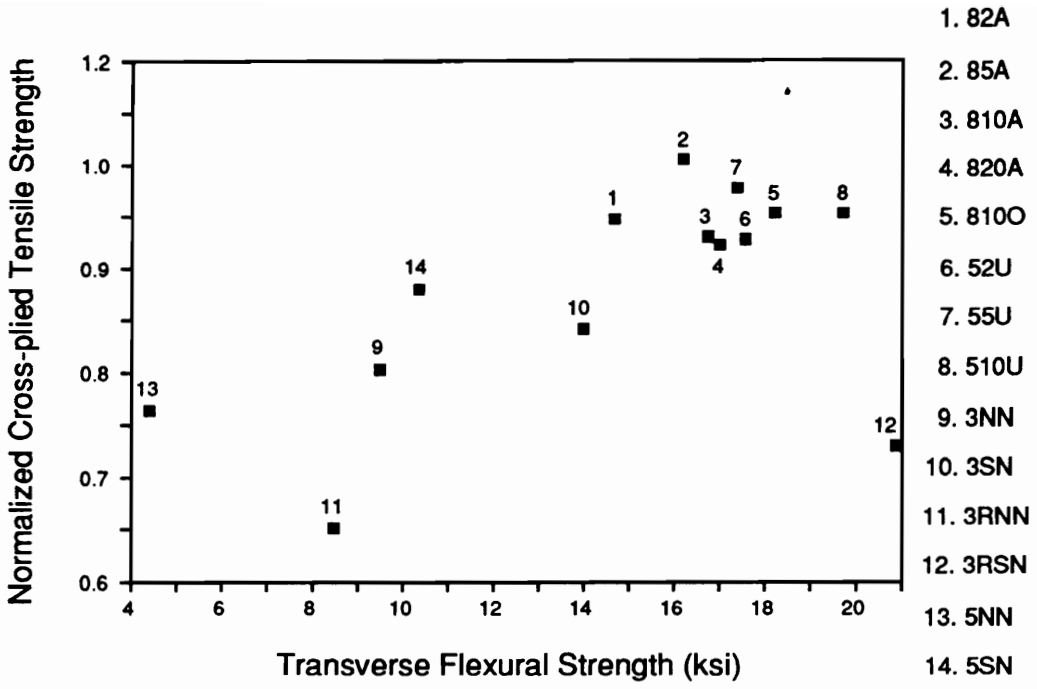

Figure 80. Normalized Cross-plied Tensile Strength versus Transverse Flexural Strength of the McAir and Northrop Materials [37,40].

had the pleasure of using the software package, "Mathematica"™ [100], which reduces the task of solving the eighth-order equations of (4.5) and (4.6) dramatically. One need only to input the values for $K_{\mathcal{P}}$ (which were calculated via spreadsheet computations) and the ratio of the notched tensile strength over the unnotched tensile strength, along with the symbolically-written equations ((4.5) and (4.6)) and request the program to solve for "NRoots". Seconds later, a total of eight (real and imaginary) roots appear.

This procedure was followed to calculate the average-stress criteria parameter, a_o. This parameter was chosen for display rather than the point-stress parameter (with no loss in generality). The calculated a_o values for all fourteen material systems are presented in Figure 81. Large values of a_o connote notch *insensitivity*, i.e., the strength of the notched specimen reflects more a reduction in load-carrying area than it does a stress-concentration-driven phenomena. Considering the arguments of Kortschot and Beaumont (discussed above), the higher the value of a_o, the greater the ability of the laminate to reduce the global stress concentrator (according to them, through longitudinal splitting). The data in Figure 81 seems to follow a definite trend. All of the systems that received 0% surface treatment reveal noticeably larger values for a_o than their 100% surface treated counterparts. Looking at the McAir material, with the exception of a few points (82A and 55U), as the level of surface treatment increases, the value of a_o decreases. These observations led the present author to compare the calculated value of a_o to a measure of the interphase strength, namely the transverse flexural strength; a plot of these two variables for all fourteen material systems is shown in Figure 82.

The relationship seen between the value a_o and the TFS confirmed the hypothesis put forward in the previous chapter: notched cross-plied tensile strength intimately depends on interphase strength. Within the extent of experimental spread, it is clearly seen that as the strength of the interphase increases, the composite becomes more notch sensitive, i.e., the ratio of notched strength to unnotched strength *decreases*. While many may have suspected such a relationship, it is very surprising to find such a *linear* relationship with the *transverse strength* of the interphase. It would seem more plausible that such a relationship might exist between notched strength and the *shear*

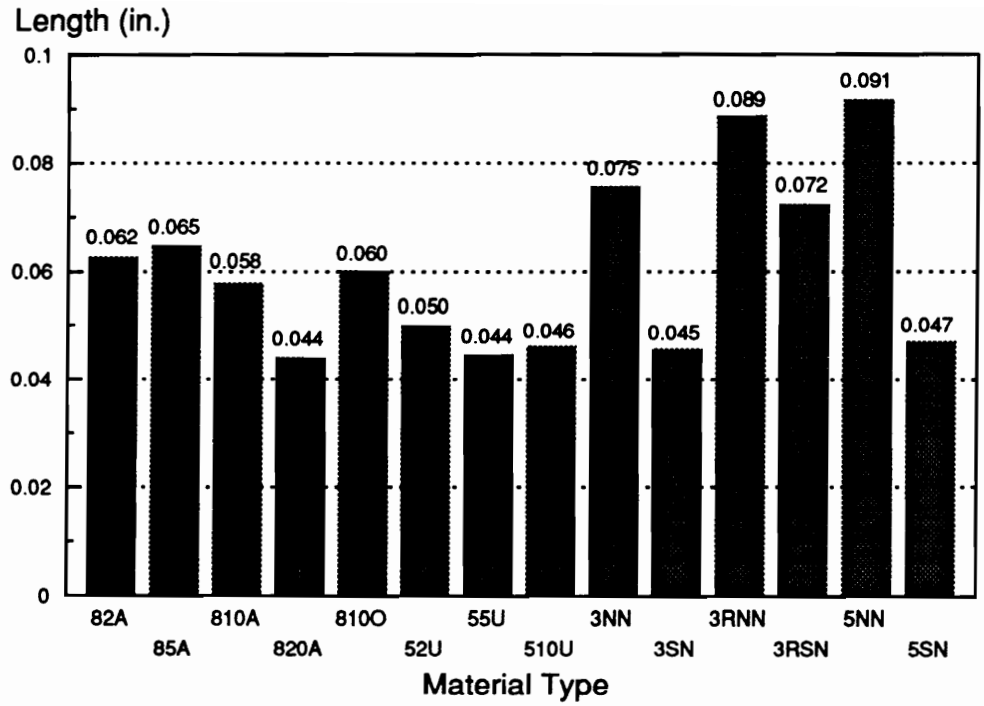

Numbers above the column represent calculated values

Figure 81. The Calculated Average-Stress Criteria Parameters of the McAir and Northrop Materials.

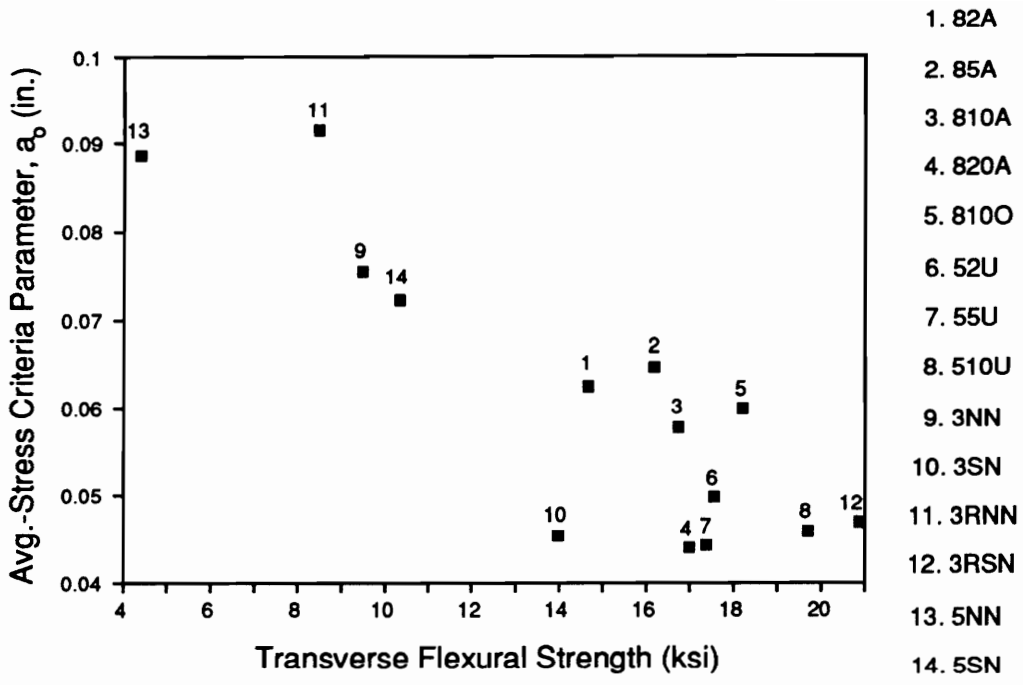

Figure 82. The Calculated Average-Stress Criteria Parameter versus the Transverse Flexural Strength of the McAir & Northrop Materials.

strength of the interphase. If one plots a_o versus MMHP, the relationship is linear only in as much as the relationship between TFS and MMHP is linear (recall Figure 11).

It is the functional relationship between a_o and the bond strength that reconciles the Whitney-Nuismer analysis and the Kortschot and Beaumont analysis of notched tensile strength. The value a_o is created out of *a priori* knowledge of notched strength. The merit of the Whitney-Nuismer analysis is not in the value of a_o *per se*, but in its ability to be used in strength predictions where the size of the hole changes. When the hole size changes, a_o is said to remain constant for the given laminate. It is the present author's claim that imbedded within the computation of a_o is an account of the *damaged state of the material.* Because notched strength is input into the calculation of a_o, this value necessarily *reflects* the damage that has taken place in the material. Therefore, buried deep within a_o is the degree in which the material was able to relieve the global stress concentration; it arrives at a_o through the value of the notched strength. Yet, this argument can now be turned completely around. From the results of Figure 82 it seems that the notched strength (or, more precisely, the ratio of the notched strength to the unnotched strength) is a function of the strength of the interphase (and of the geometry, and of the elastic moduli of the laminate, etc.). This is the point that Kortschot and Beaumont were trying to make, without explicitly proving it. By attributing the notched strength to the ability of the laminate to form longitudinal splits, they implicitly formed a relationship between notched cross-plied tensile strength and interphase strength. The energy analysis used in their derivation of longitudinal split length as a function of applied stress yielded a quantity that characterized the material's resistance to debonding — albeit resistance to delamination — namely, the critical strain energy release rate for delamination. Perhaps this quantity and the transverse flexural strength (TFS) are related. It was shown in Figure 26 that the Edge Delamination Strength (EDS) of the Northrop material was linearly related to its $\pm 45°$ tensile strength, and in Figure 23 it was shown that $\pm 45°$ tensile strength strongly correlates with TFS. O'Brien [101] has shown that the critical strain energy release rate for delamination, G_d, is proportional to the square of the Edge Delamination Strength. Thus, if one accepts a linear relationship between EDS and TFS, then it should follow that G_d is proportional to the square of the TFS.

The form of the relationship between the ratio of the split length to the notch width, l/a, and G_d, derived by Kortschot and Beaumont, has the form:

$$\frac{l}{a} \propto \frac{\sigma_\infty^2}{G_d} , \tag{4.10}$$

where,

σ_∞ is the applied stress.

If one were to replace G_d with a constant times the square of the TFS, then the expression in (4.10) would look similar to the expression Tirosh derives for split length as a function of applied stress [102], namely:

$$\frac{l}{a} \propto \left(\frac{\sigma_\infty}{\tau_o}\right)^2 , \tag{4.11}$$

where,

τ_o is the "maximum shear strength the matrix can sustain" [102].

If one were to replace the word "matrix" with "interphase", and apply the present finding that the shear strength of the interphase is well-characterized by the TFS (which is nearly proportional to the MMHP), then one can fully appreciate the manner in which the interphase strength physically and mathematically enters a model of notched cross-plied tensile strength.

Introducing the Interphase into Predictions of Notched Cross-plied Compressive Strength

In this section an attempt will be made to introduce the interphase into a micromechanical model of the unidirectional compressive strength. Prior to delving into this subject, it will be prudent to review the current philosophy and achievement attained in micromechanical compressive

modelling. This review is in no way complete — it is meant to introduce to the reader the key variables and issues that attend such modelling. For a more complete treatment, the reader is urged to peruse the thorough reviews found in References [103-105].

A Survey of the Micromechanical Theories of Compressive Strength

For the past twenty-five years, a myriad of scientists have attempted to formulate a model for the compressive strength of 0° unidirectional laminates. The constructed theories may be categorized into two general groups; instability analyses and constituent failure theories. This survey shall examine each group.

Instability Analyses: Rosen [65] is credited with one of the first mathematical analyses of compression-loaded unidirectional composite laminates. He postulated that fibers would deform in either an "extension" or "shear" mode; laminates with fiber volume fractions above 20%, however, usually deform in the latter mode. Microbuckling of the fibers would occur in the shear mode when the laminate achieved a critical stress given by the equation:

$$\sigma_c = \frac{G_m}{1 - V_f} + \frac{\pi^2 E_f V_f}{12} \left(\frac{h}{\lambda}\right)^2, \tag{4.12}$$

where,

σ_c is the laminate critical stress,

G_m is the shear modulus of the matrix,

V_f is the fiber volume fraction,

E_f is the fiber axial modulus,

h is the fiber width, and,

λ is the buckle half-wavelength.

Rosen simplified (4.12) by assuming that the ratio, $\frac{h}{\lambda}$, when squared, is negligible. Thus, (4.12) reduces to:

$$\sigma_c = \frac{G_m}{1 - V_f} \ . \tag{4.13}$$

Experimental results have shown that equation (4.13) over-estimates the unidirectional strength by a factor of two to three. Rosen, in an attempt to explain this disparity, claimed that the matrix shear modulus likely decays as the applied load increases.

Since the publication of [65], several researchers have attempted the compression/instability problem by employing a number of different techniques. Hayashi [106] and Foye [107] concluded from their separate analyses that the critical failure stress is simply:

$$\sigma_c = G_{LT} \ , \tag{4.14}$$

where,

G_{LT} is the effective in-plane composite shear modulus.

One may calculate the composite shear modulus, G_{LT}, from its constituents [108], resulting in:

$$G_{LT} = \frac{G_m}{V_f \frac{G_m}{G_f} + (1 - V_f)} \ , \tag{4.15}$$

where,

G_f is the fiber shear modulus.

If one assumes that the ratio, $\frac{G_m}{G_f}$, is negligible, then (4.15) becomes:

$$G_{LT} = \frac{G_m}{1 - V_f} \ , \tag{4.16}$$

which, when inserted in (4.14), concurs with (4.13). Instability analyses by Shuerch [109], Chung and Testa [110], Wang [111], Shuart [103], and Hyer [112], may all be reduced — under similar assumptions — to equation (4.13) or (4.14).

Many researchers have balked at equation (4.13) or (4.14) because of its inflated strength prediction. They have suggested that the modulus appearing in each of these equations should be a secant, rather than tangent measurement. Still others have introduced new variables into their instability analyses. Foye [107] multiplied (4.13) by a constant, η, representing a "void factor". Its mathematical expression is:

$$\eta = \frac{1 - 2(\frac{v}{1 - V_f}) + (\frac{v}{1 - V_f})^2}{1 + (\frac{v}{1 - V_f})}\ , \tag{4.17}$$

where,

v is the void volume fraction.

Kulkarni [113], in conjunction with Rosen and Rice, modified (4.13) by quantifying the effects of fiber shear deformation and fiber/matrix adhesion. Their result appears as:

$$\sigma_c = G_m[\frac{1 - (1 - k)V_f}{1 - (1 - \frac{G_m}{G_f} k)V_f}]^2 [1 - (1 - \frac{G_m}{G_f})V_f]\ , \tag{4.18}$$

where,

k is a measure of the degree of fiber/matrix bonding such that $-(\frac{1 - V_f}{V_f}) \leq k \leq 1$.

Hahn and Williams's [114] instability analysis examined a single fiber instead of a fiber-matrix system. Their results differ from (4.14) by a factor of V_f. Shuart [103] recognized that Rosen's model was only applicable to interior fibers. Surface fibers, he reasoned, would receive half of the

support of interior fibers. His "fiber-plate" analysis derived a factor of 0.5, multiplying equation (4.13).

Greszczuk [115] modified equation (4.12) for instances when the laminate's ends are *not* simply-supported — an assumption made in Rosen's model. He developed an "end fixity parameter" which multiplies the second term in (4.12). He claimed that the value of this parameter varies from 1 (the simply-supported case) to 4 (the fixed-fixed case).

Waas, *et al.* [116], on the basis of their thorough experimental work [117], identified the absence of free-edge tractions as critical to the analysis of unidirectional compressive failure. Their two-dimensional mechanical model predicts reasonable buckling strains at low fiber volume fractions (FVFs), yet, at higher FVFs, buckling wavelengths are predicted that invalidate the assumptions of the model.

Lessard and Chang [118], basing their analysis on the work of Hyer [112], reasoned that fiber-fiber interactions come into play when the applied stress is non-uniform. They devised a methodology to account for the deformation of each fiber in a two-dimensional array based upon the principle of influence coefficients. Using this technique, they were able to recover the expression (4.12) when the applied stress was uniform. In the case of non-uniform loading — the load distribution that would result due to the presence of a center-hole stress concentrator, for example — they predict that the *local* fiber buckling stress is 1.79 times higher than the buckling stress calculated under conditions of uniform loading.

Constituent Failure Theories: Despite the consistent outcome achieved from the various instability analyses, there are some who maintain that such analyses poorly represent the physical situation. Inherent laminate imperfections, i.e., fiber waviness, likely control the laminate strength. Besides, most elastic systems possess post-buckling strength [112]. For these and other reasons, some researchers have attempted to limit composite strength by the strength of its constituents.

Wang [111] modelled post-cured fiber waviness with a simple sin curve ($w_o = f_o \sin \frac{\pi x}{L}$). Element equilibrium resulted in the following equation for the laminate compressive strength:

$$\sigma = G_{LT}(1 - \frac{f_o}{f_c}), \tag{4.19}$$

where,

f_o is the amplitude of the initial imperfection, and,

f_c is the amplitude of the imperfection at failure.

In order to determine f_c, Tsai and Hahn [119], basing their analysis on Wang's work [110], cited two possible failure modes: local shear failure and bending failure in the fibers. They concluded that the former mode is more likely to occur and determined f_c from this limiting condition. Their final expression reads:

$$\sigma = G_{LT}[\frac{1}{1 + (\pi \frac{f_o}{L})\frac{G_{LT}}{\tau_c}}], \tag{4.20}$$

where,

L is half-wavelength of the initial imperfection, and,

τ_c is the shear strength of the composite.

The modulus G_{LT} may be resolved [118] such that:

$$G_{LT} = \frac{E_f V_f}{2}(\frac{h}{L})^2[1 + (\frac{h}{L})^2 \frac{E_f}{4G_f}], \tag{4.21}$$

where all the variables have been defined earlier.

From (4.20), if f_o is zero (all fibers are initially straight), then (4.20) reduces to (4.14). Hahn and Williams [114] derived the same equation as (4.20), yet, again, a factor of V_f accompanied their expression.

Batdorf and Ko [61] analyzed the geometry of a "kinked" fiber. They arrived at a simple expression for the unidirectional compressive strength:

$$\sigma = \frac{\tau_f'}{\alpha_o + \gamma_f} \quad , \tag{4.22}$$

where,

τ_f' is the shear strength of the composite in the material axes,

α_o is the angle between the load and material axes, and,

γ_f is the shear strain to failure of the composite.

If the matrix in (4.22) is assumed to be elastic-perfectly plastic, then (4.22) concurs with the relation derived by Budiansky [120]:

$$\sigma = \frac{\tau_y}{\phi + \gamma_y} \quad , \tag{4.23}$$

where the subscript, y, refers to *yield*, and,

ϕ is the angle of initial fiber misalignment.

Hyer [112] has approached the compression problem by modelling the initial fiber imperfection as a sin curve in the same manner as Wang [111]. Employing an energy formulation, he arrived at the following equation for the unidirectional compressive strength:

$$\sigma = [\frac{G_m}{1 - V_f} + \frac{\pi^2 E_f V_f}{12} (\frac{h}{L})^2](\frac{\overline{A} - \overline{A}^o}{\overline{A}}) \, , \tag{4.24}$$

where,

$\overline{A}^o = \frac{f_o}{h}$, and,

$\overline{A} = \frac{f}{h}$ (f and h are defined earlier).

Failure occurs in (4.24) when $\overline{A}$ reaches a critical value. This value is achieved upon constituent failure in one of two modes: fiber failure due to the sum of bending and axial strain (ε_{max}) or matrix shear failure (γ_{max}). These two relations may be expressed mathematically as:

$$\varepsilon_{max} = \frac{\pi^2}{2}\left(\frac{h}{L}\right)^2 \overline{A} + \frac{\overline{\sigma}}{E_f}\ , \tag{4.25}$$

where,

$\overline{\sigma}$ is the axial stress in the fiber, and,

$$\gamma_{max} = \frac{\pi}{1 - V_f}\left(\frac{h}{L}\right)(\overline{A} - \overline{A}^o)\ . \tag{4.26}$$

When either strength condition is violated, $\overline{A}$ is defined, and the laminate strength may be determined from equation (4.24). From (4.24), if $\overline{A}^o$ is zero (initially straight fibers), equation (4.24) reduces to equation (4.12).

Steif [121,122], after observing that fiber failure accompanies kink failure in composites, poses a very fundamental question: Does fiber failure precede kinking, or is fiber failure a result of kinking? To answer this question, he analyzes two scenarios in an attempt to calculate the critical applied strain that produces: 1.) fiber failure in an initially-misaligned fibrous composite, and, 2.) the minimum applied strain that will maintain a kink band. In his analysis of fiber failure, he discards the limiting assumptions of classical linear beam theory, and permits finite fiber deflections. His final strain-to-failure values are cast as a function of critical fiber half-wavelength — a variable that must be input into the analysis. The critical fiber half-wavelength can be determined either from experimental observation or approximated from the critical half-wavelength calculation that falls naturally from the extension-mode analysis of Rosen [65]:

$$L_c = \pi\left[\frac{EI}{E_T}\right]^{\frac{1}{4}}\ , \tag{4.27}$$

where,

EI is the bending stiffness of the fiber bundle, and,

E_T is the transverse modulus of the foundation, "a value somewhere between the matrix modulus and the composite transverse modulus" [121].

Adaptation of the Present Unidirectional Micromechanical Model

In attempting to introduce the interphase into a micromechanical model of unidirectional compressive strength, the first decision one must make is whether to pursue an instability (microbuckling) analysis or a constituent failure analysis. There are persuasive arguments on both sides of this issue. The final failure mode for most standard fiber volume fraction composites is kinking (which may or may not be a manifestation of microbuckling) — truly resembling an instability failure (or, collapse). The vast majority of buckling analyses are performed in the classical sense, i.e., they assume a perfectly straight fiber and calculate the conditions upon which the fiber can maintain a non-straight configuration; these problems reduce to linear eigenvalue problems. It seems unreasonable to consider that *every* fiber in a composite is perfectly straight. The assumption of initially-misaligned fibers helps to explain why composites "stiffen" when loaded in tension, and why their compressive modulus is rarely as high as their tensile modulus. Given these conditions, the assumption of initial fiber misalignment seems to be physically acceptable. Therefore, the work performed in the class of micromechanical models entitled "Constituent Failure Theories" will be given greater attention than the "Instability Analyses".

Having studied the positive contributions of each micromechanical theory, one can form a "checklist" of attributes their own model should have. The ideal model would take into account the effect of the free-edge, since, as many researchers have observed, compressive failure nearly always initiates at this location. The ideal model would take into account the role of matrix and/or fiber failure, and analyze the composite's response to this local failure. The perfect model would be three-dimensional in nature, not restricting the deformation field of the fibers. Yet, in falling short of perfection, sacrifices must be made. Waas, *et al.* [116], and Shuart [103] have published earnest attempts at accounting for the free edge; both analyzes, however, suffer somewhat from computational intractability. This would also be a disadvantage for any three-dimensional analysis. Given present limitations (perhaps in imagination and computer literacy) it is the author's opinion, and one shared by other researchers [118], that the model of Hyer possesses sufficient generality to

account for many important parameters. Therefore, the framework of Hyer's model will serve as the starting point in the present analysis.

Beginning with the equations and the philosophy behind the equations (4.24)-(4.26), the first scenario examined will be when fiber failure occurs due to shear failure of the supporting media. In Hyer's model, this supporting media is considered the matrix; in this case it will be consider a hybrid of the matrix and interphase. In the shear failure scenario, as the array of fibers deform in the "shear" mode (where it is assumed the supporting material carries only shear stresses and no transverse stresses) the shear strain of the supporting media increases at the nodal points of the assumed sin wave fiber deformation. Once the shear strain reaches its maximum value, γ_{max}, the fibers are thought to "unzip", that is, create a catastrophic sequence in which the local failure progresses along the length of the fiber causing complete failure [123]. Equation (4.26) equates the normalized amplitude of fiber deformation, $\overline{A}$, to the maximum shear strain of the supporting media. The claim can be made that since it is the interphase that is in intimate contact with the fiber, and, assuming the interphase is the "weak link" in the system, the interphase shear *yield* strain should define γ_{max}. If one solves equation (4.26) for $\overline{A}$ and then inserts this expression into (4.24), after some manipulation, the final result is:

$$\sigma_{=}[\frac{G_m}{1-V_f}+\frac{\pi^2 E_f V_f}{12}(\frac{h}{L})^2][1+(\pi\frac{f_o}{L})(\frac{G_{LT}}{\tau_{max}})(\frac{1}{1-V_f})]^{-1}, \tag{4.28}$$

where,

τ_{max} would then become the shear strength (or, yield strength) of the interphase,

G_{LT} is the effective shear modulus of the composite, again, reflecting the presence of the interphase, and,

L is the half-wavelength of the resulting failure mode, to be addressed below.

The expressions in (4.28) that merit further discussion are the ratio $\frac{G_{LT}}{\tau_{max}}$ and $\frac{h}{L}$. Recognize that $\frac{G_{LT}}{\tau_{max}}$ represents the inverse of the γ_{max} (if G_{LT} is a secant measurement). The $\pm 45°$ shear strength data could ultimately represent τ_{max} in (4.28). These values are shear stresses at failure, not yield stresses. Realistically, the yield strength should be approximately 70-80% of the ultimate

strength (see Figures 28 and 29). This was not done, however, since the ratio, $\frac{G_{LT}}{\tau_{max}}$, produced physically reasonable values when the *ultimate* shear strength was input into τ_{max}. This is one location where interfacial properties could enter the analysis. If one had a reliable method to measure the maximum shear strain that the interphase could tolerate prior to yielding, this would be an ideal location to insert this value. Without having such a value, the present procedure was adopted. It was necessary to quantify the presence of the interphase in another manner.

The ratio $\frac{h}{L}$ represents the ratio of the fiber diameter over the half-wavelength of the initial imperfection shape. In many micromechanical models of compressive strength the value, L, is treated as an input variable since there are only two realistic ways in which it can be measured: initially (in the virgin material) [124] or post-mortem — given the assumption that the catastrophic microbuckle wavelength is simply an amplification of the initial shape. The inability to know (or accurately measure) L *a priori* is a profound "stumbling block" for most analyses. The sinusoidally-shaped fiber with an arbitrarily-chosen half-wavelength of L is a mathematical idealization introduced to "force" the composite to collapse over experimentally determined wavelengths. It *must* be that the wavelength of the kink band (or microbuckle) in a real failed composite is an intrinsic property of the composite. Its state variables must *dictate* the wavelength over which it collapses. No rigorous micromechanical analysis predicts this wavelength from the properties of the composite, with the exception of the prediction that arises from considering extensional deformation in a low fiber volume fraction composite [65]. The "critical" half-wavelength of buckling predicted from this analysis is given in (4.27). This equation is employed in the present analysis, drawing inspiration from Steif [121]. In the present case, however, the moment of inertia of a *single fiber* is used (instead of a fiber bundle [121]). The ratio of the critical half-wavelength (which serves as the shape of the initially-misaligned fiber) to the fiber diameter then becomes:

$$\frac{L}{h} = \frac{\pi}{2}\left[\left(\frac{\pi}{4}\right)\left(\frac{E_f}{\psi E_T}\right)\right]^{\frac{1}{4}}, \tag{4.29}$$

where,

E_T is the transverse modulus of the "foundation", and,

ψ is equal to one (and will be discussed below).

The presence of the interphase is inserted in (4.29). The motivation for adjusting (4.29) through the parameter ψ comes from the thought that the interphase likely influences the critical wavelength over which the fibers collapse. In other words, strong bonding probably minimizes this wavelength, while weak bonding promotes long buckling wavelengths. This hypothesis is currently being tested by Lesko [125], and preliminary results seem encouraging. The scaling factor, ψ, is positioned in front of the transverse foundation modulus E_T in (4.29). This factor represents the ratio of the $\pm 45°$ tensile strength of the particular material system was under investigation (which has been shown to correlate linearly with the transverse flexural strength, and, therefore, is able to characterize the bond strength well) to the $\pm 45°$ tensile strength of the *strongest* material system (of the systems for which data was available [39]). In order to represent the product ψE_T, ψ is simply multiplied by the unidirectional transverse (90°) tensile stiffness (data that was supplied by Northrop [39]). The manner in which the interphase is introduced into the model (via ψ) lacks mathematical rigor; yet, the wavelength values that result from (4.29) are physically satisfying and concur reasonably well with experimental numbers.

In order to get numerical predictions out of equation (4.28), several material properties must be input. These values have been gleaned from the material characterization tests Northrop ran on their 20 different material systems [39] (of which six of the twenty have been investigated herein). The shear modulus computed from tensile testing of $\pm 45°$ laminates is used to represent G_{LT}, the fiber modulus (as determined from the manufacturer) represents E_f, V_f is taken from the FVF data that accompanied Northrop's longitudinal compressive strength data [39], h is the fiber diameter (as determined from the manufacturer), τ_{max} is the ultimate shear strength determined from $\pm 45°$ tensile coupons [39], L is calculated according to (4.29), and f_o is an adjustable parameter representing the amplitude of sin wave that characterizes the initial fiber misalignment. Using these values, the prediction of (4.28) is plotted against the actual, experimentally-determined unidirectional compressive strengths [39] (both axes are normalized to protect proprietary information) in Figure 83. It is obvious that (4.28) fails to reasonably characterize the actual compressive data. The free parameter, f_o, when divided by the critical half-wavelength, L, is proportional to the maximum an-

gular deviation of the initially-misaligned fiber; in Figure 83 this angle is 11.0% — a nearly unrealistic value. The major consequence of decreasing (increasing) the ratio of $\frac{f_o}{L}$ is to shift the data vertically upward (downward), i.e., the prediction becomes much greater than the actual strength.

It appears that the equations derived from the "shear failure" scenario are unable to predict the actual unidirectional compressive strength. Therefore, it was necessary to consider the "bending failure" scenario delineated by equations (4.24) and (4.25). In this scenario, the fiber "bows" under the applied compressive stress. The bending moment (hence, the bending stress) in the fiber becomes greatest at the antinodes. When the strain that has developed in each fiber — as a consequence of its exaggerated curvature and the compressive load it carries — exceeds its intrinsic strain limit, failure is said to occur. This failure then triggers the process of sequential failure that ultimately takes the shape of kinking. Therefore, once the strain to failure of the fiber, ε_{max}, is known, this value is related to the final deformation state of the fiber, $\overline{A}$. Solving for $\overline{A}$ in (4.25) and inserting this into (4.24) yields a quadratic expression that is solved using the quadratic formula, or:

$$\sigma_{=} \frac{\alpha - \{\alpha^2 - 4\beta\chi\kappa\}^{\frac{1}{2}}}{2}, \tag{4.30}$$

where,

$$\beta = E_f V_f, \tag{4.31}$$

$$\chi = G_{LT} + \frac{\pi^2}{12}\beta\left(\frac{h}{L}\right)^2, \tag{4.32}$$

$$\alpha = \chi + \beta\varepsilon_{max}, \text{ and,} \tag{4.33}$$

$$\kappa = \varepsilon_{max} - \frac{\pi^2}{2}\left(\frac{f_o}{L}\right)\left(\frac{h}{L}\right). \tag{4.34}$$

The only variable in equations (4.31)-(4.34) that has not been discussed is ε_{max}. One should recognize that the strain in the fiber is a superposition of axial compressive strain and the strain due to fiber curvature. Under these particular circumstances, the critical fiber strain should be

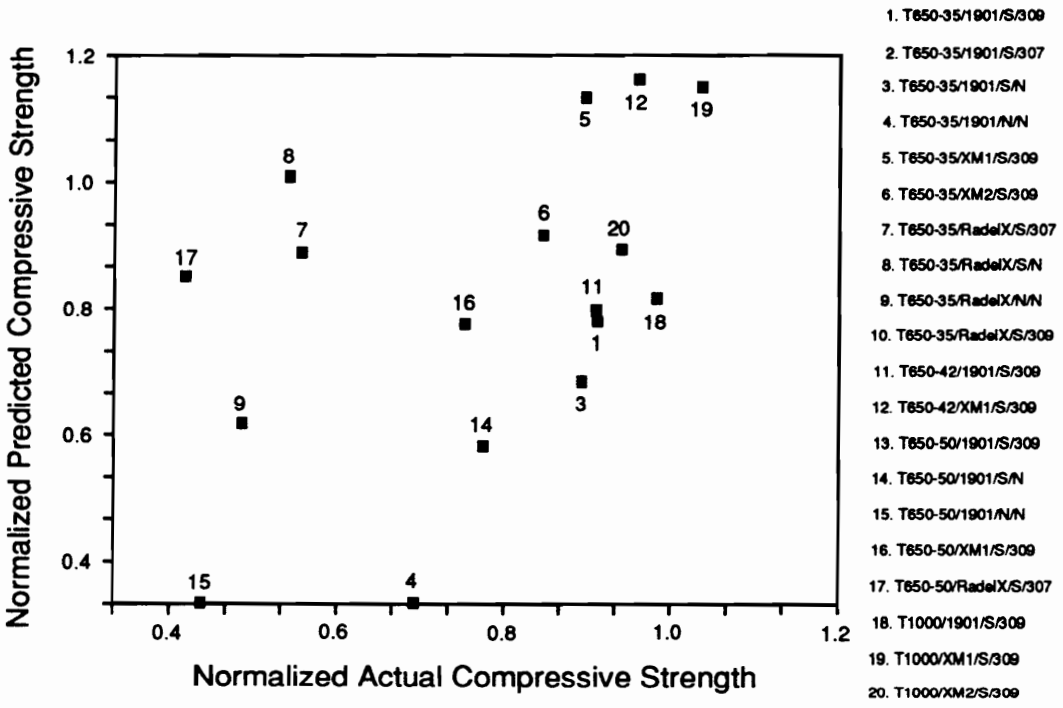

Figure 83. Normalized Unidirectional Compressive Strength; Predicted Values versus Actual Values (Shear Failure Scenario) [39].

compressive since the applied axial strain and the strain on the compressive face of the bent fiber would be additive. Unfortunately, the intrinsic compressive strain to failure of the fiber systems investigated is unknown. The "Elastica Loop Test" [126,127] could possibly be used to obtain these values. In place of the compressive value, as a first approximation, the *tensile* strain to failure of unidirectional composite specimens was used [39]. This could be a true source of error in this analysis, yet, no other data was available to enable the author to improve this approximation.

As in the "shear failure" scenario, the independent variable is f_o. Having assigned the same material properties to their respective variables (as in the "shear failure" scenario), the values predicted from equation (4.30) are plotted against the actual, experimentally-determined compressive strengths [39] in Figure 84. Despite some points that fail to correlate, a fair number of points fall *very* close to the line of perfect correlation. The angle of initial misalignment that was assumed in order to produce this plot was 1.4%, *much* less than the angle needed to produce reasonable "shear failure" values. An attempt was made to determine *why* certain points failed to be predicted — was there a common thread between the systems, such as fiber type, matrix type, presence of sizing, etc.? No one parameter seemed to be consistent among those points that fell way off of the mark. The thought arose that perhaps the points that could not be predicted using the "bending failure" scenario, *could* be predicted using the "shear failure" scenario. This was not the case, however.

Seeing nearly half of the twenty specimen types — specimens that were systematically altered with respect to fiber, matrix, surface treatment and sizing — fall close to their predicted values lends some confidence in the "bending failure" scenario of the present analysis. The true engineering confidence level, however, would be very slight, since, in some instances the prediction differed by more than 100%. Yet, it does *not* seem that the agreement between the actual and predicted values is purely coincidence; many of the key variables in the compression problem have been identified using this analysis. It is quite satisfying to see as much correlation as is witnessed in Figure 84 given the assumptions made and the inherent imprecision of experimental data. The author concludes that this methodology deserves some respect and future research, having shown that it can characterize the compressive response of such fantastically different material systems based solely on their micromechanical properties.

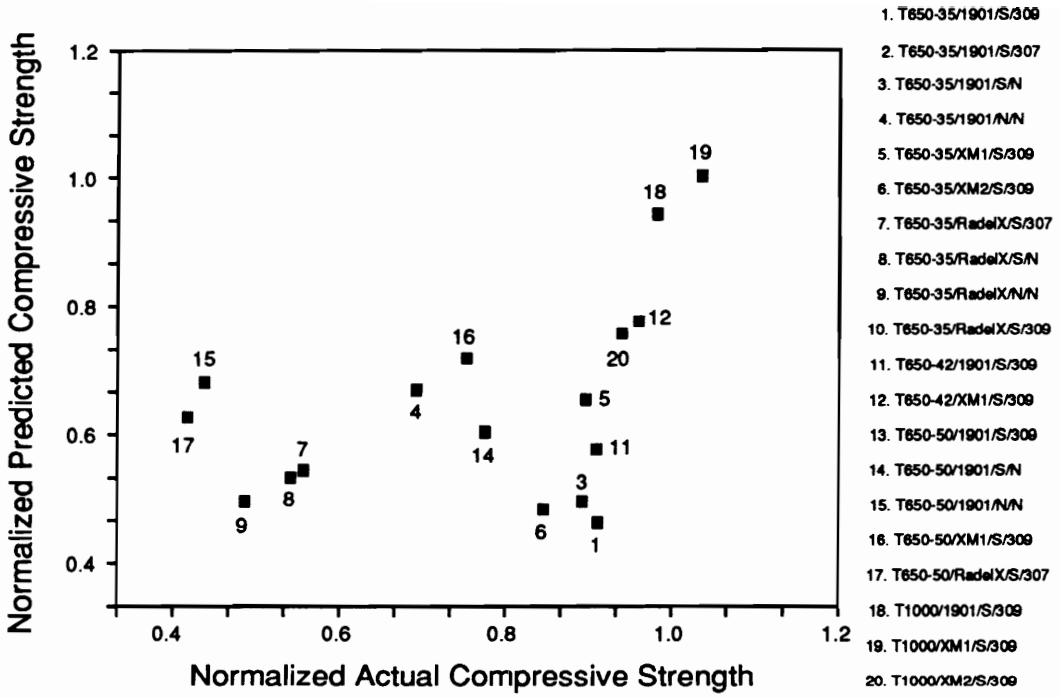

Figure 84. Normalized Unidirectional Compressive Strength; Predicted Values versus Actual Values (Bending Failure Scenario) [39].

Prediction of Unnotched Cross-plied Compressive Strength

One would normally expect cross-plied compressive data to correlate with unidirectional data. Load sharing concepts from mechanics of materials indicate that the compressive strength of a 32-ply cross-plied laminate would be approximately half of the compressive strength of a 16-ply 0° laminate, since the same number of 0° plies carry the load, but the cross-plied specimen has double the area. The two strength values are not exactly equal because the 90° plies carry some of the load, thus driving the value to greater than one-half of the unidirectional compressive strength. Sohi and Hahn [128] indicate that the presence of other off-axis plies help contain the 0° failures that occur, instead of allowing them to run unabated throughout the laminate. This finding tends to increase the ratio of 32-ply cross-ply compressive strength to 16-ply 0° compressive strength even further. One would think that 90° compressive failure must be detrimental to the stability of the neighboring plies, however. In any event, one should expect cross-ply compressive strength to correlate with unidirectional compressive strength. These two data were plotted using Northrop's data [39,40] (normalized on both axes) in Figure 85. It is interesting to note that beyond a certain strength a linear relationship is formed, yet, below this transition point, the strengths of the cross-plied specimens remain nearly constant. One may hypothesize that this constant strength level represents the influence of the *in situ* compressive strength of the 90° plies. If the linear relationship had continued below this transition point, the cross-plied strength would be predicted to be much lower than it actually is. Perhaps the presence of the 90° plies prevents a particular damage mode common in the weak 0° unidirectional specimens from materializing.

The actual compressive strengths of the unidirectional specimens were obtained with 8-ply laminates [39]. The compressive strengths of the cross-plied specimens were determined using 16-ply specimens [40]. From the above arguments, the slope of the linear portion found in Figure 85 should be greater than one-half. The least-squares fit of the data (above the transition point) reveals a slope of 0.50 — a reasonable value considering experimental error. The major point of Figure 85 is that once the unidirectional compressive strength is predicted, the cross-plied

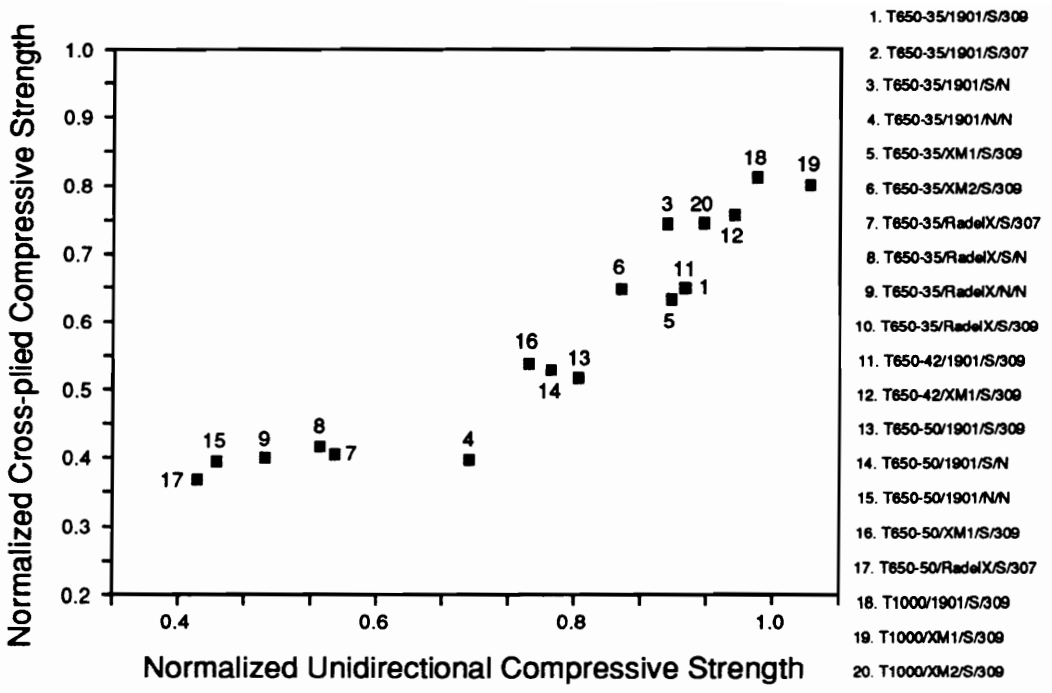

Figure 85. Normalized Cross-plied Compressive Strength vs. Normalized Unidirectional Compressive Strength; Northrop Materials [39,40].

compressive strength can be predicted with reasonable accuracy simply by accounting for load sharing arguments, *unless* the compressive strength of the 0° lamina is uncharacteristically low.

Prediction of Notched Cross-plied Compressive Strength

If one wanted to predict the notched compressive strength of a laminate, he might ask to what degree is this strength dictated by the strength of the unidirectional material. Figure 86 is a plot of the normalized "open-hole" compressive strength from a $[\pm 45/90/0_4/\pm 45/0_3]_s$ laminates versus the normalized unidirectional compressive strength of the respective Northrop materials [39]. The data is spread out throughout the plot, showing no obvious correlation. This indicates that a laminate effect comes into play and/or a hole effect influences the data (unfortunately, no unnotched compressive data was available for the above laminate configuration). It is was shown earlier that the cross-plied laminate strength correlates to the unidirectional strength. Thus, in the case of a cross-plied laminate, if any lack of correlation is seen between the notched compressive strength and the compressive strength of the unidirectional material, it *should* be attributable to the hole effect. A plot of the notched cross-plied compressive strength versus the normalized unidirectional compressive strength of the Northrop material [39] is seen in Figure 87. Due to the limited data, no sweeping conclusions can be made, yet, it does seem that the two sets of data reveal little correlation.

In the analysis of notched *tensile* strength, it was determined that the "hole effect" (quantified by the average-stress criteria parameter, a_o) was directly related to the bond strength. Several researchers [128-131] have applied the Whitney-Nuismer analysis to the compressive-loading case in order to predict the effect of hole size on strength; each has reported success when used within this capacity. Encouraged by these results, the procedure for determining a_o was replicated, this time using the ratio of the notched compressive strength to the unnotched compressive strength (K_T^∞ does not change since the compressive effective moduli are assumed to be equal to the tensile moduli — not necessarily a good assumption, but a practical assumption without having the compressive

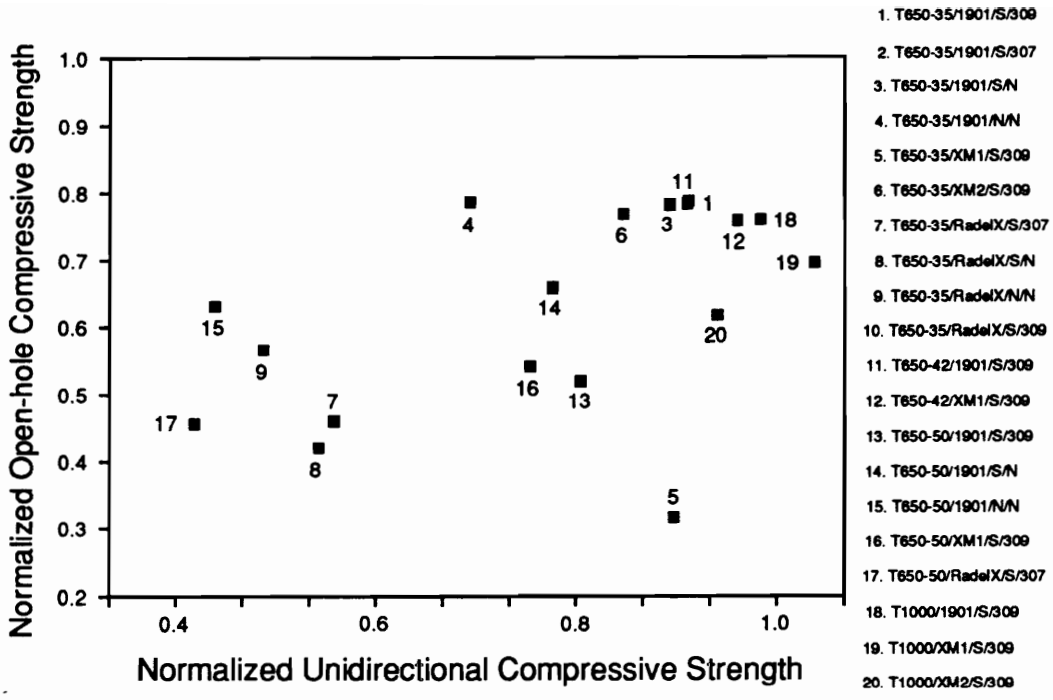

Figure 86. Normalized Open-hole Compressive Strength versus Normalized Unidirectional Compressive Strength; Northrop Materials [39].

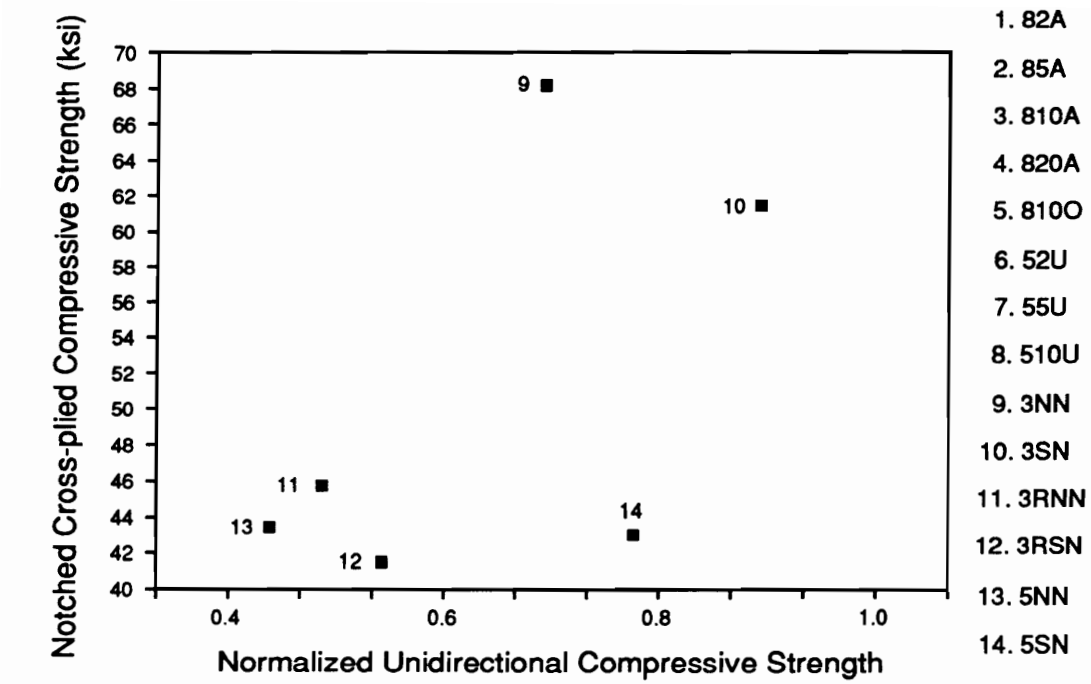

Figure 87. Notched Cross-plied Compressive Strength versus Normalized Unidirectional Compressive Strength; Northrop Materials [39].

moduli provided). This time, however, *no correlation was seen between a_o and TFS* (or any other measure used to characterize the bond condition, i.e., MMHP or $\pm 45°$ tensile strength). This indicates that: 1.) the bond strength does *not* enter the compressive problem in the same manner as the tensile problem, or, 2.) several strength measurements were uncharacteristic and/or suspect. Realistically, a combination of both points probably influences the lack of correlation.

Insisting that the bond strength *should* somehow enter the calculations of the compressive notched strength, another notched laminate configuration was investigated. Compressive data on the "open-hole" laminate (described above) were published by Northrop in Ref. [39]. The input data needed to perform the Whitney-Nuismer average-stress criteria includes the value of the notched laminate strength, the value of the unnotched laminate strength, and the notch stress concentration factor, K_T^{∞}. The stress concentration factor can be calculated (using equation (4.4)) by inputting effective laminate material properties; these were obtained from lamina properties (published by Northrop [39]) and simple lamination theory. The only unknown, therefore, is the unnotched laminate compressive strength. Unfortunately, this value was not supplied. It was necessary, therefore, to make the assumption that the unnotched laminate strength of the "open-hole" configuration was *proportional* to the unnotched strength of the cross-plied laminate made from the same material. Since both laminates are "fiber-dominated" lay-ups (one possessing 58% 0° plies, the other 50% 0° plies) this may not be a bad assumption. The unnotched compressive strength of the cross-plied laminates (published in [40]) was used to normalize the notched compressive strength of the "open-hole" laminates instead of its unnotched laminate compressive strength.

This ratio, along with the calculated value for K_T^{∞} is inserted into equation (4.6). Given this normalization procedure, it is incorrect to characterize the resulting distance as the average-stress criteria parameter, a_o. In order to differentiate the distance calculated in the present manner, it will be known as a_o^*. This value is plotted against the normalized $\pm 45°$ tensile strength data [39] (shown to be linearly related to TFS, and used in its absence) in Figure 88. While it is clear that certain points fail to follow the general trend of the data, it is obvious that as the $\pm 45°$ tensile strength (used to characterize the interphase strength) increases, the parameter, a_o^*, decreases. One source

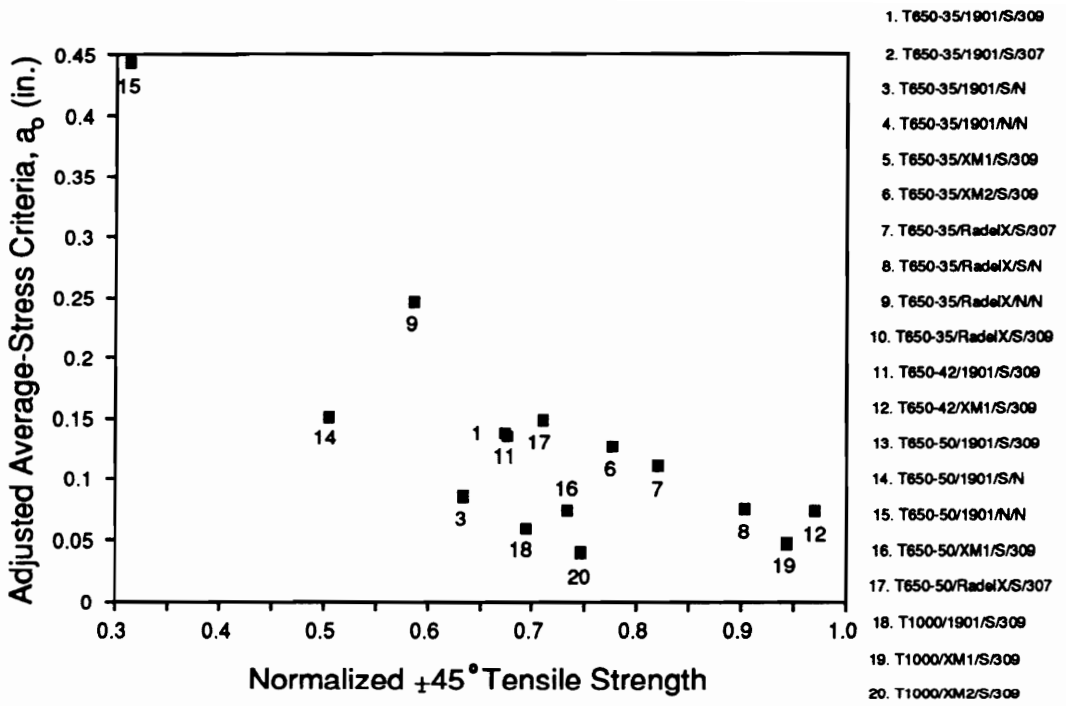

Figure 88. Adjusted Average-Stress Criteria Parameter versus Normalized ±45° Tensile Strength; Northrop Materials [39].

of error could be the normalization procedure, of course. The major point to take from Figure 88 is that the interphase strength influences the notched performance of this laminate. As the interphase strength increases, the notch sensitivity of the *compressively-loaded* laminate increases. Given Figure 88, it is unknown why the notched cross-plied compressive data failed to reveal this trend. Carefully controlled compressive test methods along with high-quality-controlled laminates under identical laboratory conditions are absolutely necessary to obtain representative and reproducible compressive strength data that can be used as input into modelling work.

It has been illustrated that a representation of the interphase belongs in the expressions of unidirectional compressive strength and in the formulation of notched compressive strength. These findings open the door for future researchers to clearly identify in what manner interphase strength (and stiffness) measures should be introduced into various micromechanical models. This study has presented possible routes and has indicated, with some satisfaction, that the introduction of the interphase into those routes produced positive correlation with macroscopic measures of notched strength. This chapter concludes with a discussion on how one can use these interphase/notched strength relationships in a performance simulation model of fatigue behavior.

Evolution Concepts as Applied to Fatigue Performance Modelling

The essence of fatigue is that stress and strength *evolve* over cyclic time. Damage to sub-critical elements causes an increase in the stress state of the critical elements due to a subsequent increase in load sharing, the effect of local stress concentrations, the introduction of moisture ingression pathways, etc. Thus, the stress state that the critical elements (those elements whose failure is equated with system failure) must endure *changes with time*. Simultaneous (though not necessarily at the same rate) to the change in stress is the change in the state of the material. If one focuses just on a laminate's response to an applied cyclic stress, the critical change of state is the change in the strength the material possesses. The very word "fatigue" connotes that the material is "getting tired" or "weak", so that it gradually loses its ability to perform its task. In a composite material

system, however, only certain constituents contribute to the evolution of strength. Studies over several years [89] have concluded that fatigue failure is *not* attributable to the degradation of graphite fibers; i.e., graphite fibers do not "fatigue". Why, then, do unidirectional (0°) laminates fail in fatigue? Damage mechanisms such as longitudinal splitting change the stress state in the composite and re-direct how stress in the composite is carried. It seems, therefore, that the matrix response — even in so-called "fiber-dominated" laminates — is fundamental in dictating the fatigue response. This thought, however, is not completely satisfying. In the case of a unidirectional laminate in fatigue, the evolution in strength does not occur in the fibers, nor is the matrix completely responsible for the laminate's fatigue behavior; it appears that the *system*, or the way the constituents interact, evolves. This "system" is conveniently embodied within the notion of the interphase. It is, in fact, the interphase that defines the level of interaction between the fiber and the matrix — forming a synergistic system response instead of an "additive" system response. The concept of interfacial evolution or degradation is a fairly novel approach to understanding the fatigue behavior of composite laminates.

The hypothesis that the state of the interphase changes and that it is intimately responsible for the change of state in the material, could and should be experimentally verified. One possible technique might involve the indentation procedure adopted in this investigation. One could measure the characteristic MMHP and representative strain (d/D at MMHP) values of the virgin material system and then monitor their evolution as a function of fatigue cycles. The indentation technique is well-suited for this, since it monitors the response of actual laminates, not model composite systems. It was hoped that such information would be gathered during this study, however, several obstacles precluded this development. It was felt that the indentation response of a cross-plied laminate would be corrupted by the presence of the 90° layers — especially with the indenter size currently employed. It would be necessary to terminate a specimen after so many cycles in order to section and mount the material for indentation studies. In the present case, not enough specimens were available for this systematic approach. Yet, with slight modification, this seems to be an ideal method to monitor the *degradation* of interfacial behavior.

Once this information was known (i.e., does the interphase strength properties change as a function of cycles and to what degree is such change measurable?) one could simply insert these phenomenological observations into the micromechanical expressions that contain the interphase as a variable. This approach, however, replaces one experimentally-observed data set (lamina strength degradation) with another data set (interphase degradation). This would not be a bad trade-off, *if* a great degree of generality accompanied this evolution information. In other words, if one could determine the conditions that contribute to interphase degradation, e.g., specimen heating, micro-scale Poisson's contractions, creep, environmental exposure, etc., then one could proceed to the next level of micromechanical modelling — mechanistic modelling of interphase degradation.

This investigation has identified the role of the interphase in the static and fatigue behavior of polymeric matrix composite laminates. This was accomplished by a thorough experimental investigation of material systems systematically altered with respect to their bond condition. By relating the bond condition (quantified through transverse flexural strength and by indentation response) to the strength and fatigue performance of the laminate, one could identify the attributes of the interphase that contributed to the composite's behavior. Having determined the manner in which the interphase affected the performance, an attempt was made to introduce the interphase into mathematical models of composite behavior. In the analysis of notched strength, it was demonstrated that the interphase plays a fundamental role in dictating how the composite will distribute the stress concentration brought about by the center hole. Having identified the roles assumed by the interphase and discussed how the interphase enters mathematical descriptions of composite performance, this investigation proffers some valuable insight into composite material behavior. The interphase is rightfully identified as the third constituent of a composite system. It is necessary to determine the properties of the interphase in order to accurately predict static and dynamic material behavior. Finally, now that the importance of the interphase has been established, it will be necessary to study the *evolution* of the interphase in order to understand the fatigue behavior of composite materials.

Summary and Conclusions

The purpose of this chapter is to condense the findings of this investigation into a succinct record. To facilitate the exposition of this summary, the outline of the study will be maintained, i.e., this chapter will be divided into four sections (corresponding to the previous four chapters) and sub-divided further to address the topics listed under each respective chapter.

Introduction and Literature Review

The Interphase

- Researchers [3] have detected a third "phase" of the material between the bulk fiber phase and bulk matrix phase of a polymeric matrix composite. This finite-thickness region — termed the *interphase* — possesses mechanical, physical, and chemical properties that are distinct from the fiber and the matrix constituents. Thus, the interphase embodies the characteristics of the fiber/matrix bond, including strength and stiffness (possibly tensorial in nature) that may be

functions of position [3]. One should consider the interphase as a third constituent within a composite material system.

- The term, *interphase*, by emphasizing that a third phase exists between the fiber and matrix, replaces the outdated term, *interface*, which describes an idealized two-dimensional boundary.
- The interphase is created in the process of bonding the bulk fibers together with a matrix system. The nature of the fiber and matrix, the processing conditions, etc., can affect the character of the interphase. Engineers and chemists have sought to improve bond strength (or, equivalently, interphase strength) by developing fiber surface treatments and fiber sizings. The effect of a fiber surface treatment is to remove weak, unordered graphitic layers from the fiber surface [5]. The treatments tend to implant oxygen and nitrogen species that encourage chemical bonding with the matrix systems. Fiber sizings typically consist of a partially-cured epoxy that is deposited onto the fiber surface. This coating — estimated to be between 100-500 nm in thickness [21,22] — aids in the handleability of the fibers and acts as a "primer" to further encourage bonding between the fiber and matrix.

The Interphase and its Influence on Composite Properties

- Having identified the interphase as a third constituent of a composite, researchers have sought to determine the relationship between the mechanical properties of the interphase and the resultant performance of the host composite. Several investigators have published work reporting that changes in interphase properties — achieved mainly through the presence or absence of fiber surface treatment and/or sizing — *do* influence the quasi-static behavior of composites, especially when testing for "matrix-dominated" properties [8-19].
- The work mentioned above shares a common feature: laminate configurations have been extremely simple (almost exclusively unidirectional) in order to attribute composite behavior directly to the interphase. While considerable knowledge has been gained in this pursuit, there is a need to study the effect of interphase behavior on the response of engineering laminates,

i.e., multi-directional laminates that possess stress raisers. In addition, *no* work has been published that studies the role of the interphase in the *fatigue response* of *carbon* fiber/polymeric matrix composites.

- Another common feature that exists among every study that attempts to formulate an interphase/composite performance relationship is the necessity to characterize the interphase strength. Techniques for measuring interphase strength are generally separated into two groups: single fiber tests and laminate tests. Single fiber tests are performed on model composite systems and fail to address the nature of the interphase in real, as-processed, standard fiber volume fraction composites. Laminate tests depend upon a necessary level of *inference*, i.e., a macroscopic strength property is assumed to correspond to the strength of the highly local interphase region. There is an overwhelming need within the composite community to find a technique that accurately assesses the strength of the interphase in real composite systems.

Opportunities

- Recently, an Air Force contract entitled, "The Development of Ultralightweight Materials," was awarded to the McDonnell Aircraft Company (abbreviated as McAir throughout this work) [30] and to the Northrop Corporation [31]. Each company supervised the creation of over twenty material systems specifically altered with respect to the fiber/matrix interphase. The materials possessed different fiber systems, matrix systems, gradations of surface treatment, and different fiber sizing formulations. A considerable amount of quasi-static property data were published from these systems [37,39,40]. Noticeably absent from the test regimen was the characterization of the dynamic (fatigue) response of these materials. Each company provided the present investigation with a selection of materials from their material systems. This provided a unique opportunity to study the role of the interphase in the static and fatigue performance of carbon fiber/polymeric matrix composites.

Experimental Techniques

Material Systems

- Eight McAir material systems arrived in panel form as two fiber systems bound with the same HC 9106-3 toughened epoxy system. The fibers, Courtaulds's 45-850 fibers (45 Msi tensile modulus, 850 ksi tensile strength) and 32-550 fibers (32 Msi tensile modulus, 550 ksi tensile strength) were surface treated at levels ranging from 20% to 200% of the industry standard treatment. Three of the systems had unsized fibers, four of the systems received an "A" epoxy sizing, and one system received an "O" "organic" sizing. The reader is encouraged to refer to Table 1 for the complete details of these systems including the coding scheme adopted in order to abbreviate the system descriptions.
- Six Northrop material systems arrived in pre-preg form as two fibers systems bound in two distinct matrix systems. Amoco's Thornel T650-35 fibers (35 Msi tensile modulus, 650 ksi tensile strength) were bound with a standard epoxy, ERLX 1901, and an amorphous thermoplastic, Radel-X (presently designated as Radel-8320 [39]). Amoco's Thornel T650X-50 fibers (50 Msi tensile modulus, 650 tensile strength) were bound only with the ERLX 1901 standard epoxy. The fibers in every Northrop system received were unsized. Northrop chose to compare the performance of systems possessing either 100% surface treatment or 0% surface treatment. The reader is encouraged to refer to Table 2 for the complete details of these systems including the coding scheme adopted in order to abbreviate the system descriptions.

Laminate Configurations and Test Specimens

- Laminate configurations tested in this investigation include 32-ply cross-ply specimens, $[\pm 45]_{ns}$ specimens (where $n = 4$ and 8), and unidirectional specimens containing 28 and 32 plies. A 0.25″ diameter center hole was cut into a majority of the cross-ply specimens (giving a hole diameter-to-width ratio of 1:4).
- The unidirectional material was cut into diminutive 90° coupons for use in 3-point flexure testing. Other unidirectional coupons were cut and mounted in a room-cure epoxy such that the fiber ends could be polished for subsequent indentation testing and SEM work. Unidirectional McAir specimens were configured for compression testing in a Wyoming IITRI compression fixture.

Mechanical Testing

Quasi-static Strength and Stiffness Testing

- Quasi-static tension and compression strength testing was performed on notched cross-plied specimens from all fourteen material systems. The strength and modulus of each specimen was recorded. The axial tensile stiffness was measured on the McAir cross-plied specimens in the unnotched condition; these numbers were needed for future modelling work. Strength testing was performed on the McAir $\pm 45°$ laminates, allowing for the measure of tensile shear strength and shear stiffness. The unidirectional compressive strength, failure strain, and stiffness of six of the eight McAir systems were measured to serve as a comparison to the data obtained by Northrop on their material systems [39].
- Inspired by the work of Madhukar and Drzal [10] and Adams, *et al.* [34], transverse flexure testing was performed on the fourteen material systems under investigation in an attempt to

characterize their bond strength. Strength, failure strain and flexural stiffness (derived from crosshead displacement) data were collected.

Fatigue Testing

- Notched cross-plied specimens from every material system were subjected to fully-reversed (R = -1), tension-compression, axial fatigue at a maximum applied stress level of 75% of their respective ultimate compressive strength. The stress level was chosen so that one could compare the performance of all fourteen systems on a common basis. Since there was a considerable range of compressive strengths, testing at a fixed stress level would unfairly tax many of the specimens. A wide range of fatigue lives indicated that the present decision to test at a fixed percentage of ultimate strength had some merit.
- During each notched cross-plied fatigue test the following data were collected: cycles to failure, modulus (with strain measured *across* the hole) as a function of cycles, notch temperature (measured with a thermocouple positioned at the point of maximum longitudinal stress) as a function of cycles, and phase and gain data collected from a Dynamic Signal Analysis program written in-house (by Ahmad Razvan).
- Unnotched McAir $\pm 45°$ coupons were cycled at a stress ratio of R = 0.1 in tension-tension fatigue. Since this is a "matrix-dominated" laminate and the matrix was the same in each material system, it was decided to test each system under the same applied maximum stress of 24 ksi. Cycles to failure, specimen temperature as a function of cycles, and phase and gain data were collected during these tests.

Indentation Testing

- A novel indentation technique, the Continuous Ball Indentation Test [33], was performed as another approach to characterizing the interphase strength. Values reflecting the maximum

indentation pressure and the depth of the indentation were used to quantify the response of the fourteen material systems.

Measurements of Strain Gradients

- A ten-gage strip gage (see Figure 1) was adhered to an 810A and an 810O specimen in an attempt to detect the influence of the interphase on the longitudinal strain field in a ligament next to the center hole. Each specimen endured a number of tensile and compressive ramp loadings equal to the number of gages. This enabled the operators to monitor each gage without the luxury of having a myriad of strain amplifiers.

Non-destructive Testing

Fiber Volume Fraction Determination

- A fairly new technique to measure the fiber volume fraction of a composite was adopted in this study. This technique calculates the density of a composite by monitoring the weight of a coupon suspended in isopropyl alcohol (IPA) and applying Archimedes' principle. Given that the matrix density and fiber density are known *a priori*, one can calculate the fiber volume fraction from these values, the "wet" weight of the composite (wet from the immersion in IPA), and the "dry" weight of the composite (see equations (2.4) and (2.5)). This technique is seen as a *vast* improvement over the standardized matrix digestion technique [55].

Penetrant-enhanced X-ray Radiography

- Penetrant-enhanced X-ray radiography was employed to determine the extent and location of various damage modes within a fatigued laminate. The penetrant consisted of a zinc iodide solution. Optimum X-ray exposure times were determined for the material systems under investigation.

Scanning Electron Microscopy (SEM)

- A SEM was used for two distinct studies within this investigation. Unidirectional samples of the 810A, 820A, and 810O material were mounted such that the cross-section of the fibers were perpendicular to the viewing surface. These samples were polished and etched using an etchant formula typically employed in PEEK matrix studies [58]. Magnifications approaching $\times$ 20,000 were used in order to focus on the interphase region of these 5 micron fibers. The other SEM study involved examining the fracture surface of an 810A tensile specimen and an 810O tensile specimen. An attempt was made to infer the quality of bonding by visually assessing the amount of matrix remaining on the fibers.

Experimental Results and Discussion

Characterization of Interphase Strength

Transverse Flexure Testing

- Transverse flexural strength (TFS) appeared to be a sensitive measure of bond strength. In the McAir material, where the interphase was altered by gradations in the level of fiber surface treatment, an increase in TFS was noted to correspond to an increase in the percentage of surface treatment. In the Northrop material, where the interphase was altered by the presence or absence of fiber surface treatment, *large* differences in TFS were seen as the fiber went from the untreated to the surface treated condition. This observation concurs with the findings of other researchers who claim that bond strength increases by a discrete "jump" when one surface treats the fiber by as little as 10% of the industry-standard process; only moderate increases in strength are witnessed upon the application of higher levels of surface treatment [11,14,16,19,59].
- Other variables besides the level of surface treatment seem to affect the TFS results. The "O" sizing appeared to cause a slight increase in TFS over its "A" sizing counterpart. Differences in TFS were attributable to the matrix systems. The largest TFS was seen in the 3RSN system. It was hypothesized that the processing temperature of this thermoplastic system contributes to the formation of large compressive residual stresses in the interphase that must be overcome during transverse tensile loading.
- It appeared that fiber type also played a role in determining a material's TFS. In two separate cases the matrix and surface treatment remained constant while the fiber type changed. Noticeable differences in TFS were noted in each case. Three possible explanations were given for this behavior.

- Failure strain results revealed the same trends as the strength results. There was some reservation about the precision of these numbers since the failure strain was calculated from the crosshead displacement. Flexural stiffness data was relatively insensitive to the bond condition. This observation concurs with the findings of Madhukar and Drzal [10].
- Every surface treated specimen snapped into two distinct pieces upon failure. This is in stark contrast to the untreated specimens; in every instance they remained intact upon failure.

Indentation Testing

- Large differences in the Maximum Mean Hardness Pressure (MMHP) and representative strain (d/D at MMHP) were seen among the fourteen material systems. The correlation between indentation performance and the level of surface treatment was not nearly as clear as with the TFS results. Two general observations were apparent, however. Instances where a material's MMHP was high and its d/D was low (as in the 820A system) indicate that the material possesses a quality of "brittleness", while low values of MMHP accompanied by high values of d/D is indicative of a "ductile" quality of the material. These trends were later confirmed in fracture surface studies of failed notched tensile specimens. The other general observation is that MMHP is greater in surface treated specimens than it is untreated specimens. This was true in two of three instances, yet, is usually seen in the systems tested thus far by Lesko [33].
- The explanation of the lack of definitive correlation between the indentation results and the TFS results centered about the differences in the failure mechanisms in each test. It was felt that the indentation test may represent a "shear" response of the interphase rather than the "tensile" response seen in the TFS results. This explanation requires further proof, however.

Quasi-static Strength and Stiffness Testing

Notched Cross-plied Specimens

- A wide variability in the notched tensile strengths was observed for the fourteen systems. In general, the notched strength correlates with the unnotched strength of the material, yet, a definite dependence on interphase strength was noted. Systems that revealed high MMHP values seemed to perform poorly in the notched strength tests.
- The notched compressive strengths of the fourteen material systems were, without exception, much lower than the notched tensile strengths (in one instance, lower than 50% of the tensile strength). This *was not* attributed to bending failures in the laminates.
- Unlike the tensile case, the compressive strengths were remarkable in their *lack* of variability between systems whose fiber surface treatment had been altered. The compressive strength *did* differ, however, as one went from one *fiber system* to another. In every instance, if one kept the matrix system the same, as the fiber diameter increased, the strength increased. Strength differences were also attributed to the matrix system; the strength of the "3" fibers in the thermoplastic matrix was noticeably less than the strength of the same fibers in the epoxy matrix.
- There seemed to be a correlation between system modulus and the interphase condition. As surface treatment levels increased, the modulus was observed to increase in six of the eight systems. The 810O specimens displayed an obvious *decrease* in modulus over their 810A counterparts, leading one to believe that sizing formulation can affect the interphase's contribution to laminate stiffness. It was unclear whether the modulus values (obtained by measuring strain across the center hole) reflected a material response or a geometric response. The tensile stress-strain curves of surface treated and untreated systems clearly revealed differences in performance (see Figure 20).

Unnotched Cross-plied Specimens

- In contrast to the notched cross-plied 8A&O specimens, where the tensile modulus generally increased as the level of surface treatment increased, the *unnotched* stiffness was observed to decrease. The 810O system, however, still revealed a lower stiffness than its 810A counterpart.

Unnotched ±45° Specimens

- Prior to collecting data, ±45° tensile strength (45TS) data culled from References [37,39] were plotted against their respective transverse flexural strength data. Surprisingly, a nearly linear relationship was observed between these two sets of data. This result was more stunning when one recognized the distinct damage sequence that each laminate endured prior to failure. Possible explanations for this behavior were submitted.
- Bolstered by the above results, the published 45TS data were compared to published short beam shear strength data and edge delamination strength (EDS) data [39]. A general correlation was observed for the former data set. The 45TS and the EDS data sets displayed an amazing degree of correlation. Again, an explanation for this behavior was forwarded.
- The ±45° tension strengths measured from the McAir material generally correlated with their respective TFS data.
- Each ±45° tensile specimen displayed the same failure process. After sustaining an applied longitudinal strain of approximately 5%, a gross "yielding" of the laminate would occur, wherein the 45° fiber angles would align towards the loading axis. This yielding would result in an increase of nearly 10% in the longitudinal strain with no further increase in load (see Figures 28 and 29). Afterwards, the laminate would begin to carry load once again until failure. An incredible *lack* of matrix cracking was observed in an X-ray radiograph of a fatigued specimen that had undergone yielding (see Figure 76), leading one to believe that this behavior is related to matrix deformation rather than interphase (or matrix) failure.

- The ±45° tensile strengths recorded in these labs were considerably higher than the strengths published in Ref. [37]. There was no obvious explanation for this behavior.
- Measured shear stiffness values appeared insensitive to differences in the bond condition. This observation concurs with the findings of Madhukar and Drzal [9].

Unidirectional Compressive Specimens

- *No* correlation was seen between interphase strength and unidirectional IITRI compression strength of the McAir systems. Another troubling result was the occurrence of an average unidirectional compressive strength of the 55U system that was nearly equivalent to several of the 8A&O systems. This finding did not concur with the trends observed in the notched cross-plied strength results and in the published results of McAir [37]; in these instances, the 5U series compressive strength was consistently higher than the 8A&O series strength.
- The IITRI compression strength values were considerably lower than the strength values published from the Northrop systems [39]. This may reflect the fact that different test fixtures were used in each case to determine the compressive strengths.

Fatigue Testing

Notched Cross-plied Specimens

- The interphase was shown to significantly influence the cyclic life of the 8A&O series. In the 82A, 85A, and 810A systems — whose cyclic lives were nearly indistinguishable — microbuckling failure emanated from the center hole and grew towards the specimen edges. The early presence of this microbuckling severely limited the life of these specimens. The 820A specimen also failed due to microbuckling formation, yet, in this instance, the initiation and

progression of the failure was delayed. It was postulated that the stronger bonding of the system (observed in both TFS and MMHP results) may have aided in the suppression of the microbuckle failures.

- The 810O specimen *never failed* when subjected to fully-reversed cyclic loading at a maximum applied stress level of 75% of its ultimate compressive strength (UCS). An X-ray radiograph taken after 2.1 million cycles revealed a complete absence of microbuckling. This finding spawned several smaller investigations into why such an astonishing difference occurs between the behavior of the 810O system and the 810A system — two systems differing *only in the sizing applied to the fiber.*
- The 5U series fatigue life did not reveal the same dramatic differences as the 8A&O series. One is tempted to conclude for the 5U series that an increase in surface treatment caused an increase in life. More data is needed to confirm this suspicion. X-ray radiographs taken at 70% of the estimated life of each system failed to reveal the presence of microbuckling. It was confirmed, however, that final failure of the laminate was in a sublaminate buckling mode (see Figure 45). It was noted that all three 5U systems displayed fatigue lives rivaling the 820A specimens, yet, the applied stress level was significantly higher.
- Only one of the three material series in the Northrop selection of materials revealed a difference in fatigue life that was attributable to the bond condition. The 3NN system performed poorly when fatigued at 75% UCS. The unusually high stress level that it endured was held responsible for its performance. Yet, when the stress level was lowered to correspond to the level applied to the 3SN specimens, its fatigue life was indistinguishable from its 3SN counterpart. It was felt that the high applied stress level limited the possible damage modes the two material systems could experience, thus dictating their fatigue lives.
- The 3RN series systems displayed comparable fatigue lives. X-ray radiography of the specimens revealed intense cross-cracking. This cracking was thought to have occurred during the "cool-down" from their inordinately high processing temperatures. It was postulated that this cracking may have severely reduced the interphase strength of the two systems. No confirmation of this point was available, however.

- While differences in the fatigue life of the 5NN and 5SN systems were recorded, these results were hampered by the presence of significant data scatter that may have resulted from differences in panel quality.
- Strain levels were recorded as a function of cycles for each of the material systems and converted into plots of normalized modulus versus normalized life. These plots were very effective in characterizing the amount of fatigue life expended and remaining. The normalized modulus response seemed to indicate the presence (or absence) of key damage modes such as microbuckling.
- Notch temperature readings as a function of life displayed an unusual degree of reproducibility and, therefore, could be used to predict the stage of life a laminate was enduring. This data was used in conjunction with the normalized modulus measurements to terminate specimens at a fixed percentage of remaining life in order to perform damage analysis.
- It was anticipated that the interphase would play a role in the dissipation of mechanical energy that would become manifest as specimen heating. The average temperature achieved at specimen failure was recorded for each material system. Temperatures, in some instances, reached over 200°F. It appeared that the variation in the average failure temperature among the fourteen systems was related to the variation in the notched cross-plied compressive strength of the systems — the value that dictated the applied fatigue stress level. A simple analysis of rate-dependent heating was performed. It was seen that the variations in specimen heating among the systems could be accurately accounted for by considering the product of the applied stress amplitude and the resulting strain amplitude measured across the notch. These effects overwhelmed any effects that could be attributed to differences in the bond condition.
- A new and novel technique, Dynamic Signal Analysis (DSA) [35], was employed in an attempt to detect differences in dynamic performance that could arise from differences in the interphase. In its most basic form, the DSA resembles a macroscopic Dynamic Mechanical Analysis (DMA) instrument, enabling the operator to monitor dynamic phase lag and dynamic compliance. It was hoped that the phase lag signal would indicate the presence of differing bond conditions. Unfortunately, the data from the technique was not reproducible to a satisfying

degree, precluding any comparative measures. Several sources of error in the test set-up were identified and corrected. More effort and experience will be required before the DSA technique can be successfully used to interrogate dynamic behavior that arises from differences in the interphase.

- The DSA technique *did* edify its position as an effective tool in failure prediction. The gain signal, which resembles the dynamic compliance, — with few exceptions — increases dramatically as the laminate faces imminent demise. This quality will be very useful to those investigators studying late-life damage states. It should be emphasized that the primary benefit of this interrogative technique lies in the fact that it is *non-contact*. This is a very appealing attribute in those instances when one is studying the fatigue behavior of laminates in demanding environments where strain monitoring is impractical.
- In an attempt to explain the difference in the fatigue behavior between the 810A, 820A, and 810O specimens, an SEM investigation of the interphase was performed. A chemical etch was used to assist in the identification of the two-phase toughened epoxy matrix system. The 810A and 820A systems displayed a nearly uniform "honeycomb" pattern of continuous epoxy surrounding empty capsules of eroded thermoplastic. There were no distinguishing traits to indicate differences in the interphase between these two systems. The 810O micrograph was stunningly different from its counterparts, however. A distinct region different from the fibers and the honeycomb structure seen in the two previous micrographs was visible. The presence of this region helps explain the differences seen in the moduli of the 810O and 810A systems (provided that the modulus of this region is less than the matrix region). It also provides a clue as to why the fatigue life was so dramatically different in the 810O system. Detailed work should be performed to aid in understanding the structure/property relationship that may arise in systems possessing different sizings or coatings.
- Inspired by the SEM results, the thought occurred that differences in local interphase moduli may influence the manner in which the stress is distributed away from the global stress concentrator. A strip gage was applied to one 810A specimen and one 810O specimen. The strain readings confirmed that the 810O specimen was the more compliant of the two. After

applying a regimen of fatigue cycles, the strain field of each specimen was monitored to detect the effect of stress relaxation. Surprisingly, the strain field in the 810A specimen changed only slightly. The gage nearest the hole was disabled by fatigue damage. The 810O specimen, on the other hand, had its first *three* gages disabled. This was completely unexpected since X-ray radiographs of 810O specimens after millions of cycles fail to reveal damage away from the hole. Though the strip gage technique proved highly effective at monitoring the gradient of strain arising from the center hole, the results of the tests could not be easily explained.

Unnotched ±45° Specimens

- The great differences in fatigue behavior seen in the notched cross-plied 8A&O series materials was not replicated in the unnotched ±45° fatigue tests. In the 8A&O series, unnotched ±45° *strength* seemed to be a good indicator of fatigue performance, i.e., the stronger the laminate, the longer the life. This theory did not apply to the 5U specimens, however. It was generally concluded that despite the differences seen in the fatigue behavior of the McAir systems, one would be hard-pressed to correlate the performance to the to influence the fatigue behavior of these systems.
- The temperature of each specimen was monitored during fatigue. The temperature at failure was recorded and compared among the systems. In this case, the heating analysis developed for the notched cross-plied case failed to predict the variations in the temperature response. It was clear that the two 32-ply laminates (the 820A and 55U specimens) displayed the highest temperatures at failure. It was postulated that the fiber type may play a role in explaining the differences between the 8A&O and 5U temperature response.
- The investigators were, again, unable to utilize the DSA data collected from the fatigue tests due to poor reproducibility.

Modelling Considerations

Introducing the Interphase into Predictions of Notched Cross-plied Tensile Strength

Review of Notched Tensile Strength Theories

- Prior to introducing the interphase into a micromechanical model of notched tensile strength, it was prudent to review the current theories. Two approaches, the Whitney-Nuismer model [94] and the "terminal damage state" approach of Kortschot and Beaumont [64], were addressed. It is the author's opinion that these two seemingly disparate approaches are entirely reconcilable.

Discussion of Data

- Attempts to incorporate interphase behavior into micromechanical models of notched strength were temporarily discouraged by indications that unidirectional tensile strength and interphase strength (characterized by TFS and MMHP results) seemingly fail to correlate with one another (see Figures 78 and 79).
- Data published by McAir and Northrop [37,39,40], along with data collected in the present investigation were used to calculate the "average-stress criteria parameter", a_o, of Whitney and Nuismer. This parameter can qualify the "notch sensitivity" of a material, i.e., a high value of a_o indicates an insensitivity to the presence of the notch, and, therefore, relatively high notched strengths. Low values of a_o indicate a heightened sensitivity to the presence of the notch, and, therefore, relatively low values of notched strength. The values for a_o were calcu-

lated for all fourteen systems under investigation. It was seen that this parameter reveals a nearly linear dependence on the transverse flexural strength. In other words, the stronger the interphase, the more notch sensitive the laminate. This is thought to be the first instance where this relationship has been formed so convincingly; *the notched tensile strength of a cross-plied laminate strongly depends on the strength of the fiber/matrix interphase.* Reasons why such a relationship should exist were given.

Introducing the Interphase into Predictions of Notched Cross-plied Compressive Strength

A Survey of the Micromechanical Theories of Compressive Strength

- The lamina level served as the starting point for the introduction of the interphase into notched compressive strength. It was necessary, therefore, to review the large number of compression models that have been published in order to identify the salient features of each approach. These models neatly separate themselves into two groups: instability analyses and constituent failure theories. Arguments were presented towards favoring the constituent failure theory approach to unidirectional compressive strength modelling. From among the many models, it was felt that the model of Hyer [112] incorporated a number of key variables an ideal (two-dimensional) model should possess.

Adaptation of the Present Unidirectional Micromechanical Model

- Unidirectional compressive failure is dictated by one of two variables in Hyer's model [112]: shear failure of the matrix (or, in the present case, the interphase) or fiber failure due to bending. A parameter representing the influence of the interphase was introduced into each

scenario. It was determined that the "shear failure" scenario failed to represent the actual compressive data measured by Northrop [39]. The "bending scenario", on the other hand, predicted the compressive response of *many* of the diverse material systems with engineering accuracy. Several systems failed to be represented by this theory, however.

Prediction of Unnotched Cross-plied Compressive Strength

- Cross-plied compressive strength of nearly twenty material systems culled from Northrop's published report [40], were plotted against their respective unidirectional compressive strength values. It was seen that a nearly linear relationship existed between the two variables beyond a certain unidirectional strength value. Below this value, cross-ply compressive strength was seen to be nearly constant, perhaps reflecting the role of the 90° plies as laminate stabilizers. It is felt that once unidirectional strength is predicted, unnotched cross-plied compressive strength can be predicted with reasonable accuracy.

Prediction of Notched Cross-plied Compressive Strength

- Attempts at correlating a compressive "average-stress criteria parameter" with the transverse flexural strength (as was done successfully in the tensile case) proved entirely unsuccessful for the fourteen material systems under investigation.
- Another attempt was made, however, using "open-hole" compressive data supplied by Northrop [39]. Since the unnotched strength of their laminate configuration was not available, the notched strength of their materials were normalized by the unnotched cross-ply compressive strength of the respective systems; this permitted the calculation of an "adjusted" parameter, a_c^*. This parameter was plotted against the $\pm 45°$ tensile strength [39] (shown in Figure 23 to be linearly related to the TFS) of its respective system. As in the tensile case, several systems revealed a strong dependence on the characterization of the interphase strength.

This indicates that notched compressive strength is also dependent on the degree of fiber/matrix bonding.

Evolution Concepts as Applied to Fatigue Performance Modelling

- Fatigue behavior is dictated by how the states of stress and strength *evolve* over cyclic time. If one assumes that intrinsic fiber strength does not degrade as a function of fatigue, then one would normally be forced to admit that the matrix system is largely responsible for the fatigue performance of composite laminates. This thought is not completely satisfying, however. The idea that the *interphase* is critical to the fatigue performance of composites has been introduced. The next investigation into the role of the interphase in the fatigue performance of composite laminates should focus on the *degradation* of interphases as a function of cyclic time. The indentation technique used in the present investigation could be modified to allow for the interrogation of interphase strength in as-damaged *laminates*.

Future Recommendations

Several questions remained unanswered that beg for more research to be performed. The following is a brief list of research issues the author feels would illuminate the role of the interphase in the performance of composite laminates:

- A thorough investigation should follow the work of Lesko [33] to address the many questions that arose while using the indentation technique to characterize the interphase. What *exactly* is the indentation test measuring? Shear response? Compressive response?

- Once such an investigation has taken place, considerable work could be focused on using the technique to monitor the *degradation* of interphases in as-damaged *laminates* (as opposed to unidirectional specimens).
- The transverse flexure test would benefit immensely from a careful and detailed SEM analysis of the failure surfaces. Is the failure in the interphase? In the matrix? In the fiber? Is the failure ductile or brittle? These answers will help researchers understand why the TFS results mirror the bond condition so well.
- Another test technique aimed at characterizing the "shear response" of the interphase should be pursued. This approach could be modelled after the works of Newaz [132] and Nairn [133,134]. Their attempts to quantify shear behavior by analyzing longitudinal splitting has immediate applicability to the fatigue response of notched composites. It is quite possible that shear response of the present systems measured in this manner could correlate to the notched cross-plied fatigue behavior or to the $\pm 45°$ fatigue behavior.
- A whole research project could be devoted to the study of why the presence of the "O" sizing affected the fatigue (and static) performance of the 810O specimen. This study would involve intense physical and chemical analyses of the distinct region seen in the SEM micrographs. Lessons learned from this study could possibly change how composite scientists design materials for fatigue resistance.
- It is quite necessary to understand how the interphase influences the fatigue behavior at *low applied stress levels*. Several systems in this investigation failed after only a few thousand cycles. Perhaps at this high stress level, the effect of the interphase was overwhelmed by the other mechanisms that instigated rapid laminate failure.
- Finally, there is a great need for the interphase to enter micromechanical models of composite behavior in a rigorous manner. Several avenues have been opened within this study. The physics of the interphase must be described with our mathematical tools in order to accurately predict the performance of composites subjected to static and dynamic loading.

References

1. Sharpe, L. H., "The Interphase in Adhesion," *Journal of Adhesion,* Vol. 4, No. 1, 1972, pp. 51-64.

2. Sharpe, L. H., "Some Thoughts About the Mechanical Response of Composites," *Journal of Adhesion,* Vol. 6, No. 1, 1974, pp. 15-21.

3. Jayaraman, K., Reifsnider, K. L., and Swain, R. E., "The Interphase in Unidirectional Fibrous Composites, I. A Review of Characterization Methods," submitted to *Journal of Composites Technology and Research,* 1991.

4. Swain, R. E., Reifsnider, K. L., Jayaraman, K., and El-Zein, M., "Interface/Interphase Concepts in Composite Material Systems," *Journal of Thermoplastic Composite Materials,* Vol. 3, Jan. 1990, pp. 13-23.

13 5. Drzal, L. T., Rich, M. J., Lloyd, P. F., "Adhesion of Graphite Fibers to Epoxy Matrices: I. The Role of Fiber Surface Treatment," *Journal of Adhesion,* Vol. 16, No. 1, 1983, pp. 1-30.

6. Drzal, L. T., "The Interphase in Epoxy Composites," *Advances in Polymer Science, Vol. 75: Epoxy Resins and Composites II,* Springer-Verlag, 1986, pp. 1-32.

7. Drzal, L. T., "Fiber-Matrix Interphase Structure and its Effect on Adhesion and Composite Mechanical Properties," *Controlled Interphases in Composite Materials,* H. Ishida, Ed., Elsevier, 1990, pp. 309-320.

15 8. Madhukar, M. S., and Drzal, L. T., "Effect of Fiber-Matrix Adhesion on the Longitudinal Compressive Properties of Graphite/Epoxy Composites," *Proceedings of the Fifth Technical Conference of the American Society for Composites,* 1990, pp. 849-858.

16 9. Madhukar, M. S., and Drzal, L. T., "Fiber-Matrix Adhesion and its Effects on Composite Mechanical Properties. I. In-plane and Interlaminar Shear Behavior of Graphite/Epoxy Composites," *Journal of Composite Materials,* Vol. 25, Aug. 1991, pp. 932-957.

17 10. Madhukar, M. S., and Drzal, L. T., "Fiber-Matrix Adhesion and its Effects on Composite Mechanical Properties. II. Tensile and Flexural Behavior of Graphite/Epoxy Composites," *Journal of Composite Materials,* Vol. 25, Aug. 1991, pp. 958-991.

18 11. Curtis, P. T., Morton, J., "The Effect of Fibre Surface Treatment on the Compressive Strength of CFRP Laminates," *Progress in Science and Engineering of Composites,* T. Hayashi, K. Kawata, and S. Umekawa, Eds., ICCM-IV, 1982, pp. 219-226.

12. Lehmann, S., Megerdigian, C., and Papalia, R., "Carbon Fiber/Resin Matrix Interphase: Effect of Carbon Fiber Surface Treatment on Composite Performance," *SAMPE Quarterly,* April 1985, pp. 7-13.

13. Lehmann, S., Robinson, R., and Tse, M. K., "Characterization of Carbon Fiber/Resin Matrix Interphase," *Materials Sciences for the Future: 31st International SAMPE Symposium,* 1986, pp. 291-302.

14. Norita, T., Matsui, J., and Matsuda, H. S., "Effect of Surface Treatment of Carbon Fiber on Mechanical Properties of CFRP," *Composite Interfaces,* H. Ishida and J. L. Koenig, Eds., Elsevier, 1986, pp. 123-132.

15. Robinson, R., Lehmann, S., Askew, G., Wilford, D., Megerdigian, C., and Papalia, R., "A Preliminary Assessment of the Role of Fiber Surface Properties in Controlling Composite Performance," *High Tech - The Way into the Nineties,* K. Brunsch, H.-D. Gölden, and C.-M. Herkert, Eds., Elsevier, 1986, pp. 299-310.

16. Robinson, R., Lehmann, S., Wilford, D., Askew, G., Coulthard, R., Megerdigian, C., and Kirby, J., "Surface Characteristics Influencing Carbon Fibre/Matrix Adhesion Performance," *Looking Ahead for Materials and Processes,* J. de Bossu, G. Briens and P. Lissac, Eds., Elsevier Science Publishing, 1987.

17. Megerdigian, C., Robinson, R., and Lehmann, S., "Carbon Fiber/Resin Matrix Interphase: Effect of Carbon Fiber Surface Treatment and Environmental Conditioning on Composite Performance," *Materials — Pathway to the Future:* Proceedings of the International SAMPE Symposium and Exhibition, G. Carrillo, E. Newell, W. Brown, and P. Phelan, Eds., Vol. 33, 1988, pp. 571-582.

18. Verpoest, I., Desaeger, M., and Ivens, J., "The Influence of the Fiber-Matrix Interface on Damage Development in Composite Materials," *Academia Analecta,* Jan. 1989.

19. Ivens, J., Wevers, M., Verpoest, I., and De Meester, P., "The Influence of the Interface on Damage Development in CFRP," *ICCM VII: The Proceedings of the Seventh International Conference on Composite Materials,* Vol. 2, W. Yunshu, G. Zhenlong, and W. Renjie, Eds., Pergamon Press, 1989, pp. 447-453.

20. Private communication at BASF in Charlotte, North Carolina.

21. Drzal, L. T., Rich, M. J., Koenig, M. F., "Adhesion of Graphite Fibers to Epoxy Matrices: II. The Effect of Fiber Finish," *Journal of Adhesion,* Vol. 16, No. 2, 1983, pp. 133-152.

22. Hughes, J. D. H., "The Carbon Fiber/Epoxy Interface - A Review," *Composites Science and Technology,* Vol. 41, 1991, pp. 13-45.

23. Konour, O. and Matthews, F. L., "Effect of the Properties of the Constituents on the Fatigue Performance of Composites: A Review," *Composites,* Vol. 20, No. 4, July 1989, pp. 317-328.

24. Hahn, H. T., "Fatigue Behavior and Life Prediction of Composite Laminates," *Composite Materials: Testing and Design (Fifth Conference), ASTM STP 674,* S. W. Tsai, Ed., American Society for Testing and Materials, 1979, pp. 383-417.

25. Curtis, P. T., "An Investigation of the Tensile Fatigue Behaviour of Improved Carbon Fibre Composite Materials," *ICCM-VI & ECCM-II,* F. L. Matthews, N. C. R. Buskell, J. M. Hodgkinson, and J. Morton, Vol. 4, Elsevier Applied Science, 1987, pp. 4.54-4.64.

26. Spearing, S. M. and Beaumont, P. W. R., "Fatigue Damage Mechanics of Composite Materials. I. Experimental Measurement of Damage and Post-Fatigue Properties," CUED/C-MATS./TR.178, Cambridge Univ. Engineering Dept., Nov. 1990.

27. Shih, G. C., and Ebert, L. J., "The Effect of the Fiber/Matrix Interface on the Flexural Fatigue Performance of Unidirectional Fiberglass Composites," *Composites Science and Technology,* Vol. 28, 1987, pp. 137-161.

19 28. Vincent, L., Fiore, L., and Fournier, P., "Fatigue Behaviour of GFRP: Some Considerations about Interfaces," *Developments in the Science and Technology of Composite Materials: ECCM3,* A. R. Bunsell, P. Lamicq, and A. Massiah, Eds., 1988, pp. 609-614.

20 29. Dolan, G. L., Goering, J. C., and Brunner, M. D., "Development of Ultra-Lightweight Materials," First Quarterly Interim Technical Report, Air Force Contract No. F33615-88-C-5452, Aug. 1988.

30. Beck, A. R., and Yen, A., "Development of Ultralightweight Materials," First Interim Technical Report, Air Force Contract No. F33615-88-C-5447, Aug. 1988.

31. Tung, C., and Yen, A., "Development of Ultralightweight Materials," Tenth Interim Technical Report, Air Force Contract No. F33615-88-C-5447, Nov. 1990.

32. Curtis, D. C., Moore, D. R., Slater, B., and Zahlan, N., "Fatigue Testing of Multi-angle Laminates of CF/PEEK," *Composites,* Vol. 19, No. 6, 1988, pp. 446-452.

33. Lesko, J. J., Carman, G. P., Dillard, D. A., Reifsnider, K. L, "Indentation Testing of Composite Materials as a Tool for Measuring Interfacial Quality," *Composite Materials: Fatigue and Fracture (Fourth Conference), ASTM STP 1156,* accepted for publication, Nov. 1991.

34. Adams, D. F., King, T. R., Blackketter, D. M., "Evaluation of the Transverse Flexure Test Method for Composite Materials," submitted for publication in *Composites Science and Technology,* 1991.

35. Elahi, M., Razvan, A., Reifsnider, K. L., "Characterization of Composite Materials Dynamic Response Using Load/Stroke Frequency Response Measurement," presented at the *ASTM Fourth Symposium on Composite Materials: Fatigue and Fracture,* Indianapolis, Indiana, May 7, 1991.

36. Dolan, G. L., Wong, R., Wilson, D. W., "Development of Ultralightweight Materials," Fourth Quarterly Interim Technical Report, Air Force Contract No. F33615-88-C-5452, May 1989.

37. Hahn, G., Wong, R., Hwang, W.-F., Hartness, T., Drzal, L., Robinson, R., and Smith, S., "Development of Ultralightweight Materials," Tenth Quarterly Interim Technical Report, Air Force Contract No. F33615-88-C-5452, Nov. 1990.

38. Beck, A. R., and Yen, A., "Development of Ultralightweight Materials," Third Interim Technical Report, Air Force Contract No. F33615-88-C-5447, Feb. 1989, pp. 56-60.

39. Tung, C., and Yen, A., "Development of Ultralightweight Materials," Eighth Interim Technical Report, Air Force Contract No. F33615-88-C-5447, May 1990.

40. Tung, C., and Yen, A., "Development of Ultralightweight Materials," Ninth Interim Technical Report, Air Force Contract No. F33615-88-C-5447, Aug. 1990.

41. Chiao, C. C., Moore, R. L., and Chiao, T. T., "Measurement of Shear Properties of Fibre Composites: Part I. Evaluation of Test Methods," *Composites,* Vol. 8, No. 3, July 1977, pp. 161-169.

42. Lee, S., and Munro, M., "Evaluation of In-plane Shear Test Methods for Advanced Composite Materials by the Decision Analysis Technique," *Composites,* Vol. 17, No. 1, Jan. 1986, pp. 13-22.

43. ASTM Standard D 3410-87, "Standard Test Method for the Compressive Properties of Unidirectional or Crossply Fiber-Resin Composites," *Annual Book of ASTM Standards,* Vol. 15.03, 1987, pp. 187-199.

44. Swain, R. E., "The Effect of Interlayers on the Mechanical Response of Composite Laminates Subjected to In-plane Loading Conditions," M.S. Thesis, College of Engineering, Virginia Polytechnic Institute and State University, Blacksburg, Virginia, April, 1988.

45. ASTM Standard D 3518-76, "Standard Test Method for the Inplane Shear Stress-Strain Response of Unidirectional Reinforced Plastics," *Annual Book of ASTM Standards,* Vol. 15.03, 1987, pp. 204-209.

46. Kellas, S., Morton, J., and Jackson, K. E., "Damage and Failure Mechanisms in Scaled Angle-Ply Laminates," presented at the *Fourth Symposium on Composite Materials: Fatigue and Fracture,* Indianapolis, Indiana, May 7, 1991.

47. Petit, P. H., "A Simplified Method of Determining the In-Plane Shear Stress/Strain Response of Unidirectional Composites," *Composite Materials: Testing and Design, ASTM STP 460,* American Society for Testing and Materials, 1969, pp. 83-93.

48. Rosen, B. W., "A Simple Procedure for Experimental Determination of the Longitudinal Shear Modulus of Unidirectional Composites," *Journal of Composite Materials,* Vol. 6, Oct. 1972, pp. 552-554.

49. ASTM Standard D 790-90, "Standard Test Method for the Flexural Properties of Unreinforced and Reinforced Plastics and Electrical Insulating Materials," *Annual Book of ASTM Standards,* Vol. 08.01, 1990, pp. 274-283.

50. Bakis, C. E., Simonds, R. A., Vick, L. W., and Stinchcomb, W. W., "Matrix Toughness, Long-Term Behavior, and Damage Tolerance of Notched Graphite Fiber-Reinforced Composite Materials," *Composite Materials: Testing and Design (Ninth Volume), ASTM STP 1059,* S. P. Garbo, Ed., American Society for Testing and Materials, Philadelphia, 1990, pp. 349-370.

51. Simonds, R. A., Bakis, C. E., and Stinchcomb, W. W., "Effects of Matrix Toughness on Fatigue Response of Graphite Fiber Composite Laminates," *Composite Materials: Fatigue and Fracture (Second Volume), ASTM STP 1012,* P. A. Lagace, Ed., American Society for Testing and Materials, Philadelphia, 1989, pp. 5-18.

52. Kellas, S., Morton, J., and Curtis, P. T., "A Characteristic Fatigue Parameter for Notched Composites," *International Journal of Fatigue,* Vol. 13, No. 1, Jan. 1991, pp. 35-43.

53. Carman, G. P., Lesko, J. J., Reifsnider, K. L., and Dillard, D. A., "Micromechanical Model of Composite Materials Subjected to Ball Indentation," submitted to *Journal of Composite Materials,* Oct. 1991.

54. Lesko, J. J., "Indentation Testing of Composite Materials: A Novel Approach to Measuring Interfacial Characteristics and Engineering Properties," M.S. Thesis, College of Engineering, Virginia Polytechnic Institute and State University, Blacksburg, Virginia, March 1991.

55. ASTM Standard D 3171-76, "Standard Test Method for the Fiber Content of Resin-Matrix Composites by Matrix Digestion," *Annual Book of ASTM Standards,* Vol. 15.03, 1991, pp. 123-125.

56. Goodman, C., "Percent Fiber Volume Fraction in Composite Laminates," Celion Carbon Fibers Application & Product Development Specification No. CS-200-T, Nov. 1988.

57. Private communication with David Lynn of BASF Corporation.

58. Olley, R. H., Bassett, D. C., Blundell, D. J., "Permanganic Etching of PEEK," *Polymer,* Vol. 27, March 1986, pp. 344-348.

59. Peters, P. W. M., and Albertsen, H., "The Fiber/Matrix Interphase in CFRP with a Phase-Separating Matrix System," *Interfacial Phenomena in Composite Materials,* Leuven, Sept. 17-19, 1991, pp. 101-104.

60. Caldwell, D. L., and Jarvie, D. A., "Determination of the Interfacial Strength of Advanced Composites," *Materials — Pathway to the Future:* Proceedings of the International SAMPE Symposium and Exhibition, G. Carrillo, E. Newell, W. Brown, and P. Phelan, Eds., Vol. 33, 1988, pp. 1268-1275.

61. Batdorf, S. B. and Ko, R. W. C., "Stress-Strain Behavior and Failure of Uniaxial Composites in Combined Compression and Shear-I," ONR Report No. UCLA-ENG-85-25, July 1985.

62. Kress, G. R. and Stinchcomb, W. W., "Fatigue Response of Notched Graphite/Epoxy Laminates," *Recent Advances in Composites in the United States and Japan, ASTM STP 864,* J. R. Vinson and M. Taya, Eds., American Society for Testing and Materials, Philadelphia, 1985, pp. 173-196.

63. Wagnecz, L., "Mechanical Behavior and Damage Mechanisms of Woven Graphite-Polyimide Composite Materials," M.S. Thesis, College of Engineering, Virginia Polytechnic Institute and State University, Blacksburg, Virginia, June 1986.

64. Kortschot, M. T., and Beaumont, P. W. R., "Damage Mechanics of Composite Materials: II - A Damage-Based Notched Strength Model," *Composite Science and Technology,* Vol. 39, 1990, pp. 303-326.

65. Rosen, B. W., "Mechanics of Composite Strengthening," *Fiber Composite Materials,* American Society of Metals, 1964, pp. 37-75.

66. Hedgepeth, J. M., Van Dyke, P., "Local Stress Concentrations in Imperfect Filamentary Composite Materials," *Journal of Composite Materials,* Vol. 1, 1967, pp. 294-309.

67. Gao, Z., and Reifsnider, K. L., "Tensile Failure of Composites: Influence of Interfacial Bonding," submitted to *Journal of Composites Technology and Research,* July 1991.

68. Reifsnider, K., Gao, Z., and Swain, R., "Micromechanical Concepts for the Estimation of Property Evolution and Remaining Life," Proceedings of the International Conference: *Spacecraft Structures and Mechanical Testing,* Noordwijk, The Netherlands, April 1991, pp. 653-658.

69. Walrath, D. E., Ingram, A, Robinson, R., Dolan, G., Wong, R., Wilson, D., and Im, J.-H., "Development of Ultralightweight Materials," Fifth Quarterly Interim Technical Report, Air Force Contract No. F33615-88-C-5452, Aug. 1989.

70. Private Communication with Gregg Owens of Amoco Performance Products.

71. Private Communication with Scott Groves of Lawrence Livermore National Laboratory.

72. O'Brien, T. K., Johnston, N. J., Morris, D. H., and Simonds, R. A., "A Simple Test for the Interlaminar Fracture Toughness of Composites," *SAMPE Journal,* July/Aug. 1982, pp. 8-15.

73. Private communication with Melinda Schowengerdt of the McDonnell Aircraft Company.

74. ASTM Standard D 695-90, "Standard Test Method for the Compressive Properties of Rigid Plastics," *Annual Book of ASTM Standards,* Vol. 8.01, 1990, pp. 197-202.

75. ASTM Standard D 4762-88, "Standard Guide for Testing Automotive/Industrial Composite Materials," *Annual Book of ASTM Standards,* Vol. 15.03, 1988, pp. 204-210.

76. Guynn, E. G., Bradley, W. L., Elber, W., "Micromechanics of Compression Failures in Open Hole Laminates," *Composite Materials: Fatigue and Fracture (Second Volume), ASTM STP 1012,* P. Lagace, Ed., American Society for Testing and Materials, Philadelphia, 1989, pp. 118-136.

77. Soutis, C., and Fleck, N. A., "Static Compression Failure of Carbon Fibre T800/924C Composite Plate with a Single Hole," *Journal of Composite Materials,* Vol. 24, May 1990, pp. 536-558.

78. Soutis, C., and Fleck, N. A., Smith, P. A., "Compression Fatigue Behavior of Notched Carbon Fibre-Epoxy Laminates," *International Journal of Fatigue,* July 1991, pp. 303-312.

79. Kortschot, M. T., and Beaumont, P. W. R., "Damage Mechanics of Composite Materials: I - Measurements of Damage and Strength," *Composite Science and Technology,* Vol. 39, 1990, pp. 289-301.

80. Adams, D. S., Bowles, D. E., Herakovich, C. T., "Thermally Induced Transverse Cracking in Graphite-Epoxy Cross-ply Laminates," Journal of Reinforced Plastics and Composites, Vol. 5, July 1986, pp. 152-169.

81. Shulte, K., Neubert, H., and Harig, H., "Load and Damage Dependent Thermal Effects in CFRP-Laminates," *Thermal Effects in Fracture of Multiphase Materials,* K. Herrmann, and Z. Olesiak, Eds., Springer-Verlag, 1989, pp. 178-187.

82. Reifsnider, K. L. and Williams, R. S., "Determination of Fatigue-related Heat Emission in Composite Materials," *Experimental Mechanics,* Vol. 14, No. 12, Dec. 1974, pp. 479-485.

83. Frederick, D., and Chang, T. S., *Continuum Mechanics,* Scientific Publishers, 1972.

84. Dally, J. W., and Broutman, L. J., "Frequency Effects on the Fatigue of Glass Reinforced Plastics," *Journal of Composite Materials,* Vol. 1, 1967, pp. 424-442.

85. Chua, P. S., "Dynamic Mechanical Analysis Studies of the Interphase," *Polymer Composites,* Vol. 8, No. 5, 1987, pp. 308-313.

86. Banerjee, A., Ogale, A. A., Edie, D. D., "Interfacial Characterization of Composites by Dynamic Mechanical Analysis," *Tomorrow's Materials Today,* Proceedings of the 34th International SAMPE Symposium, 1989, pp. 1395-1399.

87. Ke, Y., Wang, S., Meng, X., Su, B., Tian, X., Qi, Z., and Wu, R., "Effects of Cyclic Loading on the Dynamic Viscoelastic Properties of Epoxy Composites," *Proceedings of the International Symposium on Composite Materials and Structures,* T. T. Loo, and C. T. Sun, eds., 1986, pp. 676-681.

88. Osiroff, R., and W. W. Stinchcomb, "Damage Mechanical Analysis as a Complementary Damage Characterization Technique for Composite Materials," *Damage Detection and Quality Assurance in Composites, ASTM STP 1128,* accepted for publication, 1991.

89. Private communication with Ahmad Razvan of the Materials Response Group.

90. Albertsen, H., and Peters, P. W. M., "The Influence of Fibre Surface Treatment Level on Interphase Properties in CFRP," to be presented at ECCM-V, Bordeaux, April 7-10, 1992.

91. Lekhnitskii, S. G., *Anisotropic Plates,* S. W. Tsai and T. Cheron, translators, Gordon and Breach, 1968.

92. Hasselman, D. P. H., and Johnson, L. F., "Effective Thermal Conductivity of Composites with Interfacial Thermal Barrier Resistance," *Journal of Composite Materials,* Vol. 21, June 1987, pp. 508-515.

93. *MRLife6™: Simulation of Performance & Life Prediction for Composite Laminates,* Materials Response Group, Engineering Science and Mechanics, Virginia Polytechnic Institute and State University, Blacksburg, Virginia, 1991.

94. Whitney, J. M., and Nuismer, R. J., "Stress Fracture Criteria for Laminated Composites Containing Stress Concentrations," *Journal of Composite Materials,* Vol. 8, July 1974, pp. 253-265.

95. Awerbuch, J., and Madhukar, M. S., "Notched Strength of Composite Laminates: Predictions and Experiments - A Review," *Journal of Reinforced Plastics and Composites,* Vol. 4, Jan. 1985, pp. 3-159.

96. Konish, H. J., and Whitney, J. M., "Approximate Stresses in an Orthotropic Plate Containing a Circular Hole," *Journal of Composite Materials,* Vol. 9, 1975, pp. 157-166.

97. Lagace, P., "Notch Sensitivity and Stacking Sequence of Laminated Composites," *Composite Materials: Testing and Design (Seventh Conference), ASTM STP 893,* J. M.

Whitney, Ed., American Society for Testing and Materials, Philadelphia, 1986, pp. 161-176.

98. El-Zein, M., "Strength in Notched and Impact Damaged Laminates," Ph.D. Dissertation, College of Engineering, Virginia Polytechnic Institute and State University, Blacksburg, Virginia, July 1990.

99. Kortschot, M. T., and Beaumont, P. W. R., "Damage Mechanics of Composite Materials: III - Prediction of Damage Growth and Notched Strength," *Composite Science and Technology,* Vol. 40, 1991, pp. 147-165.

100. Wolfram, S., *Mathematica™: A System for Doing Mathematics by Computer,* Addison-Wesley, 1988.

101. O'Brien, T. K., "Characterization of Delamination Onset and Growth in a Composite Laminate," *Damage in Composite Materials, ASTM STP 775,* American Society for Testing and Materials, Philadelphia, 1982, pp. 140-167.

102. Tirosh, J., "The Effect of Plasticity and Crack Blunting on the Stress Distribution in Orthotropic Composite Materials," *Journal of Applied Mechanics,* Sept. 1973, pp. 785-790.

103. Shuart, M. J., "Short-Wavelength Buckling and Shear Failures for Compression-Loaded Composite Laminates," NASA TM 87640, Dec. 1985.

104. Camponeschi, E. T., Jr., "Compression of Composite Materials: A Review", David Taylor Research Center, Report No. DTRC-87/050, Nov. 1987.

105. Beck, A. R., and Yen, A. "Development of Ultralightweight Materials," Fourth Interim Technical Report, Air Force Contract No. F33615-88-C-5447, May 1989.

106. Hayashi, T., "On the Shear Instability of Structures Caused by Compressive Load," Aircraft Design and Technology Meeting, AIAA Paper No. 65-770, Nov. 1965, pp. 1-12.

107. Foye, R. L., "Compression Strength of Unidirectional Composites," AIAA Paper No. 66-143, 1966, pp. 1-23.

108. Jones, R. M., *Mechanics of Composite Materials,* McGraw-Hill, 1975, p. 96.

109. Shuerch, H., "Prediction of Compressive Strength in Uniaxial Boron Fiber-Matrix Composite Materials," *AIAA Journal,* Vol. 4, Jan. 1966, pp. 102-106.

110. Chung, W. and Testa, R. B. "The Elastic Stability of Fibers in a Composite Plate," *Journal of Composite Materials,* Vol. 3, Jan. 1969, pp. 58-80.

111. Wang, A. S. D., "A Non-Linear Microbuckling Model Predicting the Compressive Strength of Unidirectional Composites," ASME Paper No. 78-WA/Aero-1, 1978.

112. Hyer, M. W., "Micromechanics of Compression in Unidirectional Laminates," Technical Report 86-9 prepared for Martin Marietta, Baltimore Division, Aug. 1986.

113. Kulkarni, S. V., Rice, J. R., and Rosen, B. W., "An Investigation of the Compressive Strength of Kevlar 49/Epoxy Composites," *Composites,* Vol. 6, 1975, pp. 217-225.

114. Hahn H. T. and Williams, J. G., "Compression Failure Mechanisms in Unidirectional Composites," NASA TM 85834, Aug. 1984.

115. Greszczuk, L. B., "Microbuckling of Lamina-Reinforced Composites," *Composite Materials: Testing and Design (Third Conference), ASTM STP 546,* American Society for Testing and Materials, 1974, pp. 5-29.

116. Waas, A. M., Babcock, C. D., Jr., Knauss, W. G., "A Mechanical Model for Elastic Fiber Microbuckling", *Journal of Applied Mechanics*, Vol. 57, March 1990, pp. 138-149.

117. Waas, A. M., Babcock, C. D., Knauss, W. G., "An Experimental Study of Compression Failure of Fibrous Laminated Composites in the Presence of Stress Gradients," *International Journal of Solids and Structures,* Vol. 26, No. 9/10, 1990, pp. 1071-1098.

118. Lessard, L. B., and Chang, F.-K., "Effect of Load Distribution on the Fiber Buckling Strength of Unidirectional Composites," *Journal of Composite Materials,* Vol. 25, Jan. 1991, pp. 65-87.

119. Tsai, S. W., and Hahn, H. T., *Introduction to Composite Materials,* Technomic, 1980, pp. 414-416.

120. Budiansky, B., "Micromechanics," *Computers and Structures,* Vol. 16, No. 1-4, 1983, pp. 3-12.

121. Steif, P. S., "A Model for Kinking in Fiber Composites — I. Fiber Breakage via Micro-Buckling", *International Journal of Solids and Structures*, Vol. 26, No. 5/6, 1990, pp. 549-561.

122. Steif, P. S., "A Model for Kinking in Fiber Composites — II. Kink Band Formation", *International Journal of Solids and Structures*, Vol. 26, No. 5/6, 1990, pp. 563-569.

123. Steif, P. S., "A Simple Model for the Compressive Failure of Weakly Bonded, Fiber Reinforced Composites," *Journal of Composite Materials,* Vol. 22, Sept. 1988, pp. 818-828.

124. Yurgartis, S. W., "Measurement of Small Angle Fiber Misalignments in Continuous Fiber Composites," *Composites Science and Technology*, Vol. 30, 1987, pp. 279-293.

125. Lesko, J. J., Swain, R. E., Reifsnider, K. L., and Dillard, D. A., "Micro-, Meso-, and Macro-Investigation of Compressive Strength to Determine the Influence of the Fiber/Matrix Interphase," submitted to the *ASTM Symposium on Compression Response of Composite Structures,* Dec. 1991.

126. Jones, W. R., and Johnson, J. W., "Intrinsic Strength and Non-Hookean Behavior of Carbon Fibers," *Carbon,* Vol. 9, 1971, pp. 645-655.

127. Tsushima, E., "Intrinsic Strength of Carbon Fiber by Loop Testing," *Tomorrow's Materials Today,* Proceedings of the 34th International SAMPE Symposium, 1989, pp. 2042-2053.

128. Sohi, M. M., Hahn, H. T., and Williams, J. G., "The Effect of Resin Toughness and Modulus on Compressive Failure Modes of Quasi-Isotropic Graphite/Epoxy Laminates," *Toughened Composites, ASTM STP 937,* N. J. Johnston, Ed., American Society for Testing and Materials, Philadelphia, 1987, pp. 37-60.

129. Garbo, S. P., and Ogonowski, J. M., "Strength Predictions of Composite Laminates with Unloaded Fastener Holes," *AIAA Journal,* Vol. 18, No. 5, May 1980, pp. 585-589.

130. Gürdal, Z., and Haftka, T., "Compressive Failure Model for Anisotropic Plate with a Cutout," *AIAA Journal,* Vol. 25, No. 11, Nov. 1987, pp. 1476-1481.

131. Seidensticker, D. G., Kim, K.-S., Hahn, H. T., Jensen, D. W., and Goering, J. C., "Compressive Behavior of a Thermoplastic Composite (Gr/PEEK)," *Journal of Thermoplastic Composites,* Vol. 3, July 1990, pp. 233-251.

132. Newaz, G. M., "Evaluation of Fiber-Matrix Interphasial Toughness in Unidirectional Composites," *Polymer Composites,* Vol. 7, No. 6, 1986, pp. 421-425.

133. Nairn, J. A., "Fracture Mechanics of Unidirectional Composites Using the Shear-Lag Model, I. Theory," *Journal of Composite Materials,* Vol. 22, June 1988, pp. 561-588.

134. Nairn, J. A., "Fracture Mechanics of Unidirectional Composites Using the Shear-Lag Model, II. Experiment," *Journal of Composite Materials,* Vol. 22, June 1988, pp. 569-600.

Vita

Robert E. Swain III was born on August 23, 1963, to Judith and Robert E. Swain, Jr. in Orange County, California. He grew up in the northern suburbs of Cincinnati, Ohio and attended the local, public schools. In 1981 he graduated with honors from Northwest Senior High School and came to Virginia Tech in the fall of 1981 to study engineering. Mr. Swain graduated magna cum laude with a Bachelor of Science degree from the Engineering Science and Mechanics department in 1985. He spent the summers prior to his senior year and after graduation working as an engineering intern at General Electric in Evendale, Ohio. Robert returned to VPI in the fall of 1985 to pursue a Master of Science degree in Engineering Mechanics with a focus on composite material science. He completed his degree in the spring of 1988, taking a short sabbatical in 1987 to marry Susan Reed Kordack of LaPlata, Maryland, a graduate of VPI. Robert began his doctoral work in the Engineering Mechanics department of VPI as a Presidential Fellow in the fall of 1988. He, again, studied the mechanics of composite materials under the direction of Dr. K. L. Reifsnider.

The year 1992 has brought several changes to Robert's life. He graduated with his Ph.D. in Engineering Mechanics in February. Upon graduation, he accepted a position as a Senior Research Engineer with Smith & Nephew Richards Inc., in Memphis, Tennessee. As of this writing, Robert and his wife, Susan, are awaiting the birth of their first child, due in ten weeks.

Robert E. Swain III